

Timothy M. Maus · Sonia Nhieu
Seth T. Herway *Editors*

Essential Echocardiography

Transesophageal
Echocardiography
for Non-Cardiac
Anesthesiologists

EXTRAS ONLINE

 Springer

Essential Echocardiography

Timothy M. Maus · Sonia Nhieu
Seth T. Herway
Editors

Essential Echocardiography

Transesophageal Echocardiography
for Non-Cardiac Anesthesiologists

 Springer

Editors

Timothy M. Maus, MD, FASE
Department of Anesthesiology
University of California San Diego
San Diego, CA
USA

Seth T. Herway, MD, MS
Department of Anesthesiology
University of California San Diego
San Diego, CA
USA

Sonia Nhieu, MD
Division of Cardiovascular Anesthesiology
and Critical Care
Texas Heart Institute at Baylor St. Luke's
Medical Center
Houston, TX
USA

Additional material to this book can be downloaded from
<https://link.springer.com/book/10.1007%2F978-3-319-34124-8>.

ISBN 978-3-319-34122-4 ISBN 978-3-319-34124-8 (eBook)
DOI 10.1007/978-3-319-34124-8

Library of Congress Control Number: 2016940810

© Springer International Publishing Switzerland 2016

This work is subject to copyright. All rights are reserved by the Publisher, whether the whole or part of the material is concerned, specifically the rights of translation, reprinting, reuse of illustrations, recitation, broadcasting, reproduction on microfilms or in any other physical way, and transmission or information storage and retrieval, electronic adaptation, computer software, or by similar or dissimilar methodology now known or hereafter developed.

The use of general descriptive names, registered names, trademarks, service marks, etc. in this publication does not imply, even in the absence of a specific statement, that such names are exempt from the relevant protective laws and regulations and therefore free for general use.

The publisher, the authors and the editors are safe to assume that the advice and information in this book are believed to be true and accurate at the date of publication. Neither the publisher nor the authors or the editors give a warranty, express or implied, with respect to the material contained herein or for any errors or omissions that may have been made.

Printed on acid-free paper

This Springer imprint is published by Springer Nature
The registered company is Springer International Publishing AG Switzerland

To Molly for your unwavering love and support and to William, Owen, and Winston for the overflowing happiness you bring to our life.

—Timothy M. Maus

For TayTay, whose memory reminds me everyday of the important things in life. And to Alvin, for the unconditional support during my never-ending pursuit of higher education. I am blessed to be able to share my life, love, and beagle with you.

—Sonia Nhieu

To my wife, my children, and my many mentors in the UCSD Department of Anesthesiology.

—Seth T. Herway

Preface

Transesophageal echocardiography (TEE) has a well-established history of utility in cardiac operating rooms, allowing the diagnosis of cardiac anatomical and physiological pathologies while also directing the surgical treatment. However, the notion that cardiac surgery is the only situation where perioperative care is improved by the use of TEE is simply outdated. The advances and increased availability of TEE, along with the portability of transthoracic echocardiography (TTE), have propelled both modalities into the non-cardiac realm. Whether in the emergency department, intensive care unit, or operating room in high-risk surgical patients, echocardiography's ability to monitor cardiac function, assess response to interventions, and quickly diagnose causes of hemodynamic instability have made it a necessary basic skill for practicing physicians in this era of medicine.

Utilizing both two-dimensional echocardiography and Doppler imaging, through color flow Doppler and quantitative spectral Doppler, numerous causes of hemodynamic compromise that warrant immediate intervention may be identified. Recognizing myocardial ischemia, pericardial tamponade, left ventricular outflow obstruction, severe valvular abnormalities, hypovolemia, venous air embolism, and pulmonary emboli can directly affect patient management and outcomes. By providing direct visualization of cardiac structures and function in real time, echocardiography can enable any trained practitioner to competently assess a patient who is experiencing hemodynamic compromise or may be at risk of compromise, both in an emergent and in a perioperative setting.

The editors of this textbook had a vision to share their enthusiasm and educate interested practitioners regarding the utility of basic echocardiography in everyday practice. We, along with the contributing authors who are all established as excellent and respected echocardiography instructors, set out to create an easily approachable and well-illustrated text set as a resource to learn the principles of perioperative echocardiography, evaluation of cardiac anatomy in a context outside of the cardiac operating room, and integration of such findings into current clinical practice. While numerous comprehensive echocardiography textbooks exist, this text differs by offering a unique perspective of utilizing echocardiography by

non-cardiac anesthesiologists. Therefore, advanced cardiac operating room topics such as determinations for valvular repair versus replacement are omitted. Instead, there is a distinct emphasis on identifying normal versus abnormal anatomic and physiologic states, commonly encountered perioperative pathologies, and emergent causes of hemodynamic instability.

This book aims to serve as a guide and provide a framework for the readers as they are introduced to the application of TEE. Understandably, there is often fear and frustration observed when learning a new task such as TEE. The gentle approach of the authors within the context of echocardiography for non-cardiac surgery helps to allay those fears and minimize the frustration that often comes with learning a new skill set. It is also important to remember that a multimodal approach to learning echocardiography is key, including echocardiography simulation and repetitive hands-on application during patient care.

In addition to helping the practitioner who is seeking to implement the use of TEE into their clinical practice, this text is intended as an aid for those who are seeking basic certification in echocardiography, including passing the Basic PTEeXAM[®]. Each chapter in this book is designed to address the core competencies that are tested in the basic exam and prepare the practitioner for the basic certification. In addition to being a valuable and practical guide to obtaining certification, we hope that this textbook becomes a successful resource for the application of echocardiography into your clinical practice.

San Diego, CA, USA
Houston, TX, USA
San Diego, CA, USA

Timothy M. Maus
Sonia Nhieu
Seth T. Herway

Contents

Part I Basic Perioperative Echocardiography

1	TEE in Non-cardiac Surgery: Indications, Contraindications, Probe Manipulation, and Certification	3
	Seth T. Herway	
2	Transesophageal Echocardiography: Essential Views	15
	Sonia Nhieu	
3	Basic Ultrasound Physics, Doppler Ultrasound, and Hemodynamic Assessment	45
	Gerard R. Manecke	

Part II Echocardiographic Assessment

4	Left Ventricular Systolic Function	61
	Seth T. Herway, Raimy Boban and Swapnil Khoche	
5	Regional Ventricular Function	77
	Tariq Naseem and Timothy M. Maus	
6	Mitral Valve	95
	Liem Nguyen and Neal Gerstein	
7	Aortic Valve	125
	Michael Benggon and Thomas Griffiths	
8	The Right Heart	145
	Dalia Banks	
9	Diastology	169
	Liem Nguyen and Neal Gerstein	
10	Thoracic Aorta	183
	Timothy M. Maus	

11 Rescue Echocardiography 205
Byron Ferguson and Joshua Zimmerman

12 Imaging Artifacts and Common Misdiagnoses 231
Brett Cronin

13 Adult Congenital Heart Disease 247
Swapnil Khoche

Part III Surface Ultrasound

14 Transthoracic Echocardiography: The Basic Views 265
Sonia Nhieu

15 Ultrasound for Vascular Access 279
Seth T. Herway

Index 295

Contributors

Dalia Banks MD, FASE Department of Anesthesiology, University of California San Diego, San Diego, CA, USA

Michael Benggon MD Department of Anesthesiology, Loma Linda University, Loma Linda, CA, USA

Raimy Boban MD Department of Anesthesiology, University of California San Diego, San Diego, CA, USA

Brett Cronin MD Department of Anesthesiology, University of California San Diego, San Diego, CA, USA

Byron Ferguson MD Department of Anesthesiology, University of California San Diego, San Diego, CA, USA

Neal Gerstein MD Department of Anesthesiology, University of New Mexico, Albuquerque, NM, USA

Thomas Griffiths MD Department of Anesthesiology, University of California San Diego, San Diego, CA, USA

Seth T. Herway MD, MS Department of Anesthesiology, University of California San Diego, San Diego, CA, USA

Swapnil Khoche MBBS Department of Anesthesiology, University of California San Diego, San Diego, CA, USA

Gerard R. Manecke MD Department of Anesthesiology, University of California San Diego, San Diego, CA, USA

Timothy M. Maus MD, FASE Department of Anesthesiology, University of California San Diego, San Diego, CA, USA

Tariq Naseem MD Department of Anesthesiology, University of California San Diego, San Diego, CA, USA

Liem Nguyen MD Department of Anesthesiology, University of California San Diego, San Diego, CA, USA

Sonia Nhieu MD Division of Cardiovascular Anesthesiology and Critical Care, Texas Heart Institute at Baylor St. Luke's Medical Center, Houston, TX, USA

Joshua Zimmerman MD, FASE Department of Anesthesiology, University of Utah, Salt Lake City, UT, USA

Part I
Basic Perioperative Echocardiography

Chapter 1

TEE in Non-cardiac Surgery: Indications, Contraindications, Probe Manipulation, and Certification

Seth T. Herway MD, MS

Abstract Transesophageal echocardiography (TEE) is a safe monitoring modality with broad applications in non-cardiac surgery. A moderate amount of exposure to its use and knowledge of the principles of echocardiography can yield the practitioner competent to make basic assessments of a patient's cardiac status and help guide initial management decisions. The practitioner should also be able to determine when the nature of the surgery or the patient's cardiovascular status necessitates a comprehensive examination by a board certified advanced echocardiographer. Each patient should be evaluated individually to assess for contraindications and potential complications associated with the use of TEE. Most complications are associated with probe insertion and manipulation and providers should ensure that these maneuvers are performed carefully and appropriately.

Keywords Echocardiography · Transesophageal echocardiography · Indications · Contraindications · Complications

Transesophageal Echocardiography in Non-cardiac Surgery

There is broad application for the use of transesophageal echocardiography (TEE) as both a diagnostic and monitoring modality in non-cardiac surgery. The notion that cardiac surgery is the only situation where perioperative care is improved by the use of TEE is outdated. TEE has been used in non-cardiac surgeries to identify myocardial ischemia, pericardial tamponade, left ventricular outflow obstruction, severe valvular abnormalities, hypovolemia, venous air embolism, intrapulmonary emboli, and a number of other causes of hemodynamic

S.T. Herway, MD, MS (✉)
Department of Anesthesiology, University of California San Diego,
200 W Arbor Drive MC #8770, San Diego, CA 92103, USA
e-mail: sherway@ucsd.edu

compromise of cardiac origin [1]. By providing direct visualization of cardiac structures and function, TEE can enable any trained practitioner to competently assess a patient who is experiencing hemodynamic compromise of cardiovascular origin in a way that no other monitor is able. As a provider gains experience in TEE, competency in transthoracic echocardiography (TTE) is readily acquired and with this comes the ability to non-invasively assess the patient's cardiovascular status in pre- and post-operative settings.

For anesthesiologists who have not pursued fellowship training in anesthesia for cardiac surgery or had dedicated advanced training in the use of TEE, integrating TEE into clinical practice can be an intimidating proposition. However, a moderate amount of exposure to its use and knowledge of the principles of echocardiography contained in this text will enable the practitioner to make basic assessments of a patient's cardiac status and help guide initial management decisions. Additionally, the practitioner should also be able to determine when the nature of the surgery or the patient's cardiovascular status necessitates a comprehensive examination by an echocardiographer with an advanced echocardiography skill set.

This book was intentioned for the practitioner with little to no previous experience with echocardiography who is seeking to employ this diagnostic modality in their clinical practice. The book also may serve as a review of basic echocardiography principles to those who do possess prior experience or training. Most graduates of U.S. residency programs receive their initial exposure to TEE during training. This book certainly fulfills the role as a guide during that initial exposure or as a framework for building upon the knowledge obtained during training.

Echocardiography requires several skill sets: (1) Manual dexterity which is manifested as probe manipulation and image acquisition; (2) Knowledge of normal anatomy; and (3) Recognition of pathology or diseased states. For practitioners who have never had formal exposure to TEE, a basic introduction from a competent practitioner on safe probe insertion and manipulation and initial assistance with obtaining TEE views is important to get started. This topic will be discussed below, however to become fluent with the TEE probe repetition is key. Performing exams on a regular basis will begin to engrain certain subtleties of probe manipulation in order to display the particular structure of interest. Therefore, it is recommended to physically perform the exam as much as possible either through clinical indication or TEE simulation. Repetition is certainly the key to adult learning and this is applicable to knowledge of normal anatomy. The more exams one visualizes or performs, the more data points one will have that represent normal anatomy. Similarly, the more exams performed, the more pathology one will observe and begin to develop patterns of recognition. In summary, when clinically indicated, performance of exams will increase manual dexterity as well as recognition of normal versus abnormal anatomy.

Initial attempts at performing a TEE exam can be frustrating and anxiety-ridden as the views can be challenging for the novice echocardiographer to obtain. Most

practitioners notice that it takes roughly 20–30 performed exams before they are able to reliably find the basic views. Once able to obtain the basic views, they can then start recognizing pathology and abnormal findings. Similar to other clinical skills such as appreciating heart sounds with a stethoscope, a practitioner must be able to appreciate the normal findings before the pathologic exam becomes clear.

In addition to helping the practitioner seeking to implement the use of TEE into their clinical practice, this text is intended as an aid for those who are seeking basic certification in echocardiography including passing the Basic PTEeXAM[®]. Each chapter in this book is designed to address the core competencies that are tested in the basic exam and prepare the practitioner to obtain basic certification.

Certification in Basic Perioperative Transesophageal Echocardiography

As one becomes proficient in the use of perioperative echocardiography, they ultimately may seek certification to acknowledge the new skill set they have achieved. The National Board of Echocardiography, Inc. (www.echoboards.org) is the not-for-profit corporation that administers the examination in perioperative TEE as well as the board certification process. The purpose of certification is to recognize anesthesiologists who have demonstrated their competence in basic TEE. The NBE offers two levels of certification: Basic and Advanced, which differ primarily on their scope of practice and training requirements. Certification in Basic Perioperative Transesophageal Echocardiography is provided to recognize anesthesiologists utilizing TEE in a non-diagnostic or monitoring-only manner, except in emergency situations. The use of TEE as a diagnostic tool to direct medical or surgical interventions, particularly cardiac surgical interventions, is under the purview of anesthesiologists with Certification in Advanced Perioperative Transesophageal Echocardiography. This is an important distinction when considering the pathway and certification options for the individual practitioner.

The NBE offers two statuses in relation to basic perioperative TEE: Testamur and Certification. Testamur status indicates the successful completion of the Examination of Special Competence in Basic Perioperative Transesophageal Echocardiography (Basic PTEeXAM[®]). Certification also implies a passing score on the Basic PTEeEXAM[®] in addition to meeting requirements that document proficiency. Readers are encouraged to visit the NBE's website for the most current requirements; however, the present requirements include a current license to practice medicine, current board certification in Anesthesiology, and specific training in basic perioperative TEE.

The specific training involves performing a certain number of exams and reviewing (but not performing) additional exams. There are several pathways to obtaining the specific training including a Supervised Training pathway which is

often suited to those still in a training institution, and the Extended CME pathway which is more suited to those already in practice. Both pathways require performance and interpretation of at least 50 basic perioperative TEE exams. The supervised training pathway involves reviewing (but not performing) additional exams with a supervising physician to a total of 150 basic TEE exams. The Extended CME pathway involves a review of 100 basic TEEs through the ASA/SCA Basic Perioperative TEE Education Program to result in a total of 150 basic TEE exams. Lastly, there is an additional Practice Experience pathway for those who have previously completed residency and currently perform basic TEEs in their practice. Details of each of the pathways and the required documentation may be found on the NBE's website (www.echoboards.org).

Basic TEE Examination

Indications

The use of basic TEE in non-cardiac surgery can be broadly categorized into two main areas: monitoring and diagnostic purposes. Monitoring uses of TEE occur during any type of surgery where pre-operative evaluation suggests that either the nature of the surgery or the patient's cardiovascular status has the potential to result in hemodynamic compromise. Therefore, the TEE exam can be used to monitor volume status, detect ischemia, and determine the need for inotropic or vasopressor therapy. TEE is appropriate for any surgery ranging from common elective cases in patients with cardiovascular indications to large intra-abdominal, thoracic, or neurosurgical procedures where there is potential for hemodynamic compromise in otherwise healthy patients. The basic echocardiographer can also utilize TEE as a diagnostic modality in the situation of unexplained perioperative hemodynamic compromise. The delay introduced in waiting for another imaging modality or an advanced echocardiographer may result in patient harm.

The American Society of Anesthesiologists (ASA) and the Society of Cardiovascular Anesthesiologists (SCA) have explained the use of basic TEE in monitoring and diagnostic capacities in their published practice guidelines [1]. In non-cardiac surgery, the ASA and SCA recommend that TEE *may be used* when "the nature of the planned surgery or the patient's known or suspected cardiovascular pathology may result in severe hemodynamic, pulmonary, or neurologic compromise." The published guidelines also recommend TEE *should be used* when "unexplained life-threatening circulatory instability persists despite corrective measures." Taking into account any contraindications, TEE is therefore appropriate perioperatively when either instability is present or possible. The American Society of Echocardiography (ASE) and the SCA have created a consensus statement that further delineates indications and utility of basic perioperative TEE including

evaluating ventricular function, valvular function, pericardial disease, embolism detection, and basic congenital heart disease in the adult [1].

Contraindications

Clinical judgment should be employed to determine the suitability of TEE for each individual patient. While prior practice guidelines divided contraindications by absolute and relative categories, current updated practice guidelines note that the use of TEE is a risk versus benefit evaluation even in the setting of potential contraindications [1, 2]. Absolute contraindications often involve pathology of the esophagus and include previous esophagectomy and esophagogastrectomy. Often included are a history of a tracheoesophageal fistula, esophageal trauma, esophageal surgery, esophageal stricture/mass, perforated viscus, and active upper gastrointestinal bleeding [1, 3]. Relative contraindications include pathologies of oral, esophageal and gastric location, often with less severe presentations than those listed above as absolute contraindications. A suggested list of absolute and relative contraindications is provided in Table 1.1. However, it is noteworthy that current practice guidelines report TEE can be used even in patients with oral, esophageal, or gastric disease if the expected benefit outweighs the potential risk.

Table 1.1 Contraindications to transesophageal echocardiography

Absolute contraindications
Esophagectomy or esophagogastrectomy Postesophageal surgery
Esophageal trauma, perforation, laceration
Esophageal obstruction (stricture, mass)
Tracheoesophageal fistula
Perforated viscus
Active upper gastrointestinal bleed
Relative contraindications
History of dysphagia
History of radiation to neck and mediastinum
Recent GI surgery
Barrett esophagus
Symptomatic hiatal hernia
Esophageal varices
Zenker diverticulum
Colonic interposition
Recent upper gastrointestinal bleed
Severe cervical arthritis with restricted mobility
Atlantoaxial joint disease with restricted mobility
Severe coagulopathy
Active esophagitis or peptic ulcer disease

In such cases where there is some perceived additional risk, some precautions can be considered when TEE is used. Limiting the exam either to only the views necessary or to the most experienced provider will help to avoid unnecessary probe manipulations and potentially avoid additional oropharyngeal, esophageal, or gastric trauma. For example, in the case of a patient with prior gastric surgery, limiting the exam to mid-esophageal views will still provide excellent imaging and diagnostic information without the additional risk of gastric injury. As the echocardiographer becomes more familiar with the basic TEE views and the information that can be obtained from each view, it will become apparent that only one or two views are necessary to evaluate the aspect of cardiac function that is of interest. In these cases, leaving the probe in one location (i.e., mid-esophageal) for monitoring purposes during the anesthetic may be the best course of action.

In clinical scenarios where the potential risks outweigh the benefits of TEE probe placement, the use of other non-invasive imaging modalities that provide the same information (e.g., transthoracic echocardiography) should be considered [1]. Additionally, in an elective scenario, obtaining a gastroenterology consultation prior to probe placement may provide further insight into the patient's pathology and their risk–benefit ratio.

Complications

Perioperative TEE has been demonstrated to be a safe monitoring modality. The morbidity is often associated with a traumatic placement or manipulation of the probe. Recognition of potential contraindications as well as gentle placement and manipulation of the probe are essential. The use of force is unnecessary in TEE imaging. A large study of 7200 cardiac surgical patients determined an intraoperative TEE-associated morbidity and mortality of 0.2 and 0 %, respectively [3]. The

Table 1.2 Complications associated with intraoperative transesophageal echocardiography

Complication	Incidence (%)
Odynophagia	0.1
Swallowing abnormality	0.01
Esophageal abrasions	0.06
No associated pathology	0.03
Upper gastrointestinal hemorrhage	0.03
Esophageal perforation	0.01
Dental injury	0.03
Endotracheal tube malposition	0.03
Total	0.2

Data from Kallmeyer et al. [3]

majority of complications (86 %) were associated with oropharyngeal, esophageal, or gastric trauma due to TEE probe insertion and manipulation (see Table 1.2). The reported morbidity of 0.2 % in this study of intraoperative TEE correlates with a reported 0.18 % complication rate in a large, multicenter survey of over 10,000 predominantly conscious adult patients undergoing TEE [4].

Using the TEE Probe

Insertion

In addition to consideration of contraindications to TEE prior to probe insertion, the mouth should be inspected for preexisting injuries including at-risk dental lesions. Limitations in cervical spine movement should also be considered.

The TEE probe can be inserted in a similar manner to an orogastric tube. Performing a jaw lift during insertion significantly facilitates insertion. This includes lifting the mandible with the left hand, utilizing the left thumb posterior to the lower incisors and the left fingers inferior to the mental protuberance. The right hand is used to advance the probe with constant gentle pressure. Lubrication of the probe facilitates advancement and reduces the incidence of trauma to soft tissues. Of note, non-sterile multiuse ultrasound transmission gel is not recommended as an oral lubricant for TEE procedures due to a risk of contamination and sepsis. Current FDA recommendations include the use of single-use sterile packets [5]. Ensure that the large and small knobs of the TEE probe are in the unlocked position as this will allow the distal end of the probe to remain flexible as it passes through the oropharynx. A loss of resistance is typically felt as the probe passes the upper esophageal sphincter. Again, excessive force is unnecessary. Anteflexion of the probe can help navigate the upper oropharynx while once past the upper oropharynx, retroflexion aids in guiding the probe away from the glottis and towards the esophageal inlet. If blind insertion of the probe proves difficult, a laryngoscope or even a video laryngoscope can be used to identify the glottis and esophageal inlet, and facilitate passage of the probe under direct visualization.

Manipulation

There are five primary movements of the TEE probe used to optimize the ultrasound image (Fig. 1.1). Some of these are analogous to the movement of a bronchoscope (familiar to most anesthesiologists) which include advance/withdrawal, anteflexion/retroflexion, and turning the probe to the left/right, while other functions are unique to TEE which include the image appearing perpendicular to probe tip (as opposed to in-line with the probe tip), flexion to the left/right and the omniplane function. The movements in detail are as follows:

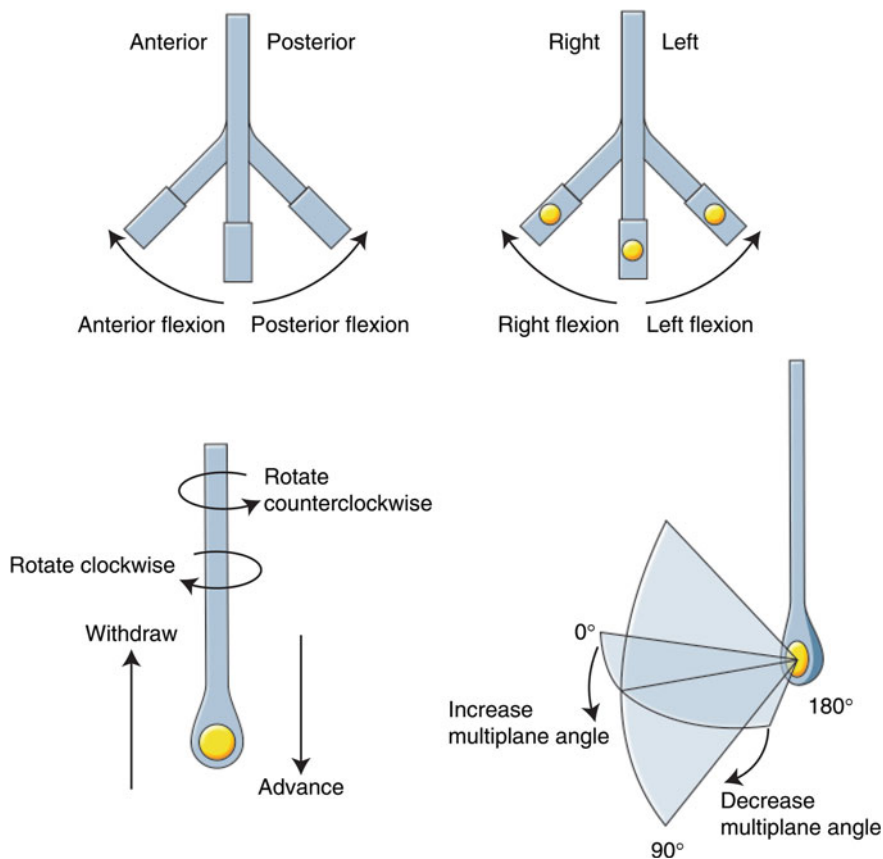
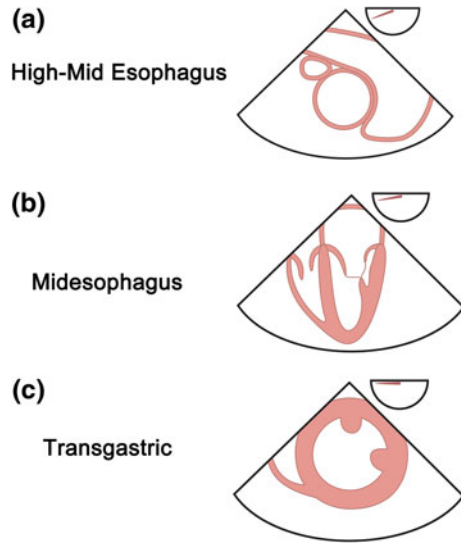


Fig. 1.1 Basic TEE probe manipulations

1. **Advance and withdraw.** The probe can be advanced (and withdrawn) to more distal (and proximal) locations within the esophagus and stomach. The primary positions at which ultrasound images are obtained are, from proximal to distal: (1) upper esophagus, (2) mid-esophagus, (3) transgastric, and (4) deep transgastric. In general, the tip of the transducer should be in the neutral position before advancing or withdrawing the probe. Brief recognition of depth can be determined by observing what is closest to the image transducer (closest to the top of the image): great vessels (high mid-esophagus), left atrium (mid-esophagus) and ventricle (transgastric) (Fig. 1.2).
2. **Anteflex and retroflex.** The large knob on the probe handle can be turned to move the tip of the probe anteriorly (anteflexion) or posteriorly (retroflexion). Again this is analogous to the flexion on a bronchoscope.
3. **Flexion to the left and right.** The small knob on the probe can be turned to flex the probe leftward or rightward. This motion is rarely utilized in basic TEE

Fig. 1.2 Depth estimation via observation of what is nearest to the probe (apex of the image). **a** Great vessels—High mid-esophagus; **b** Left atrium—Mid-esophagus; **c** Ventricle—Transgastric (illustrations adapted from Shanewise et al. [6])



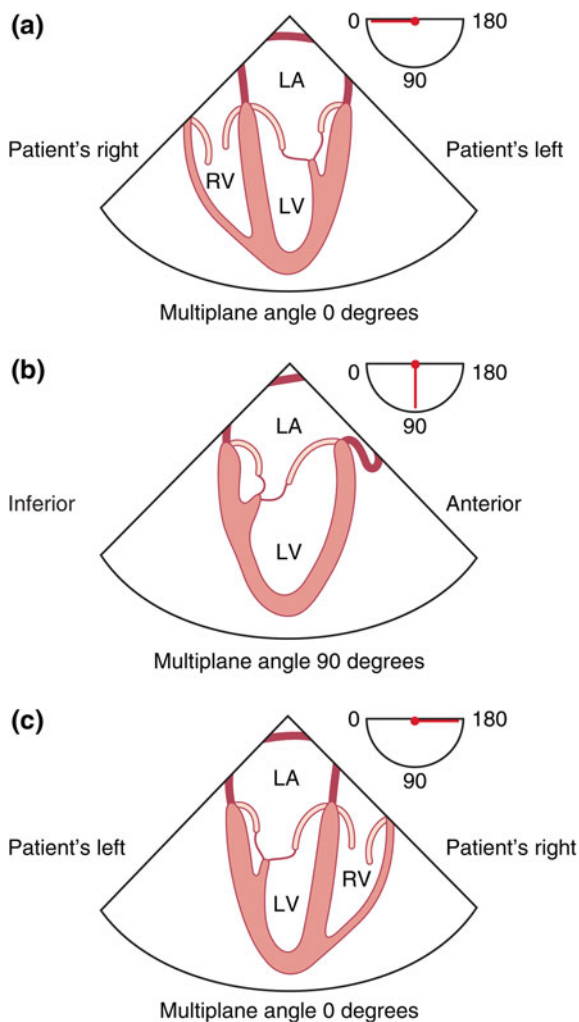
imaging as the esophagus is a relatively fixed structure. However, this motion is often necessary in the comprehensive examination for the deep transgastric long axis view to bring the tip of the probe towards the left-sided LV apex.

4. **Turn to the left and right.** The probe shaft can be rotated clockwise (called turning to the right) or counterclockwise (called turning to the left) to adjust the orientation of the ultrasound beam. This allows the imaging of the right versus left-sided structures within the chest.
5. **Increase or decrease omniplane (multiplane).** Axial rotation of the multiplane angle from 0° towards 180° is called rotating forward and from 180° towards 0° is called rotating back. This “movement” does not physically move the TEE probe, however it moves the image produced by rotating the image in an axial direction. This can be visualized by placing the right-hand palm face down in front of one’s chest with the fingers spread out, imagining this as the imaging view from the esophagus. The thumb will be the right side of the image, while the small finger will be left side of the image. Imagining a four chamber view, the left atrium and left ventricle will be displayed on the right side of the image (near the thumb), while the right atrium and right ventricle will be displayed on the left side of the image (near the small finger). Increasing the omniplane can be demonstrated by rotating the hand clockwise. A 90° rotation will display a two-chamber view with the thumb directed over the anterior wall (on the right side of the image) and the small finger over the inferior wall (on the left side of the image). The use of the hand movement with either an imagined heart or a heart model will help to understand the physical relationship of cardiac structures.

Orientation

The objects closest to the TEE probe transducer are displayed at the top of the screen while the far field is displayed at the bottom. With a multiplane angle of 0° and the TEE probe transducer angled anteriorly from the gastrointestinal tract towards the heart, the patient's right side is displayed on the left of the screen. When the multiplane is rotated towards 90° , the left side of the screen is moved inferiorly towards the patient's feet. When the multiplane is increased to 180° , the patient's right side is now displayed on the right of the screen, making it the mirror image of the display at 0° (Fig. 1.3).

Fig. 1.3 Image orientation with multiplane angles 0° – 180° (illustration adapted from Shanewise et al. [6])



Basic Echocardiography Reporting and Image Storage

Current basic perioperative TEE consensus statement recommends the image storage and reporting of all performed basic exams. Modern echocardiography machines have the ability to save exams digitally in a DICOM (Digital Imaging and Communications in Medicine) format, which allows retrieval and review when necessary. Older systems have allowed the storage of images and clips through VHS tapes or proprietary disk systems. Discussion with the echocardiography machine vendor and your information technology (IT) department is necessary to ensure the proper storage and retrieval for your institution.

In addition to image storage, a documented report of the intraoperative findings into the patient's chart is necessary. This may be performed as a written report or a clickable generated report in an electronic medical record. The report should include documentation of ventricular function, valvular function, chamber sizes, assessments of pericardium or pleura, and description of responses to interventions. The Society for Cardiovascular Anesthesiology website (www.scahq.org) hosts a template for a suggested adult TEE report.

References

1. American Society of Anesthesiologists and Society of Cardiovascular Anesthesiologists task force on transesophageal echocardiography. Practice guidelines for perioperative transesophageal echocardiography. *Anesthesiology*. 2010;112:1084–96.
2. Hahn RT, Abraham T, Adams MS, Bruce CJ, Glas KE, Lang RM, Reeves ST, Shanewise JS, Siu SC, Stewart W, Picard MH. American society of echocardiography; society of cardiovascular anesthesiologists. Guidelines for performing a comprehensive transesophageal echocardiographic examination: recommendations from the American society of echocardiography and the society of cardiovascular anesthesiologists. *Anesth Analg*. 2014;118:21–68.
3. Kallmeyer IJ, Collard CD, Fox JA, Body SC, Shernan SK. The safety of intraoperative transesophageal echocardiography: a case series of 7200 cardiac surgical patients. *Anesth Analg*. 2001;92:1126–30.
4. Daniel WC, Erbl R, Kasper W, Visser CA, Engberding R, Sutherland GR, et al. Safety of transesophageal echocardiography: a multicenter survey of 10,419 examinations. *Circulation*. 1991;83:817–21.
5. O'Rourke M, Levan P, Khan T. Current use of ultrasound transmission gel for transesophageal echocardiogram examinations: a survey of cardiothoracic anesthesiology fellowship directors. *J Cardiothorac Vasc Anesth*. 2014;28(5):1208–10.
6. Shanewise JS, et al. ASE/SCA guidelines for performing a comprehensive intraoperative multiplane transesophageal echocardiography examination: recommendations of the American Society of Echocardiography Council for Intraoperative Echocardiography and the Society of Cardiovascular Anesthesiologists Task Force for Certification in Perioperative Transesophageal Echocardiography. *J Am Soc Echocardiogr*. 1999;12(10):884–900.

Chapter 2

Transesophageal Echocardiography: Essential Views

Sonia Nhieu, MD

Abstract The use of a noncomprehensive basic perioperative transesophageal echocardiographic (PTE) examination, both for intraoperative monitoring and outside of the operating room, is increasing in practice. Cardiac causes of hemodynamic instability, such as ventricular dysfunction, valvular abnormalities, volume status changes, and pericardial abnormalities can be identified with the basic PTE examination. A basic PTE exam is intended to be complementary to comprehensive echocardiography, and thus the practitioner must also recognize when further investigation of an abnormality by an echocardiographer with advanced imaging skills may be required. While the consensus statement of the American Society of Echocardiography (ASE) and Society of Cardiovascular Anesthesiologists (SCA) identifies 11 views for the basic PTE examination, the additional 9 views that comprise the comprehensive examination will also be discussed for completeness.

Keywords Transesophageal echocardiography · Comprehensive perioperative transesophageal examination · Basic perioperative transesophageal echocardiography examination · Basic perioperative TEE certification · TEE perioperative guidelines

Abbreviations

TEE	Transesophageal echocardiography
PTE	Perioperative transesophageal
ASE	American Society of Echocardiography
SCA	Society of Cardiovascular Anesthesiologists
ME	Midesophageal

Electronic supplementary material The online version of this chapter (doi:[10.1007/978-3-319-34124-8_2](https://doi.org/10.1007/978-3-319-34124-8_2)) contains supplementary material, which is available to authorized users.

S. Nhieu, MD (✉)

Division of Cardiovascular Anesthesiology and Critical Care, Texas Heart Institute at Baylor St. Luke's Medical Center, 6720 Bertner Ave, MC1-226, Houston, TX 77030, USA
e-mail: Sonia.nhieu@gmail.com

AV	Aortic valve
LVOT	Left ventricular outflow tract
RA	Right atrium
LA	Left atrium
RV	Right ventricle
LV	Left ventricle
TV	Tricuspid valve
MV	Mitral valve
LAX	Long axis
SVC	Superior vena cava
IVC	Inferior vena cava
ASD	Atrial septal defect
PFO	Patent foramen ovale
RVOT	Right ventricular outflow tract
SAX	Short axis
TG	Transgastric
UE	Upper esophageal

The goal of this chapter is for the echocardiographer to become familiar with the imaging views required to perform a basic perioperative transesophageal (PTE) examination. Specific pathologies that can be appreciated in each view are discussed in subsequent chapters. As outlined by the consensus statement of the American Society of Echocardiography (ASE) and Society of Cardiovascular Anesthesiologists (SCA), the basic PTE examination focuses on acquiring the 11 most relevant views [1]. Though prior guidelines for performing a comprehensive PTE examination consists of acquiring 20 views [2], with the expansion of indications for TEE the most recent guidelines have expanded with the addition of 8 views [3] for a total of 28 views in a complete comprehensive exam. While the 11 views of a basic PTE examination will provide the information needed to monitor patients perioperatively and diagnose general etiologies of hemodynamic instability (e.g., ventricular dysfunction, valvular abnormalities, volume status changes, and pericardial abnormalities), the basic PTE echocardiographer should also be familiar with how to perform the comprehensive examination. This textbook will describe the additional views to complete a 20-view comprehensive exam. The recent addition of 8 views focus on structures such as the different pulmonary veins, left atrial appendage, and the right ventricular outflow and pulmonic valve views which would rarely be indicated in a basic PTE exam. The basic PTE examination is designed to be complementary to a comprehensive TEE examination. Therefore, consultation with an advanced PTE echocardiographer should be requested when complex pathology is anticipated or when further investigation of abnormality is desired.

Beginning echocardiographers often exhibit anxiety and fear when learning the examination with a focus on the order of the exam. Each echocardiographer will have a different approach to the TEE examination and the order of the examination is not critical. Completeness of the examination without missing important data is the most important aspect. This text will offer a suggested order of views for both a basic and comprehensive examination based upon minimizing significant probe movement between views and maximizing the data obtained (Tables 2.1 and 2.2). It is suggested for the beginning echocardiographer to perform PTE exams as often as possible, when clinically indicated, in order to develop a comfort level when moving from one view to the next and to learn anatomical relationships.

In addition to obtaining the particular image, there are specific anatomical and physiologic interrogations that should occur within the image. These interrogations are divided into two-dimensional (2D) analysis, color flow Doppler (CFD) and spectral Doppler (pulsed wave and continuous wave) interrogation. It is recommended for the beginning echocardiographer to develop a systematic approach to the interrogations as well as simply obtaining the images. For example, when obtaining the midesophageal four-chamber view, a 2D image is acquired, color flow Doppler interrogation of the mitral valve and tricuspid valve is acquired, followed by a pulsed wave or continuous wave Doppler interrogation of mitral valve and tricuspid valve inflow and regurgitation. This approach of 2D > CFD > Spectral allows an echocardiographer to develop an approach to the examination without missing data and prevents “bouncing” around the exam. Additionally, pathologies in this textbook will be summarized in the 2D > CFD > Spectral format, highlighting important findings for each interrogation.

Basic PTE Examination

The following are the 11 views as described by the ASE and SCA for performing a basic PTE examination. The additional 9 views that comprise the comprehensive exam will be subsequently discussed. Many practitioners will find that a complete 20-view examination is rarely necessary for a basic perioperative echocardiographic assessment. However, becoming familiar with all 20 views will allow the echocardiographer to become adept at choosing which views to obtain in a focused examination to evaluate for specific pathologies.

Midesophageal (ME) Four-Chamber View

The ME four-chamber view is obtained by inserting the TEE probe approximately 30–35 cm. A midesophageal position is identified by observing the left atrium at the apex of the imaging display. If the aortic valve (AV) and left ventricular outflow tract (LVOT) are visible (five-chamber view), then retroflexion of the probe and

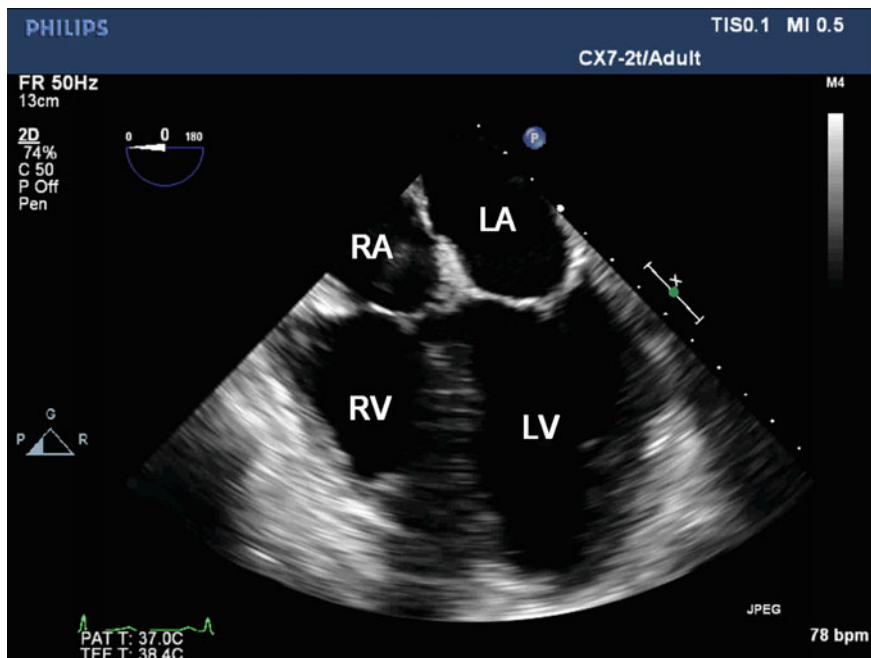


Fig. 2.1 ME four-chamber view. RA right atrium; RV right ventricle; LA left atrium; LV left ventricle

adjustment of the multiplane angle to 10° may be necessary to obtain the ME four-chamber view. Structures that should be visible in this view include the right atrium (RA), interatrial septum, left atrium (LA), right ventricle (RV), interventricular septum, left ventricle (LV), tricuspid valve (TV), and mitral valve (MV). The image depth should be adjusted so that the apex of the LV is visible as well.

The ME four-chamber view is often a readily identified and very useful view to acquire. It provides significant amounts of information, typically without any manipulation of the multiplane. Returning to this zero degree view is recommended if the echocardiographer becomes disoriented during their TEE evaluation. The ME four-chamber view allows evaluation of chamber sizes, function, valvular function, and regional wall motion of the septal and lateral walls of the LV (Fig. 2.1; Video 2.1). Two-dimensional evaluation allows inspection of LV and RV size and systolic function, evidence of wall motion abnormalities (WMA), tricuspid and mitral valve anatomy and motion, chamber sizes of RA, LA, LV and RV, and motion of the interatrial and interventricular septums. Color flow Doppler is utilized to interrogate the mitral and tricuspid valves for stenosis and regurgitation. Spectral Doppler is often utilized to measure mitral valve inflow in the evaluation of diastology and mitral stenosis.

ME Two-Chamber View

To obtain the ME two-chamber view, the multiplane angle is rotated to 80–100° until the right-sided cardiac structures are no longer visible. The probe is turned to the left and right until the LV apex is visualized in the far field. Structures that are visible in the ME two-chamber view are the left atrium, mitral valve, left ventricle, left atrial appendage (LAA), and left upper pulmonary vein (Fig. 2.2; Video 2.2). A short axis view of the coronary sinus can also be appreciated in this view. 2D evaluation focuses on regional wall motion of the anterior and inferior walls of the LV, mitral valve motion, and thrombus in the LV apex or left atrial appendage. Color flow Doppler of the MV and LAA are helpful in evaluating for regurgitation and thrombus formation respectively. Spectral Doppler can be helpful in evaluating mitral inflow and thrombus formation in the MV and LAA, respectively.

ME Long Axis (LAX) View

From the ME two-chamber view, the multiplane angle is advanced to approximately 120° when the LVOT is seen to obtain the ME LAX view. All patients are

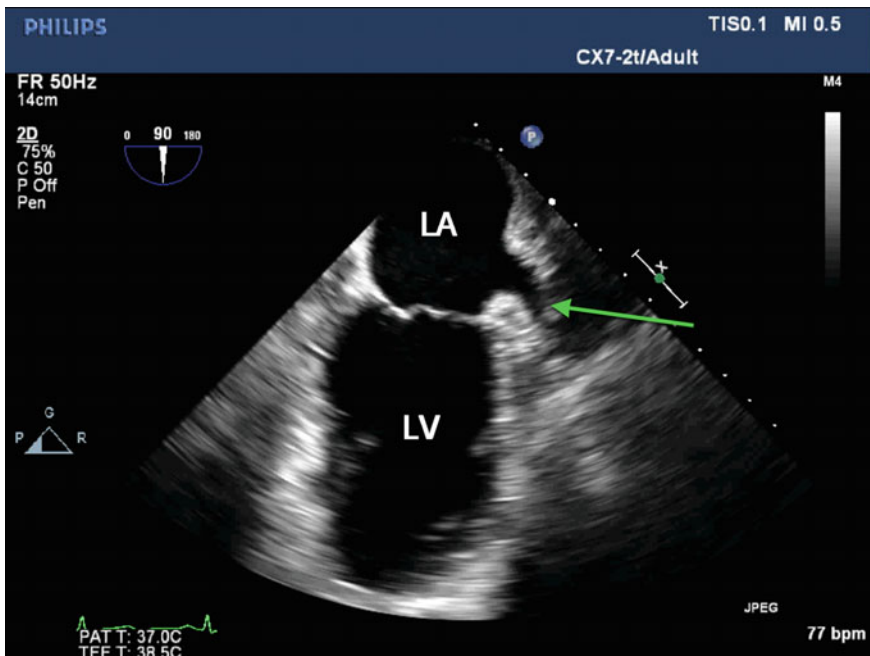


Fig. 2.2 ME two-chamber view with *green arrow* indicating the left atrial appendage. *LA* left atrium; *LV* left ventricle

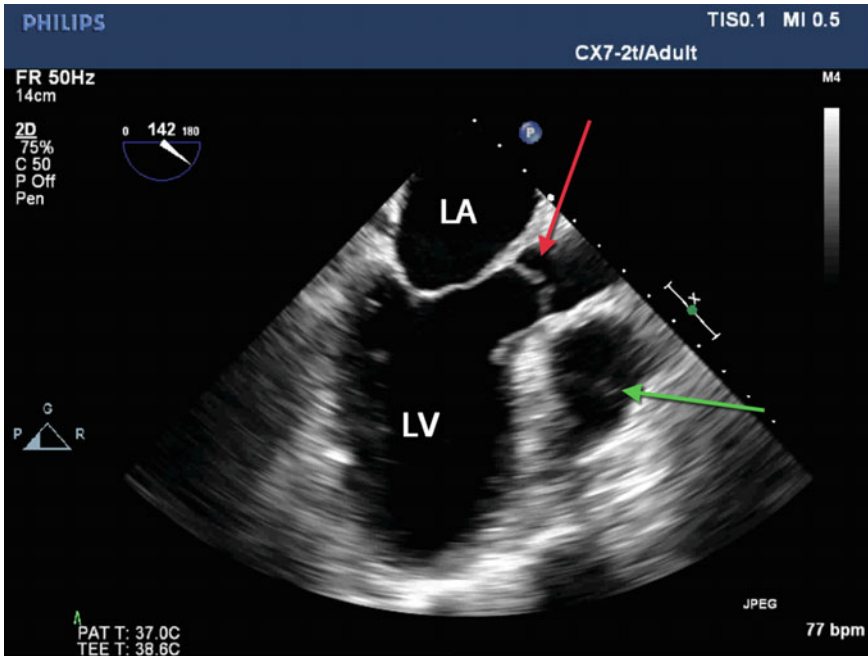


Fig. 2.3 ME LAX view with a *red arrow* indicating the aortic valve and a *green arrow* indicating the right ventricular outflow tract. *LA* left atrium; *LV* left ventricle

obviously different and therefore the multiplane degree is simply an estimate; this view may be developed in some patients as far out as 160°. The left atrium, mitral valve, left ventricle, LVOT, and aortic valve (AV) should be visible in this view (Fig. 2.3; Video 2.3). This view is similar to the ME AV LAX (see “Additional Views” below). However, rather than focusing on the AV, the LV inflow and outflow tract as well as the entirety of the LV cavity can be seen in this view. 2D assessments that can be made in the ME LAX view include chamber sizes, regional wall motion of the anteroseptal and inferolateral walls of the LV, and mitral valve and aortic valve anatomy and motion. Color flow Doppler interrogation of the MV and AV and spectral Doppler interrogation of the mitral valve is possible as well. The AV is often positioned perpendicular to the probe in this view and is therefore not conducive to spectral Doppler interrogation.

ME AV Short Axis (SAX) View

In TEE, when rotating the multiplane by 90°, the object in the center of the image will be rotated from a long axis to a short axis orientation and vice versa. From the ME LAX view, centering the AV by slowly withdrawing the probe and then

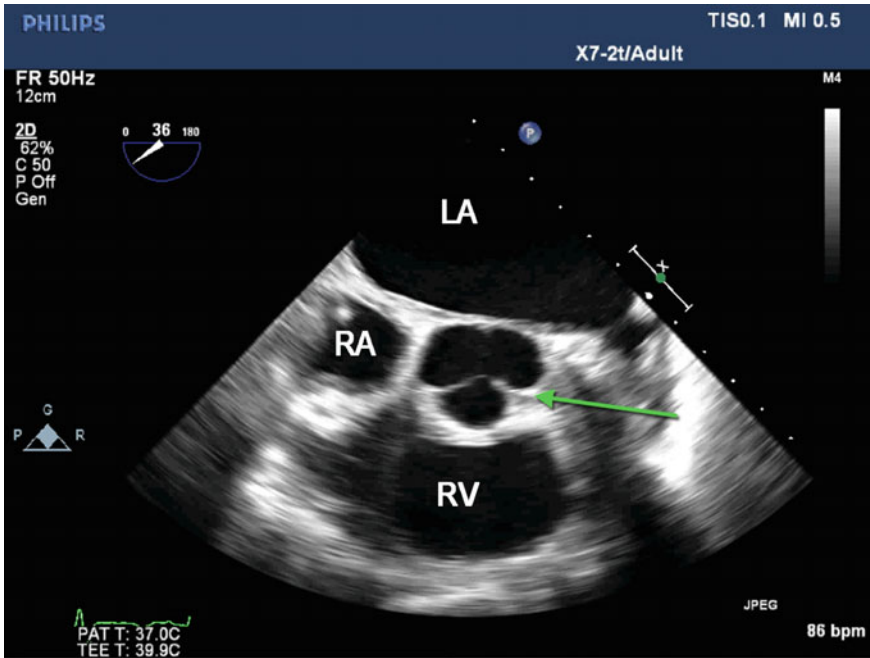


Fig. 2.4 ME AV SAX view with a *green arrow* indicating the aortic valve in short axis. *LA* left atrium; *RA* right atrium; *AV* aortic valve; *RV* right ventricle

rotating the multiplane back to 30° represents a 90° change. This will develop the ME AV SAX view with the cusps of the AV clearly seen (Fig. 2.4; Video 2.4). Two-dimensional assessment includes the general morphology of the AV (tricuspid versus bicuspid) as well as calcifications and mobility of the aortic leaflets. Color flow Doppler allows for interrogation of aortic regurgitation. Again the perpendicular orientation of the AV precludes spectral Doppler interrogation. Lastly, the interatrial septum can be identified proximal to the AV and can be evaluated for an atrial septal defect (ASD) or a patent foramen ovale (PFO).

ME Right Ventricular (RV) Inflow–Outflow View

The far field of the ME AV SAX view demonstrates the right ventricle (anterior to the aortic valve). Often the RA and part of the tricuspid valve may be visualized. Maintaining the RA and RV in view and increasing the multiplane to $60\text{--}90^\circ$ will bring the right ventricular outflow tract (RVOT) and pulmonic valve into view, constituting the ME right ventricular inflow–outflow view (Fig. 2.5; Video 2.5). While

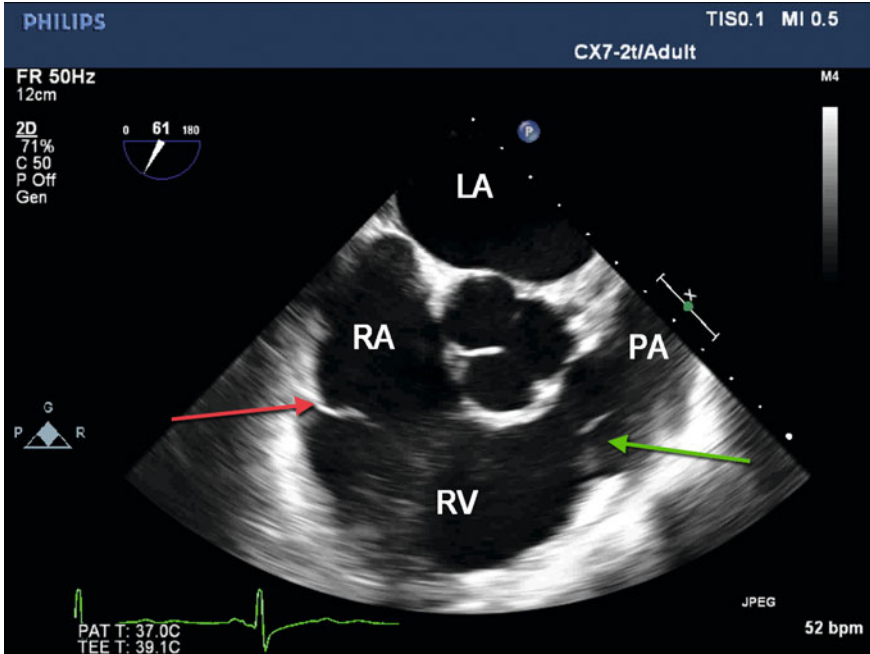


Fig. 2.5 ME RV inflow–outflow view with the *red arrow* indicating the tricuspid valve and the *green arrow* indicating the pulmonic valve. *LA* left atrium; *RA* right atrium; *RV* right ventricle; *PA* pulmonary artery

some of the AV may still be in view, the focus of this view is the RA, tricuspid valve, RV, RVOT, pulmonic valve, and the proximal pulmonary artery. The “wrapping around” nature of the right heart is demonstrated by seeing the RA, RV, and PA come around anteriorly to the AV. Two-dimensional assessment includes RV size and function, TV and PV anatomy and motion, and the position of the interatrial septum (the septum will bow away from the chamber with higher pressure). Color flow Doppler assessment focuses on the TV and PV for regurgitation and stenosis as well as the interatrial septum for a PFO or an ASD. Spectral Doppler interrogation of the TV may prove helpful in estimating PA pressure (see Chaps. 3 and 8).

ME Bicaval View

The ME bicaval view is obtained by rotating the multiplane angle to 90–110° and physically turning the probe clockwise. As a midesophageal view, the left atrium remains closest to the probe (apex of the imaging window), however, turning the

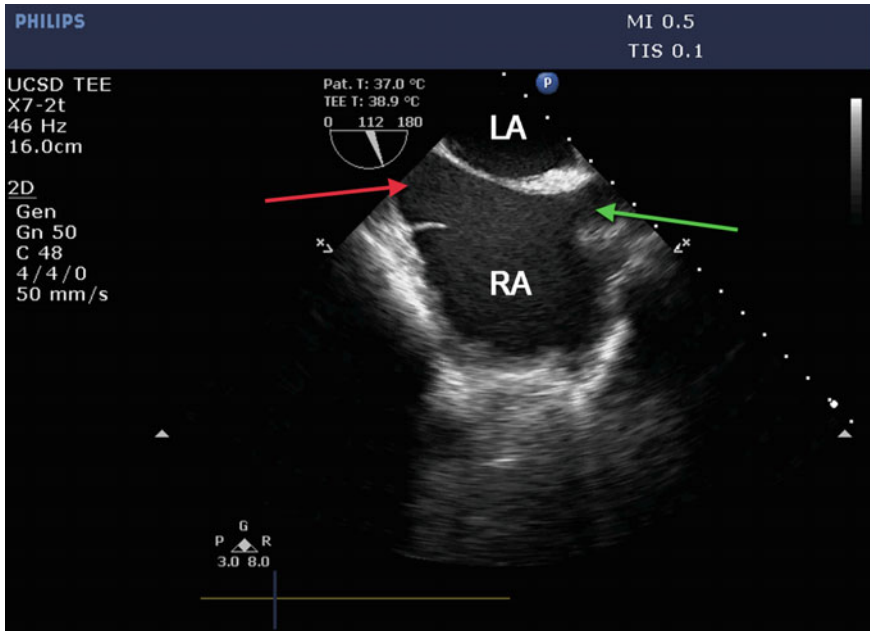


Fig. 2.6 ME bicaval view with the *red* arrow indicating the inferior vena cava and the *green* arrow indicating the superior vena cava. *LA* left atrium; *RA* right atrium

probe clockwise moves the interatrial septum into the center of the image and the right atrium into the far field. The 90° orientation places the superior vena cava (SVC) on the right and the inferior vena cava (IVC) on the left of the RA (Fig. 2.6; Video 2.6). Two-dimensional assessment focuses on atrial size, interatrial septum competency and direction (the septum bows away from the chamber with higher pressure) and anatomical variants (see Chap. 12). Additionally, the ME bicaval view can aid in the placement of central venous catheters by observing the initial wire placement in the RA. Color flow Doppler interrogation aids in detection of an ASD or a PFO. An agitated saline study may also be utilized in this view to demonstrate a PFO. Spectral Doppler is not typically employed in a ME bicaval view.

ME Ascending Aortic SAX and LAX Views

Returning the multiplane to zero degrees (roughly the ME Four-Chamber view) and then withdrawing the probe allows the development of the ME ascending aortic SAX view which provides an image of the proximal ascending aorta and bifurcation of the main pulmonary artery is visualized. Slight anteflexion of the probe and rotation of the multiplane angle from 0 to 45° may be necessary to optimize the

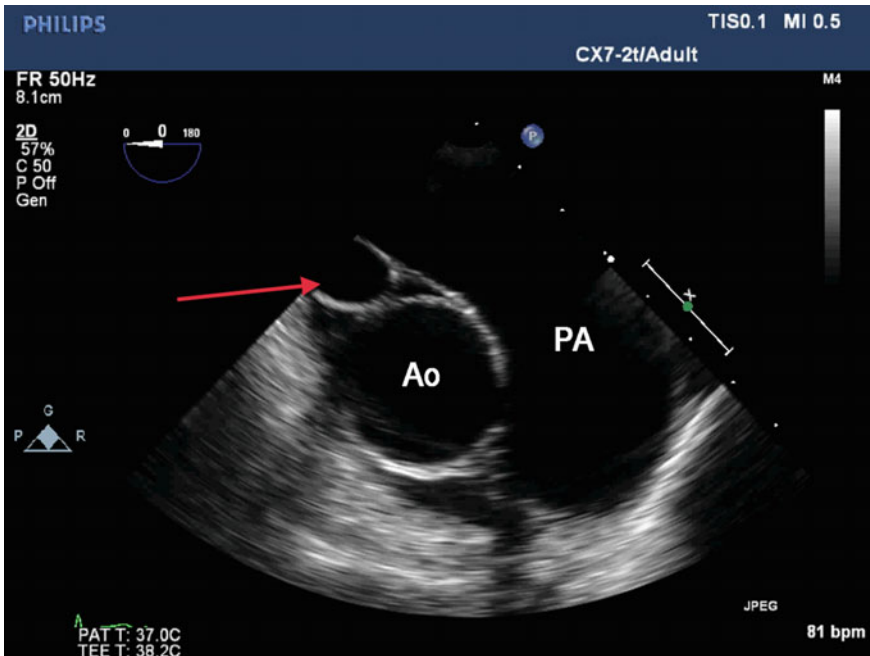


Fig. 2.7 ME Ascending Aortic SAX view with a *red arrow* indicating the superior vena cava. *Ao* ascending aorta; *PA* pulmonary artery

image (Fig. 2.7; Video 2.7). The right pulmonary artery in this view lies immediately posterior to the proximal ascending aorta in a long axis orientation. The left pulmonary artery is typically not visualized due to the interposed air-filled left main bronchus. Two-dimensional assessment is utilized for identification of aneurysms, plaque, and dissections of the ascending aorta as well as for identifying thrombus in the main or right pulmonary artery. Color flow Doppler may be helpful in the setting of aortic dissection (see Chap. 10). Spectral Doppler is often not employed in this view during a basic examination.

To obtain the ME ascending aortic LAX view, the aorta is centered in the image and the multiplane angle is rotated to approximately 90° until the right pulmonary artery is seen in the short axis while the ascending aorta is seen in the long axis (Fig. 2.8; Video 2.8). Similarly, two-dimensional assessment is utilized for identifications of aneurysms, plaque, and dissections of the ascending aorta as well as for identifying thrombus in the right pulmonary artery. Color flow Doppler may be helpful in the setting of aortic dissection while spectral Doppler is often not employed in this view during a basic examination.

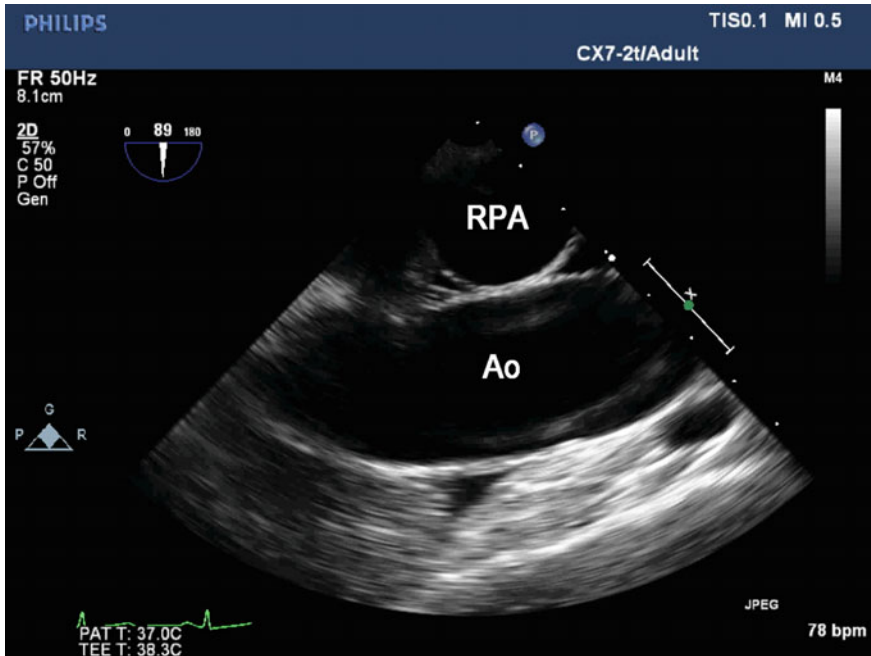


Fig. 2.8 ME Ascending Aortic LAX view. *Ao* ascending aorta; *RPA* right pulmonary artery

Transgastric (TG) Midpapillary SAX View

In order to obtain the TG midpapillary SAX view, the probe is returned to the ME four-chamber view at 0° and then advanced into the stomach. When advancing, the image on the screen will often disappear when entering into the stomach as the probe is no longer adjacent to tissue (free floating in the stomach). While keeping the multiplane angle at 0° , the probe is gradually anteflexed while the depth is adjusted until the posteromedial and anterolateral papillary muscles are visualized. A proper TG midpapillary SAX view can be difficult to obtain since proper depth and anteflexion are required to obtain a true short axis cross section of the LV. Since the posteromedial papillary muscle is closest to the TEE probe, the depth of the probe should first be adjusted until it is visualized. If the MV chordae tendinae are visible, then the probe is too high and should be advanced. Once the depth is appropriate, small adjustments to the degree of anteflexion should be made until the anterolateral papillary muscle comes into view (Fig. 2.9; Video 2.9).

The TG midpapillary SAX view is commonly used during intraoperative monitoring and may frequently be the first view assessed during hemodynamic instability. Two-dimensional assessment includes volume status, LV systolic function, and regional wall motion. The TG midpapillary SAX view is especially useful because all three coronary arteries that perfuse the different segments of the

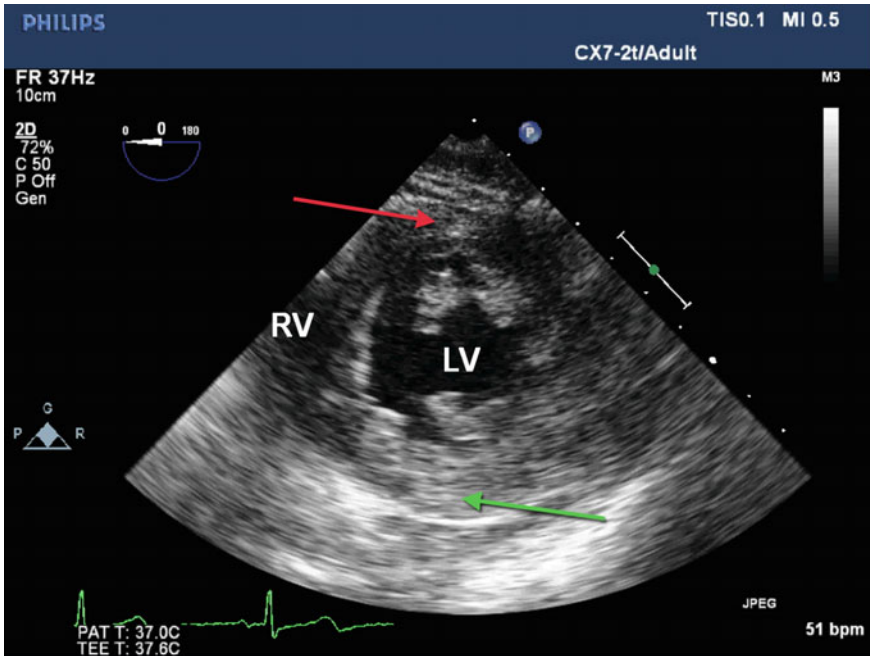


Fig. 2.9 TG midpapillary SAX view. The *green arrow* indicates the anterior wall of the left ventricle (LV), while the *red arrow* indicates the inferior wall of the LV. RV right ventricle

myocardium can be assessed simultaneously. However, it is important to remember that this view only provides a single cross-sectional view of the LV and inadequate coronary perfusion to the base and apex of the LV will not be detected (see Chap. 4—Left Ventricular Systolic Function). Color flow Doppler and spectral Doppler are typically not employed in this view.

Descending Aortic SAX and LAX Views

To obtain the descending aortic SAX view, the probe is returned to the ME four-chamber view at 0° and turned counterclockwise until the circular-shaped descending aorta appears in the apex of the image display. To enlarge and optimize the image, the image depth is decreased and the focus moved to the near field (Fig. 2.10; Video 2.10). The probe can then be withdrawn and advanced, imaging the entire descending aorta in short axis. The aortic arch is reached when the aorta appears elongated at the apex of image display (see “Additional Views” below). At any point during the evaluation of the SAX of the descending aorta, the multiplane

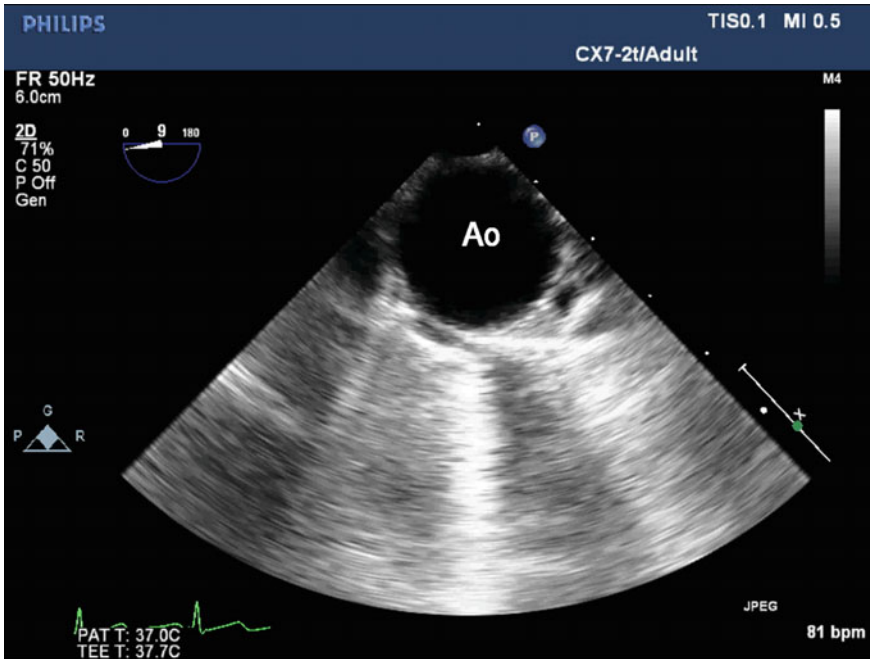


Fig. 2.10 Descending aortic SAX view. *Ao* descending aorta

angle can be rotated to approximately 90° to obtain the descending aortic LAX view (Fig. 2.11; Video 2.11). Two-dimensional assessment in these views includes aortic diameter, degree of atherosclerosis, and presence of a dissection. Color flow Doppler may be helpful in a dissection (see Chap. 10) while spectral Doppler of a descending aortic LAX view may be helpful in assessing aortic valve regurgitation (see Chap. 7). In addition, the presence of a left pleural effusion (anterior to the descending aorta) can be identified in the descending aortic SAX view (Fig. 2.12; Video 2.12).

Additional Views

When added to the basic PTE exam, the following 9 additional views described below make up a comprehensive TEE examination and are included for completeness.

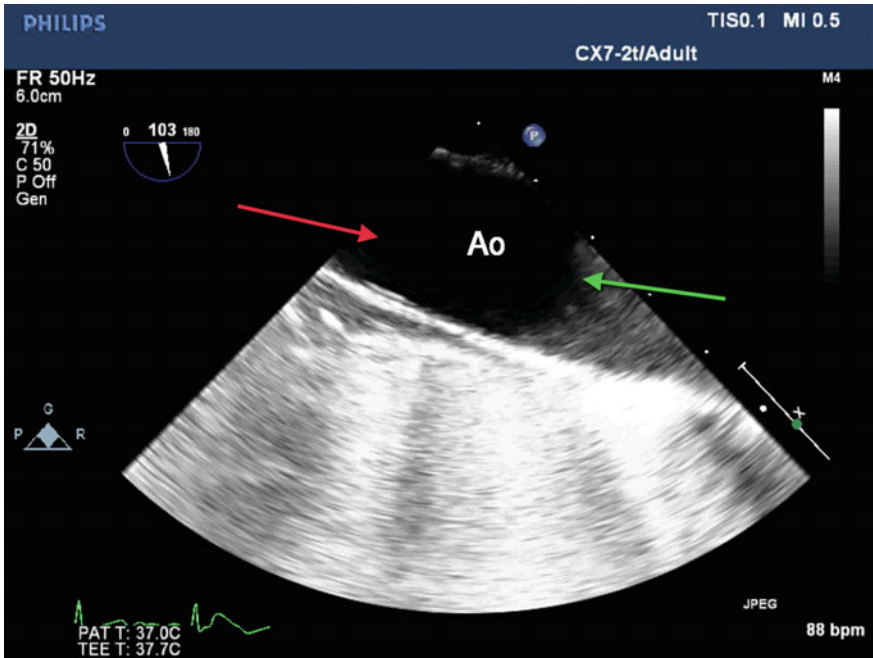


Fig. 2.11 Descending aortic LAX view. The *green arrow* indicates proximal while the *red arrow* indicates distal aortic segments. *Ao* descending aorta

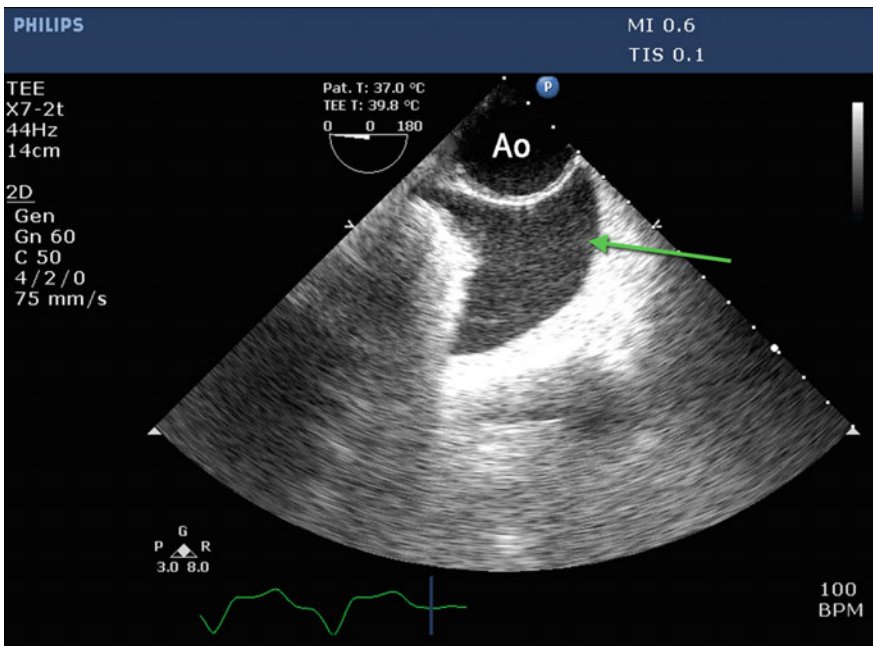


Fig. 2.12 Descending aortic SAX view with a left pleural effusion (*green arrow*). *Ao* descending aorta

ME Mitral Commissural View

From the ME four-chamber view with the mitral valve positioned in the center of the image, the multiplane angle is rotated to approximately 60° to obtain the ME mitral commissural view. As the coaptation line of the MV is curved (“smile shaped”), the ME mitral commissural view will image through the coaptation line twice, giving the appearance of a posterior leaflet on the left and right with a central anterior leaflet portion. This view is helpful in evaluating the location of mitral valve pathology given that multiple scallops (P3-A2-P1) of the mitral valve can be seen (see Chap. 6). Other structures that can be seen include papillary muscles, chordae tendinae, and the coronary sinus (Fig. 2.13; Video 2.13). This view generally involves a 2D assessment of MV leaflet motion as well CFD for localizing regurgitation.

ME AV LAX View

To obtain the ME AV LAX view, the multiplane angle is rotated to $120\text{--}140^\circ$ followed by a slight clockwise turn of the probe. In this view, the LVOT, aortic

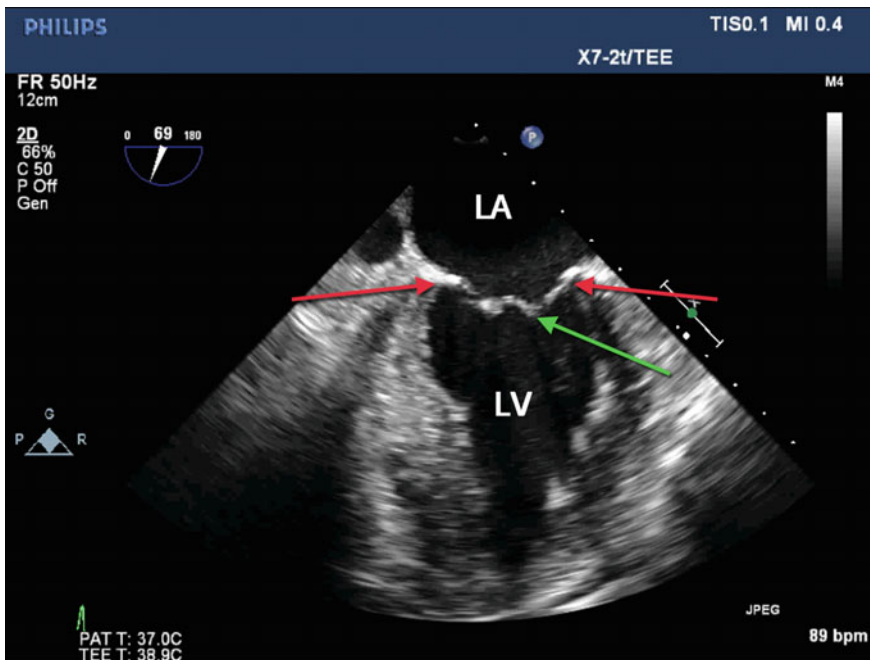


Fig. 2.13 ME mitral commissural view. The *red arrows* indicate posterior mitral valve leaflet, while the *green arrow* indicates anterior mitral valve leaflet. *LA* left atrium; *LV* left ventricle

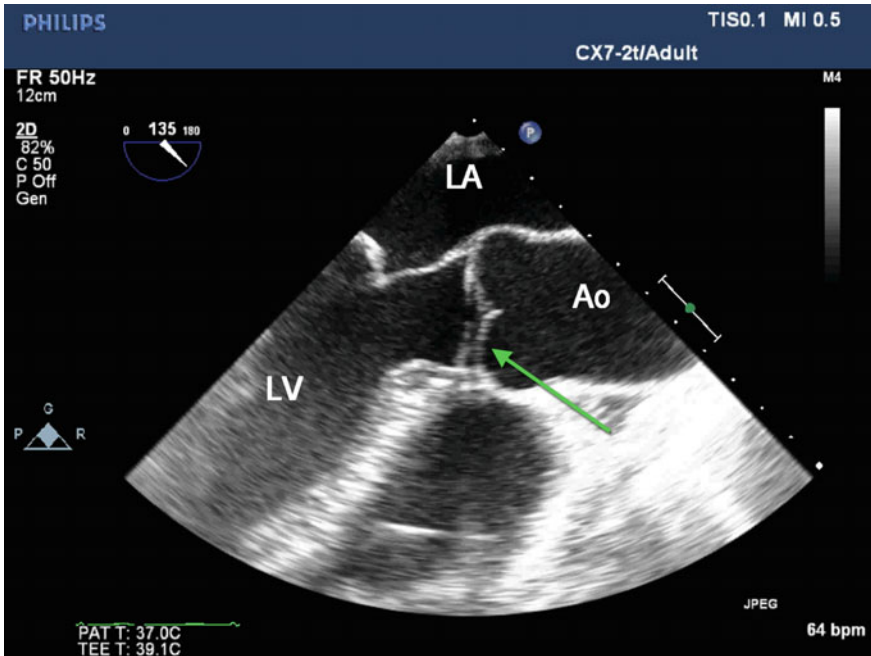


Fig. 2.14 ME AV LAX view with the aortic valve indicated by the *green arrow*. LA left atrium; LV left ventricle; Ao proximal ascending aorta

valve, sinus of Valsalva, sinotubular junction, and proximal ascending aorta should be visualized well (Fig. 2.14; Video 2.14). Compared to the ME LAX view, the ME AV LAX view allows better evaluation of aortic valve function both structurally and with color flow Doppler, measurements of structures from the annulus to the proximal ascending aorta, as well as appreciation of atherosclerotic plaques and dissections.

TG Basal SAX View

From the ME four-chamber view, the probe is advanced into the stomach and then anteflexed to obtain the TG basal SAX view of the LV. If the papillary muscles of the LV (TG midpapillary SAX view) are seen, then the probe is slowly withdrawn until the mitral valve or “fish mouth” comes into view (Fig. 2.15; Video 2.15). This view can be used to evaluate calcifications of the mitral valve and estimate mitral

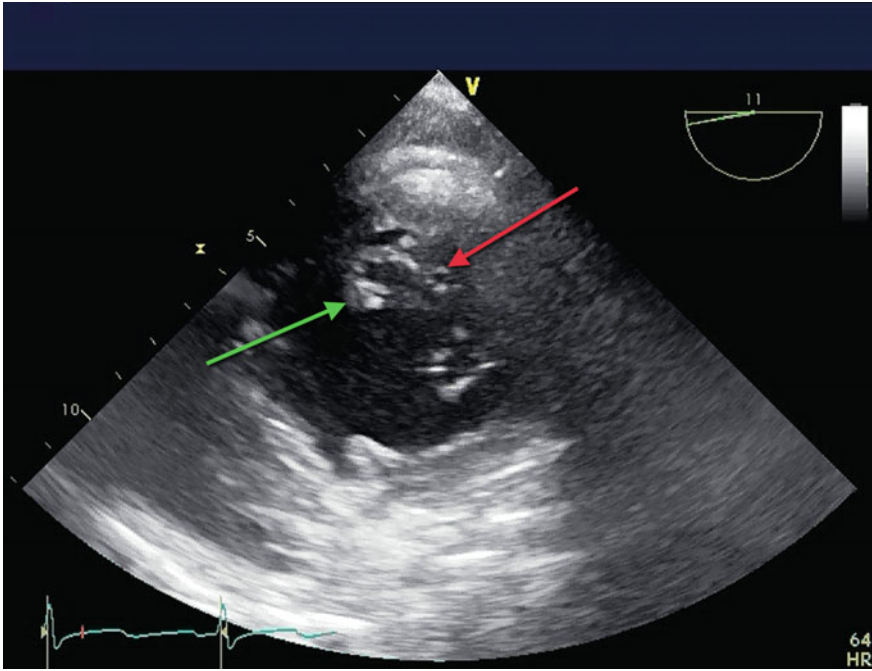


Fig. 2.15 TG basal SAX view with the *green arrow* indicating edge of the anterior mitral valve leaflet and the *red arrow* indicating the posterior mitral valve leaflet

valve area using planimetry for 2D assessment and localizing regurgitation using CFD (see Chap. 6).

TG Two-Chamber View

From the TG midpapillary SAX view, the multiplane angle is rotated to approximately $90\text{--}110^\circ$ to obtain the TG two-chamber view. This view provides a lengthwise view of the LV for evaluation of regional wall motion abnormalities. The posterior wall is located at the apex of imaging sector while the anterior wall is located at the bottom, allowing visualization of the base, mid and apical segments of both walls (Fig. 2.16; Video 2.16).

TG LAX View

From the TG two-chamber view, the multiplane angle is rotated further to approximately $120\text{--}140^\circ$ until the LVOT and aortic valve comes into view at the 4

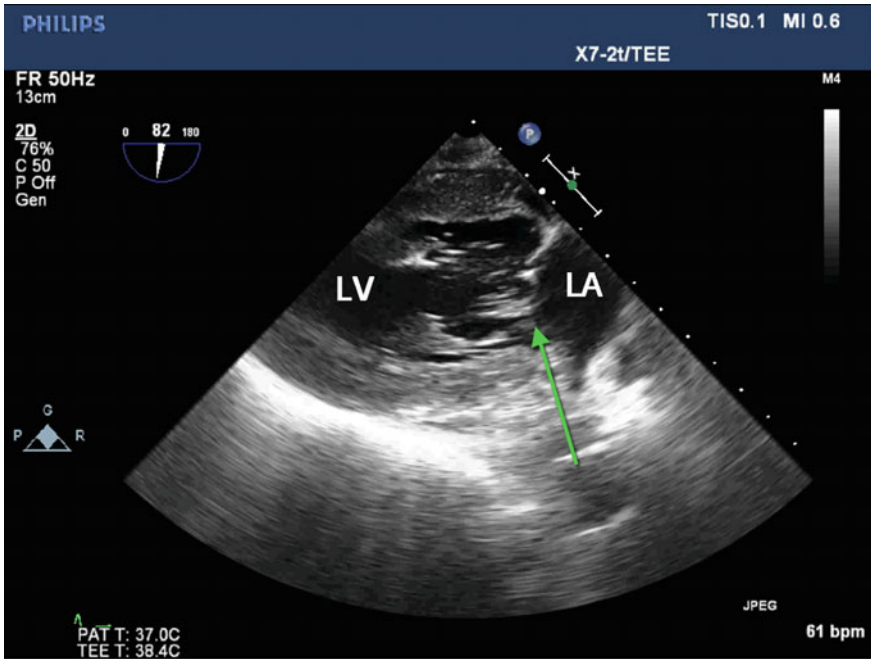


Fig. 2.16 TG two-chamber view with the *green arrow* indicating the mitral valve. Note the papillary muscles and chordae attached to the mitral valve. LA left atrium; LV left ventricle

o'clock position. In addition to the deep TG LAX view (see below), this view is useful for spectral Doppler interrogation of the LVOT and aortic valve (Fig. 2.17; Video 2.17).

Deep TG LAX View

With the multiplane angle at 0° , the probe is advanced deep into the stomach, anteflexed, left-flexed, and then slowly withdrawn until the deep TG LAX view is imaged (Fig. 2.18; Video 2.18). In this view, the LVOT and aortic valve are aligned parallel with the ultrasound beam. This parallel orientation allows for optimal spectral Doppler interrogation. Slow turning of the probe to the left or right may be needed for proper alignment. Two-dimensional interrogation focuses on the LV apex (at the apex of the image sector), the mitral and aortic valves, as well as the ventricular walls. Color flow Doppler interrogation focuses on the MV and AV.

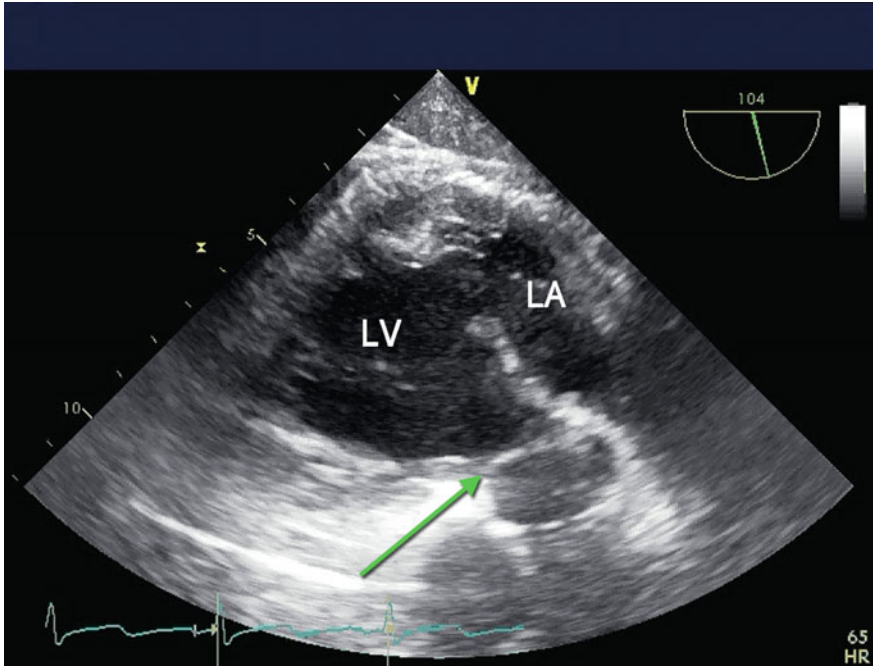


Fig. 2.17 TG LAX view with the *green arrow* indicating the aortic valve. *LA* left atrium; *LV* left ventricle

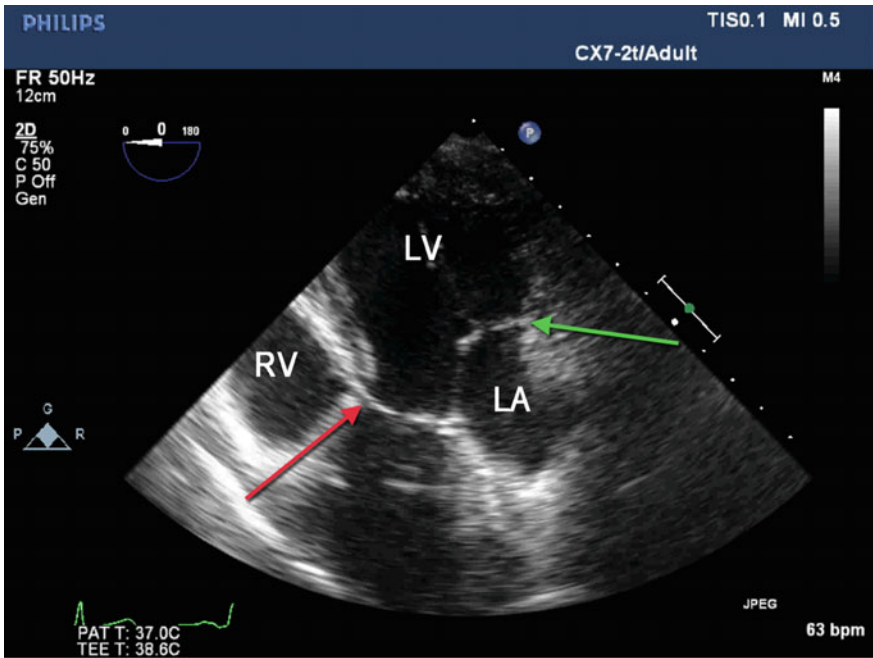


Fig. 2.18 Deep TG LAX view. The *green arrow* denotes the mitral valve, while the *red arrow* indicates the aortic valve. *LA* left atrium; *LV* left ventricle; *RV* right ventricle

Spectral Doppler interrogation includes pulsed wave Doppler evaluation of the LVOT as well as continuous wave Doppler evaluation of the AV. This information will be helpful in detecting aortic valve gradients, aortic valve area, and cardiac output (see Chap. 3).

TG RV Inflow View

Starting from the TG midpapillary SAX view, the probe is turned slightly clockwise until the RV is in the center of the image sector and the multiplane angle subsequently advanced to 90–110° until the TG RV inflow view is seen (Fig. 2.19; Video 2.19). This view can be used to evaluate the function and thickness of the RV free wall as well as tricuspid valve annular size and leaflet motion. The perpendicular orientation of the TV precludes spectral Doppler analysis of the TV.

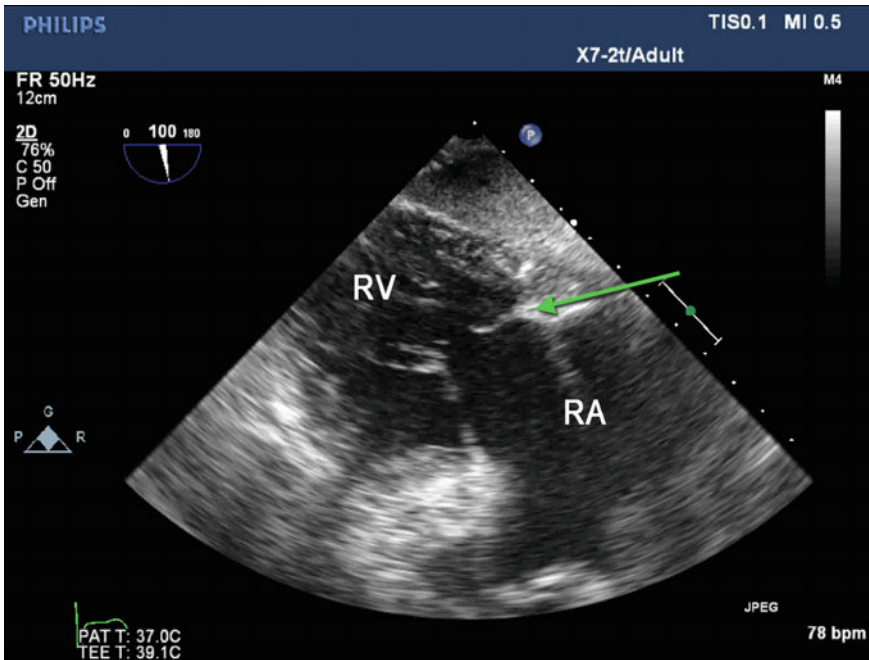


Fig. 2.19 TG RV inflow view. The *green arrow* indicates the tricuspid valve. RA right atrium; RV right ventricle

Upper Esophageal (UE) Aortic Arch LAX and SAX Views

From the ME descending aortic SAX view (Fig. 2.10; Video 2.10), the probe is slowly withdrawn and turned clockwise (to maintain the aorta in the center of the imaging sector) until the aorta begins to elongate. Once the aorta has elongated into an oval shape, the UE aortic arch LAX view has been developed. The image depth may need to be decreased to optimize visualization (Fig. 2.20; Video 2.20). This view can be used to evaluate atherosclerotic plaques in the aortic arch as well as aneurysms and dissections. To obtain the UE aortic arch SAX view, the mutiplane angle is rotated to 70–90°. This places the aortic arch in a SAX view as well as brings the pulmonic valve and main pulmonary artery into view on the left-hand side of the screen. Because of the parallel alignment of the pulmonic valve and main pulmonary artery with the spectral Doppler line, Doppler interrogation of the pulmonary valve can be performed in this view. Other structures that can also be visualized include the left subclavian artery and the brachiocephalic vein (Fig. 2.21; Video 2.21).

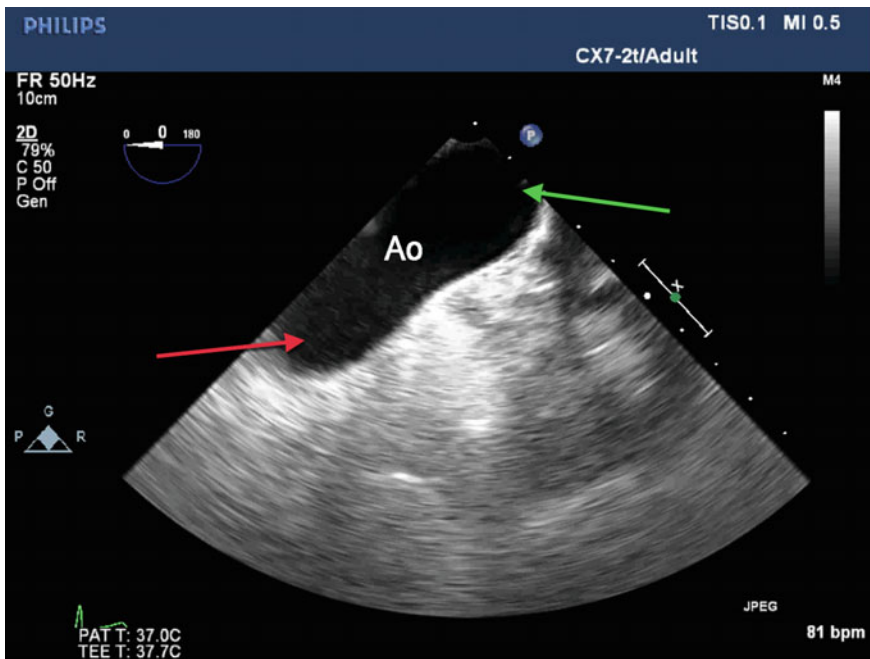


Fig. 2.20 UE aortic arch LAX view with the *green arrow* denoting distal aortic arch (Ao) and the *red arrow* denoting proximal aortic arch

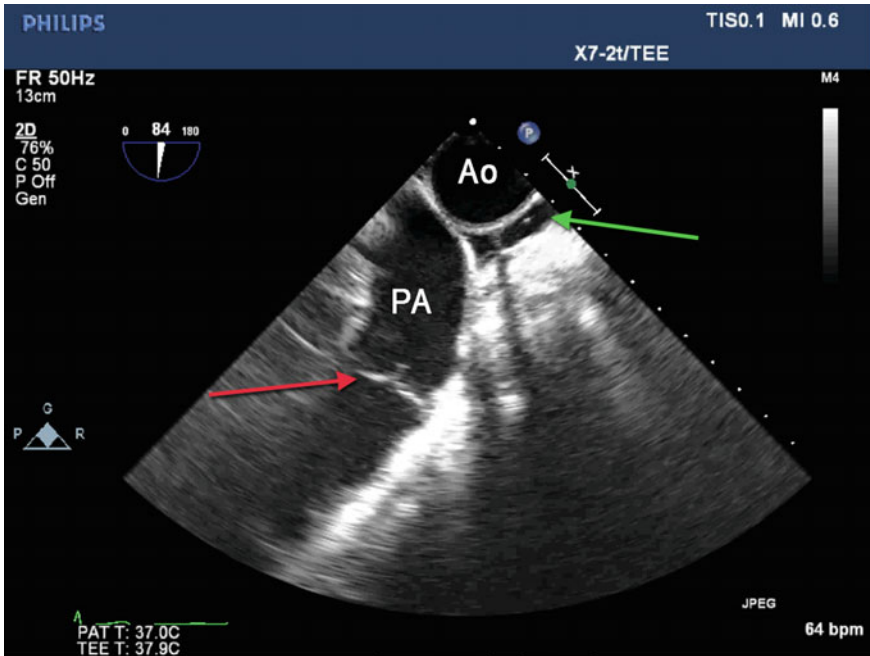

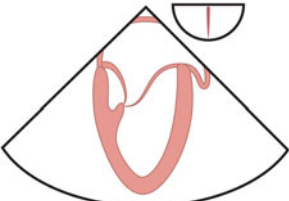

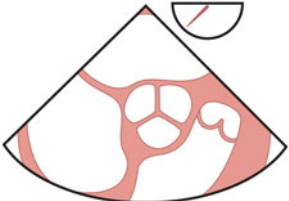


Fig. 2.21 UE aortic arch SAX view. The *red arrow* indicates the pulmonic valve while the *green arrow* indicates the brachiocephalic vein. PA main pulmonary artery; Ao aortic arch

Conclusion


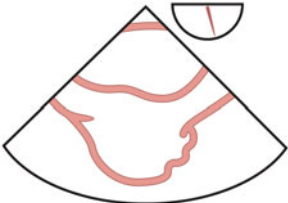
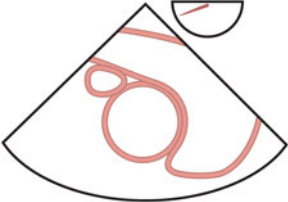
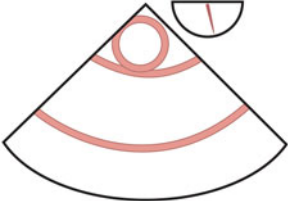
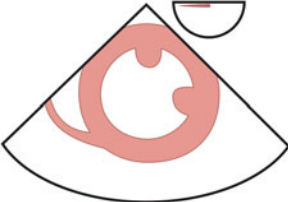
The individual views of the basic and comprehensive PTE exam are discussed above. Again the performed order of the views is not essential. Developing a systematic approach to the order of the views as well as modalities of interrogation is important in order to establish a consistent approach to perioperative echocardiography. Tables 2.1 and 2.2 outline a suggested order of views for the basic and comprehensive PTE exam, respectively.

Table 2.1 Basic perioperative transesophageal echocardiography exam

Image order	Image name	Image depiction	2D > CFD > Spectral
1	ME four chamber		<p><i>2D</i></p> <ul style="list-style-type: none"> Chamber sizes: RA/LA/RV/LV Systolic function: RV/LV Ischemia detection: RV/LV Valvular anatomy/motion: TV/MV <p><i>CFD</i></p> <ul style="list-style-type: none"> Valvular pathology: TV/MV Interatrial septum: PFO/ASD <p><i>Spectral</i></p> <ul style="list-style-type: none"> Inflow velocities: TV/MV Estimating PASP: TV
2	ME two chamber		<p><i>2D</i></p> <ul style="list-style-type: none"> Chamber sizes: LA/LV Systolic function: LV Ischemia detection: Anterior/Inferior LV Valvular anatomy/motion: MV <p><i>CFD</i></p> <ul style="list-style-type: none"> Valvular pathology: MV Thrombus: LAA <p><i>Spectral</i></p> <ul style="list-style-type: none"> Inflow velocities: MV; LUPV Thrombus: LAA
3	ME long axis		<p><i>2D</i></p> <ul style="list-style-type: none"> Chamber sizes: LA/LV/LVOT/AV/Ao Systolic function: LV Ischemia detection: AntSept/InfLat LV Valvular anatomy/motion: MV/AV <p><i>CFD</i></p> <ul style="list-style-type: none"> Valvular pathology: MV/AV <p><i>Spectral</i></p> <ul style="list-style-type: none"> Inflow velocities: MV
4	ME AV short axis		<p><i>2D</i></p> <ul style="list-style-type: none"> Chamber sizes: LA Valvular anatomy/motion: AV <p><i>CFD</i></p> <ul style="list-style-type: none"> Valvular pathology: AV Interatrial septum: ASD/PFO <p><i>Spectral</i></p> <ul style="list-style-type: none"> Not typically utilized

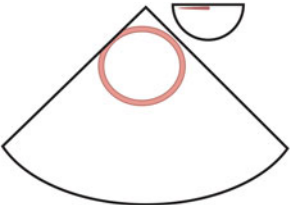
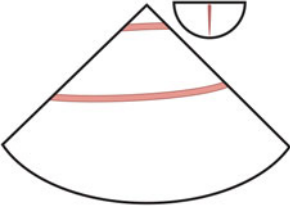
(continued)

Table 2.1 (continued)

Image order	Image name	Image depiction	2D > CFD > Spectral
5	ME RV inflow–outflow		<p>2D</p> <ul style="list-style-type: none"> Chamber sizes: RA/RV/PA/LA Systolic function: RV Ischemia detection: RV Valvular anatomy/motion: TV/PV <p>CFD</p> <ul style="list-style-type: none"> Valvular pathology: TV/PV <p>Spectral</p> <ul style="list-style-type: none"> Estimating PASP: TV
6	ME bicaval		<p>2D</p> <ul style="list-style-type: none"> Chamber Sizes: LA/RA Interatrial Septum: Competency <p>CFD</p> <ul style="list-style-type: none"> Interatrial Septum: ASD/PFO <p>Spectral</p> <ul style="list-style-type: none"> Not typically utilized
7	ME ascending aortic SAX		<p>2D</p> <ul style="list-style-type: none"> Vessel sizes: Ao/PA/SVC Dissection/Plaque: Ao Thrombus: PA/RPA <p>CFD</p> <ul style="list-style-type: none"> Dissection: Ao <p>Spectral</p> <ul style="list-style-type: none"> Not typically utilized
8	ME ascending aortic LAX		<p>2D</p> <ul style="list-style-type: none"> Vessel sizes: Ao/RPA Dissection/Plaque: Ao Thrombus: RPA <p>CFD</p> <ul style="list-style-type: none"> Dissection: Ao <p>Spectral</p> <ul style="list-style-type: none"> Not typically utilized
9	TG midpapillary SAX		<p>2D</p> <ul style="list-style-type: none"> Chamber size: LV Ischemia detection: LV (3 Coronaries)/RV <p>CFD</p> <ul style="list-style-type: none"> Not typically utilized <p>Spectral</p> <ul style="list-style-type: none"> Not typically utilized

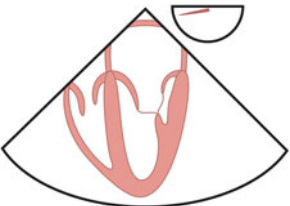
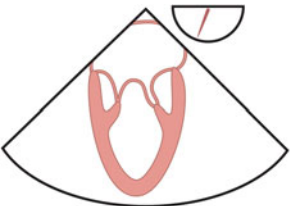
(continued)

Table 2.1 (continued)

Image order	Image name	Image depiction	2D > CFD > Spectral
10	Descending aortic SAX		<p>2D</p> <ul style="list-style-type: none"> • Vessel size: Ao • Dissection/Plaque: Ao <p>CFD</p> <ul style="list-style-type: none"> • Dissection: Ao <p>Spectral</p> <ul style="list-style-type: none"> • Not typically utilized
11	Descending aortic LAX		<p>2D</p> <ul style="list-style-type: none"> • Vessel size: Ao • Dissection/Plaque: Ao <p>CFD</p> <ul style="list-style-type: none"> • Dissection: Ao <p>Spectral</p> <ul style="list-style-type: none"> • Not typically utilized

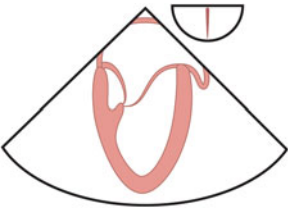
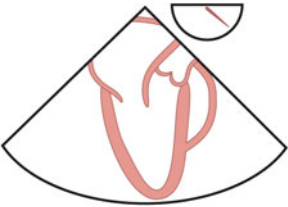
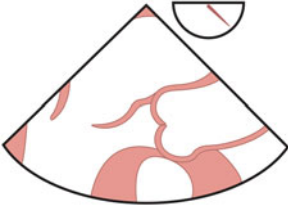
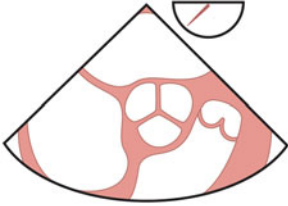
Abbreviations ME midesophageal; TG transgastric; LAX long axis; SAX short axis; 2D two dimensional; CFD color flow doppler; RA right atrium; LA left atrium; RV right ventricle; LV left ventricle; MV mitral valve; AV aortic valve; TV tricuspid valve; PV pulmonic valve; LVOT left ventricular outflow tract; PFO patent foramen ovale; ASD atrial septal defect; LAA left atrial appendage; LUPV left upper pulmonary vein; Ao aorta; PA pulmonary artery; RPA right pulmonary artery; AntSept anterior septal wall; InfLat inferolateral wall; SVC superior vena cava
 Adapted from Shanewise et al. [2]

Table 2.2 Comprehensive perioperative transesophageal echocardiography exam

Image order	Image name	Image depiction	2D > CFD > Spectral
1	ME four chamber		<p>2D</p> <ul style="list-style-type: none"> • Chamber sizes: RA/LA/RV/LV • Systolic function: RV/LV • Ischemia detection: RV/LV • Valvular anatomy/motion: TV/MV <p>CFD</p> <ul style="list-style-type: none"> • Valvular pathology: TV/MV • Interatrial septum: PFO/ASD <p>Spectral</p> <ul style="list-style-type: none"> • Inflow velocities: TV/MV • Estimating PASP: TV
2	ME mitral commissural		<p>2D</p> <ul style="list-style-type: none"> • Chamber sizes: LA/LV • Valvular anatomy/motion: MV <p>CFD</p> <ul style="list-style-type: none"> • Valvular pathology: MV • Thrombus: LAA <p>Spectral</p> <ul style="list-style-type: none"> • Inflow velocities: MV • Thrombus: LAA


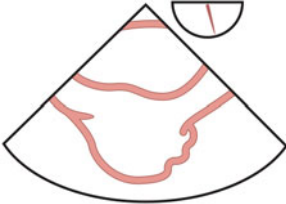
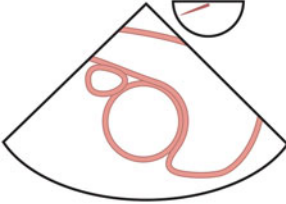
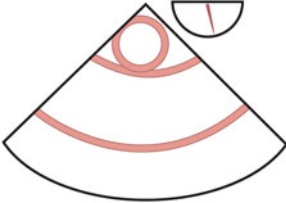
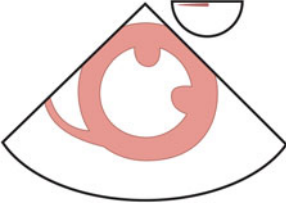
(continued)

Table 2.2 (continued)

Image order	Image name	Image depiction	2D > CFD > Spectral
3	ME two chamber		<p><i>2D</i></p> <ul style="list-style-type: none"> • Chamber sizes: LA/LV • Systolic function: LV • Ischemia detection: Anterior/Inferior LV • Valvular anatomy/motion: MV <p><i>CFD</i></p> <ul style="list-style-type: none"> • Valvular pathology: MV • Thrombus: LAA <p><i>Spectral</i></p> <ul style="list-style-type: none"> • Inflow velocities: MV; LUPV • Thrombus: LAA
4	ME long axis		<p><i>2D</i></p> <ul style="list-style-type: none"> • Chamber sizes: LA/LV/LVOT/AV/Ao • Systolic function: LV • Ischemia detection: AntSept/InfLat LV • Valvular anatomy/motion: MV/AV <p><i>CFD</i></p> <ul style="list-style-type: none"> • Valvular pathology: MV/AV <p><i>Spectral</i></p> <ul style="list-style-type: none"> • Inflow velocities: MV
5	ME AV LAX		<p><i>2D</i></p> <ul style="list-style-type: none"> • Chamber sizes: LVOT/AV Annulus/Ao • Valvular anatomy/motion: AV <p><i>CFD</i></p> <ul style="list-style-type: none"> • Valvular pathology: AV <p><i>Spectral</i></p> <ul style="list-style-type: none"> • Typically not utilized
6	ME AV short axis		<p><i>2D</i></p> <ul style="list-style-type: none"> • Chamber sizes: LA • Valvular anatomy/motion: AV <p><i>CFD</i></p> <ul style="list-style-type: none"> • Valvular pathology: AV • Interatrial septum: ASD/PFO <p><i>Spectral</i></p> <ul style="list-style-type: none"> • Not typically utilized

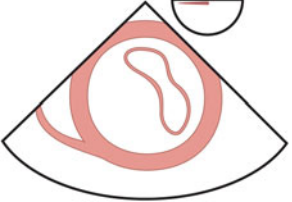

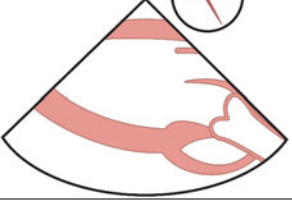
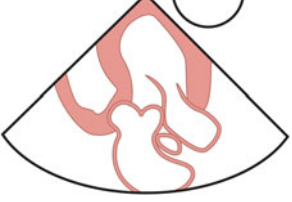
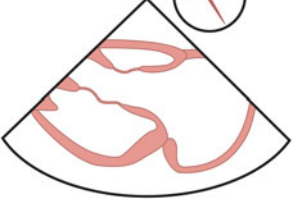
(continued)

Table 2.2 (continued)

Image order	Image name	Image depiction	2D > CFD > Spectral
7	ME RV inflow–outflow		<p>2D</p> <ul style="list-style-type: none"> Chamber sizes: RA/RV/PA/LA Systolic function: RV Ischemia detection: RV Valvular anatomy/motion: TV/PV <p>CFD</p> <ul style="list-style-type: none"> Valvular pathology: TV/PV <p>Spectral</p> <ul style="list-style-type: none"> Estimating PASP: TV
8	ME bicaval		<p>2D</p> <ul style="list-style-type: none"> Chamber sizes: LA/RA Interatrial septum: competency <p>CFD</p> <ul style="list-style-type: none"> Interatrial septum: ASD/PFO <p>Spectral</p> <ul style="list-style-type: none"> Not typically utilized
9	ME ascending aortic SAX		<p>2D</p> <ul style="list-style-type: none"> Vessel sizes: Ao/PA/SVC Dissection/Plaque: Ao Thrombus: PA/RPA <p>CFD</p> <ul style="list-style-type: none"> Dissection: Ao <p>Spectral</p> <ul style="list-style-type: none"> Not typically utilized
10	ME ascending aortic LAX		<p>2D</p> <ul style="list-style-type: none"> Vessel sizes: Ao/RPA Dissection/Plaque: Ao Thrombus: RPA <p>CFD</p> <ul style="list-style-type: none"> Dissection: Ao <p>Spectral</p> <ul style="list-style-type: none"> Not typically utilized
11	TG midpapillary SAX		<p>2D</p> <ul style="list-style-type: none"> Chamber size: LV Ischemia detection: LV (3 Coronaries)/RV <p>CFD</p> <ul style="list-style-type: none"> Not typically utilized <p>Spectral</p> <ul style="list-style-type: none"> Not typically utilized

(continued)

Table 2.2 (continued)

Image order	Image name	Image depiction	2D > CFD > Spectral
12	TG basal SAX		<p><i>2D</i></p> <ul style="list-style-type: none"> • Chamber size: LV • Ischemia detection: LV (3 Coronaries)/RV • Valvular anatomy/motion: MV <p><i>CFD</i></p> <ul style="list-style-type: none"> • Valvular pathology: MV <p><i>Spectral</i></p> <ul style="list-style-type: none"> • Not typically utilized
13	TG two chamber		<p><i>2D</i></p> <ul style="list-style-type: none"> • Chamber size: LV • Ischemia detection: Anterior/Inferior LV <p><i>CFD</i></p> <ul style="list-style-type: none"> • Not typically utilized <p><i>Spectral</i></p> <ul style="list-style-type: none"> • Not typically utilized
14	TG LAX		<p><i>2D</i></p> <ul style="list-style-type: none"> • Chamber size: LV <p><i>CFD</i></p> <ul style="list-style-type: none"> • Valvular pathology: AV <p><i>Spectral</i></p> <ul style="list-style-type: none"> • Outflow velocities: LVOT/AV
15	Deep TG LAX		<p><i>2D</i></p> <ul style="list-style-type: none"> • Chamber size: LV • Ischemia detection: Sept/Lat/Apex LV • Valvular anatomy and motion: MV/AV <p><i>CFD</i></p> <ul style="list-style-type: none"> • Valvular pathology: MV/AV <p><i>Spectral</i></p> <ul style="list-style-type: none"> • Outflow velocities: LVOT/AV
16	TG RV inflow		<p><i>2D</i></p> <ul style="list-style-type: none"> • Chamber sizes: RV/RA/TV Annulus • Ischemia detection: RV Free Wall • Valvular anatomy and motion: TV <p><i>CFD</i></p> <ul style="list-style-type: none"> • Valvular pathology: TV <p><i>Spectral</i></p> <ul style="list-style-type: none"> • Typically not utilized

(continued)

Table 2.2 (continued)

Image order	Image name	Image depiction	2D > CFD > Spectral
17	Descending aortic SAX		<p>2D</p> <ul style="list-style-type: none"> • Vessel size: Ao • Dissection/Plaque: Ao <p>CFD</p> <ul style="list-style-type: none"> • Dissection: Ao <p>Spectral</p> <ul style="list-style-type: none"> • Not typically utilized
18	Descending aortic LAX		<p>2D</p> <ul style="list-style-type: none"> • Vessel size: Ao • Dissection/Plaque: Ao <p>CFD</p> <ul style="list-style-type: none"> • Dissection: Ao <p>Spectral</p> <ul style="list-style-type: none"> • Not typically utilized
19	UE aortic arch LAX		<p>2D</p> <ul style="list-style-type: none"> • Vessel size: Ao • Dissection/Plaque: Ao <p>CFD</p> <ul style="list-style-type: none"> • Dissection: Ao <p>Spectral</p> <ul style="list-style-type: none"> • Not typically utilized
20	UE aortic arch SAX		<p>2D</p> <ul style="list-style-type: none"> • Vessel size: Ao/PA • Dissection/Plaque: Ao <p>CFD</p> <ul style="list-style-type: none"> • Dissection: Ao • Valvular pathology: PV <p>Spectral</p> <ul style="list-style-type: none"> • Valvular/PA velocities: PV/Main PA

Abbreviations ME midesophageal; TG transgastric; UE upper esophageal; LAX long axis; SAX short axis; 2D two dimensional; CFD color flow Doppler; RA right atrium; LA left atrium; RV right ventricle; LV left ventricle; MV mitral valve; AV aortic valve; TV tricuspid valve; PV pulmonic valve; LVOT left ventricular outflow tract; PFO patent foramen ovale; ASD atrial septal defect; LAA left atrial appendage; LUPV left upper pulmonary vein; Ao aorta; PA pulmonary artery; RPA right pulmonary artery; AntSept anterior septal wall; InfLat inferolateral wall; Sept septal wall; Lat lateral wall; SVC superior vena cava

Adapted from Shanewise et al. [2]

References

1. Reeves ST, Finley AC, Skubas NJ, Swaminathan M, Whitley WS, Glas KE, et al. Basic perioperative transesophageal echocardiography examination: a consensus statement of the American Society of Echocardiography and the Society of Cardiovascular Anesthesiologists. *J Am Soc Echocardiogr.* 2013;26(5):443–56.
2. Shanewise JS, Cheung AT, Aronson S, Stewart WJ, Weiss RL, Mark JB, et al. ASE/SCA guidelines for performing a comprehensive intraoperative multiplane transesophageal echocardiography examination: recommendations of the American Society of Echocardiography Council for Intraoperative Echocardiography and the Society of Cardiovascular Anesthesiologists Task Force for Certification in Perioperative Transesophageal Echocardiography. *J Am Soc Echocardiogr.* 1999;12(10):884–900.
3. Hahn RT, Abraham T, Adams MS, Bruce CJ, Glas KE, Lang RM, et al. Guidelines for performing a comprehensive transesophageal echocardiographic examination: recommendations from the American Society of Echocardiography and the Society of Cardiovascular Anesthesiologists. *J Am Soc Echocardiogr.* 2013;26(9):921–64.

Chapter 3

Basic Ultrasound Physics, Doppler Ultrasound, and Hemodynamic Assessment

Gerard R. Manecke, MD

Abstract A basic understanding of physics is necessary for effective clinical use of ultrasound, and it allows appreciation of the wonderful technology we now use. Rapid waveform analysis and massive data storage capability make high-resolution imaging and complex hemodynamic assessment accessible at the bedside. Understanding the principles of ultrasound physics and applying them to echocardiography help us to understand the anatomy and function of the heart, while use of Doppler principles allows us to make assessments of blood flow, valve areas, and pressure gradients.

Keywords Transesophageal echocardiography · Ultrasound physics · Doppler principles · Doppler ultrasound · Hemodynamic assessment

Basic Ultrasound Physics

Some animals make use of sound wave reflections to determine their position and direction of motion (echolocation) [1, 2]. Bats, with their poor vision, transmit ultrasonic signals and are particularly adept at echolocation [3, 4]. Visually impaired humans can develop similar capabilities using audible sound, resulting in an impressive ability to navigate surroundings [5, 6]. Ultrasound in the form of Sound Navigation and Ranging (SONAR) was developed in early twentieth century, and was first employed for military purposes shortly after the First World War [7]. Medical ultrasound was first introduced by George Ludwig in 1949 [8] and cardiac ultrasound was first employed in 1953 [9]. An explosion in computer technology in the 1980s allowed the development of two-dimensional (2D) ultrasound for continuous imaging, Doppler blood flow, and tissue movement measurements. Further advances in computer technology provide the high-resolution

G.R. Manecke, MD (✉)

Department of Anesthesiology, University of California San Diego, 200 West Arbor Drive,
MC 8770, San Diego, CA, USA
e-mail: gmanecke@ucsd.edu

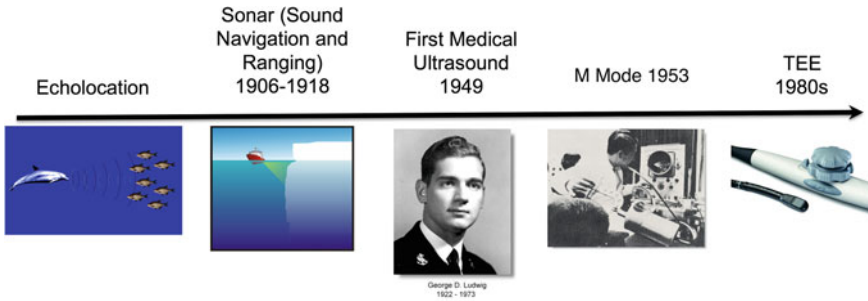
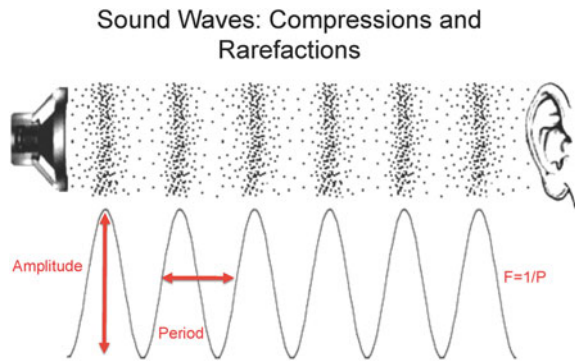


Fig. 3.1 Timeline of the history of ultrasound

Fig. 3.2 Characteristics of sound waves. F frequency, P Period



three-dimensional imaging with continuous display we currently enjoy [10]. A timeline of the history of ultrasound is shown in Fig. 3.1.

Physics of Ultrasound

Sound waves are pressure waves: compressions and rarefactions of the molecules occur in the medium in which they are traveling. Like all waves, sound waves have amplitude (loudness) and frequency (pitch) (Fig. 3.2). Humans can hear sounds within the range of 20–20,000 cycles per second (Hz). Ultrasound is sound at frequencies above the audible range (>20,000 Hz), while medical ultrasound is in the mega-Hz (MHz) range, or millions of Hz (Fig. 3.3).

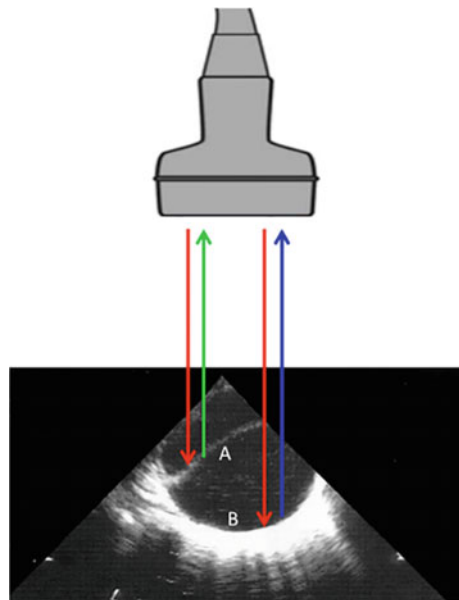
Sound transmission depends upon the density of the medium, with higher density substances such as liquid transmitting sound more rapidly and efficiently than air. Ultrasound does not travel well through gas, so gas-filled spaces such as bronchi and gastric air result in “blackout” of the ultrasound image. Lower frequency sound tends to propagate farther than high frequency sound. One notices this when a storm is approaching. When the storm is distant, thunder sounds like a

Fig. 3.3 Sound frequencies. Medical ultrasound is in the Mega-Hz (million Hz) range



- 1 Hz = 1 cycle/sec
- Sound (Audible) 20-20,000 Hz
- Ultrasound: >20,000 Hz
- Medical Ultrasound MHz
- 1 MHz=1,000,000 Hz

Fig. 3.4 “Specular Echoes.” Ultrasound waves bouncing off tissues of varying density, *A* is the intimal flap of an aortic dissection, *B* is the distal wall of the aorta



low-pitched “rumble.” As the storm approaches, the sound of thunder includes higher frequencies, resulting in a “thunder clap.” Ultrasound behaves similarly, so imaging objects distant from the transducer requires lower frequencies than imaging close objects.

When sound waves strike an interface of a different density, they bounce off that interface. This is the principle upon which two-dimensional ultrasound is based [11]. The ultrasound transducer emits ultrasound, the ultrasound bounces off a density interface (object) back to the transducer, and the time required allows calculation of the distance the object is from the transducer. As demonstrated in

Fig. 3.4, a cross-sectional image of the descending aorta shows ultrasound waves bouncing off of two density interfaces: a dissection intimal flap (A) and the distal wall of the aorta (B). A perpendicular orientation of the object to the ultrasound probe is optimal for return of echo signals. A parallel orientation may not provide a sufficient reflection of signals, leading to drop out.

Ultrasound Probes

Ultrasound probes have both emission and sensing capabilities. Each probe contains an array of pressure-electric (piezoelectric) crystals that convert electrical energy to pressure waves (for emitting ultrasound) and pressure waves to electricity (for sensing). The lateral resolution of the image depends upon the distance between the crystals aligned within the probe, with a smaller distance associated with better resolution (Fig. 3.5). The lateral resolution may also be altered by focusing. Akin to utilizing a magnifying glass in the sunshine to focus the sunlight into a narrow beam, modern ultrasound machines have an adjustable focal point that represents the narrowest part of the beam (Fig. 3.6). Lateral resolution is best at the focal point, but is quite poor in the far field (distal to the focal point). Therefore, it is recommended to place the focal point at the level of the structure of interest.

The longitudinal, or axial resolution depends on the pulse length, with shorter pulse length resulting in better resolution (Fig. 3.7). Pulse length can be decreased either by increasing the frequency of the probe (and thus decreasing the wavelength), or decreasing the cycles/pulse Eq. 3.1 and Eq. 3.2. Higher frequency probes with shorter wavelengths thus have better resolution Eq. 3.3. Note that resolution is expressed as distance, so a *lower* number indicates *better* resolution.

Fig. 3.5 Lateral resolution depends upon the distance between piezoelectric crystals in the probe

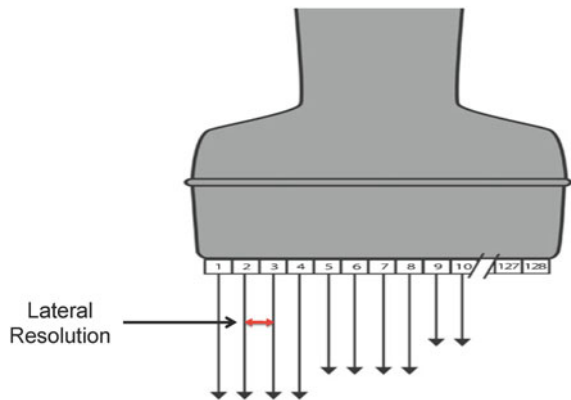


Fig. 3.6 Focus influence on beam width. The narrowest portion of the beam is at the focal point with poorer resolution in the far zone

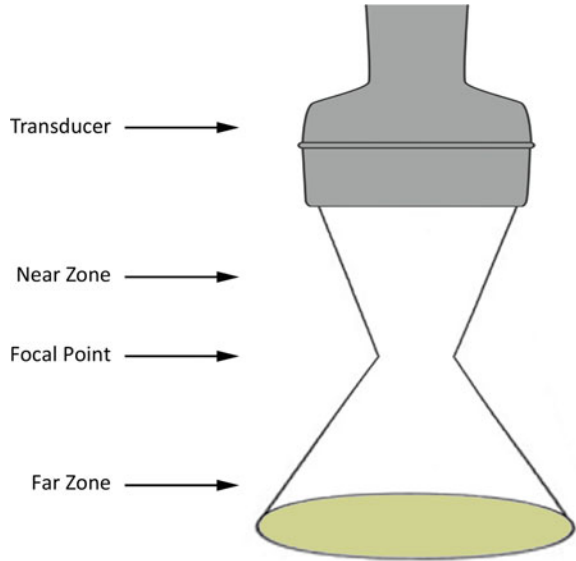
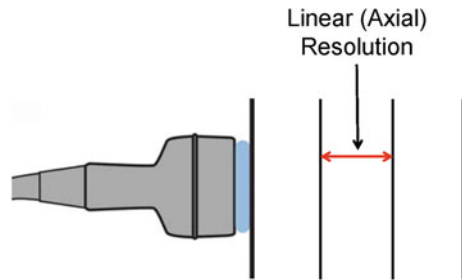


Fig. 3.7 Axial resolution depends upon the pulse length and the probe frequency



$$\text{Frequency} = 1/\text{wavelength} \tag{3.1}$$

$$\text{Pulse length} = \text{wavelength} \times \text{cycles/pulse} \tag{3.2}$$

$$\text{Axial Resolution} = \frac{0.77 \times \frac{\text{cycles}}{\text{pulse}}}{\text{Frequency}} \tag{3.3}$$

The effects of probe frequency on ultrasound imaging are summarized in Table 3.1, with the general rule that distant objects can be viewed best using a low frequency probe, however, the resolution will be poorer at the lower frequency. Likewise, small objects close to the probe, such as the radial artery with surface ultrasound, are best visualized using a high frequency probe because of the associated high resolution. The trade-off of high frequency imaging is the inability to visualize deeper structures due to energy dissipation.

Table 3.1 The effects of probe frequency on ultrasound imaging

<ul style="list-style-type: none"> • High frequency – More energy dissipation – Better linear resolution – Close objects with high resolution
<ul style="list-style-type: none"> • Low frequency – Less energy dissipation – Poor linear resolution – Far objects viewed but less resolution

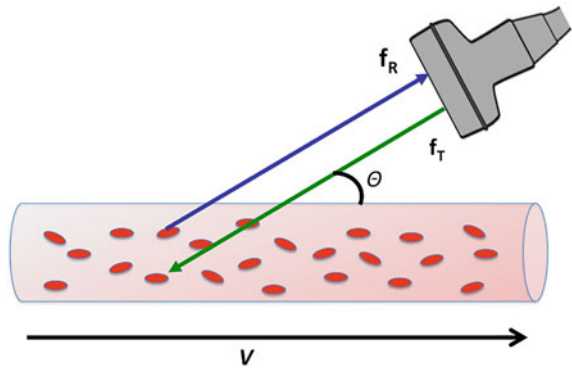
While lateral and axial resolution represent the spatial resolutions of ultrasound, cardiac ultrasound requires interpreting moving clips as opposed to still images. Therefore, one must consider temporal resolution. This is similar to movie and television images where at an analog movie theater one would note a flickering of the image, however, at home on a television there is no longer a flickering of the image. With modern televisions, the high-definition frame rate is high enough such that even fast moving objects (e.g., sporting events) appear smoothly. This is due to the improved frame rate moving from analog movie theater to television to high-definition television.

With ultrasound, the machine has to produce numerous ultrasound pulses in a fan-like fashion to develop one single image. Repeating this process will provide subsequent images yielding a moving clip. The number of images developed per second is termed the frame rate. The more imaging (e.g., deeper or wider) and processing (e.g., color flow Doppler in addition to 2D) that a machine is requested to do, the longer it will take to generate a single image, subsequently reducing the frame rate. If the frame rate is too slow, the video will begin to appear choppy or flip-book like, reducing the ability to detect fine cardiac movement. Therefore, only the depth needed and the color flow Doppler box size needed should be utilized to maintain the best frame rate.

Doppler Ultrasound

In 1842, Austrian physicist Christian Doppler postulated that the difference in color between double stars could be explained by their motion. The effect of an object's motion on the frequency of waves detected from it is known as the "Doppler Effect." An example of the Doppler effect is the change in pitch of a train whistle as the train passes by an observer. This principle is applied in ultrasound with blood flow velocity measurements as illustrated in Fig. 3.8. Ultrasound at a known frequency (f_T) is transmitted from the probe, bounces off a moving object (blood cells), and the reflected sound is detected by the probe. The frequency of the returning ultrasound (f_r) is calculated, and the frequency shift between the transmitted and returning ultrasound (Δf) is used to calculate the velocity of blood flow (V):

Fig. 3.8 Doppler assessment of blood flow velocity. The closer the alignment of blood flow with the Doppler beam (angle $\theta = 0$), the more accurate the result. V is blood flow velocity, f_T is transmitted frequency (known), F_R is the returning frequency (calculated). The difference between f_T and F_R is the frequency shift, Δf



$$V = \frac{C(\Delta f)}{2f_T \cos \theta} \tag{3.4}$$

V = velocity of blood flow, C = speed of sound, Δf = frequency shift (difference between transmitted and received frequency), Θ = angle between blood flow path and Doppler beam.

Closer alignment of the blood flow and the Doppler beam (Θ) yields a more accurate measurement ($\cos 0^\circ = 1$). Of note, the $\cos 90^\circ = 0$ and therefore, measurement of flow perpendicular to the probe cannot be calculated. As opposed to 2D imaging which prefers the object to be perpendicular to the probe, Doppler imaging prefers the object to be parallel in orientation.

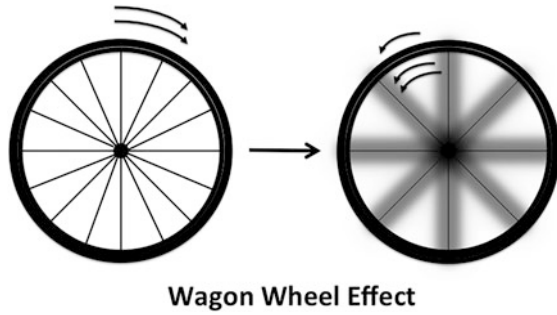
The Doppler Principle is used clinically in three ways: color flow Doppler (CFD), pulse wave Doppler (PWD), and continuous wave Doppler (CWD). CFD results in a real-time color flow diagram, PWD determines the velocity at a discrete area in space (“sample volume”), and CWD determines flow velocity along an axis. Tissue Doppler is simply a variation of PWD, used to determine the velocity of tissue movement (e.g., the mitral annulus) as opposed to blood movement. The characteristics, uses, and limitations of Doppler techniques are summarized in Table 3.2.

An important and sometimes useful artifact is *aliasing*. Aliasing is a false frequency wave or image resulting when the sampling rate of the sensor is too low to

Table 3.2 Characteristics and clinical use of Doppler techniques

	Color flow Doppler	Pulse wave Doppler	Continuous wave Doppler
Color map	+	–	–
Assess flow at a discrete area	+	+	–
Assess flow along an axis	–	–	+
Qualitative assessment	Very useful	Useful	Less useful
Quantitative assessment high flow	Less useful	Less useful	Very useful
Aliasing	+	+	–

Fig. 3.9 “Wagon Wheel Effect.” Rapid movement of spokes is interpreted as slow moving, large “blurred” spokes, often in the opposite direction



accurately detect the high frequency of the returning signal. The *Nyquist Theorem* states that the sampling rate must be at least twice the frequency of the wave being sampled. The *Nyquist Limit* is the highest frequency that can be accurately sampled at a given sampling rate. Aliasing is often called the “Stroboscopic” or “Wagon Wheel” effect, in which rapidly moving spokes of a wheel in one direction appear as slow moving blurred spokes (Fig. 3.9, <https://www.youtube.com/watch?v=jHS9JGkEOmA>). This results from either, in a video, the frame rate being too slow to pick up the actual speed of the spokes, or in real time, the inability of the human central nervous system to process the fast spoke motion. If the “snapshots” (samples) of the moving spokes are not frequent enough, the spokes appear to be moving slowly, sometimes in the opposite direction.

After transmitting an ultrasound wave, the probe “samples” the returning wave. In CFD and PWD, the probe “waits” until a transmitted signal bounces off the target and is received, so the sampling rate is limited by this process. Aliasing thus results if the returning frequency is higher than half the sampling rate. In CWD, the sampling and transmission are simultaneous—the probe does not wait for the returning signal, so aliasing does not occur. CWD is thus preferred for measurement of high velocity (high returning frequency) flow. Aliasing results in the “wrap around” appearance of PWD tracings (Fig. 3.10) and the appearance of flow in the opposite direction of the actual flow in CFD (Fig. 3.11). The latter may be useful, since the velocity at which aliasing occurs is known and can be applied to calculations such as Proximal Isovelocity Surface Area (PISA) [12].

Hemodynamic Assessment

Echocardiography can be used for an accurate assessment of hemodynamics. The most common applications are quantifications of flow, valvular area, and pressure gradients.

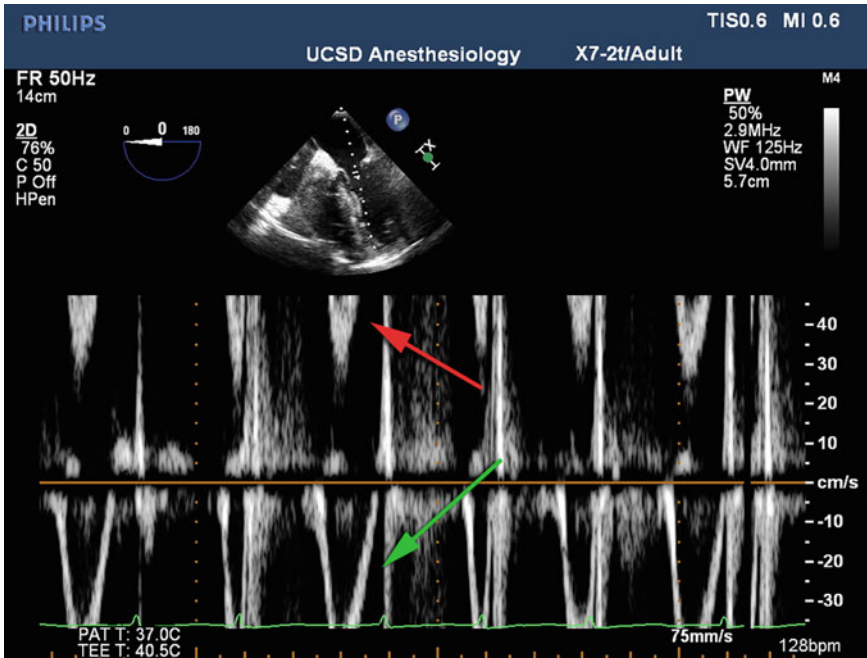


Fig. 3.10 Pulse Wave Doppler of transmitral flow. Flow away from the transducer is displayed as below the zero line. Flow becomes so rapid (*green arrow*) that it is displayed as flow in the opposite direction (*red arrow*, “Wrap Around”)

Flow

Blood flow measurement is typically utilized in determining stroke volume and subsequently cardiac output. A stroke volume is determined by calculating the cross-sectional area of the blood vessel and multiplying it by the area under the Doppler velocity–time curve. The area under the Doppler velocity–time curve is called the “Velocity Time Integral” (VTI), or the “Stroke Distance.” Figure 3.12a explains how the area under the curve provides a distance by plotting velocity and time of a traveling car. In the example, a car traveling at 75 miles per hour for 2 h will have traveled a distance of 150 miles (analogous to “Stroke Distance”). The cross-sectional area of the blood vessel is estimated by determining the radius of the vessel (diameter divided by 2) and assuming the shape is circular (area = πr^2) (Fig. 3.12b).

$$\text{Stroke Volume} = \text{Area} * \text{VTI} \quad (3.5)$$

For example, to calculate the left ventricular stroke volume, one can measure the diameter of the left ventricular outflow tract (LVOT) using the midesophageal aortic valve long axis view (Fig. 3.13a), with Area = $\pi(D/2)^2$. Using the deep

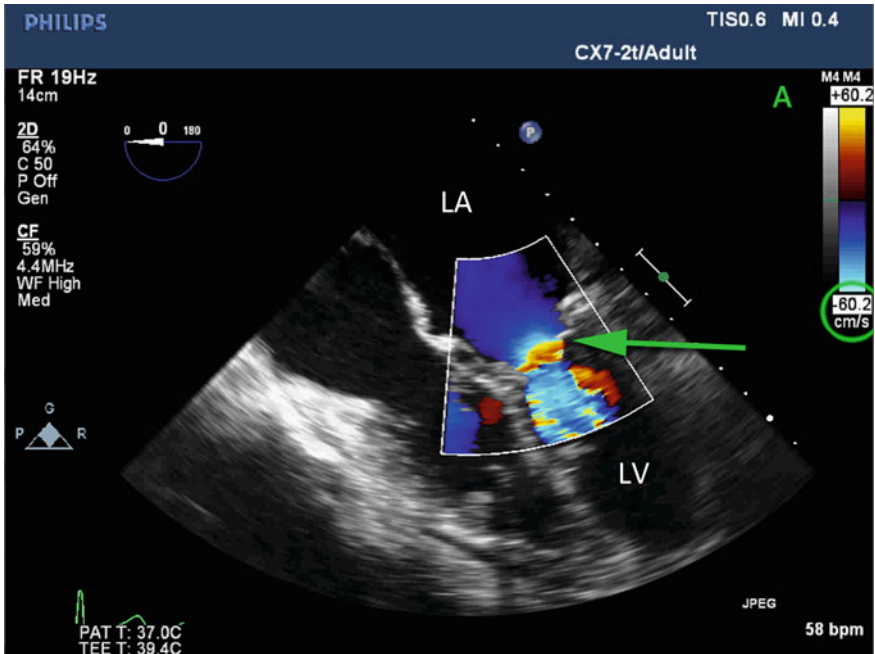


Fig. 3.11 Midesophageal four-chamber view with transmitral color flow Doppler demonstrating aliasing. The flow map (A) indicates that flow away from the probe is *blue*, flow toward the probe is *yellow*, and the limit below which aliasing does not occur is 60.2 cm/sec. The *arrow* shows an aliasing line, where flow exceeds 60.2 cm/sec, and downward flow turns from *blue* to *yellow*. LA left atrium; LV left ventricle

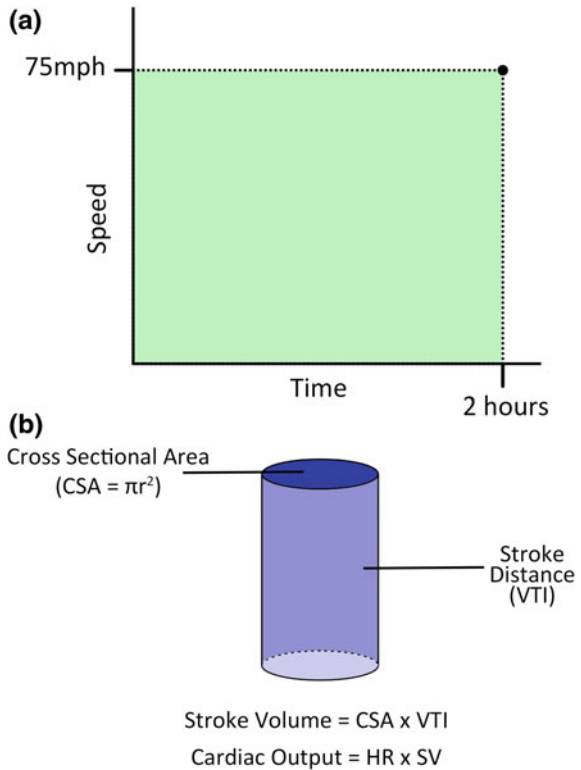
transgastric long axis view, CWD can be used to obtain the LVOT systolic Doppler wave, and the VTI can be determined by tracing the wave. Stroke volume is then calculated by multiplying the LVOT area by the VTI.

Valvular Area

In a closed fluid system, the amount of flow through one section is the same as the amount of flow through another. This conservation of mass principle is described by the Continuity Equation. Most commonly utilized in the case of aortic stenosis (see Chap. 7—Aortic Valve), the flow through the aortic valve is the same as the flow through the LVOT, so the valve area of the stenotic valve can be determined:

$$A_1 * V_1 = A_2 * V_2 \quad (3.6)$$

Fig. 3.12 **a** Graph of the speed of a car versus time. The area under the curve which is shaded green demonstrates the distance the car traveled. **b** Depiction of the cross-sectional area of a cardiac structure multiplied by its velocity time integral (“Stroke Distance” will yield a stroke volume). *CSA* Cross-Sectional Area; *VTI* Velocity Time Integral; *HR* Heart Rate; *SV* Stroke Volume



In this example, $A_{LVOT} * V_{LVOT} = A_{AV} * V_{AV}$, where AV is aortic valve and LVOT is Left Ventricular Outflow Tract. One measures the area of the LVOT, and the VTIs for the AV and LVOT (Fig. 3.13a, b). Solving for the area of the AV:

$$A_{AV} = (A_{LVOT} * V_{LVOT}) / V_{AV}$$

Pressure Gradient Estimation

Clinically, practitioners often think in terms of pressure (mmHg) while echocardiography measures velocities. Therefore, a relationship between velocity and pressure is necessary to provide appropriate clinical estimations. The pressure gradient across a valve or orifice can be determined using the modified Bernoulli Equation,

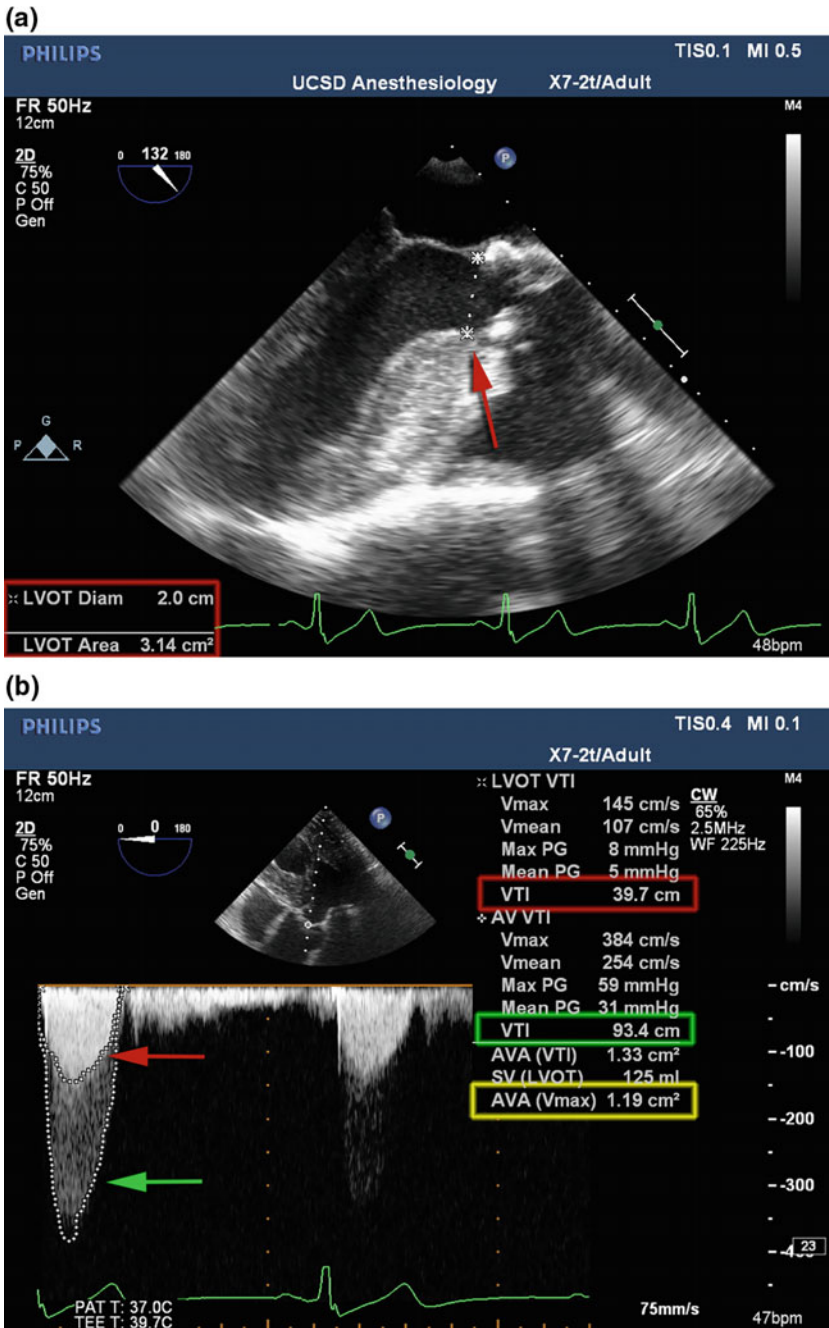


Fig. 3.13 **a** Measurement of the diameter (*red arrow*) of the left ventricular outflow tract (LVOT) using the midesophageal aortic valve long axis view. **b** The “Double Envelope,” showing a velocity envelope for the LVOT (*red arrow, red box*) and a higher velocity envelope for the aortic valve (*green arrow, green box*). Velocity Time Integrals (VTI) are used in the Continuity Equation for calculation of the aortic valve area (*yellow box*)

$$P = 4V^2 \tag{3.7}$$

where P is the pressure gradient, and V is the peak velocity in m/sec. For example, the systolic right ventricular pressure gradient between right ventricle and right atrium can be determined by CWD across the tricuspid valve. The peak velocity of the regurgitant jet, in m/sec, is used in Eq. 3.7. The right ventricular systolic pressure can then be estimated by adding the value of the gradient to the right atrial or central venous pressure (CVP). In the absence of pulmonic valve stenosis, right ventricular systolic pressure is equal to pulmonary artery systolic pressure. Therefore, the application of the modified Bernoulli equation to a tricuspid regurgitation jet in addition to CVP provides an estimation of pulmonary artery pressures (Fig. 3.14).

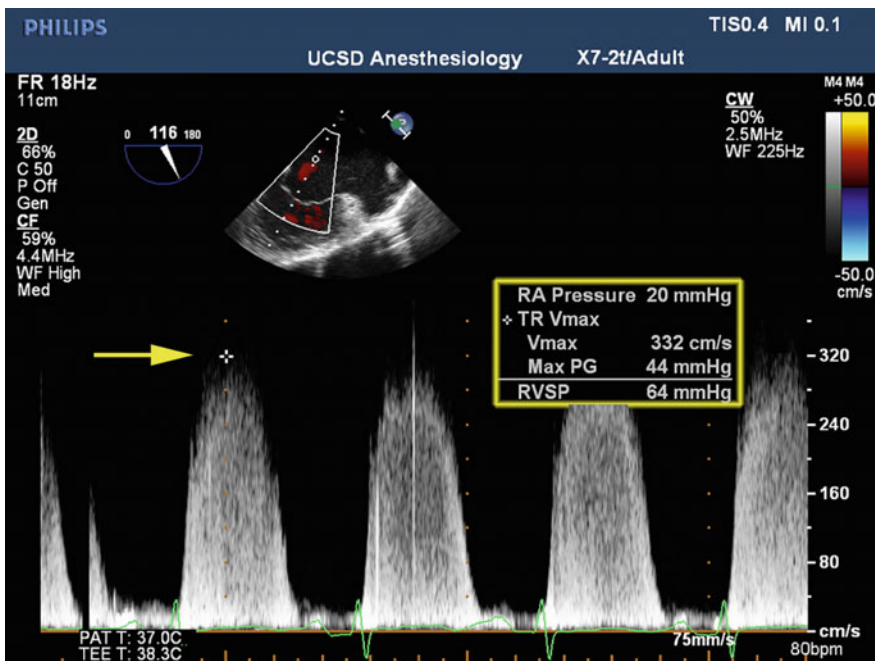


Fig. 3.14 A continuous wave Doppler profile of a tricuspid regurgitation (TR) jet. The right ventricular systolic pressure (RVSP), which is an estimation of pulmonary artery systolic pressure, is determined by applying the modified Bernoulli equation to the peak regurgitant velocity in addition to the CVP (RA Pressure). RA right atrial; Vmax maximum velocity; PG pressure gradient

Summary

Understanding basic principles of sound wave reflection, propagation, and frequency, as well as digital sampling facilitates the effective clinical use of ultrasound technology. These principles can be applied to understand the anatomy and function of the heart, as well as the assessment of blood flow, valve areas, and pressure gradients.

References

1. Brinklov S, Fenton MB, Ratcliffe JM. Echolocation in Oilbirds and swiftlets. *Front Physiol.* 2013;4:123.
2. Harmon, K. Homing in on Mammalian Echolocation. *Scientific American*, 2010.
3. Ryckegham, AV. How do bats echolocate and how are they adapted to this activity? *Scientific American*, 1998.
4. Ulanovsky N, Moss CF. What the bat's voice tells the bat's brain. *Proc Natl Acad Sci USA.* 2008;105(25):8491–8.
5. Kolarik AJ, et al. A summary of research investigating echolocation abilities of blind and sighted humans. *Hear Res.* 2014;310:60–8.
6. Schornich S, et al. Psychophysics of human echolocation. *Adv Exp Med Biol.* 2013;787:311–9.
7. D'Amico A, Pittenger R. A brief history of active sonar. *Aquat Mammals.* 2009;35(4):426–34.
8. Ludwig G, Struthers F. Considerations underlying the use of ultrasound to detect gallstones and foreign bodies in tissue. *Naval medical research institutes reports*, 1949. Project 004001 (Report Number 4): p. 20.
9. Singh S, Goya A. the origin of echocardiography. *Tex Heart Inst J.* 2007;34(4):431–8.
10. Lang RM, et al. Three-dimensional echocardiography: the benefits of the additional dimension. *J Am Coll Cardiol.* 2006;48(10):2053–69.
11. Aldrich JE. Basic physics of ultrasound imaging. *Crit Care Med.* 2007;35(5 Suppl):S131–7.
12. Enriquez-Sarano M, et al. Effective mitral regurgitant orifice area: clinical use and pitfalls of the proximal isovelocity surface area method. *J Am Coll Cardiol.* 1995;25(3):703–9.

Part II
Echocardiographic Assessment

Chapter 4

Left Ventricular Systolic Function

Seth T. Herway, MD, MS, Raimy Boban, MD
and Swapnil Khoche, MBBS

Abstract The estimation of left ventricular systolic function, both qualitative and quantitative, remains essential to the perioperative management of the cardiovascular status of the surgical patient. As a result of its portability and versatility, echocardiography is now widely used for this purpose (Lang et al. in *European Journal of Echocardiography* 7(2):79–108, 2006 [1]). The spectrum of techniques for assessment of left ventricular systolic function is wide. This chapter provides an overview of some of the techniques that are essential for the basic echocardiographer and delineates the advantages, disadvantages, and pitfalls of each.

Keywords Echocardiography · Ejection fraction · Fractional shortening · Systolic function · dP/dt · Myocardial performance

Echocardiography has long been used for the assessment of left ventricular function and the diagnosis of heart failure [2]. However, because a gold standard to measure true efficacy of cardiac contraction (adequate blood propulsion with low filling pressures that lead to adequate tissue perfusion) does not exist, surrogates such as ejection fraction (EF) are employed [3].

The ejection fraction is a measure of the left ventricle's (LV) ability to project forward a proportion of volume it contains at the end of diastole. End diastole is noted by mitral valve closure and correlates with the onset of the QRS complex on the electrocardiogram (ECG). End systole immediately precedes the mitral valve

Electronic supplementary material The online version of this chapter (doi:[10.1007/978-3-319-34124-8_4](https://doi.org/10.1007/978-3-319-34124-8_4)) contains supplementary material, which is available to authorized users.

S.T. Herway, MD, MS · R. Boban, MD · S. Khoche, MBBS (✉)
Department of Anesthesiology, University of California San Diego,
200 W Arbor Drive MC #8770, San Diego, CA 92103, USA
e-mail: skhoche@ucsd.edu

S.T. Herway, MD, MS
e-mail: sherway@ucsd.edu

opening and correlates with the end of the T wave on ECG [4]. The American Society of Echocardiography (ASE) defines normal ejection fraction as greater than 52 % for men and 54 % for women [5]. As the amount of blood ejected is the difference between end-diastolic and end-systolic volumes, EF is mathematically represented as

$$EF = [(LVEDV - LVESV) / LVEDV] \times 100$$

LVEDV = LV end diastolic volume

LVESV = LV end systolic volume

For a majority of echocardiography-derived parameters, the above formula is utilized with other measurements substituted for the volumes such that

$$EF = [(LV ED parameter - LV ES parameter) / LV ED parameter] \times 100$$

The methods described in this text provide estimations of EF or surrogate measures of left ventricular systolic function (refer below table). Methods that should be familiar to the basic echocardiographer include visual estimation of EF, fractional shortening, fractional area change, the modified Simpsons method, the rate of rise of ventricular pressure, and mitral annular motion utilizing tissue Doppler imaging. Advanced techniques such as three-dimensional (3D) EF measurement and global longitudinal strain analysis will be briefly mentioned, however, these methods are beyond the scope of this text.

LV systolic function

2D	<ul style="list-style-type: none"> • Reduced FS, FAC, EF • EF Determination: Modified Simpson's method or Visual Estimation • Secondary changes—LAE, biventricular dysfunction
CFD	<ul style="list-style-type: none"> • Typically not utilized
Spectral	<ul style="list-style-type: none"> • dP/dt determination • S'—Tissue Doppler Imaging

LV left ventricle, *FS* fractional shortening; *FAC* fractional area of change; *EF* ejection fraction; *LAE* left atrial enlargement; *dP/dt* rise in pressure over time; *S'* lateral mitral annular velocity

Visual Estimation of Ejection Fraction

The most basic way to determine a patient's ejection fraction is to qualitatively estimate it based on visual evaluation on echocardiography. Although objective measures of LV function result in reduced interobserver variability and better reproducibility, visual estimation of ejection fraction by skilled echocardiographers can approach objective measurements [6]. For the basic echocardiographer, a simple qualitative estimate of poor, moderate, or good ventricular function is often all that is needed. Over time, as experience is gained in obtaining objective measurements of EF, the practitioner will be better able to calibrate their visual estimate of the patient's EF with the actual quantitative estimate. The mid-esophageal four-chamber and the transgastric mid-papillary short axis windows are excellent views for visual estimation of EF by visually comparing the size of the chamber at end diastole versus end systole.

It is important to note that both quantitative and qualitative estimates of EF can be prone to error in cases of arrhythmia, extremes of heart rate, and presence of significant wall motion abnormalities. Most two-dimensional (2D) measurements rely heavily on adequate endocardial border definitions, which require gain optimization to improve the blood-tissue interface. Contrast agents may be used to better delineate LV volumes, but their use for this purpose has not been well verified [5].

Fractional Shortening

Fractional shortening is a linear measurement of changes in the LV cavity, expressed as a percentage. In order to calculate the percentage of fractional shortening, a transgastric mid-papillary short axis view is obtained and endocardial border-to-border measurements of the LV cavity during systole and diastole is acquired. Measurements of the endocardial borders can be made directly from the transgastric mid-papillary short axis window or using M-mode with the interrogation line along the inferior and anterior wall. As described in the equation below, fractional shortening is calculated as a percentage of the difference between the internal diameters of the LV at systole and diastole. Care should be taken to exclude the papillary muscles from the measurement to avoid error. Normal values for fractional shortening are 25–45 % [5] (Figs. 4.1a, b and 4.2).

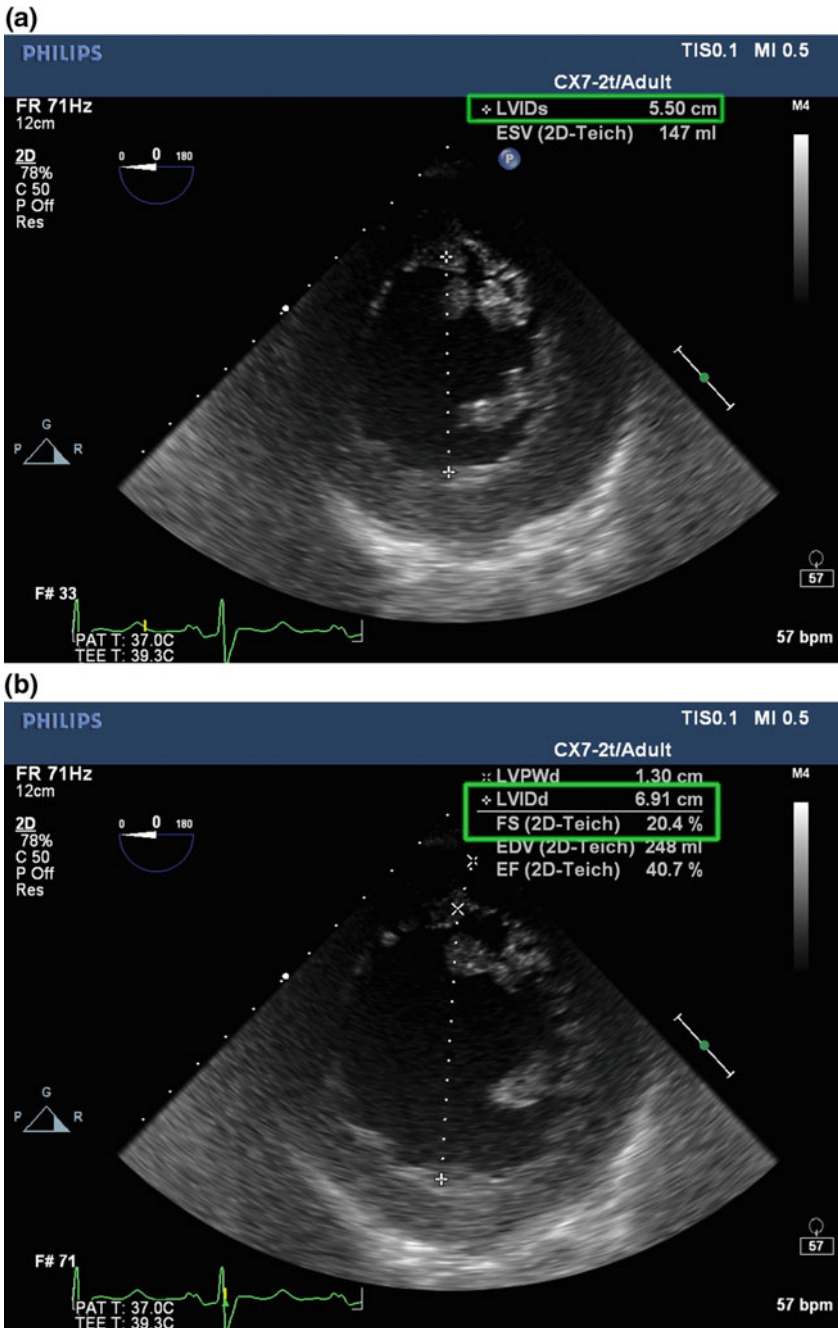


Fig. 4.1 **a** The TG mid-papillary SAX view in systole where endocardium to endocardium measurements are obtained. The machine calculates an end-systolic volume based on a predetermined algorithm. **b** The acquisition of an end-diastolic dimension results in a calculation of fractional shortening (FS) as well as estimations of end-diastolic volume and EF based on predetermined algorithms. The case demonstrates the LV function as being reduced. (low FS)

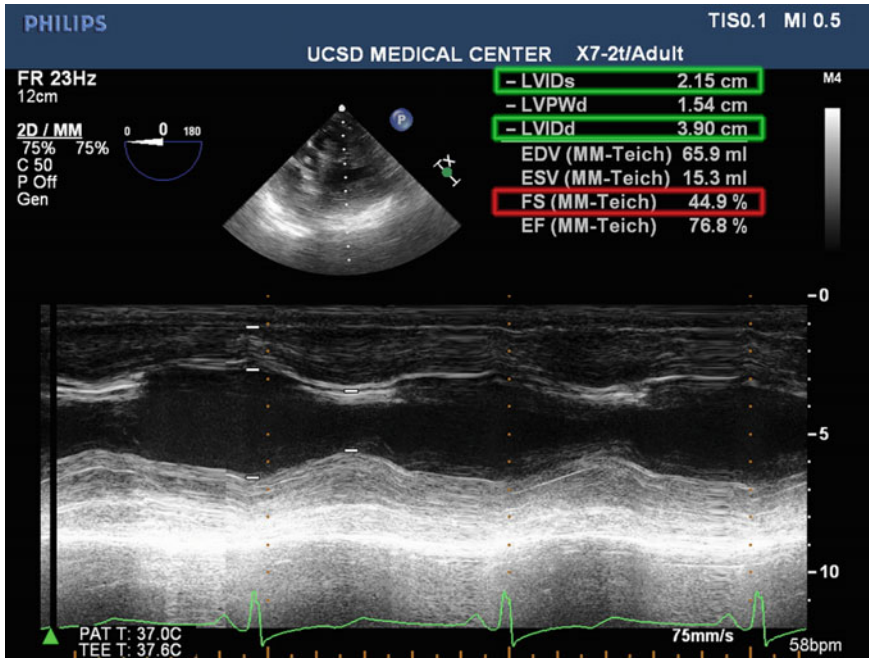


Fig. 4.2 M-mode-based FS calculation along a one-dimensional axis from inferior to anterior walls. The dark portions denote the LV cavity, while the echogenic lines indicate inferior and anterior wall motion over time. Note that care has been taken to exclude the papillary muscles, which encroach on the LV cavity during systolic measurement. Fractional shortening is obtained by noting the internal diameter in systole and diastole

$$\text{Fractional shortening of the LV (\%)} = [(LVIDd - LVIDs)/LVIDd] \times 100$$

LVIDd = LV internal diameter at end diastole

LVIDs = LV internal diameter at end systole

Whether it is from traditional 2D imaging or M-mode, fractional shortening can provide an estimate of LV systolic function, however, it is the least representative of overall global function, especially with regional abnormalities and distorted LV geometry. This limitation results from the fact that fractional shortening is a measurement of just one dimension along two isolated points along the LV and is not representative of the entire LV. This measurement does not take into account septal and lateral wall motion as well as basal and apical function. Another source for error is the need for appropriate beam orientation, since an off-axis ultrasound beam orientation can result in inappropriate measurements of LV internal diameters [5]. It is also vital to remember that most reference values for fractional changes, in either ventricular dimensions or area, are different from the reference values for EF.

For instance, a fractional shortening of 30 %, while “appearing” as a low percentage actually represents normal systolic function [1]. However, most machines will provide a corresponding EF value extrapolated from the values being measured.

Fractional Area Change

Fractional area change extends the principle of fractional shortening to two dimensions, evaluating the change in the cross-sectional area of the LV during systole and diastole to estimate LV systolic function rather than just the change in the LV cavity along a straight line (single dimension). Fractional area change is easy to perform, reproducible, and provides a more accurate surrogate for EF than fractional shortening. Although multiple methods have been devised to put this principle into practice, measuring fractional area change at the transgastric mid-papillary short axis view is the quickest since it requires just one view to be obtained. However, it should be noted that calculating fractional area change in a single plane is still not a global representation of LV function and can become very inaccurate in the setting of wall motion abnormalities and LV distortion. In particular, simply utilizing the TG mid-papillary short axis view will not account for wall motion of the basal and apical LV segments.

In order to calculate the fractional area change, the internal area of the LV cavity can be traced out manually at end systole and end diastole, carefully excluding the papillary muscles from the tracing. The difference in the area of the LV at end systole and diastole is then calculated as a percentage according to the equation below:

$$\text{Fractional Area Change of the LV (\%)} = [(LV\ EDA - LV\ ESA)/LV\ EDA] \times 100$$

LV EDA = End diastolic area of the left ventricle

LV ESA = End systolic area of the left ventricle

Some machines have algorithms that automate this process using semiautomatic endocardial border detection. Normal values are defined as 56–62 % for males and 59–65 % for females [7].

Left Ventricular Volumes

Determination of ejection fraction requires calculation of ventricular volumes at end diastole and end systole. While a volume is a three-dimensional measurement, performing this calculation from two-dimensional images can be challenging and often requires geometrical assumption of the left ventricular shape. Multiple

methods exist (ellipsoid method, bullet method, etc.) to provide this estimation of the left ventricle, however, the modified Simpson’s method described below is the most often utilized.

The ellipsoid method recognizes the nonspherical shape of the LV, and attempts to calculate its volume as a symmetrical ellipsoid. A line connecting the insertion points of the mitral leaflets (the mitral annulus) forms the base of the ellipsoid. In a ME four-chamber, ME two-chamber, or a TG two-chamber view, the LV is divided into two axes along its length and width, and its volume using the single plane

Fig. 4.3 A diagrammatic explanation of the ellipsoid method for determining LV volume which is based on the LV internal diameter (LVID) and the LV length

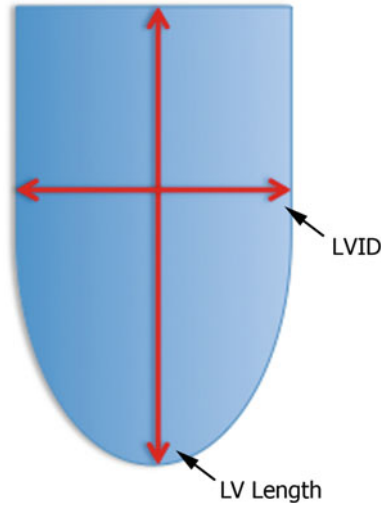
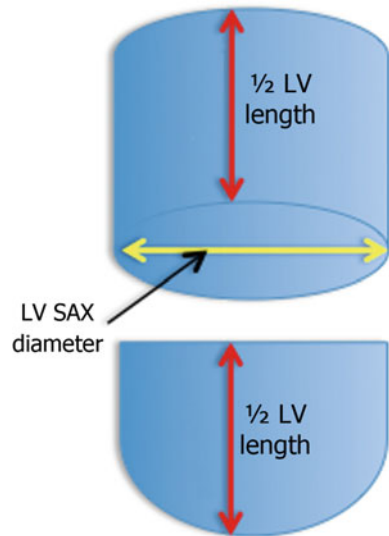


Fig. 4.4 Diagram explaining the assumption that LV is a “bullet” shape where part is cylindrical while the remainder is hemispheric



ellipsoid method is calculated utilizing a formula involving the left ventricular area in the long axis view and the diameter of left ventricle. To further increase the accuracy of the estimation, the biplane ellipsoid method uses the above parameters in addition to minor axis and short axis area measurements. Another form of LV volume estimation is the bullet formula or the hemisphere-cylinder formula. It assumes that the LV is shaped like a hemisphere sitting on top of a cylinder [8] (Figs. 4.3 and 4.4). These methods have not gained popularity in LVEF estimation, likely related to the complexity of the techniques, introduction of errors in measurement of the LV area and interobserver variability.

Modified Simpson's Method

The modified Simpsons method is the preferred technique of two-dimensional echocardiography-based LV volume estimation and EF determination per the ASE [5]. This method is an extension of the previously discussed fractional area change method, except the fractional area change is now calculated at multiple points across the LV instead of a single "slice," thus essentially providing a measure of fractional volume change. The modified Simpsons method divides the LV into a series (typically 20) of symmetrical discs. The volume of each disc is calculated based on the height and the diameter of the disc and summated to obtain an LV volume. This is analogous to calculating the volume of a stack of different diameter coins, where the diameter of the coins corresponds to the diameter of that particular segment of the left ventricle. The mid-esophageal four-chamber and two-chamber views are commonly used for this method [8]. Although it can be done using either single view, combining the two increases accuracy. The endocardium is either manually or automatically traced (if available) by the machine software in both the mid-esophageal four-chamber and two-chamber views at end diastole and end systole. The ultrasound machine software splits the designated area into 20 discs and calculates the volume of each disc as well as a summation of all discs (i.e., LV volume estimation). This process is repeated for end-diastolic and systolic volumes in both views (i.e., septal-lateral in the ME four-chamber view and anterior-posterior in the ME two-chamber view), thus generating a biplane EF (Fig. 4.5a-d).

The modified Simpson's method is easy to perform and has been shown to have low interobserver variability [9]. Although this technique overcomes some of the difficulties in estimating EF in patients with altered LV geometry and segmental dysfunction, it is important to remember that only two views of the LV are used to predict global function. Therefore, it is still possible to miss dysfunction of segments not visualized and therefore may not truly be representative of the entire LV. Adequate 2D imaging is essential to reduce foreshortening, which results in reduced volume estimation and errors in EF estimation [10]. To ensure foreshortening of the LV is not causing errors in calculation, there should be less than a 10 % discrepancy between the measurements in the ME four-chamber view and the ME two-chamber view for both phases of the cardiac cycle [5].

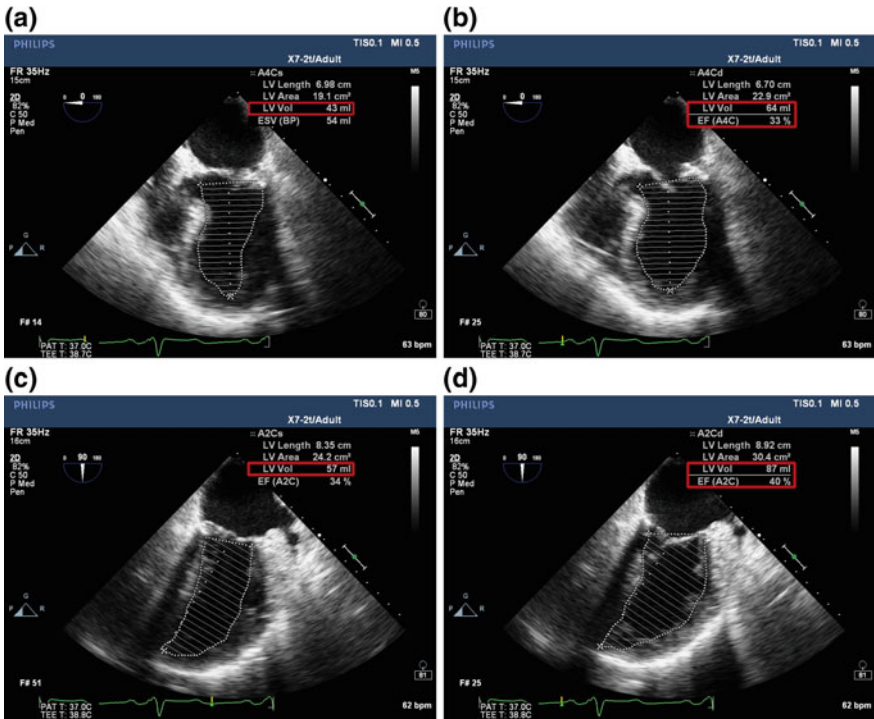


Fig. 4.5 Modified Simpson’s method of EF calculation. The dotted line from mitral valve annulus describes the length of the LV while the numerous horizontal lines depict the stack of “discs” from which the volume of the LV is calculated. **a** ME four-chamber view in systole. **b** ME four-chamber view in diastole. **c** ME two-chamber view in systole. **d** ME two-chamber view in diastole

Rate of Rise of Ventricular Pressure (dP/dt)

The rate of rise of left ventricular pressure (dP/dt) is used as a single measure to evaluate left ventricular systolic function. The left atrial (LA) pressure changes during systole are negligible, and therefore the mitral regurgitant velocity used to estimate the pressure gradient that forms is primarily a result of the rise in LV pressure only. LV contractility determines how swiftly the pressure gradient develops between the LV and LA, making dP/dt an appropriate surrogate for measurement of left ventricular systolic function.

The basis of this method is the modified Bernoulli equation: $P = 4v^2$, discussed in Chap. 3. The ME four-chamber view is used with a focus on the mitral valve and the mitral regurgitant (MR) jet. Other views of the mitral valve from the mid-esophageal position can also be considered if alignment of the jet is improved

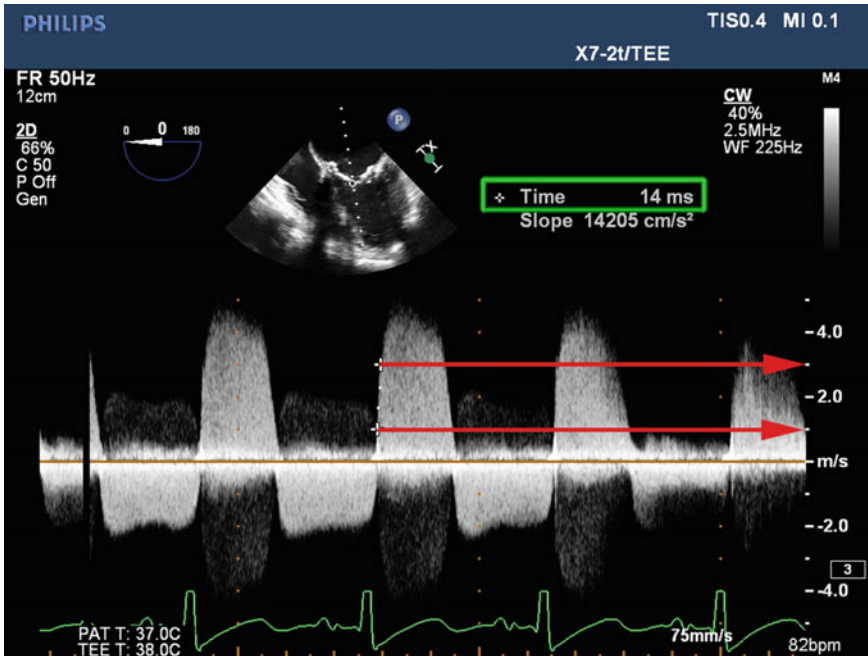


Fig. 4.6 The measurement for the rate of ventricular pressure rise (dP/dt). The determination of $dP/dt = 32 \text{ mmHg}/0.014 \text{ s} = 2285 \text{ mmHg/s}$, which denotes a normal ventricle. The *red arrows* indicate the pressure gradient determinations at 1 and 3 m/s respectively. The time required to increase pressure is calculated as 14 ms

with the Doppler interrogation line. The cursor is placed over the MR jet during systole, and a continuous wave Doppler waveform is obtained, ensuring the scale is appropriately set to at least 5 m/s. The caliper is placed on the ascending edge of the MR jet envelope at 1 m/s and 3 m/s and the time needed for this transition is measured and converted to seconds (t) [11] (Fig. 4.6).

The pressure gradient that drives the mitral jet changes from 4 mmHg when the velocity is 1 m/s ($4v^2 = 4 \times (1)^2 = 4$) to 36 mmHg when the velocity is 3 m/s ($4v^2 = 4 \times (3)^2 = 36$). The pressure gradient change (dP) is therefore 32 mmHg, which remains constant for the calculation [12]. The time to change (dt) from 4 mmHg to 36 mmHg is therefore determined from the measurement. The following equation is used to measure the rate of change in the pressure gradient:

$$dP/dt = [4(3)^2 - 4(1)^2]/t \rightarrow (36 - 4)/t \rightarrow 32/t; \text{ therefore,}$$

$$dP/dt = 32/t, \text{ with } t \text{ in seconds}$$

A value of greater than 1000 mmHg/s is considered normal. The advantages of this technique include ease of performance and relative load independence. The

measurement also correlates well with other parameters of systolic function. However, it requires the presence of a well-aligned mitral regurgitation jet, and is prone to error with significant alterations in left atrial pressure.

Tissue Doppler Imaging

During systolic contraction, the piston-like contraction of the LV pulls the mitral annulus downward toward the LV apex and the speed of this displacement can be used as a surrogate for left ventricular systolic function. Utilizing tissue Doppler imaging which uses an inverted filter to measure the velocity of lower speed, high intensity signals (i.e., myocardium) filtering out higher speed, low intensity signals (i.e., blood), the peak velocity that the mitral annulus attains can be measured. Mitral annular velocity (S') reflects the longitudinal motion of the left ventricle and correlates well with global systolic function, analogous to the use of Tricuspid Annular Motion for the right ventricle (see Chap. 8). As well, this measurement can be predictive of cardiac mortality in patients over time [13].

A mid-esophageal four-chamber view is used, with focus on the lateral mitral annulus. Tissue Doppler Imaging (TDI) modality is used, which generates a color-coded image on the screen, reflecting tissue motion towards and away from the ultrasound probe. Pulsed-wave Doppler is used with the sample volume cursor placed over the lateral mitral annulus. The height of the S' wave, the deflection below the baseline during systole, is measured and represents the peak systolic velocity of the lateral mitral annulus. Healthy subjects generally have a velocity of more than 7.5 cm/s; though placing the cutoff at 10 cm/s makes this measurement even more specific [14]. In LV failure, this velocity is almost always below 5 cm/s (Fig. 4.7). This method offers ease of performance, reliability, and relative load independence as its advantages [8]. Additionally, no endocardial tracing is needed [15]. However, a calcified mitral valve can confound the measurement, since the lack of movement of a calcified annulus can underestimate LV function. It is also not accurate in the presence of a prosthetic mitral valve.

Advanced Methods

Three-Dimensional (3D) EF Calculation

This modality correlates well with the gold standard, cardiac MRI, and with recent improvements in technology, can be carried out relatively quickly [16]. It involves post-capture processing of a full volume dataset, typically with multi-beat acquisition (Fig. 4.8; Video 4.1). Since it involves visualization of the entire LV, wall motion anomalies and altered LV geometry typically do not impact the results. It is,

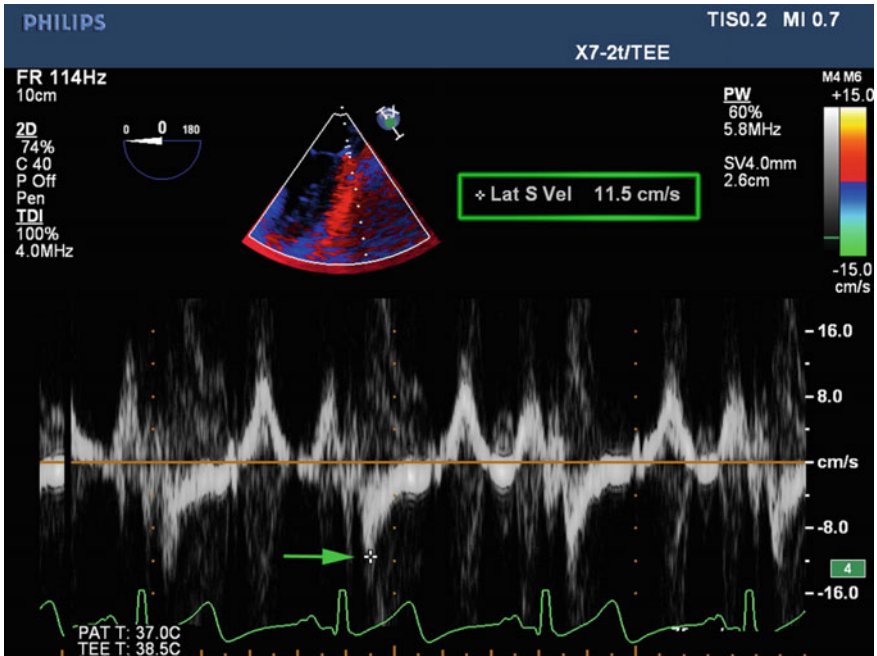


Fig. 4.7 Tissue Doppler-based calculation of the lateral mitral annular velocity during systole (*green arrow*). The measurement is obtained below the baseline since during systole the annulus movement is downward toward the apex

however, technically difficult and time consuming and relies heavily on excellent 2D visualization in all segments. In the presence of arrhythmias, multi-beat acquisition is not possible, degrading the temporal resolution, as well as the accuracy of the results. The details of this methodology are outside the scope of this text, but can be found elsewhere [16]. Data regarding its efficacy continues to emerge, and this may become the modality of the future as workflow becomes less complicated [17].

Global Longitudinal Strain (GLS)

Strain measurement is a load-independent variable that uses the analysis of individual bright spots on the ultrasound image (speckles), and calculates the myocardial deformation and strain based on the separation of individual speckles during the cardiac cycle. Strain can be calculated using tissue Doppler as well, but speckle tracking is becoming the preferred modality [3]. The complete methodology of this technique is outside the scope of this text, but it is important to note that normal strain values are reported as negative numbers, since systolic myocardial

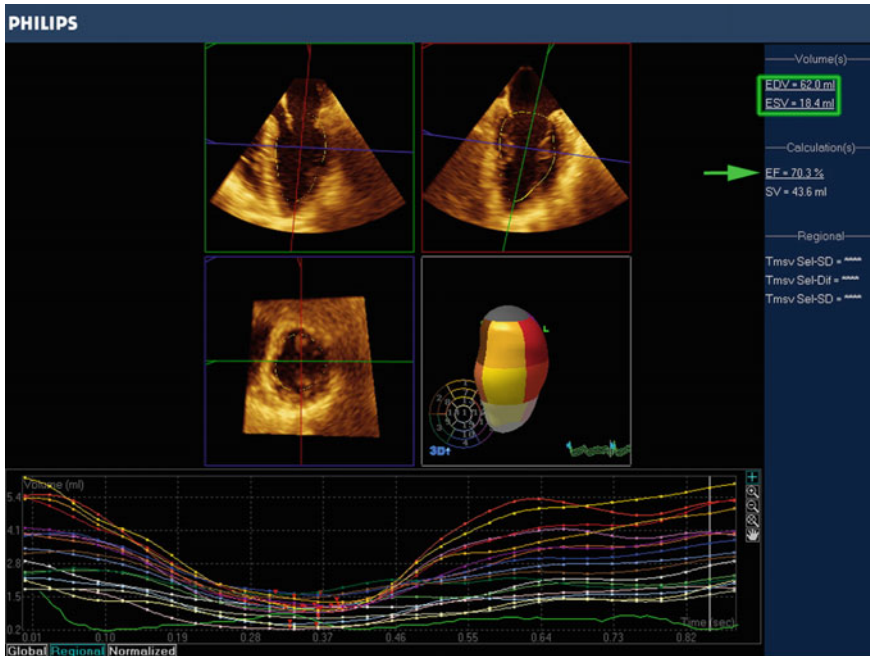


Fig. 4.8 Calculation of EF using 3D echocardiography. The *individual lines* represent contribution from all LV segments. The global EF is displayed on the *panel to the right* (green arrow)

length is shorter than diastolic (due to the contraction). Scant data and time-consuming calculations have prevented widespread use and it remains primarily a research tool [5] (Fig. 4.9; Video 4.2).

Measurements of Left Ventricular Geometry

Left Ventricular Wall Thickness

The wall thickness of the LV during diastole is a measure of its hypertrophy, and is generally measured from the transgastric short axis view at the level of the papillary muscles. Both 2D and M-mode can be used. The septal wall is measured from the endocardium to the endocardium, whereas the inferolateral wall is measured from the endocardium to the epicardium. Sources of error can include measurement of an oblique section of the wall, a regional aneurysm, and inclusion of pericardial structures or papillary muscles. While LV hypertrophy does not contribute directly to abnormal systolic function, its identification may indicate the presence of LV diastolic dysfunction. Normal values are 0.6–1.0 cm and 0.6–0.9 cm for males and females, respectively [5].

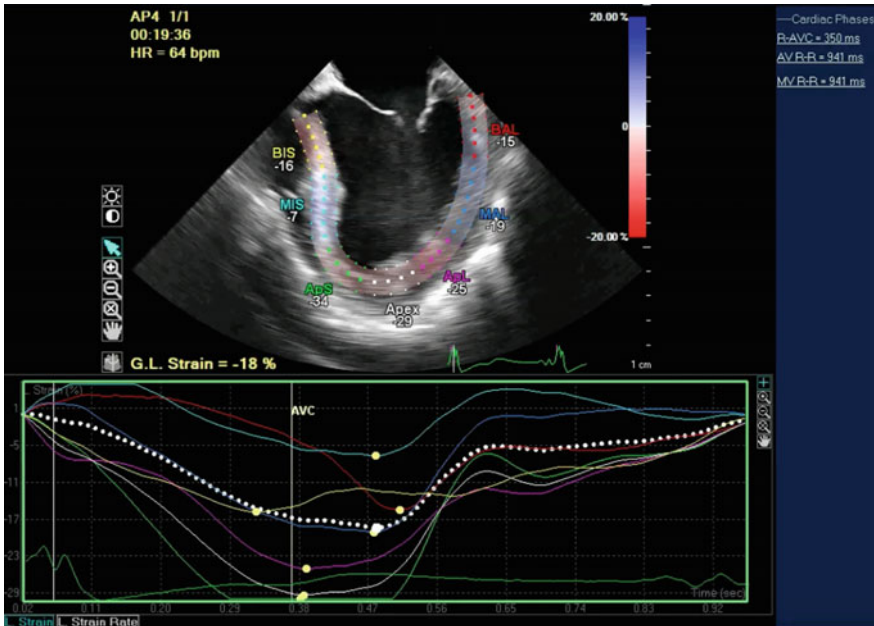


Fig. 4.9 Measurement of global longitudinal strain using speckle tracking in 2D echocardiography. The *individual lines* represent individual segments, while the *white dotted line* represents the global summation of individual strain measurements

LV Mass Calculation

While not typically utilized in noncardiac surgery, LV mass is a strong predictor of adverse cardiovascular events and can be calculated from M-mode, 2D, or 3D images. M-mode is generally used for screening large population samples, whereas 2D methodology is used in cases of altered LV geometry and for serial measurements in one patient. All measurements are done in diastole and the myocardial volume calculated is then multiplied by its density (1.05 g/ml) to calculate the mass. The 2D measurements are made from the transgastric mid-papillary short axis view, with the LV mass calculated by the formula recommended by the ASE [1]:

$$\text{LV mass} = 0.8 \times 1.04 \times \left[(\text{LVIDd} + \text{PWT} + \text{IVS})^3 - \text{LVIDd}^3 \right] + 0.6$$

LVID = LV internal diameter in diastole

PWT = Inferolateral (posterior) wall thickness

IVS = Interventricular septum thickness

The ASE recommends the 2D modality for this purpose since 2D is easy and the most studied technique, but 3D estimation of LV mass has been validated as well

[5, 16]. This technique suffers from the fault of overestimating the LV mass and the need for good beam alignment. The normal values range from 67–162 g for women and 88–224 g for men [1]. A calculation of relative wall thickness (based on the ratio of posterior wall thickness and the diastolic LV diameter) can help differentiate between concentric and eccentric hypertrophy.

Conclusion

For the basic echocardiographer, the main use of transesophageal echocardiography is to identify causes or potential causes of hemodynamic instability. Identifying changes in LV systolic function and being able to quantify changes in EF can be valuable for management in the perioperative setting. While there are many methods available to evaluate LV systolic function, it is important to remember the limitations of each method. The modified Simpson's method may give a more accurate result because it takes into account two planes of the LV, however, it can be time consuming and tedious. It also requires distinct endocardial borders. Simpler methods such as fractional shortening, fractional area change, the rate of rise of ventricular pressure, and tissue Doppler imaging may be easier to acquire in time-sensitive situations, but may not take into account altered LV geometry and regional wall motion. The results also do not directly equate to an EF and may simply tell you whether LV systolic function is normal or abnormal. With experience over time, visual estimation of EF can approximate the calculated EF and may be all that is needed in an emergent situation.

References

1. Lang R, Bierig M, Devereux R, et al. Recommendations for chamber quantification. *Eur J Echocardiogr.* 2006;7(2):79–108.
2. Parameashwar J, Keegan J, Sparrow J, Sutton GC, Poole-Wilson PA. Predictors of prognosis in severe chronic heart failure. *Am Heart J.* 1992;123(2):421–6.
3. Thomas JD, Popović ZB. Assessment of left ventricular function by cardiac ultrasound. *J Am Coll Cardiol.* 2006;48(10):2012–25.
4. Fukuta H, Little WC. The cardiac cycle and the physiologic basis of left ventricular contraction, ejection, relaxation, and filling. *Heart Fail Clin.* 2008;4(1):1–11.
5. Lang RM, Badano LP, Mor-Avi V, et al. Recommendations for cardiac chamber quantification by echocardiography in adults: an update from the american society of echocardiography and the European association of cardiovascular imaging. *J Am Soc Echocardiogr.* 2015;28(1):1–39.e14.
6. Foster E, Cahalan MK. The search for intelligent quantitation in echocardiography: “Eyeball”, “trackball” and beyond. *J Am Coll Cardiol.* 1993;22(3):848–50.
7. Skarvan K, Lambert A, Filipovic M, Seeberger M. Reference values for left ventricular function in subjects under general anaesthesia and controlled ventilation assessed by two-dimensional transoesophageal echocardiography. *Eur J Anaesthesiol.* 2001;18(11):713–22.

8. Gottdiener J, Bednarz J, Devereux R, et al. American Society of Echocardiography recommendations for use of echocardiography in clinical trials: a report from the American Society of Echocardiography's guidelines and standards committee and the task force on echocardiography in clinical trials. *J Am Soc Echocardiogr.* 2004;17(10):1086–119.
9. Nijland F. Early prediction of improvement in ejection fraction after acute myocardial infarction using low dose dobutamine echocardiography. *Heart.* 2002;88(6):592–6.
10. McGowan JH, Cleland JGF. Reliability of reporting left ventricular systolic function by echocardiography: A systematic review of 3 methods. *Am Heart J.* 2003;146(3):388–97.
11. Bargiggia GS, Bertucci C, Recusani F, et al. A new method for estimating left ventricular dP/dt by continuous wave Doppler-echocardiography validation studies at cardiac catheterization. *Circulation.* 1989;80(5):1287–92.
12. Koliass TJ, Aaronson KE, Armstrong WF. Doppler-Derived dP/dt and -dP/dt predict survival in congestive heart failure. *J Am Coll Cardiol.* 2000;36:1594–9. *ACC Current Journal Review.* 2001;10(2):43–44.
13. Yu C-M, Sanderson JE, Marwick TH, Oh JK. Tissue doppler imaging. *J Am Coll Cardiol.* 2007;49(19):1903–14.
14. Kadappu KK, Thomas L. Tissue doppler imaging in echocardiography: value and limitations. *Heart, Lung Circ.* 2015;24(3):224–33.
15. Marwick TH. Techniques for comprehensive two dimensional echocardiographic assessment of left ventricular systolic function. *Heart.* 2003;89(90003):2iii–8.
16. Kühl HP, Bucker A, Franke A, et al. Transesophageal 3-Dimensional echocardiography. In vivo Determination of left ventricular mass in comparison with magnetic resonance imaging. *J Am Soc Echocardiogr.* 2000;13(3):205–15.
17. Monaghan MJ. Role of real time 3D echocardiography in evaluating the left ventricle. *Heart.* 2006;92(1):131–6.

Chapter 5

Regional Ventricular Function

Tariq Naseem, MD and Timothy M. Maus, MD, FASE

Abstract One of the most useful applications of intra-operative 2D transesophageal echocardiography (TEE) in noncardiac surgery is qualitative assessment of myocardial function in acutely unstable patients. When hemodynamic instability occurs intraoperatively, TEE can serve as an adjunct to other modalities in diagnosing or ruling out an ischemic event. In fact, compared to other monitoring methods, regional wall motion abnormality (RWMA) observed on echocardiography is the most sensitive method for early detection of ischemic changes in the heart. In noncardiac surgery, this can be especially useful in patients with no existing invasive or detailed monitoring that shows a sudden change in clinical status. Knowledge of normal coronary anatomy and its myocardial distribution is key in determining the location of an ischemic event. Recognizing the attributes of a wall motion abnormality such as decreased wall excursion or decreased wall thickening is key in diagnosing ischemic events, while recognizing that not all wall motion abnormalities are ischemic events (e.g., pacing effect).

Keywords Ischemia · Infarction · Regional wall motion abnormalities · Ischemic detection · Coronary artery · Coronary blood flow

Electronic supplementary material The online version of this chapter (doi:[10.1007/978-3-319-34124-8_5](https://doi.org/10.1007/978-3-319-34124-8_5)) contains supplementary material, which is available to authorized users.

T. Naseem, MD (✉) · T.M. Maus, MD, FASE
Department of Anesthesiology, University of California San Diego,
9300 Campus Pointe Drive, #7651, La Jolla, San Diego, CA 92037-7651, USA
e-mail: tariqnaseem@gmail.com

T.M. Maus, MD, FASE
e-mail: tmaus@ucsd.edu

Regional Ventricular Function

One of the most useful applications of intra-operative transesophageal echocardiography (TEE) in noncardiac surgery is qualitative assessment of myocardial function in acutely unstable patients. When hemodynamic instability occurs intraoperatively, TEE can serve as an adjunct to other modalities in diagnosing or ruling out an ischemic event. In fact, compared to arterial blood pressure, EKG changes and pulmonary artery catheter measurements, regional wall motion abnormality (RWMA) observed on echocardiography is the most sensitive method for early detection of ischemic changes in the heart [1–3]. In noncardiac surgery, this can be especially useful in patients with no existing invasive or detailed monitoring that may exhibit a sudden change in clinical status. This chapter will describe the normal coronary anatomy and distribution including echocardiography correlates, as well as describe normal and abnormal regional myocardial function. Finally, caveats of regional wall motion abnormalities and complications of ischemic events are discussed.

Coronary Anatomy

Basic understanding of the vascular anatomy of the heart is key to interpreting TEE images of ventricular wall function (Fig. 5.1). There is a significant amount of variability in the normal coronary circulation; however, the most common anatomic presentation is discussed here. The heart is supplied by two major arteries: left coronary artery (LCA) and the right coronary artery (RCA). They arise from just above the left and right coronary cusps of the aortic valve respectively. The LCA bifurcates into the left anterior descending (LAD) and the left circumflex (LCx) arteries. Less commonly, the LCA trifurcates into an LAD, LCx, and a ramus intermedius (RI). The LAD descends anteriorly toward the apex traveling within the anterior interventricular groove. Its major branches are the diagonal branches that supply the free wall of the LV and the septal branches that feed into the interventricular septum. Therefore, the LAD is commonly responsible for blood flow to the apex as well as the anterior, anterolateral, and anteroapical walls of the left ventricle (LV).

The LCx takes a path along the atrioventricular groove towards the left side after emerging from the LCA and travels posteriorly towards the crux, the meeting point of the interventricular septum (IVS) and atrioventricular groove. In 15–20 % of patients, the LCx supplies the posterior descending artery (PDA), resulting in left dominant circulation. In these patients, left coronary circulation supplies the interventricular septum (IVS) and often the atrioventricular (AV) node. Along its path toward the crux, the LCx provides branches termed obtuse marginal (OM) arteries which supply the lateral wall of the LV. Therefore, the LCx is commonly responsible for the blood flow to the lateral aspect of the LV and the infero-apical aspect in patients with left heart dominant circulation. It's notable that the LCx shares supply to the lateral wall with the LAD anterolaterally and RCA inferolaterally.

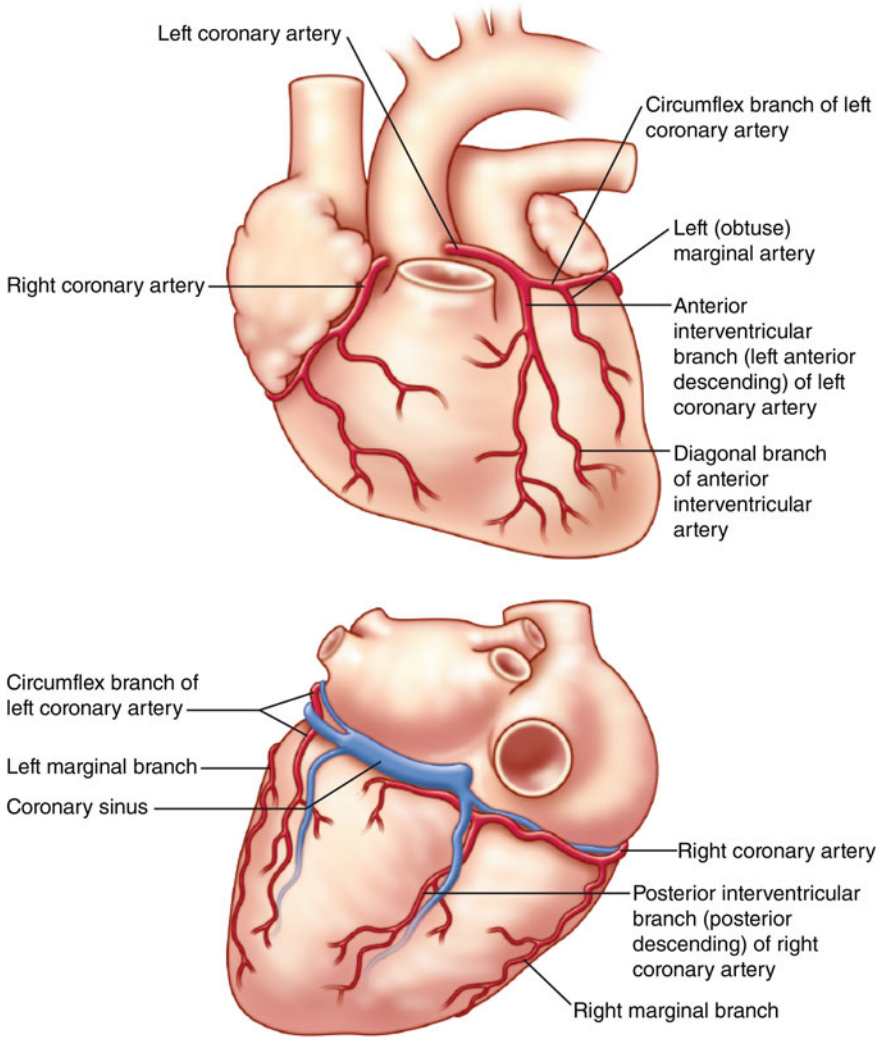


Fig. 5.1 Coronary artery anatomy. **a** Anterior aspect; **b** Posterior aspect

The RCA travels in the right atrioventricular groove and turns posteriorly toward the crux. The RCA provides branches, termed acute marginal arteries, supplying the right ventricle free wall, sinoatrial (SA) and AV node. In 80–85 % of patients, the RCA terminates as the PDA supplying the inferior IVS. This constitutes a right dominant circulation. The RCA is also responsible for providing blood flow to the inferior wall of the LV. Therefore, the RCA is commonly responsible for the blood flow to the right ventricle and inferior wall of the LV as well as the infero-apical aspect of the LV in patients with right heart dominant circulation. It shares supply with the LAD to the inferoseptal wall of the left ventricle.

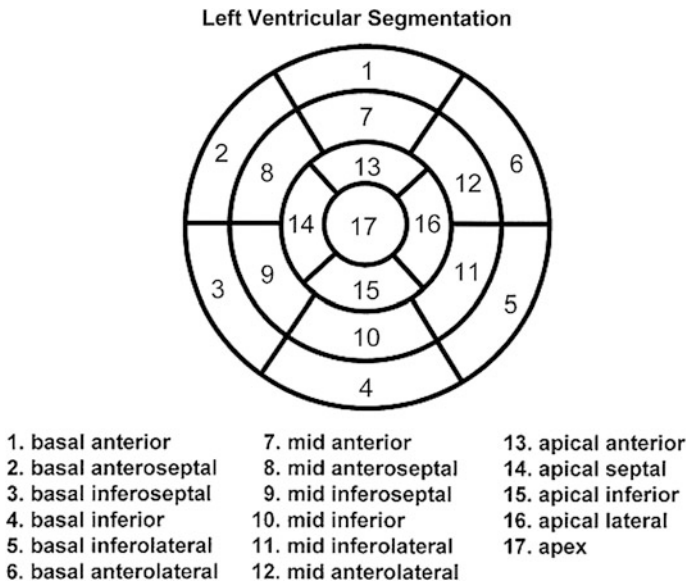


Fig. 5.2 Seventeen-segment model. Reprinted from [14]

The segmentation of the heart is intended to match that of the coronary blood supply. While several segmentation models exist, recent guidelines suggest the use of a 17-segment model [4] (Fig. 5.2). The purpose of the model is to improve communication between specialties (e.g., cardiologists, intensivists, anesthesiologists, etc.) as well as between imaging modalities (e.g., echocardiography, nuclear medicine imaging). In this model, the LV is broadly divided into basal, mid-cavitary, and apical areas which are then divided into segments. The basal and mid-cavitary areas are divided similarly into anterior, inferior, anteroseptal, inferoseptal, anterolateral and inferolateral segments. The apical area is divided into four segments: anterior, inferior, septal, and lateral with the apical cap comprising the seventeenth segment. The echocardiography correlation of which segments are perfused by certain coronary arteries is discussed below.

Application of Coronary Topography to Echocardiography

Coronary perfusion to the myocardium can be assessed qualitatively with echocardiography, with attention to the coronary blood flow distribution to each segment as described. This concept is depicted in Fig. 5.3 which describes the common perfusion anatomy of the heart utilizing TEE views. The overlap in the depicted coronary supply is explained by normal anatomic variability in coronary perfusion (e.g., the inferolateral wall may be supplied by the LCx in some patients

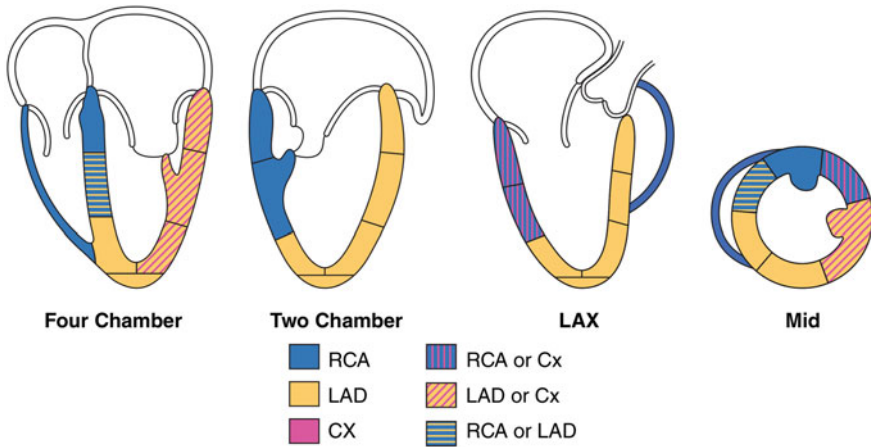


Fig. 5.3 Transesophageal views with the representative coronary blood supply and segmentation. The views are the midesophageal (ME) four chamber, ME two chamber, ME long axis (LAX), and transgastric midpapillary short axis (Mid). *RCA* right coronary artery, *LAD* left anterior descending artery and *Cx* left circumflex artery

while by the RCA in others). This can present as variability in the appearance of the wall motion abnormality during an ischemic event. In one patient, an LAD lesion may lead to a WMA of just the anterior and anteroseptal wall, while in another patient the WMA may extend to cover the entire anterior half of the LV (inclusive of the anterolateral wall). Therefore, it is important when assessing for WMAs in a busy perioperative setting to not become over-focused on interpretation of the “normal” coronary distribution.

The transesophageal echocardiography examination for ischemia involves transgastric and midesophageal imaging. The transgastric midpapillary short axis view is useful in that in one view all three coronary distributions are represented: the LAD covers the anterior, anterolateral (shared with LCx), anteroseptal and inferoseptal (shared with RCA) segments, the LCx covers the anterolateral and inferolateral segments, while the RCA typically covers the inferior wall, inferolateral (shares with LCx), inferoseptal (shares with LAD) segments and the right ventricle (Fig. 5.4). While it is convenient that all three coronary distributions are observed in one view, it is important to recognize that this view may not detect all wall motion abnormalities (e.g., basal and apical segments). One study noted that the midpapillary short axis view only recognized 17 % of wall motion abnormalities, while adding other short axis orientations as well as long axis imaging significantly increased the recognition of WMAs [5]. Therefore, midesophageal imaging with various omniplane orientations is necessary and complementary to imaging of the transgastric midpapillary short axis view.

When envisioning the myocardial walls in the midesophageal views, it is helpful to think of the direction of the omniplane “slice” through a transgastric view (Fig. 5.5). Therefore, the ME four-chamber view will present the septal and lateral walls, the ME two-chamber view will present the anterior and inferior walls, while

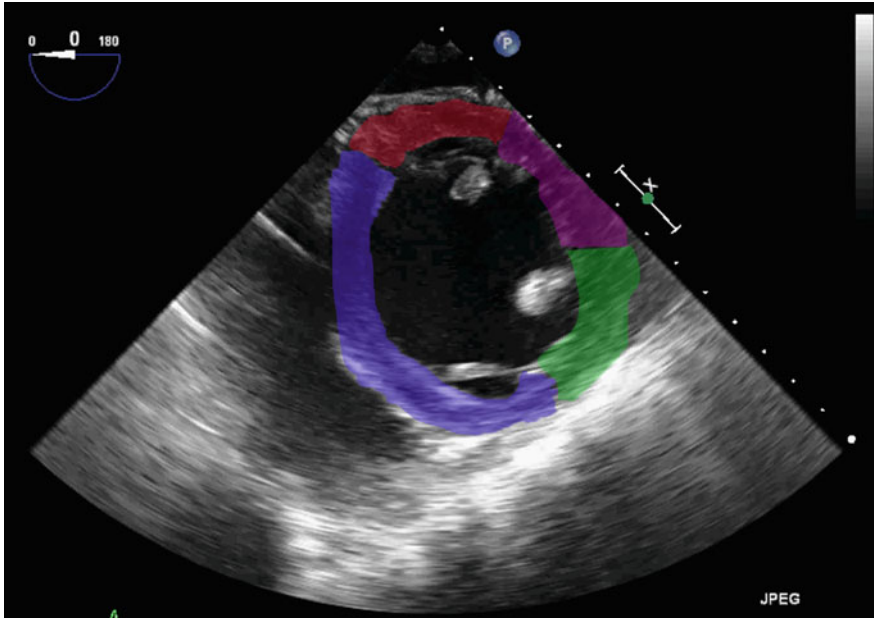
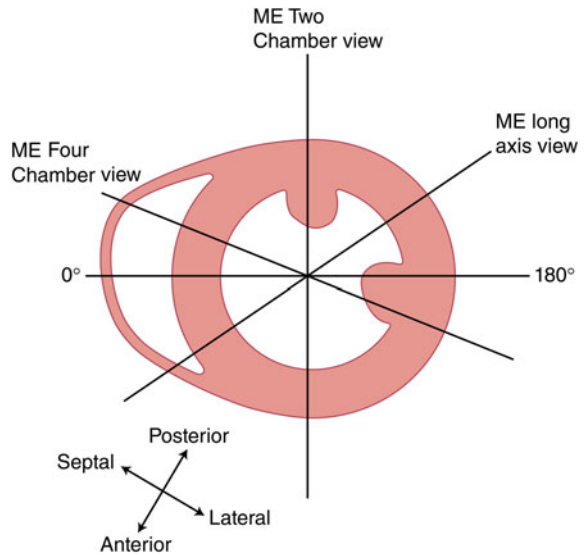


Fig. 5.4 Transgastric midpapillary short axis view with overlaying color representation of coronary perfusion. *Blue* left anterior descending artery (LAD), *red* right coronary artery (RCA), *purple* RCA or left circumflex artery (LCx), *green* LAD or LCx

Fig. 5.5 Transgastric midpapillary short axis representation with indications of the walls visualized in respective midesophageal views



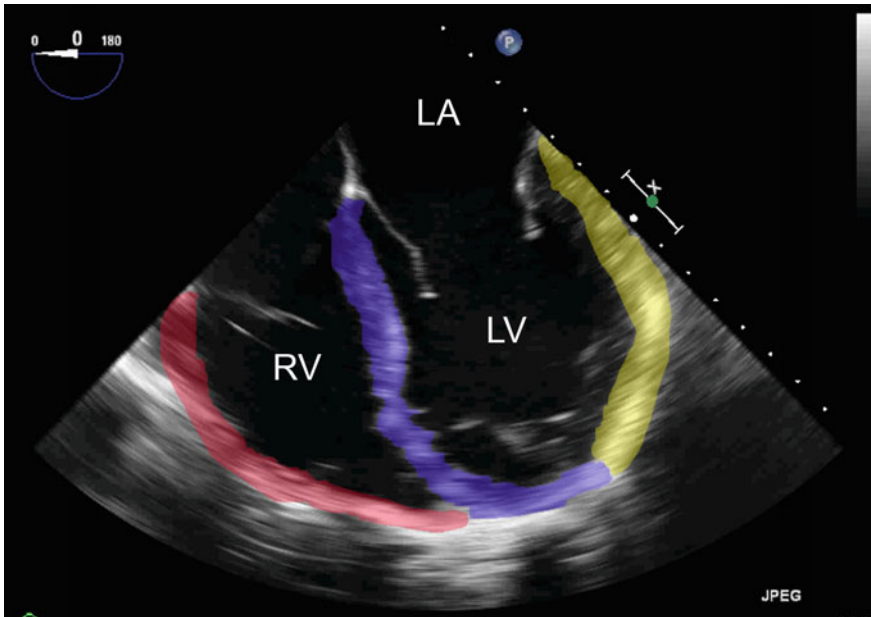


Fig. 5.6 Midesophageal four-chamber view with overlaying color representation of coronary perfusion. *Blue* left anterior descending artery (LAD), *red* right coronary artery (RCA), *yellow* left circumflex artery (LCx). LA left atrium; LV left ventricle; RV right ventricle

the ME long axis will present the anteroseptal and inferolateral walls. The advantage of midesophageal views is the ability to display basal, mid-cavitary and apical segments of a particular wall, allowing detection of abnormalities beyond just the mid-cavitary segments.

The midesophageal four-chamber view is an excellent view for ischemia detection due to its ability to observe all three coronary distributions in one view including observation of basal, mid-cavitary, and apical function (Fig. 5.6). Depending upon the flexion of the probe, the septum is most commonly perfused by the LAD, the lateral wall is perfused by the LCx, while the RV is perfused by the RCA. Flexion or retroflexion of the probe in a midesophageal four-chamber view allows the observation of anteroseptal/anterolateral and inferoseptal/inferolateral segments, respectively.

Rotation of the omniplane to roughly 90° develops the ME two-chamber view (Fig. 5.7). This view nicely displays the basal, mid-cavitary and apical segments of the anterior and inferior walls. In the majority of patients, the anterior wall and LV apex will be covered by the LAD while the inferior wall will be perfused by the RCA. Right heart dominant patients will have the LV apex covered by the RCA and LAD.

The ME long axis view, at approximately 120° of omniplane rotation, will develop the anteroseptal and inferolateral walls of the LV, while also displaying a portion of left ventricular outflow tract (LVOT) (Fig. 5.8). The wall motion of basal, mid-cavitary and apical segments should be assessed. The LAD typically

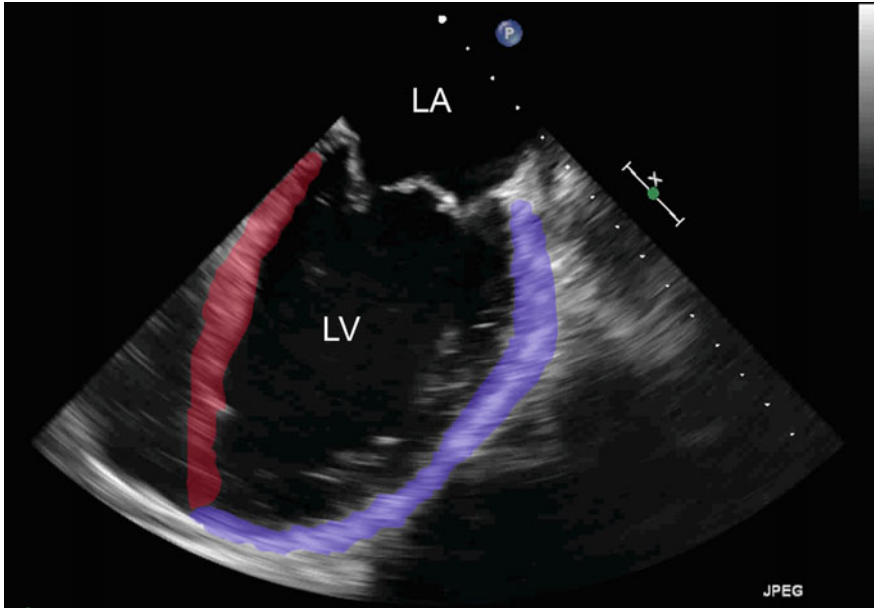


Fig. 5.7 Midesophageal two-chamber view with overlaying color representation of coronary perfusion. *Blue* left anterior descending artery (LAD), *red* right coronary artery (RCA). *LA* left atrium; *LV* left ventricle

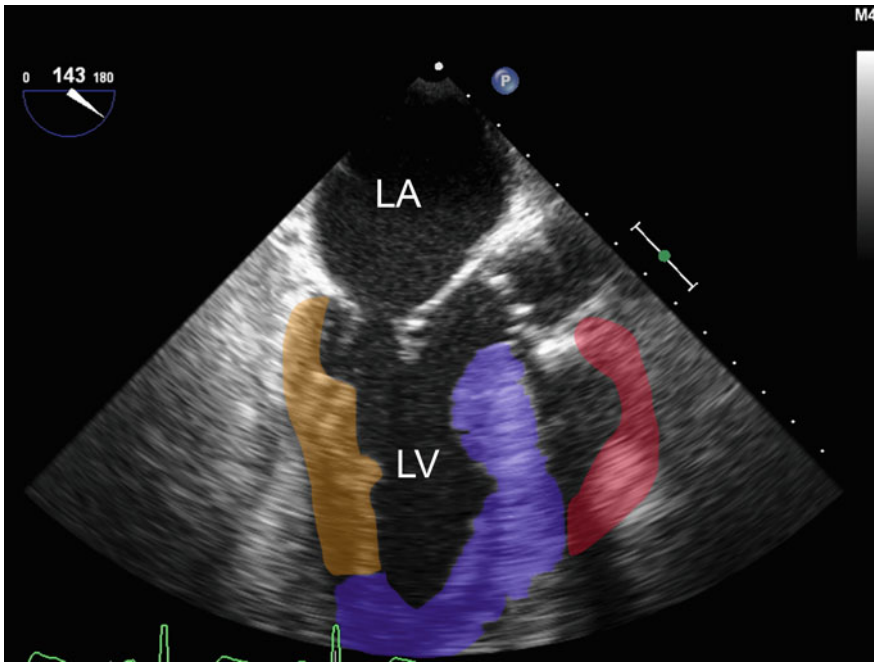


Fig. 5.8 Midesophageal long axis view with overlaying color representation of coronary perfusion. *Blue* left anterior descending artery (LAD), *red* right coronary artery (RCA), *orange* RCA or left circumflex artery (LCx). *LA* left atrium; *LV* left ventricle

covers the anteroseptal wall and apex, while the RCA or LCx perfuses the inferolateral wall. The RVOT is perfused by the RCA. Again, the combination of midesophageal and transgastric imaging allows the echocardiographer to provide a composite analysis of wall motion throughout all segments of the LV and RV.

Grading of Regional Wall Motion Abnormalities

Regional Ventricular Function	
2D	<ul style="list-style-type: none"> • Left ventricular systolic assessment (Chap. 4) • Regional wall motion abnormalities • Systolic wall thickening • Concentric myocardial movement • M-mode assessment • Dilated LV with chronic ischemic changes
CFD	<ul style="list-style-type: none"> • New onset mitral regurgitation
Spectral	<ul style="list-style-type: none"> • Worsening diastolic function (Chap. 9) • Worsening pHTN

LV left ventricle, *pHTN* pulmonary hypertension

Regional myocardial function can be quantified on the basis of observed wall thickening and endocardial motion of the myocardial segment. These two measurements can be graded separately and each segment should be analyzed in multiple views, ensuring that an appreciation of thickening and motion be obtained for all 17 segments. During systolic contraction, normal healthy myocardial tissue should thicken and also move concentrically toward the center of the left ventricular cavity by more than 30 %. A reduction below this level of thickening or excursion rate constitutes as hypokinesis (Video 5.1) (Table 5.1). Akinesis is the near complete cessation of any wall movement along with absent or minimal thickening of the wall (Fig. 5.9; Videos 5.2 and 5.3). Significant ischemia or frank infarction can

Table 5.1 Grading of RWMA

Grade	Endocardial motion (%)	Wall thickening (%)
Normal or hyperkinetic	>30 %	30–50 %
Hypokinesis	10–30 %	<30 %
Akinesis	None	Absent or minimal thickening
Dyskinesia	Outward movement	Systolic stretching or thinning (e.g., aneurysm)

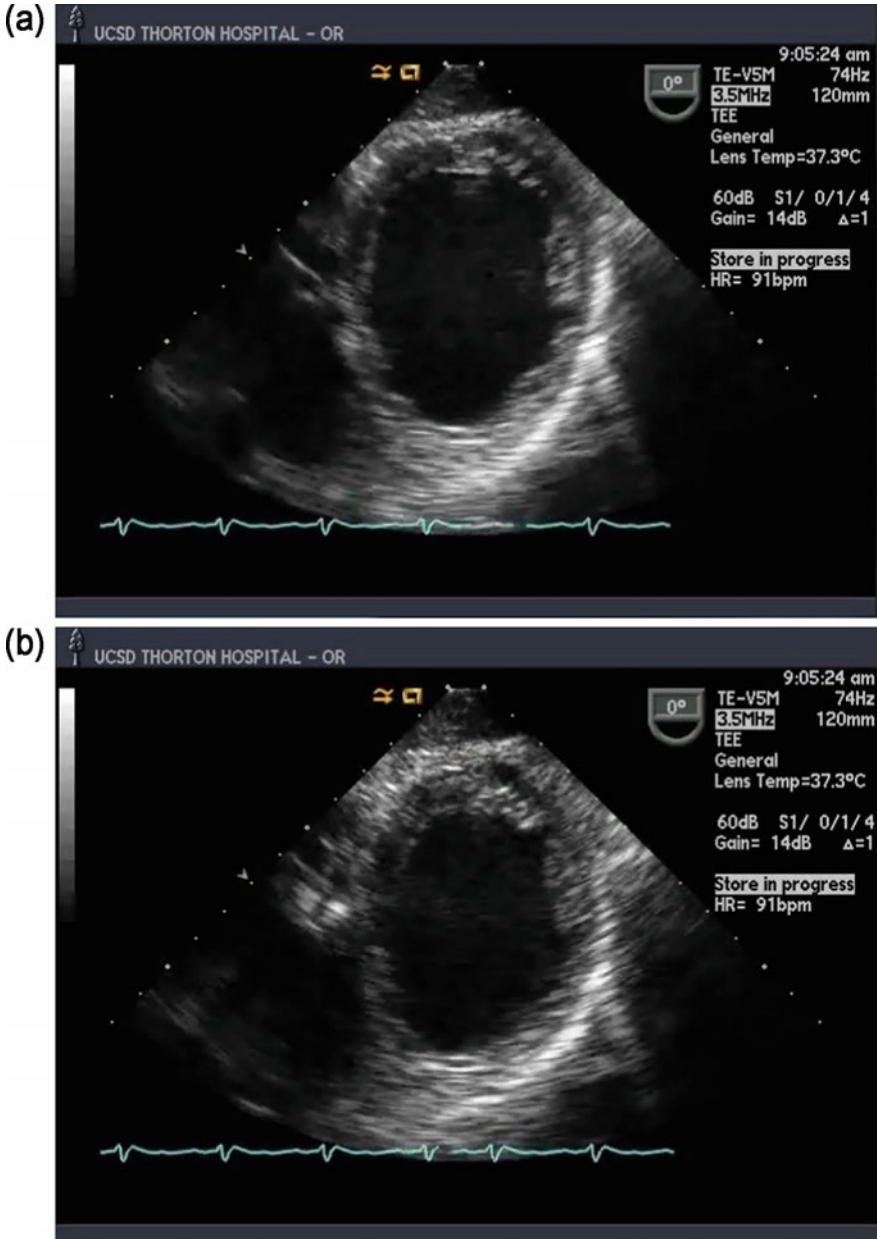


Fig. 5.9 Transgastric midpapillary short axis view in a patient with an akinetic anterior wall secondary to a left anterior descending lesion (LAD). Note the lack of thickening and central wall excursion in the anterior portion of the left ventricle. **a** Diastole. **b** Systole

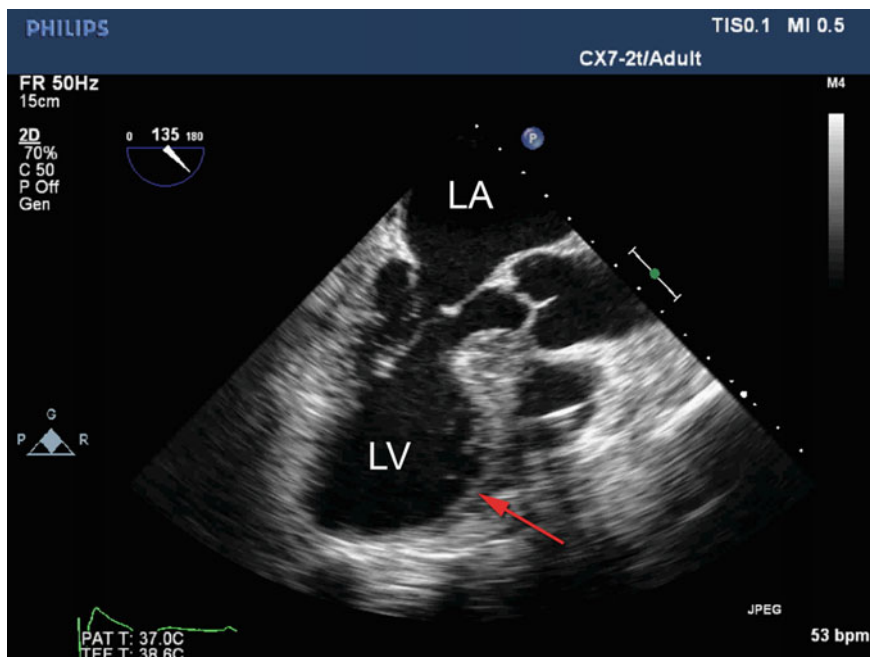


Fig. 5.10 Mid esophageal long axis view in a patient with a prior anterior myocardial infarction, now with a resultant anteroseptal left ventricular aneurysm (*red arrow*). LA left atrium; LV left ventricle

lead to akinesia. Finally, dyskinesia is seen when the myocardial wall moves in the opposite outward direction during contraction with thinning of the myocardium (Video 5.4). Recent American Society of Echocardiography (ASE) guidelines have classified an LV aneurysm (i.e., focal LV dilation) under the category of akinesia or dyskinesia [4] (Fig. 5.10; Video 5.5).

There are some caveats to interpreting RWMA in that all that does not move is not necessarily ischemia. There may be regional differences in wall motion due to anatomic location. For example, the basal portion of the anteroseptal wall often contracts toward the left ventricular outflow tract (LVOT) as opposed to direct concentric contraction. This may give the appearance of a hypokinetic segment. Additionally, there is interventricular septal dependence between the LV and RV, such that RV dysfunction may cause septal RWMA (see Chap. 8). This septal flattening may be interpreted as septal akinesia or dyskinesia. Other causes of non-ischemic RWMA include abnormal conduction (e.g., pacing or bundle branch block), post-pericardiotomy (e.g., abnormal septal bounce), and hemodynamic changes (e.g., acute loading changes and anesthetic-induced myocardial depression). Finally, since the myocardium is contiguous and not 17 discrete segments, abnormal motion in one segment can “tether” additional segments. This can cause the interpretation of RWMA in segments that may have normal perfusion.

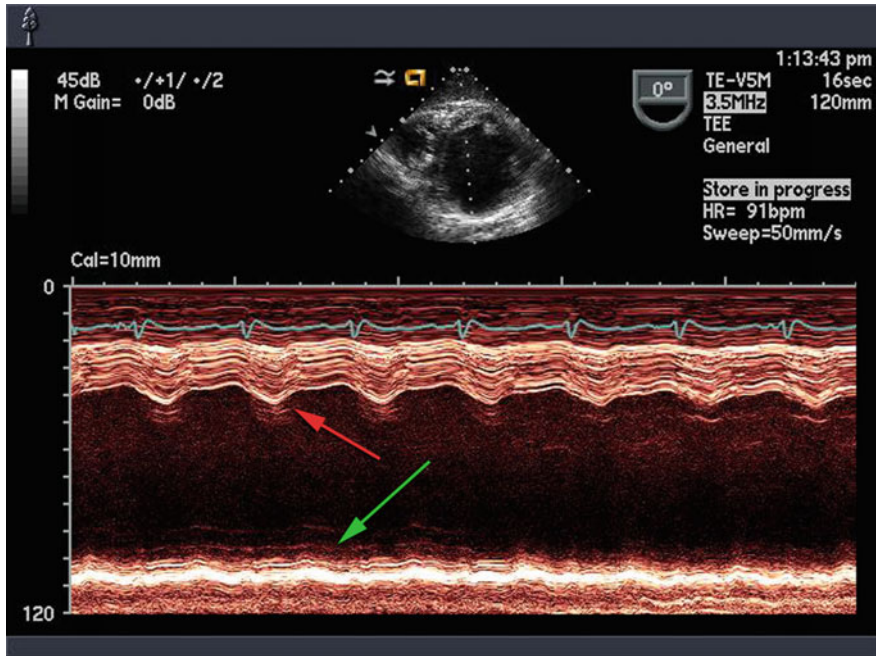


Fig. 5.11 M-mode imaging in a transgastric midpapillary short axis view. The *red arrow* indicates the systolic thickening and wall excursion of the inferior wall. The *green arrow* indicates the akinetic anterior wall

Therefore, it is imperative to integrate the echocardiographic findings clinically before instituting therapy for an abnormal myocardial wall motion.

With the understanding of coronary blood supply and its echocardiographic correlation, it is important to have an approach to the exam when focusing on ischemic changes. A standard approach of evaluating the basal, mid-cavitary, and apical segment in each midesophageal view as well as transgastric short axis imaging is helpful. Unlike other pathologies, wall motion abnormalities generally do not benefit from color flow Doppler (CFD) or spectral Doppler interrogation and therefore, detection largely rests upon two-dimensional interrogations. However, the implementation of M-mode two-dimensional imaging can prove quite helpful; M-mode provides a single ultrasound pathway displayed on a graph format with depth on the Y axis and time on the X-axis. A transgastric midpapillary short axis view with the M-mode cursor through the inferior and anterior walls will demonstrate wall motion with excellent temporal resolution (Fig. 5.11).

Complications from Myocardial Ischemia

While ischemia typically manifests on echocardiography as a RWMA, ischemic damage can lead to other complications which may be detected echocardiographically. These can largely be categorized into reversible changes, which will resolve with return of coronary blood flow, and irreversible changes which are typically related to infarction and result in permanent structural damage.

Reversible secondary changes include diastolic dysfunction, stunned myocardium, and mitral regurgitation. As diastology is an energy-dependent function, diastolic dysfunction is a common occurrence with new ischemia. As explained further in Chap. 9, diastolic dysfunction is a dynamic process where patients may shift from varying degrees of diastolic function. For example, a patient with normal diastology experiencing an acute ischemic event will progress to impaired relaxation. With restoration of coronary blood flow, their diastolic profile may improve back to normal.

Stunned myocardium refers to cardiac tissue that has experienced an ischemic insult and despite restoration of blood flow, still has transient persistent dysfunction. This is commonly seen after coronary artery bypass grafting surgery where an aortic cross clamp and a cardioplegic state has resulted in a brief ischemic insult that requires inotropes until the reperfused myocardium recovers. Stunned myocardium differs from hibernating myocardium, which is a portion of cardiac tissue that is chronically underperfused (e.g., long-term coronary artery disease). In an attempt to preserve structural integrity, the contractility in hibernating myocardium is reduced [6]. Stunned myocardium benefits from exogenous inotropy and time while hibernating myocardium will benefit from revascularization.

As discussed in Chap. 6, the mitral apparatus consists not just of the mitral valve itself but also the supporting annulus, the left atrium, papillary muscles as well as the ventricular walls attached to the papillary muscles. There are two supporting papillary muscles, the anterolateral and posteromedial muscles that attach to the mitral valve via multiple chordae. Myocardial ischemia can lead to the cessation of blood flow supplying the papillary muscles or to the myocardial segments underlying those papillary muscles. Dysfunction of either the papillary muscle or underlying segment will lead to abnormal motion of the papillary muscle, chordae, and attachments to the mitral valve leaflets. This leaflet restriction leads to malcoaptation and mitral insufficiency (Fig. 5.12; Video 5.6). The posteromedial papillary muscle is at greater risk due to its single blood supply from the RCA (in right dominant patients), as opposed the anterolateral papillary muscle which has a dual blood supply from the LAD and LCx circulations. It is therefore especially prudent to evaluate the mitral valve in the setting of ischemic insult to the RCA territory (e.g., when inferior and/or inferoseptal wall motion abnormalities are evident). The converse is true: new mitral insufficiency should prompt the search for evidence of ischemia (e.g., RWMA).

Irreversible secondary changes, which do not immediately recover with restoration of blood flow, include papillary muscle rupture, ischemic ventricular

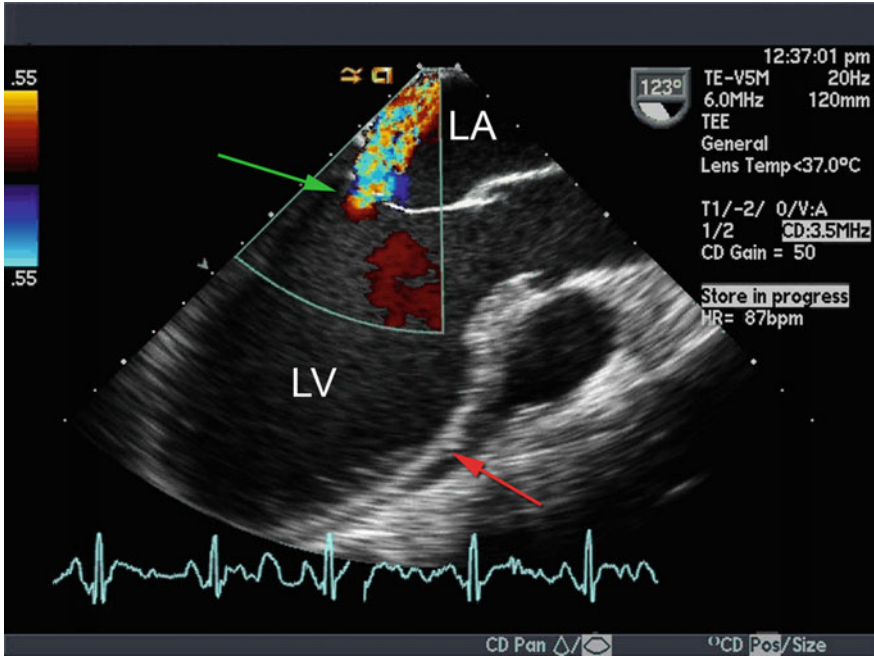


Fig. 5.12 Mid esophageal long axis view in a patient with an acute LAD ischemic event and significant ischemic MR (*green arrow*). Note the lack of thickening during systole of the anteroseptal wall (*red arrow*). LA left atrium; LV left ventricle

septal defects, ventricular free wall rupture, ventricular dilation, and aneurysm formation. Papillary muscle rupture is an extension of the papillary muscle dysfunction previously described, with significant hemodynamic and functional consequences. As mentioned above, this is most commonly seen with the posteromedial papillary muscle that has the RCA as a single feeding vessel, as opposed to the anterolateral papillary muscle that is supplied by both LAD and LCx [7]. Frank infarction of the territory including the papillary muscle may lead to rupture and separation of the papillary head. Papillary muscle rupture is a surgical emergency requiring an urgent evaluation for possible mitral valve replacement [8].

The most serious complication of myocardial infarction may be ventricular rupture, which includes both septal and ventricular free wall rupture. Ventricular free wall rupture is more common and is one of the most fatal outcomes of an acute myocardial infarction [9–11]. Both pathologies can be diagnosed effectively with TEE with the addition of CFD. Using CFD, turbulent blood flow can be seen moving from the ventricular cavity into the pericardial space in the case of free wall rupture. Likewise, in the setting of septal rupture, blood flow can be seen moving from the LV into the right ventricle, creating a left-to-right shunt. If there is pre-existing pulmonary hypertension or elevated right-sided pressures, the septal

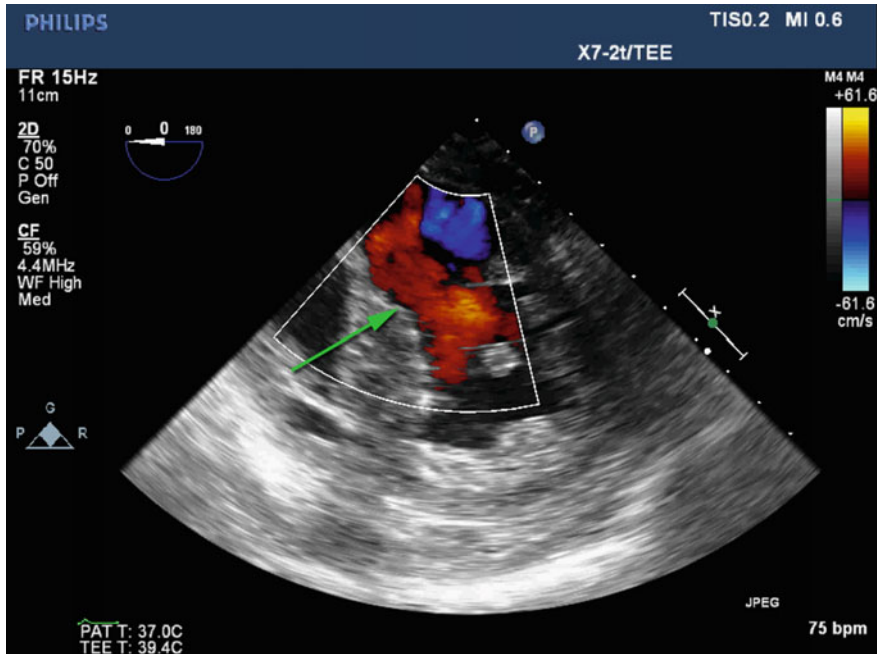


Fig. 5.13 Transgastric midpapillary short axis view with color flow Doppler in a patient status post inferior myocardial infarction and inferior wall rupture (*green arrow*). Note the contained rupture with flow exiting the ventricular cavity

rupture can then cause a right-to-left shunt and hypoxia and cyanosis may ensue (Fig. 5.13; Video 5.7).

Left ventricular remodeling and dilatation resulting in myocardial dysfunction is frequently observed after an acute myocardial infarction [12]. With chronic ischemia, the dilation and loss of contractile function leads to an echocardiographic presentation similar to non-ischemic cardiomyopathy. This can be evaluated using TEE by looking at parameters such as left ventricular end-diastolic and end-systolic volumes (LVEDV, LVESV), ejection fraction (LVEF), and myocardial strain models (see Chap. 4).

The incidence of aneurysm formation has decreased in recent years with the evolution of improved therapy. However, up to 15 % of patients may suffer from a left ventricular aneurysm after an acute myocardial infarction [13]. Over 70 % of aneurysms are seen in the anterior wall and apex due to an LAD infarct. Another 10–15 % of patients may show involvement of inferior wall due to RCA disease. Pseudoaneurysms are mostly seen after inferior wall myocardial infarctions. On TEE, an outpouching of the myocardial segment is seen with no contraction or systolic contribution. See Fig. 5.10; Video 5.5.

Conclusion

The interpretation of myocardial function and detection of an ischemic event is a fundamental application of TEE. In a busy clinical setting that demands a quick and definitive diagnosis, echocardiography's ability to detect regional wall motion abnormalities before other diagnostic tools makes it an indispensable resource. Recognizing the attributes of a wall motion abnormality such as decreased wall excursion or decreased wall thickening is key to ischemia detection, while recognizing that not all wall motion abnormalities are ischemic events (e.g. pacing effect). Additionally, echocardiography allows the interrogation of secondary changes, both reversible and irreversible.

References

1. Beaupre PN, Kremer PF, Cahalan MK, et al. Intraoperative detection of changes in left ventricular segmental wall motion by transesophageal two-dimensional echocardiography. *Am Heart J.* 1984;107:1021.
2. van Daele ME, Sutherland GR, Mitchell MM, et al. Do changes in pulmonary capillary wedge pressure adequately reflect myocardial ischemia during anesthesia? A correlative preoperative hemodynamic, electrocardiographic, and transesophageal echocardiographic study. *Circulation.* 1990;81:865.
3. Akchurin RS, Tkachuk LM, Lepilin MG, et al. Intraoperative transesophageal echocardiography for detection of myocardial ischemia. *Herz.* 1993;18:372.
4. Lang RM, Badano LP, Mor-Avi V, et al. Recommendations for cardiac chamber quantification by echocardiography in Adults: An update from the American Society of Echocardiography and the European Association of Cardiovascular Imaging. *J Am Soc Echocardiogr* 2015, 28:1–39.
5. Rouine-Rapp, et al. Detection of intraoperative segmental wall-motion abnormalities by transesophageal echocardiography: The incremental value of additional cross sections in the transverse and longitudinal planes. *Anesthesia & Analgesia* 1996, 83:6, 1141–1148.
6. Braunwald RA. Kloner: The stunned myocardium: Prolonged, postischemic ventricular dysfunction. *Circulation.* 1982;66:1146–1149 (tmn).
7. Otsuji Y, Handschumacher MD, Kisanuki A, et al. Functional mitral regurgitation. *Cardiologia.* 1998;43:1011–6.
8. Russo A, Suri RM, Grigioni F, Roger VL, Oh JK, Mahoney DW, et al. Clinical outcome after surgical correction of mitral regurgitation due to papillary muscle rupture. *Circulation.* 2008;118:1528–34.
9. Reeder GS. Identification and treatment of complications of myocardial infarction. *Mayo Clin Proc.* 1995;70:880.
10. López-Sendón J, González A, López de Sá E, et al. Diagnosis of subacute ventricular wall rupture after acute myocardial infarction: sensitivity and specificity of clinical, hemodynamic and echocardiographic criteria. *J Am Coll Cardiol.* 1992;19:1145.

11. Figueras J, Alcalde O, Barrabés JA, et al. Changes in hospital mortality rates in 425 patients with acute ST-elevation myocardial infarction and cardiac rupture over a 30-year period. *Circulation*. 2008;118:2783.
12. Giannuzzi P, Temporelli PL, Bosimini E, et al. Heterogeneity of left ventricular remodeling after acute myocardial infarction: results of the Gruppo Italiano per lo Studio della Sopravvivenza nell'Infarto Miocardico-3 Echo Substudy. *Am Heart J*. 2001;141:131.
13. Glower DG, Lowe EL. Left ventricular aneurysm. In: *Cardiac surgery in the adult*. Edmunds LH (ed) McGraw-Hill, New York 1997. p. 677.
14. Douglas PS, et al. ACCF/ACR/AHA/ASE/ASNC/HRS/NASCI/RSNA/SAIP/SCAI/SCCT/SCMR 2008 health policy statement on structured reporting in cardiovascular imaging. *J Am Coll Cardiol*. 2009;53(1):76–90.

Chapter 6

Mitral Valve

Liem Nguyen, MD and Neal Gerstein, MD

Abstract The mitral valve is a complex apparatus consisting of the annulus, leaflets, chordae tendineae, papillary muscle, myocardium, and its attendant chambers, the left atrium and ventricle. The function and competency of the mitral valve apparatus is intricately dependent on the structural integrity and coordination of each and all of its components. Structural or functional abnormalities contributing to mitral stenosis or mitral regurgitation and post-procedural changes can be evaluated with transesophageal echocardiography (TEE). With advancements in technology and the evolution of three-dimensional (3D) imaging, TEE is a necessary tool and modality for evaluating the mitral valve perioperatively.

Keywords Transesophageal echocardiography (TEE) • Mitral valve • Mitral regurgitation • Mitral stenosis • Proximal isovelocity surface area (PISA)

Anatomy and Function of the Mitral Valve Apparatus

The mitral valve apparatus consists of the annulus, leaflets, chordae tendineae, papillary muscle, myocardium, and its attendant chambers, the left atrium and ventricle (Fig. 6.1). Essentially, the entire left heart contributes to the function of

Electronic supplementary material The online version of this chapter (doi:[10.1007/978-3-319-34124-8_6](https://doi.org/10.1007/978-3-319-34124-8_6)) contains supplementary material, which is available to authorized users.

L. Nguyen, MD (✉)

Department of Anesthesiology, University of California San Diego, 9300 Campus Point Drive #7651, San Diego, CA 92037-7651, USA
e-mail: liem@ucsd.edu

N. Gerstein, MD

Department of Anesthesiology, University of New Mexico, 2211 Lomas Blvd NE, Albuquerque, NM 87106, USA
e-mail: ngerstein@gmail.com

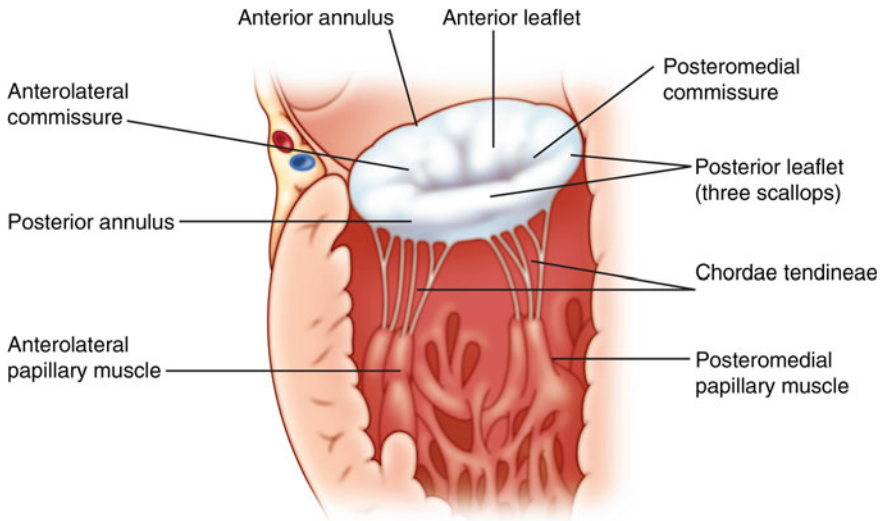


Fig. 6.1 Components of the mitral valve apparatus

the mitral valve. The function and competency of the mitral valve apparatus is intricately dependent on the structural integrity and coordination of each and all of its components [1–4].

The bicuspid mitral valve is composed of two anatomically distinct leaflets, the anterior and posterior leaflet. The anterior leaflet is located in close juxtaposition to the left and noncoronary cusps of the aortic valve, separated by a thin piece of tissue termed the aorto-mitral curtain. The posterior leaflet is unique in that it contains three identifiable subunits called scallops. In the commonly utilized Carpentier description of mitral valve anatomy, the scallops are labeled from anterior to posterior as P1, P2, and P3. While smaller in area than the anterior leaflet, the posterior leaflet subtends approximately two-thirds of the circumference of the annulus [1, 2, 4]. By contrast, the larger anterior leaflet in surface area only covers about one-third of the circumference of the annulus. The anterior leaflet is devoid of individual scallops, providing a smooth surface designed to promote systolic ejection of blood into the left ventricular outflow tract. Despite a lack of scallops, the Carpentier description notes segments A1, A2, and A3 which correspond to the posterior scallops (e.g., P1 coapts with A1, P2 coapts with A2, etc.) (Fig. 6.2). The anterior and posterior leaflets adjoin at two distinct points near the edges of the annulus (described below), which are termed the anterolateral and posteromedial commissures (Fig. 6.2) [2–4]. As an interdependent unit, the anterior and posterior leaflets come together and contact each other during systole to form a coaptation line resembling a semicircle (Figs. 6.2 and 6.3) [2, 3, 5]. The mitral leaflets are circumferentially supported by a fibrous-tissue reinforced ring structure referred to as the mitral annulus. The mitral annulus geometrically resembles a hyperbolic paraboloid or saddle shape, and anatomically serves as the attachment points for

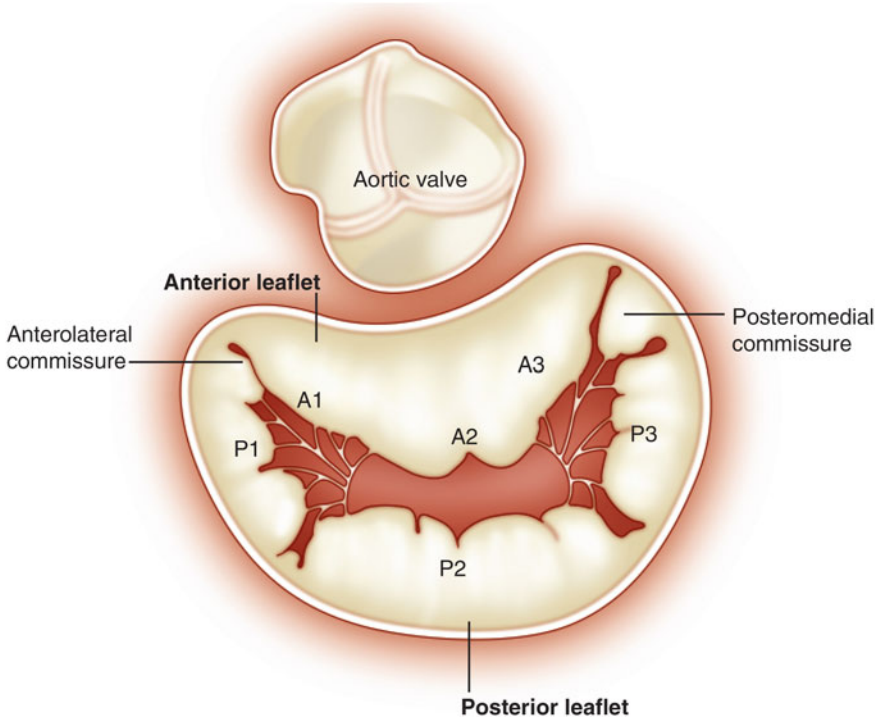


Fig. 6.2 Nomenclature of the bicuspid mitral valve according to the Carpentier classification

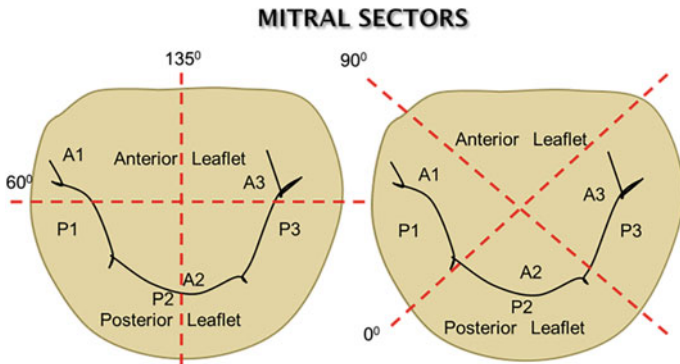


Fig. 6.3 Mitral sectors with representative leaflet segments expected from the midesophageal transesophageal views

both mitral leaflets. While a saddle has two high points (the front and back of a saddle) and two low points (the sides of the saddle), a mitral valve is similarly shaped with high and low points. The anterior–posterior (front to back) axis of the annulus defines the higher peak to peak dimension whereas the lateral axis (side to side or commissure to commissure) defines the trough to trough dimension, which is positioned at a lower point (Fig. 6.4a, b; Video 6.1). The posterior aspect of the mitral annulus is structurally thinner and contains less fibrous support, lending it to be more prone to dilation and flattening compared to the more reinforced anterior portion of the mitral annulus. Overall, the unique geometry of the saddle-shaped annulus serves to reduce the tension on both of the mitral leaflets during systole [5–9]. Underneath the mitral leaflets emerges a complex network of chordae tendineae that attach to both leaflets. The chordae tendineae are attached to the anterolateral and posteromedial papillary muscles and contract in concert to prevent the prolapse of the mitral leaflets into the atrium during systole [1, 4]. In summary, the coordinated movements of the mitral valve apparatus results in the closure of the mitral valve during systole and prevention of regurgitant flow into the left atrium.

TEE Imaging of the Mitral Valve

Assessment of the mitral valve begins with two-dimensional imaging of the entire mitral apparatus (Fig. 6.5a–f; Videos 2.1–2.3, 2.13, 2.15, and 2.16) [2, 3, 10, 11]. This can be performed by first starting in the midesophageal four-chamber view and obtaining multiplane images of all components of the mitral apparatus [2, 3, 10, 12]. The leaflet subunits of the mitral valve can be individually viewed as a two-dimensional slice using the available sector planes of the TEE probe at various multiplane angles (Figs. 6.3 and 6.5a–f). Instructions for how to obtain the various views discussed in this chapter can be found in Chap. 2.

Midesophageal Four-Chamber View (ME Four-Chamber View)

In the ME four-chamber view at 0° (Figs. 6.3 and 6.5a; Video 2.1), the anterior leaflet appears on the left side of the screen whereas the posterior leaflet is visualized on the right of the screen. The ME four-chamber view is useful for obtaining a global evaluation of bileaflet motion and the corresponding changes that may occur as a result of volume stress in the upstream atrium and downstream ventricle. The ME four-chamber is also useful to evaluate the degree of mitral regurgitation using color flow Doppler [2, 3, 10].

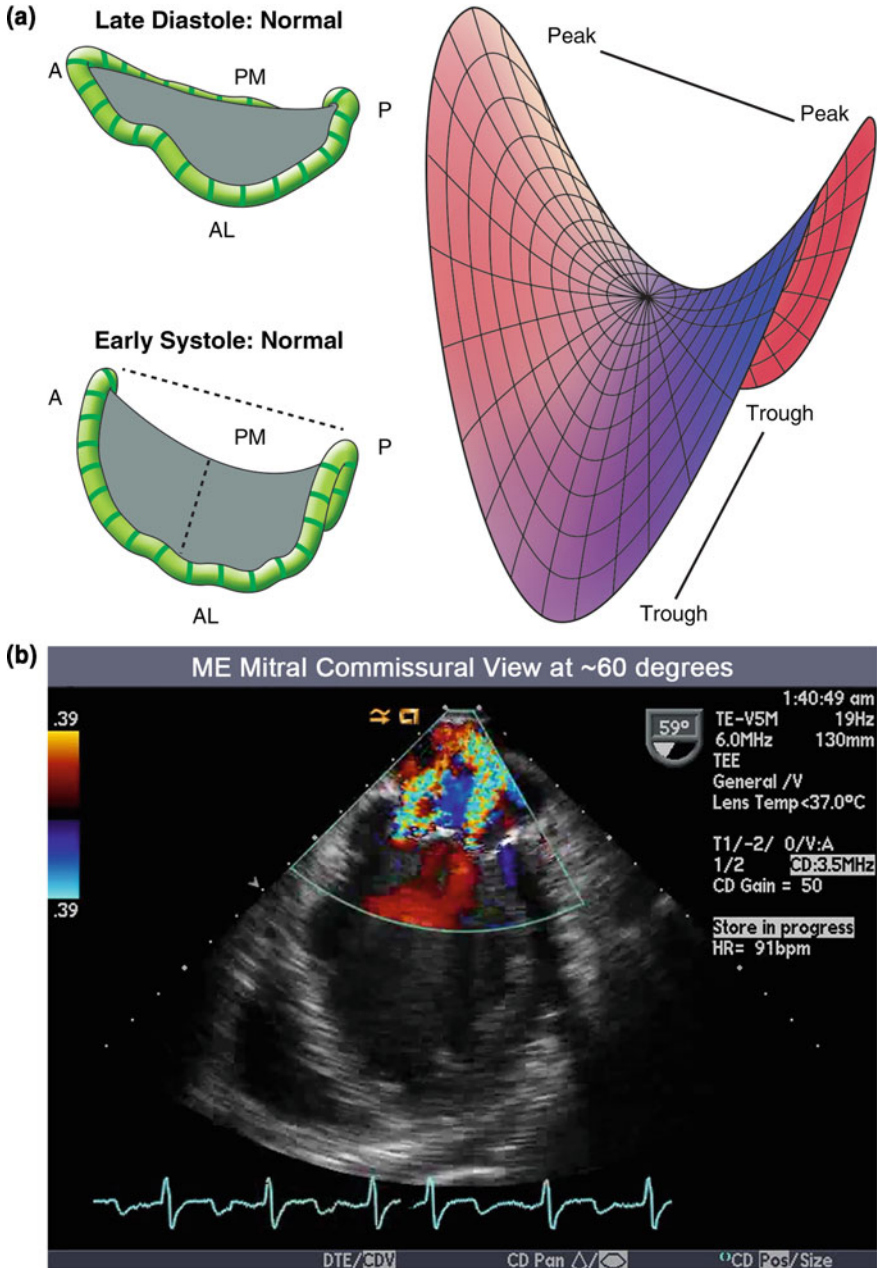


Fig. 6.4 a Rendition of mitral annulus depicting the characteristic saddle-shaped geometry. The anterior–posterior axis (ME LAX view) encompasses the peak to peak distance, whereas the lateral axis (ME mitral commissural view) corresponds to the trough to trough distance. b ME mitral commissural view with color flow Doppler demonstrating two distinct jets due to a sector plane that captures the two outer edges of the jet and omitting the central portion

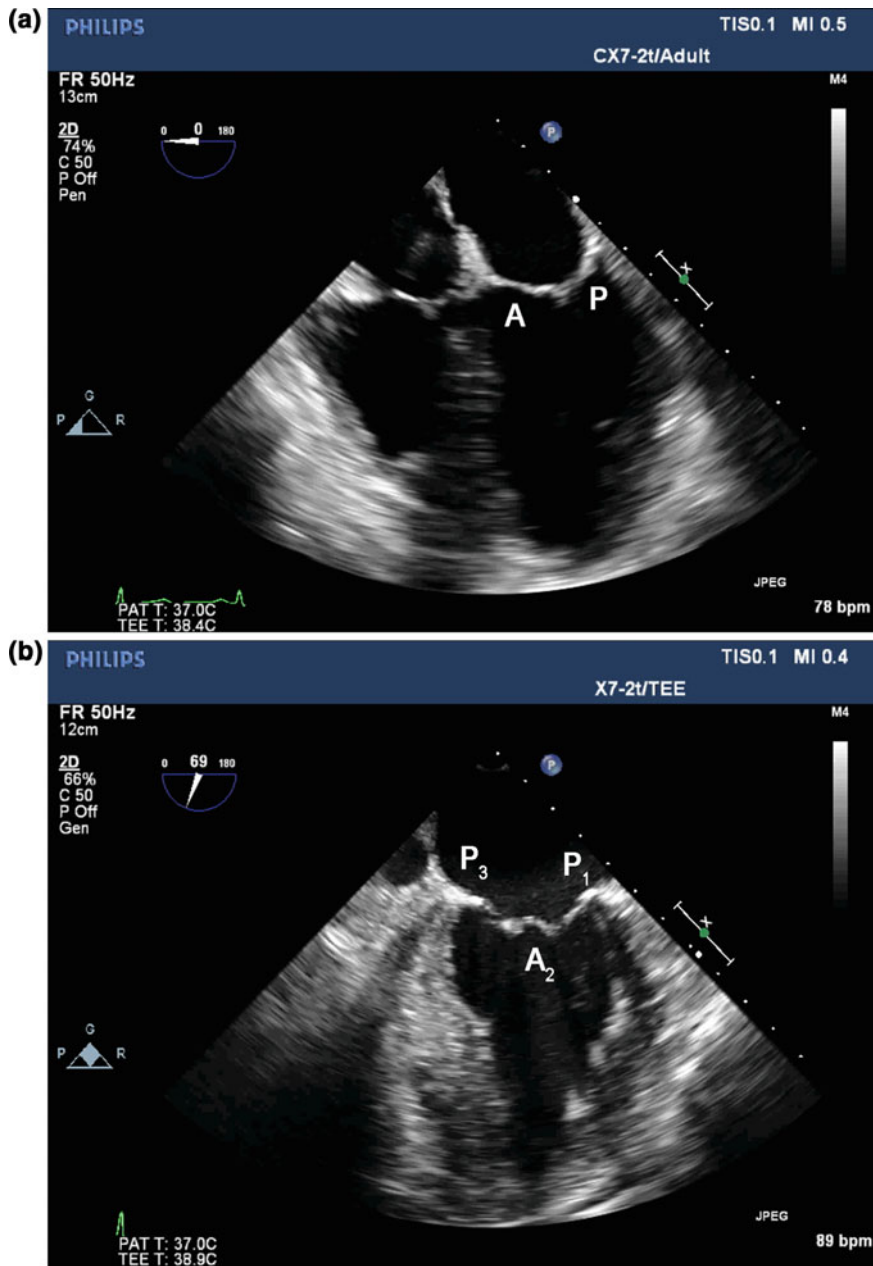


Fig. 6.5 TEE imaging of the mitral valve apparatus. **a** ME four-chamber view. **b** ME mitral commissural view. **c** ME two-chamber view. **d** ME LAX view. **e** TG basal SAX view. **f** TG two-chamber view. *A* anterior leaflet, *P* posterior leaflet

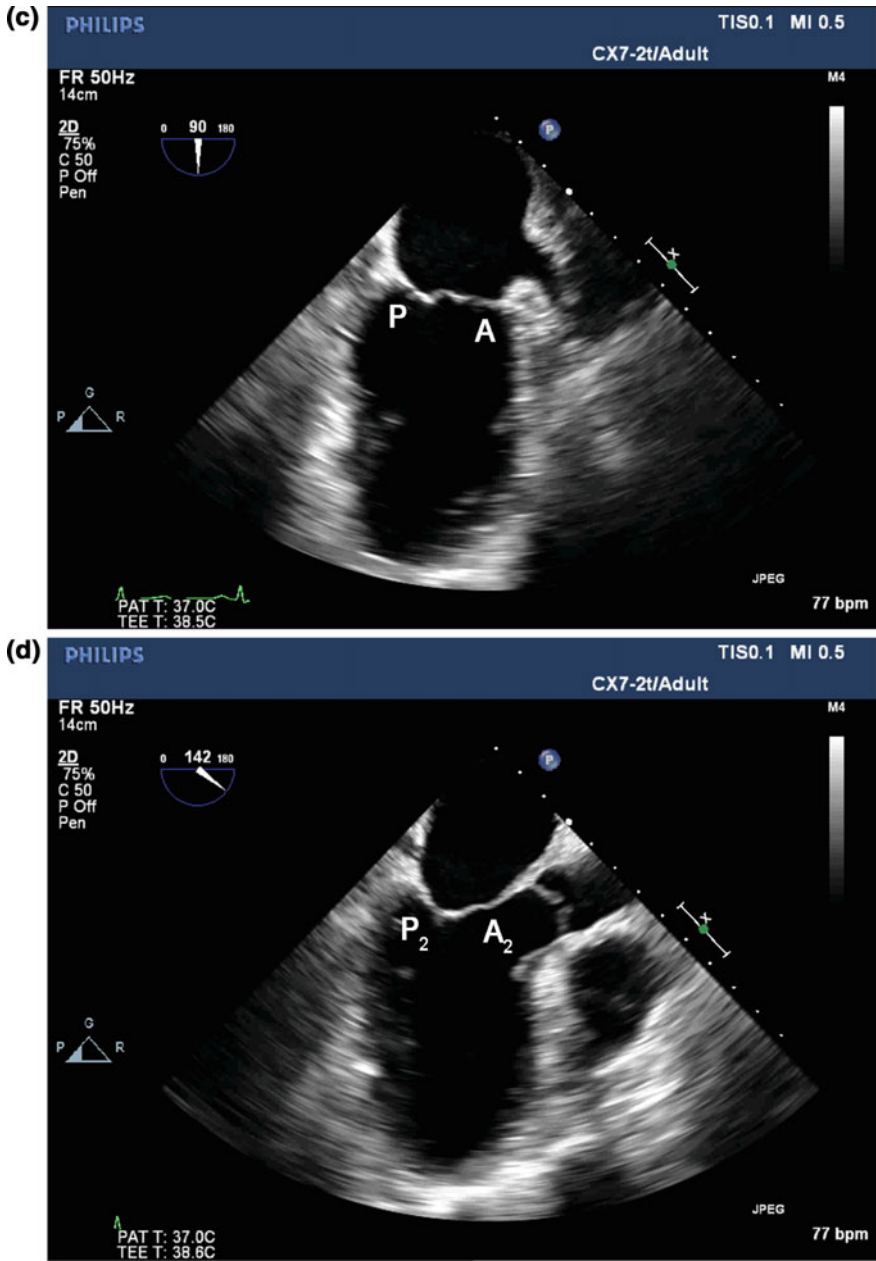


Fig. 6.5 (continued)

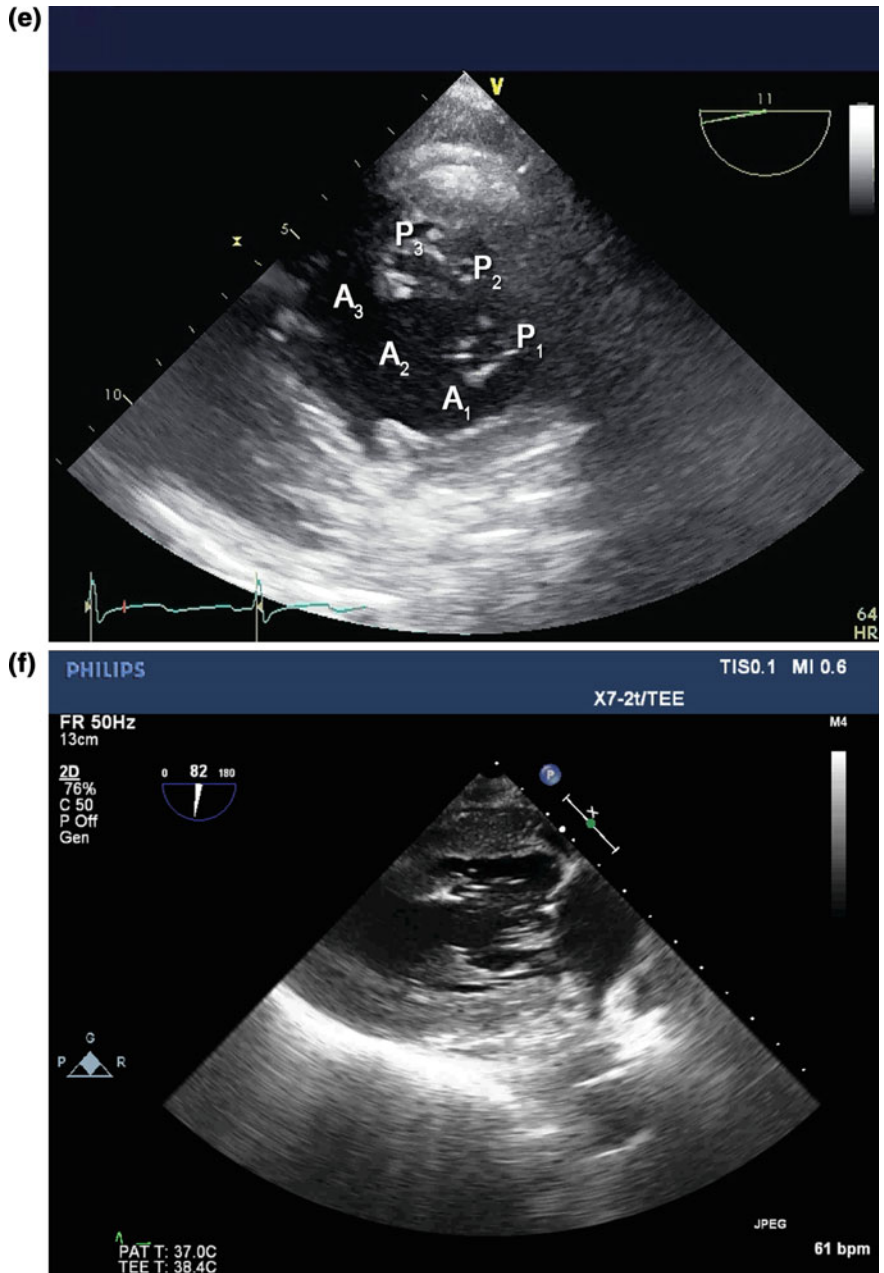


Fig. 6.5 (continued)

ME Mitral Commissural View

The ME mitral commissural view is obtained by starting at the ME four-chamber view and rotating the multiplane angle to approximately 45–60°. In this view of the mitral valve, the middle A2 segment is flanked by the P3 segment on the left and P1 segment on the right (Figs. 6.3 and 6.5b; Video 2.13) [2, 3, 10]. The ME mitral commissural view may also provide a view of the papillary muscles and their associated chordae tendineae. It is important to note that the ME mitral commissural view displays an imaging slice corresponding to a line that traverses the semicircle or curved coaptation point and the anterolateral and posteromedial commissures. Accordingly, Doppler color flow assessment of a regurgitant jet may appear as two distinct jets because the sector plane captures the two outer edges of the jet and omits the central portion (Fig. 6.4b; Video 6.1). This often results in the incorrect echocardiographic diagnosis of two distinct jets, when in fact the image merely represents the edges of one jet.

ME Two-Chamber View

The ME two-chamber view is obtained by rotating the multiplane angle to approximately 90° (Figs. 6.3 and 6.5c; Video 2.2). In this image plane, the anterior leaflet is positioned on the right and the posterior leaflet is on the left of the screen. The left atrial appendage and Coumadin ridge (a band of tissue separating the left atrial appendage and the left upper pulmonary vein) are often observed above and to the right of the anterior mitral leaflet. Withdrawing the probe from this position and turning slightly to the left often brings the left upper pulmonary vein into view, allowing for Doppler interrogation of left atrial inflow [2, 10].

ME Long-Axis View (ME LAX View)

The ME LAX view is obtained by increasing the multiplane angle to 120–140° until the aortic and mitral valve leaflets are seen opening and closing in the same image plane (Figs. 6.3 and 6.5d; Video 2.3) [2, 3, 10]. This imaging plane displays a slice of the mitral leaflets along the anterior–posterior dimension (A2–P2), perpendicular to the coaptation line. The A2 segment is displayed on the right of the screen nearest the aortic valve leaflets and the P2 segment appears on the left side of the screen. The ME LAX view allows for the echocardiographer to assess the anterior–posterior dimension of both the diameter of the mitral regurgitant jet and peak to peak distance of the mitral annulus (Fig. 6.4a). This view plane therefore offers a more accurate measurement of the width of the vena contracta, the narrowest part of a regurgitant jet at the level of the valve leaflets as measured by color flow Doppler, compared to other imaging planes [2, 3, 10].

Transgastric Basal Short-Axis View (TG Basal SAX)

The TG basal SAX view at 0° (Fig. 6.5e; Video 2.15) is obtained by either slightly withdrawing the probe or exerting anteflexion from the true transgastric midpapillary short-axis view of the left ventricle. The imaging plane is achieved when both the anterior and posterior mitral leaflets are visualized in a short axis, “fishmouth” view. The “fishmouth view” of the mitral valve allows for all the mitral segments to be viewed, providing a means to assess valve opening and closure from the left ventricular aspect. The TG basal SAX view may also reveal a ruptured chordae or flail segment from this vantage point. Moreover, color flow mapping of the regurgitant jet in the TG basal SAX view may reveal the origin of the coaptation defect and provide insight into the mechanism of regurgitation [3, 10].

TG Two-Chamber View

The TG two-chamber view at 90° (Fig. 6.5f; Video 2.16) provides a perpendicular scan plane that facilitates the assessment of the subvalvular apparatus (i.e., chordae tendineae and papillary muscle-LV wall complex) [10]. The anterolateral papillary muscle occupies a position furthest from the probe and the posteromedial papillary muscle is situated in the near field. This view is useful for evaluating the position and geometry of the papillary muscles, chordae tendineae and ventricular wall complex.

Mitral Regurgitation

Mitral regurgitation

2D	<ul style="list-style-type: none"> • Mitral leaflet motion (normal, excessive, restrictive) • Mitral calcification • Annular dimensions (dilated) • Left atrial enlargement, eccentric LV hypertrophy • LV wall motion abnormalities
CFD	<ul style="list-style-type: none"> • Qualitative assessment (Jet Area/LA Area ratio) • Coanda effect (wall hugging jet) • Vena contracta measurement
Spectral	<ul style="list-style-type: none"> • Pulmonary venous doppler (PWD) • Density of regurgitation jet profile (CWD) • PISA-based calculation of EROA

LV left ventricle, *LA* left atrium, *PWD* pulsed wave Doppler, *CWD* continuous wave Doppler, *PISA* proximal isovelocity surface area, *EROA* effective regurgitant orifice area

Although the final common pathway of an incompetent mitral apparatus is a regurgitant jet at the level of the leaflet tips due to a coaptation defect, a significant portion of MR is due to dysfunction of structures above and below the valve in the presence of normal leaflet motion [2, 3, 5, 13]. When considering the etiology or mechanism of MR, it may therefore be prudent to examine all the structures above and below the leaflets that comprise the mitral valve apparatus in order to fully characterize the mechanism. Furthermore, examination of leaflet motion according to Carpentier's classification can yield important clues into the mechanism of MR [2, 3]. The classification categorizes the mechanisms of MR into three types based upon the motion of the mitral valve leaflets: Type 1—normal leaflet motion; Type 2—excessive leaflet motion; Type 3—restricted leaflet motion. This categorization helps to organize the thought process around the types of MR as well as to help guide surgical therapy for the mitral valve.

MR associated with normal leaflet motion (Type 1) can be a result of mitral valve clefts, perforations, or most commonly annular dilation [2, 5]. The mitral annulus is reinforced by a network of fibroelastic tissue that serves to maintain the unique saddle-like geometry during systole (Fig. 6.4a) [5, 14–16]. Annular dilation, measured in the anterior–posterior dimension in the ME LAX view using caliper-based measurements, or distortion of the saddle-shaped geometry during systole may lead to a coaptation defect and represents an important mechanism of MR [6, 9, 16–20]. Left atrial enlargement (e.g., due to atrial fibrillation or ventricular dysfunction) and secondary annular dilation may contribute to MR in the setting of normal leaflet anatomy and motion. Dilation of the mitral annulus has also been implicated as a contributing etiology in ischemic MR [2, 3, 13, 19, 21, 22].

The ventricular myocardium, anterolateral and posteromedial papillary muscles, and network of chordae tendineae provide the strong foundation required for normal leaflet motion and competency (Fig. 6.1). The interpapillary distance (lateral distance) and location of the papillary muscles (i.e., apical displacement) in relation to the ventricular wall and coaptation point plays a significant role in the overall competency of the mitral valve complex [4, 5]. The major responsibility of the papillary muscle-chordae tendineae complex is to regulate leaflet movement. Excessive leaflet motion (Type 2), such as in the presence of a ruptured chord, results in leaflet prolapse and acute MR demonstrating that the papillary muscle and chordae tendineae work together to prevent leaflet displacement into the left atrium.

Abnormalities in leaflet anatomy such as seen in degenerative disease and endocarditis, may also result excessive leaflet motion, a coaptation defect and subsequent MR [2]. Degenerative mitral disease (i.e., Barlow's disease and fibroelastic deficiency) comprises a range of leaflet abnormalities characterized by chordal and leaflet thickening, mitral tissue redundancy, and excessive leaflet motion in the form of prolapse (Fig. 6.6a, b; Videos 6.2 and 6.3) or flail, leading to valve incompetency [5, 23]. Infective endocarditis and the presence of bacterial vegetations on the atrial side often causes leaflet damage, leading to marked destruction of both the anatomy and function of the leaflets (Fig. 6.6c, d; Videos 6.4 and 6.5). Extensive damage may result in excessive leaflet motion and be classified

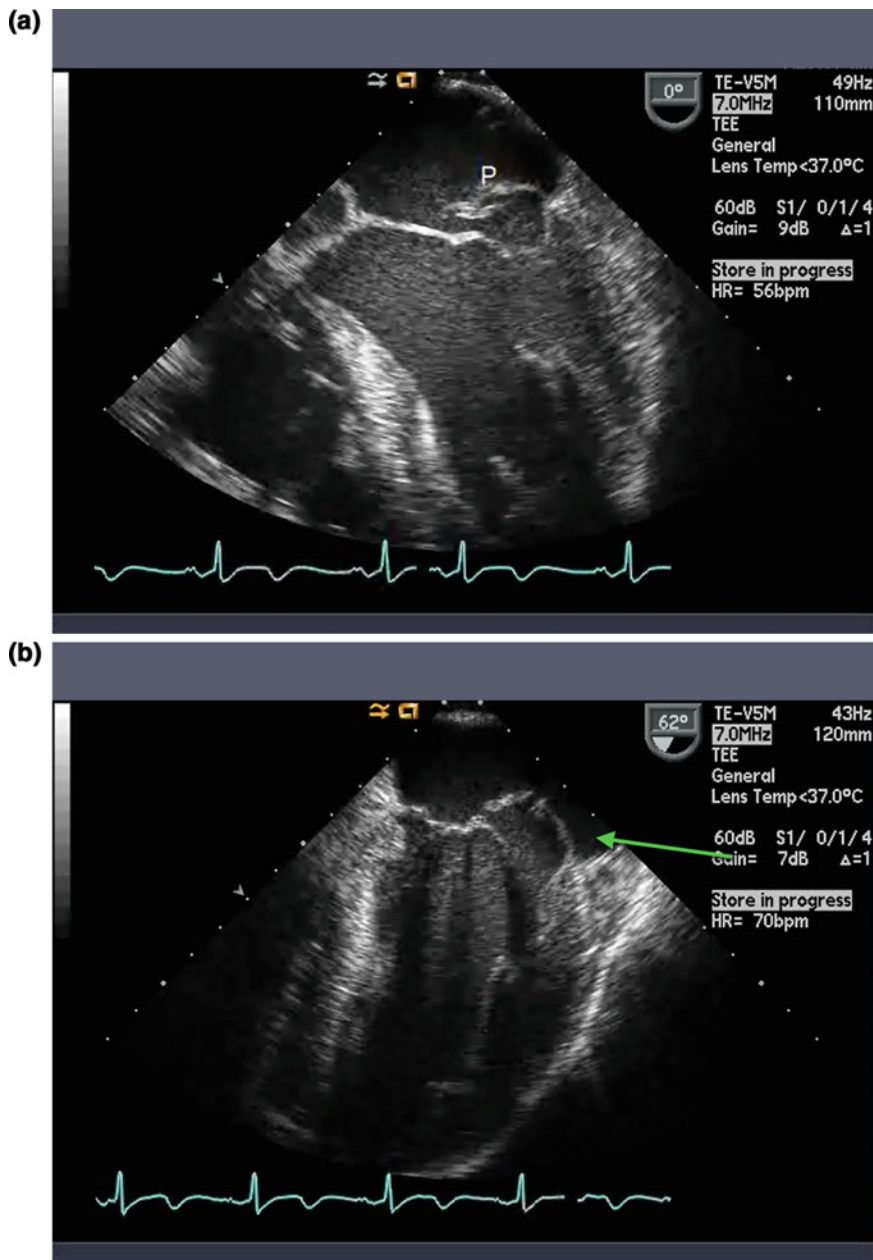


Fig. 6.6 **a** ME four-chamber view with posterior leaflet prolapse (P). **b** ME mitral commissural view of the same patient with posterior leaflet prolapse (green arrow). **c** ME four-chamber view with anterior leaflet vegetation (red arrow). **d** ME LAX view of the same patient with an anterior leaflet vegetation (red arrow)

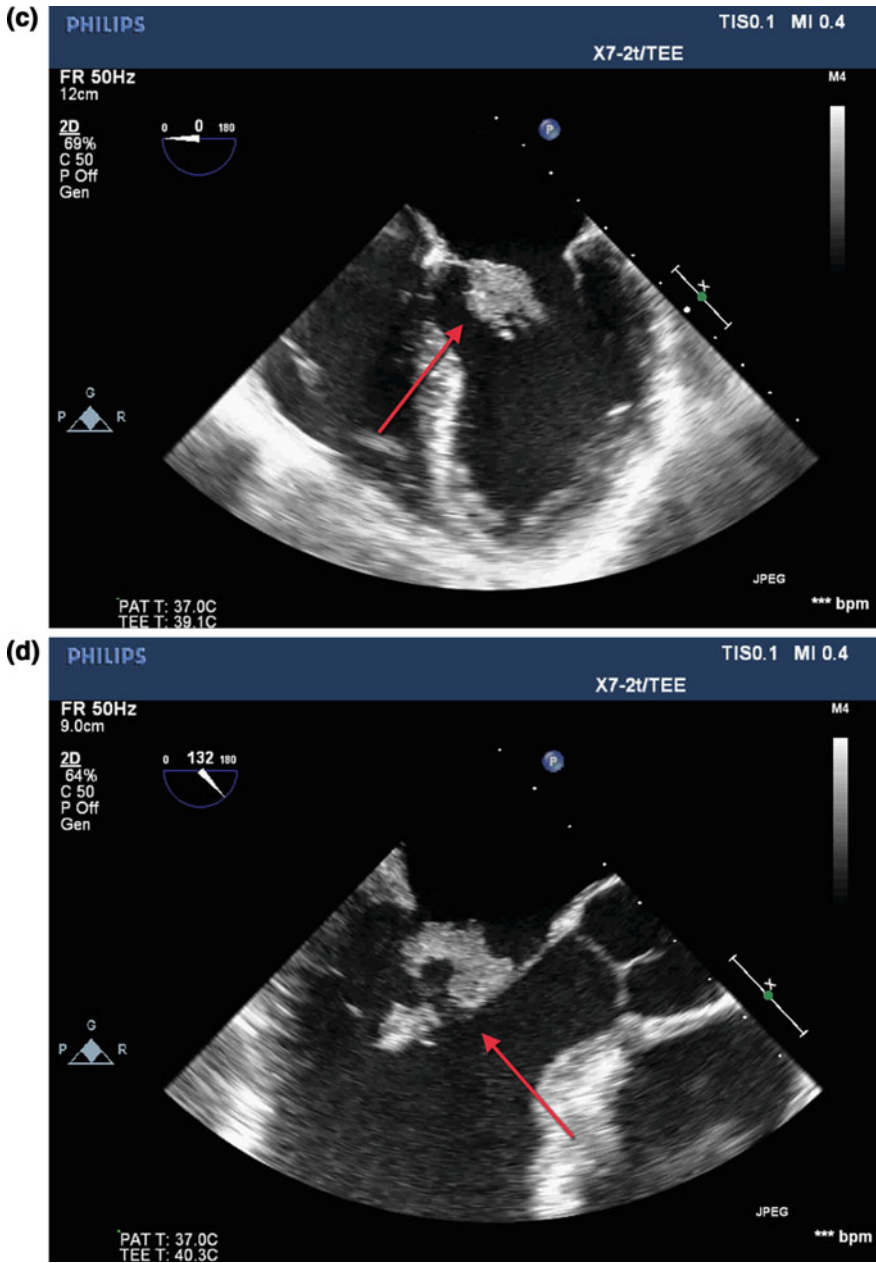


Fig. 6.6 (continued)

as Type 2 MR, while healed endocarditis may have a resultant perforation in a leaflet but otherwise normal leaflet motion and be classified as Type 1.

Restriction of the mitral valve leaflet motion is classified as Type 3 and may be subdivided based upon the restriction in systole and diastole (Type 3a) and during systole only (Type 3b). Leaflet calcification and fusion as seen in rheumatic disease (Type 3a) is an underappreciated etiology of MR where leaflet motion is impaired in systole and diastole. In addition to marked leaflet immobility, the annulus and entire subvalvular apparatus may also deteriorate from marked calcification.

Patients with functional mitral regurgitation (FMR) (Type 3b) underscore the critical geometrical relationship of the ventricular wall, papillary muscle, and chordal elements in providing a strong foundation for normal leaflet coaptation. The term “functional mitral regurgitation” refers to the dysfunction of the left ventricle as the underlying cause of MR in the setting of normal leaflet anatomy. Most commonly, FMR is a result of myocardial ischemia or dilated cardiomyopathy with distortion of the normal geometry of the ventricular myocardium, papillary muscles, and chordae network. Indeed, the proper interpapillary distance (lateral distance) and location of the papillary muscles (i.e., apical displacement) in relation to the ventricular wall and coaptation point is critical in regulating the overall competency of the mitral valve complex [4]. In the setting of myocardial ischemia, displacement of the papillary muscles toward the apex of the heart and concomitant tethering of attached chordae culminates in leaflet restriction and formation of a coaptation defect [13, 21].

In summary, the closing forces of the mitral apparatus are dependent on the intricate relationship of the leaflets, annulus, chordae tendineae, papillary muscles, atrial, and ventricular myocardium. Disruption of any component in the chain may result in mitral incompetency.

Grading Severity (Table 6.1)

Two-dimensional Echocardiography

Prior to quantifying the severity of MR, it may be prudent to examine the upstream and downstream chambers (left atrium and left ventricle, respectively) for signs of adaptation to volume stress. Adaptation to chronic volume overload may lead to

Table 6.1 Mitral valve regurgitation quantitative assessment

	Mild	Moderate	Severe
Vena contracta (mm)	<3	3–7	>7
Pulmonary venous Doppler	Normal	S wave blunted	S wave reversal
EROA by PISA (cm ²)	<0.20	0.20–0.40	>0.40

Criteria for severe MR is highlighted in bold

chamber dilation of the left atrium and left ventricle, which may be appreciated on two-dimensional imaging [5, 10]. Upstream effects of left atrial volume overload and pulmonary hypertension may result in echocardiographic signs of right ventricular (RV) dilation, tricuspid regurgitation, and septal bowing suggestive of RV dysfunction. Echocardiographic signs of the downstream effects of MR may include the presence of eccentric LV hypertrophy, elevated end diastolic volumes, and increased (presence of ventricular dysfunction) or decreased (supranormal ejection fraction in compensated chronic MR) end systolic dimensions. After examining the chambers of the heart for the effects of volume overload, specific attention can then be afforded to the rest of the mitral apparatus.

While two-dimensional echocardiography does not directly allow gradation of severity of MR, it certainly alludes to a mechanism for the MR. Observation of a significant coaptation defect (lack of anterior and posterior leaflets coming together in systole) suggests that MR will exist. The cause of the coaptation defect may be categorized under one of the three types of leaflet motion described above. Evidence of excessive leaflet motion (Type 2) is generally a result of degenerative disease of the mitral valve leading to prolapse, flail, or billowing of a leaflet segment above the annular plane [2, 23]. More specifically, prolapse is defined as a translation of the leaflet tip above the annulus due to excess leaflet and/or chordal length during systole (Figs. 6.6a, b and 6.7; Video 6.6). The term flail refers to the movement of leaflet tip above the annular plane as a result of a ruptured chordae. The presence of a ruptured chordae may often be obscured, rendering the echocardiographic distinction between prolapse and flail challenging. Billowing or scalloping is a projection of leaflet body or segment (not leaflet tip as in prolapse) above the annulus with the point of coaptation remaining below the annular plane [5, 23]. MR as a result of excessive motion of an isolated leaflet often results in an eccentric jet directed away from the diseased leaflet as it emerges through the coaptation defect (Fig. 6.7). Although uncommon, eccentric jets may be present in bileaflet disease if one of the leaflets is more affected than the other. Nevertheless, the appearance of an eccentric jet often signifies the presence of a structural abnormality in the mitral apparatus and thus warrants close examination.

Restricted leaflet motion in systole and diastole (Type 3a) is associated with rheumatic disease [24]. This differs from functional MR (Type 3b) in which restricted leaflet motion is only in systole due to leaflet tethering as a result of a dilated ventricle or papillary muscle ischemia. The direction of the jet often emerges toward the affected leaflet if the restricted leaflet motion is asymmetric. In the case of symmetric bileaflet tethering, a central jet may result [2, 3].

Color Flow Doppler

Color flow Doppler enables the echocardiographer to initially screen and map the mitral regurgitant jet as it occupies the left atrium (Fig. 6.8a–d; Videos 6.7–6.10) [3, 10]. To optimize the image quality, it may help to utilize the zoom function to increase the window size of the chamber of interest. With a Doppler flow sector

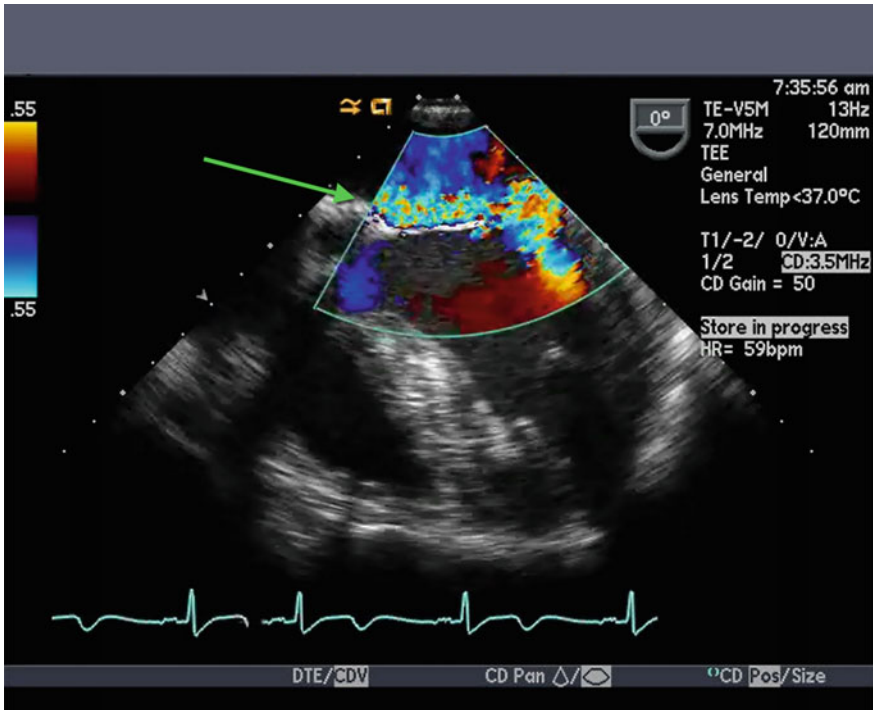


Fig. 6.7 ME four-chamber view with CFD in the patient from Fig. 6.6. Posterior leaflet prolapse with corresponding jet directed away from affected leaflet

window set to capture only the left atrium, mapping of the MR jet can then be optimized by setting the Nyquist limit (the maximum detectable velocity of the Color Map Scale, see Chap. 3) to approximately 50–70 cm/s. It may be prudent to visualize the jet in multiple views to gain a complete picture of the nature and contour of the regurgitant volume. In this way, jets that are difficult to visualize (e.g. wall hugging or eccentric jets) are not missed or underappreciated. It may also be helpful to make small adjustments to the probe position to maximize the quality of the image and capture the most representative jet possible. This may require slight anteflexion/retroflexion, advancement/withdrawal, or leftward/rightward turn of the probe while imaging the MR jet with color flow Doppler. Once the MR jet is fully imaged, it is important to make a qualitative assessment of the regurgitant flow focusing on the jet shape, direction, width, area, presence of eccentricity, and distance traveled into the left atrium. Color flow Doppler examination of the MR jet is an important first step to obtaining an initial impression and grading the severity of regurgitation [3, 5].

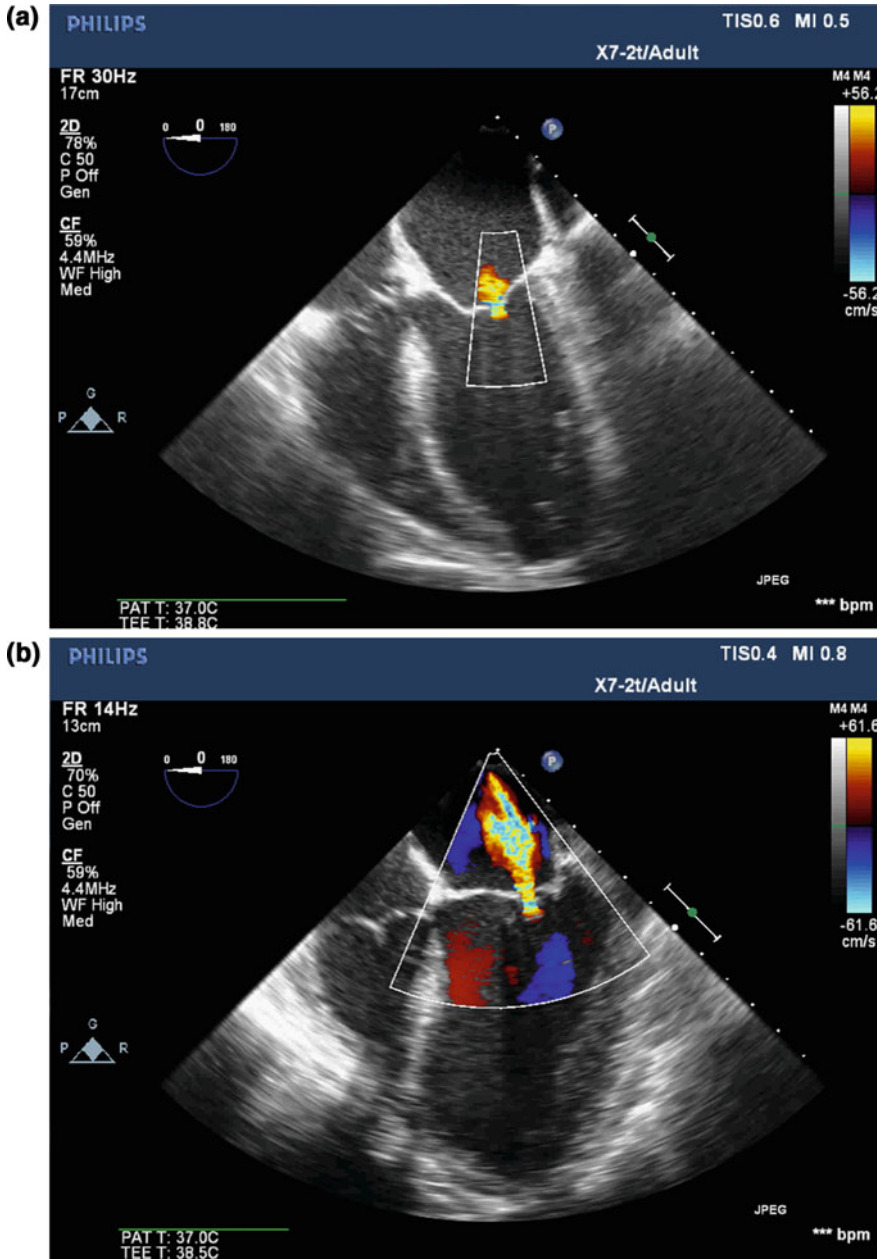


Fig. 6.8 Color flow Doppler showing increasing MR severity. **a** Trace MR (1+), **b** mild MR (2+), **c** moderate MR (3+), **d** severe MR (4+)

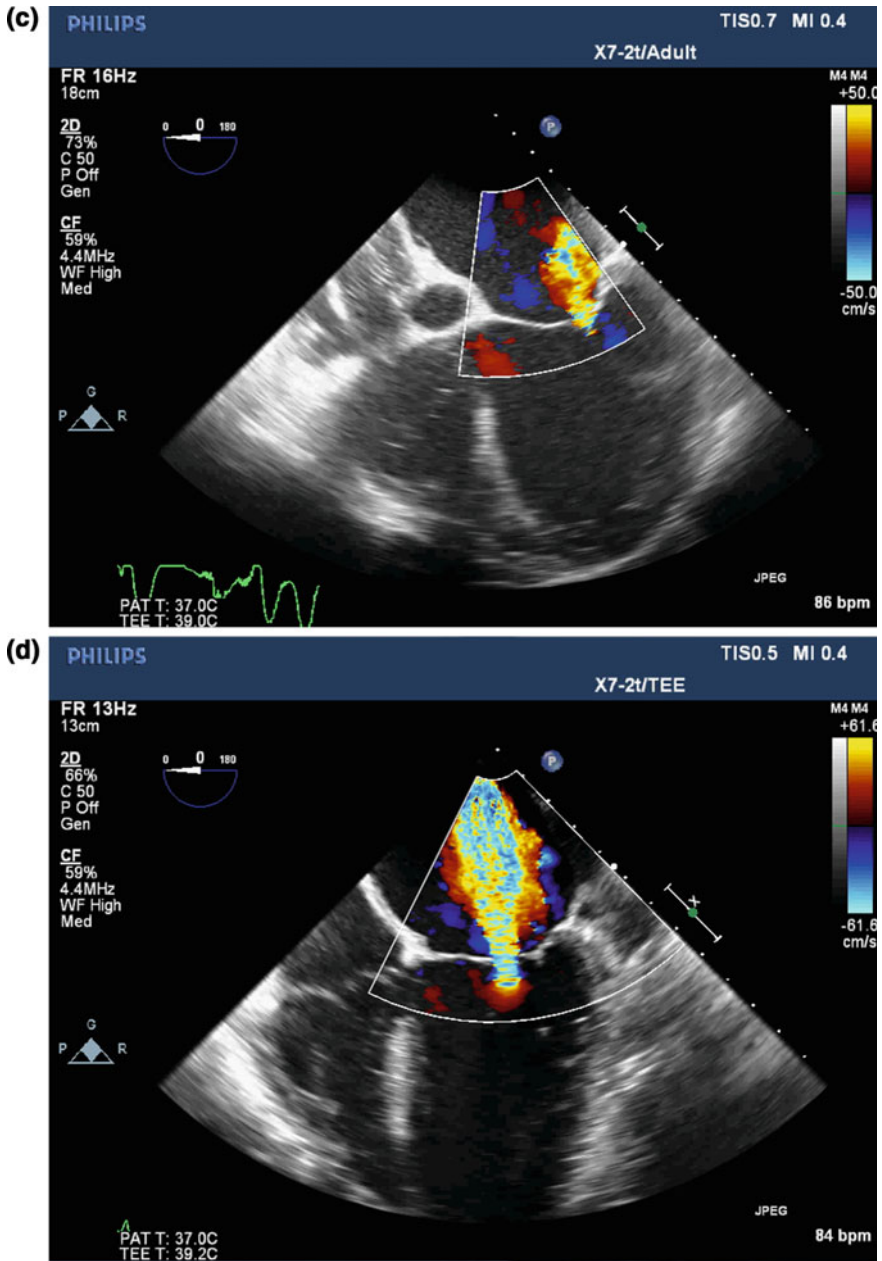


Fig. 6.8 (continued)

Vena Contracta

Measurement of vena contracta (Fig. 6.9a) is a quick and useful method to assess the severity of mitral regurgitation [3, 5, 25, 26]. The vena contracta is the narrowest part of the regurgitant jet visualized with color flow Doppler as it emerges from the regurgitant orifice at the level of the leaflet tips [2, 3]. The ideal image captures a jet profile that consists of a proximal convergence zone (area of flow acceleration on ventricular side) and a narrow neck at the plane of the coaptation point. The vena contracta measurement is advantageous as it is relatively independent of machine settings and loading conditions [5]. However, precise measurement of the vena contracta width can often be challenging due to difficulties in proper image acquisition and the small dimensions of the jet width. The image of the jet can be optimized using the zoom function and setting the Nyquist limit to approximately 50–70 cm/s. The ideal acoustic window to capture the anterior–posterior dimensions (perpendicular to coaptation point) of the regurgitant jet corresponds to the ME LAX view (at $\sim 120\text{--}150^\circ$). It may be necessary to fine-tune the image by turning the probe leftward or rightward to obtain an optimal jet profile. If a jet is not visualized in the ME LAX view, the vena contracta can also be measured in the ME four-chamber view, but this measurement should be interpreted with caution as it does not measure the jet perpendicular to the coaptation line. It may be helpful to take several measurements to obtain a more precise vena contracta measurement. Vena contracta measurements above 7 mm constitute severe MR and values below 3 mm constitute mild MR [2, 5].

Pulmonary Venous Flow Profile

Doppler interrogation of the pulmonary venous flow or left atrial inflow (Fig. 6.9b) can be used as a semi-quantitative method for grading MR severity [2, 3, 10, 26]. Using pulse wave Doppler, a sample volume of left atrial inflow can be captured, usually using the left upper pulmonary vein. With the point of interrogation cursor set approximately 1 cm into the pulmonary vein, velocities are measured as flow moves into the left atrium. The speed or velocity of blood flow traveling towards the left atrium during systole is typically greater than the speed during diastole, yielding a systolic dominant pulmonary venous pattern ($S_{\text{velocity}} > D_{\text{velocity}}$ or $S/D > 1$).

The presence of systolic mitral regurgitation may reduce the peak systolic velocity of the pulmonary venous flow as the regurgitant jet accelerates back through the atrium and into the pulmonary venous bed. As the regurgitant jet flows into the pulmonary veins and meets the incoming left atrial flow during systole, blunting ($S_{\text{velocity}} < D_{\text{velocity}}$ or $S/D < 1$, Fig. 6.9b) or reversal (below baseline) of the systolic component of the pulmonary Doppler profile is observed. Systolic reversal of flow in the pulmonary venous profile is a specific but not sensitive

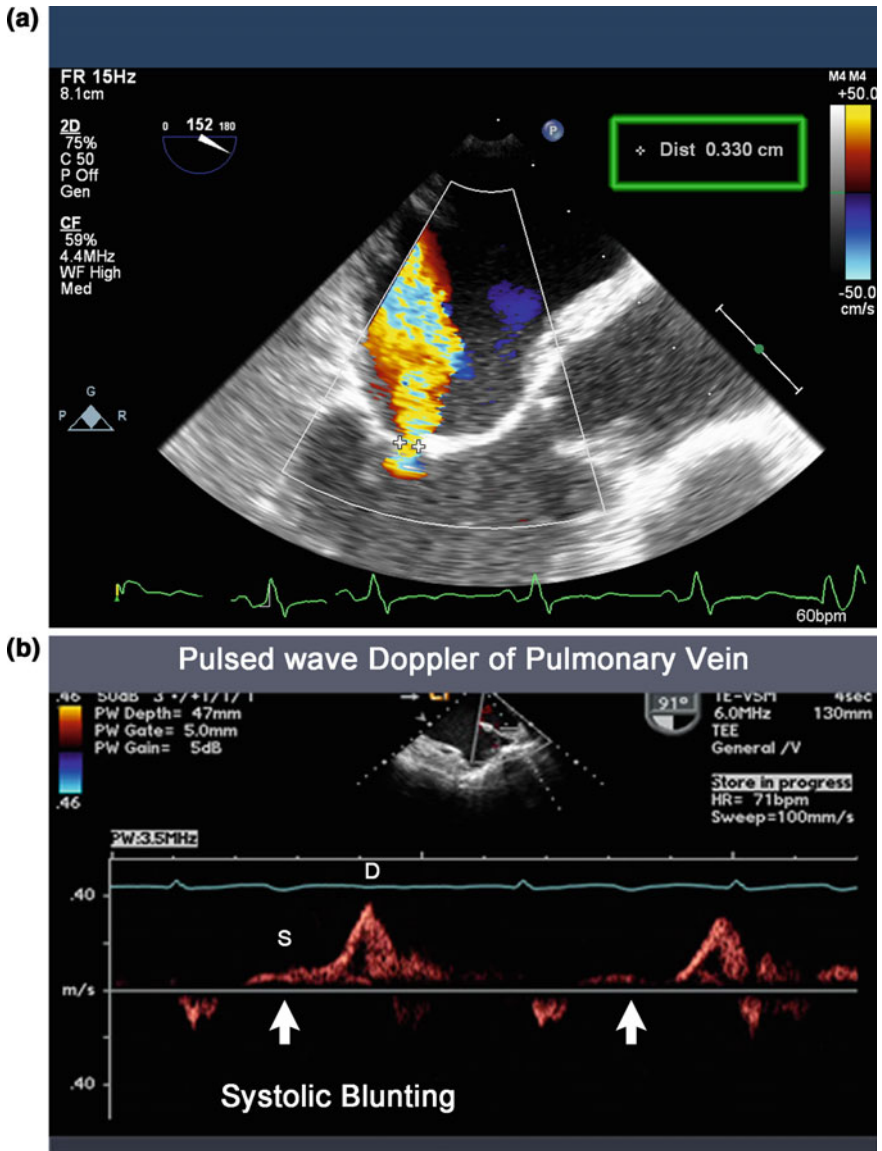


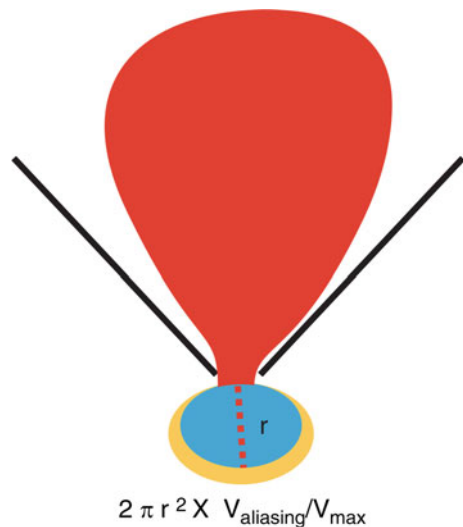
Fig. 6.9 **a** Vena contracta measurement. Notice that the measurement is taken at the narrowest portion or neck of the jet as it crosses the plane of coaptation. **b** Pulse wave Doppler interrogation of pulmonary veins demonstrating systolic blunting in a patient with moderate MR

finding of severe MR, with systolic blunting representing a more moderate degree of MR [5]. The poor sensitivity of the pulmonary venous flow in detecting MR is partly due to the varying degrees of left atrial compliance in certain patients and the challenge of interrogating all four pulmonary veins on TEE [2, 3].

Proximal Isovelocity Surface Area (PISA)

The proximal isovelocity surface area (PISA) method is a quantitative modality for grading MR (Fig. 6.10) [26–28]. The PISA method is an application of the continuity equation and provides a means to calculate the effective regurgitant orifice area (EROA). In simple terms, the volume or flow of blood below the mitral valve is equal to the volume or flow of blood above the mitral valve. As a regurgitant jet travels towards the narrowed mitral orifice, the column of blood accelerates and a series of concentric hemispheres are generated on the ventricular side of the mitral valve. When blood velocity increases beyond the limit of detection of the Doppler (i.e., Nyquist limit), the color flow map near the mitral orifice displays a high velocity region with evidence of aliasing (blood velocities above the limit of detection appear to reverse). Volume or flow of blood in the convergence zone (ventricular side) is equal to the product of the surface area of the first hemisphere or isovelocity shell and its associated aliasing velocity (Flow = $2\pi r^2 \times V_{\text{aliasing}}$). The radius (r) of the isovelocity shell is defined by the distance from the regurgitant orifice to the border of the first aliasing velocity. Volume or flow on the atrial side is calculated as the product of the effective regurgitant orifice area (EROA) and peak

Fig. 6.10 Calculation of the effective regurgitant orifice area of MR by PISA



velocity of the MR jet ($V_{MR \text{ Jet}}$). For this calculation, the peak velocity of the MR jet is measured using continuous wave Doppler interrogation along or parallel to the regurgitant flow.

Applying the continuity principle of equal flow on the atrial and ventricular side of the regurgitant orifice, the EROA can be calculated as follows:

$$\text{EROA} = 2\pi r^2 \times V_{\text{aliasing}} / V_{\text{MR jet}}$$

r = radius of the first isovelocity shell; V_{aliasing} = Nyquist limit; $V_{\text{MR jet}}$ is the peak velocity of the MR jet and $\pi = 3.14$.

The PISA method allows for calculation of the EROA and represents a true quantitative measurement of MR severity. An EROA $>0.4 \text{ cm}^2$ corresponds to severe MR while an EROA $<0.2 \text{ cm}^2$ corresponds to mild MR. It is important to highlight that the PISA method is fraught with several limitations. The PISA calculation requires several steps and is based on meticulous measurements of small dimensions, rendering this technique time-consuming and laborious for clinical application in the operating room. The shape of the isovelocity shells are also assumed to be hemispheres when indeed they may not be. Nevertheless, the PISA method may prove useful in cases where quantitative analysis is necessary to distinguish between moderate MR from mild or severe forms [27, 28].

Hemodynamics

The MR jet is one of the most dynamic and load dependent lesions owing to the large pressure gradient between the LV and LA during systole. The degree of MR at any point in time is extremely sensitive to hemodynamics with numerous studies demonstrating the dynamic nature of MR under different loading conditions. The degree of MR has been shown to decrease with the reduction of preload and afterload that is associated induction of general anesthesia. By contrast, increasing afterload with phenylephrine and preload augmentation with fluid administration has been shown to provoke or worsen the MR jet under general anesthesia. The effects of general anesthesia often poses a challenge for the intraoperative echocardiographer as the preoperative awake hemodynamics may significantly differ from that found in the operating room. It may prove useful to make note of the precise hemodynamic state of the patient at the time of intraoperative echocardiographic assessment and compare the parameters to the baseline or preoperative loading conditions [5].

Mitral Stenosis

Mitral Stenosis

2D	<ul style="list-style-type: none"> • Mitral leaflet motion (restrictive) • Mitral annular and leaflet calcification • Left atrial enlargement • LA spontaneous echo contrast (LAA thrombus identification) • Small LV dimensions (underfilled) • Planimetry
CFD	<ul style="list-style-type: none"> • Flow acceleration on left atrial aspect • Turbulent flow entering LV
Spectral	<ul style="list-style-type: none"> • PHT–CWD • Mean gradient–CWD • MVA–PHT-based calculation, PISA-based calculation

LA left atrium, *LV* left ventricle, *LAA* left atrial appendage, *PHT* pressure half time, *CWD* continuous wave Doppler, *MVA* mitral valve area, *PISA* proximal isovelocity surface area

The mitral valve (MV) assumes its largest area during diastole as it serves as a conduit for left ventricular filling. The normal mitral valve area is approximately 4–6 cm², with significant elevations in the gradient across the MV as the area approaches 1.0 cm². Upstream from the stenotic mitral valve, a marked increase in left atrial pressure is observed followed by chamber enlargement, stagnant blood flow, and atrial dysrhythmias. As the disease process progresses, marked elevations in left atrial pressure and pulmonary hypertension can precipitate right heart dysfunction. As blood converges near the narrow orifice, flow accelerates across the valve as it enters the left ventricle. Downstream from the MV stenosis, an LV with lower end diastolic volume from restricted filling is often evident on two-dimensional echo [3, 24, 29].

Two-dimensional Echocardiography

Mitral stenosis (MS) is the result of a reduction in the valve area during diastole from impaired valve opening. Although rheumatic heart disease is commonly associated with mitral stenosis, nonrheumatic causes of MS have recently become more important causes of MS [2, 24]. Nonrheumatic causes of mitral stenosis include severe leaflet and annular calcification, congenital mitral defects like parachute deformity (in which all chordae originate from a single papillary muscle), infective endocarditis, LA thrombus or myxoma, carcinoid syndrome, and post-repair or valve replacement associated MS [24]. The anatomic changes

associated with the above-mentioned processes are often discernible on two-dimensional echocardiography. Besides appreciating a reduction in valve opening in the TG basal SAX view and ME views, echocardiographic signs of calcific MS may include evidence of leaflet thickening, echogenic calcification, retraction or shortening, fusion of the commissures and leaflet immobility. Two-dimensional echocardiography often reveals calcium deposition extending to the subvalvular apparatus and mitral annulus, which may be visualized in the ME mitral commissural and TG LAX views.

In the case of rheumatic MS, the characteristic doming of the anterior leaflet or formation of a “hockey stick” like appearance may be appreciated in the ME four chamber and ME LAX views (Fig. 6.11; Video 6.11). The unique pattern of calcification beginning at the leaflet tips renders this portion relatively immobile compared to the remaining mobile midportion or body. By contrast, calcific MS usually starts near the annulus and extends into the leaflets near the base and usually does not involve the commissures or leaflet tips until later in the disease process. Two-dimensional examination of the upstream effects of MS may reveal signs of adaptation to LV inflow obstruction. Upstream echocardiographic signs of chronic MS may include the presence of spontaneous echo contrast or early thrombus formation, marked LA enlargement, systolic blunting of the pulmonary venous flow, concomitant MR, RV dysfunction with paradoxical septal motion, RA enlargement with bulging of the interatrial septum, and tricuspid regurgitation. Just

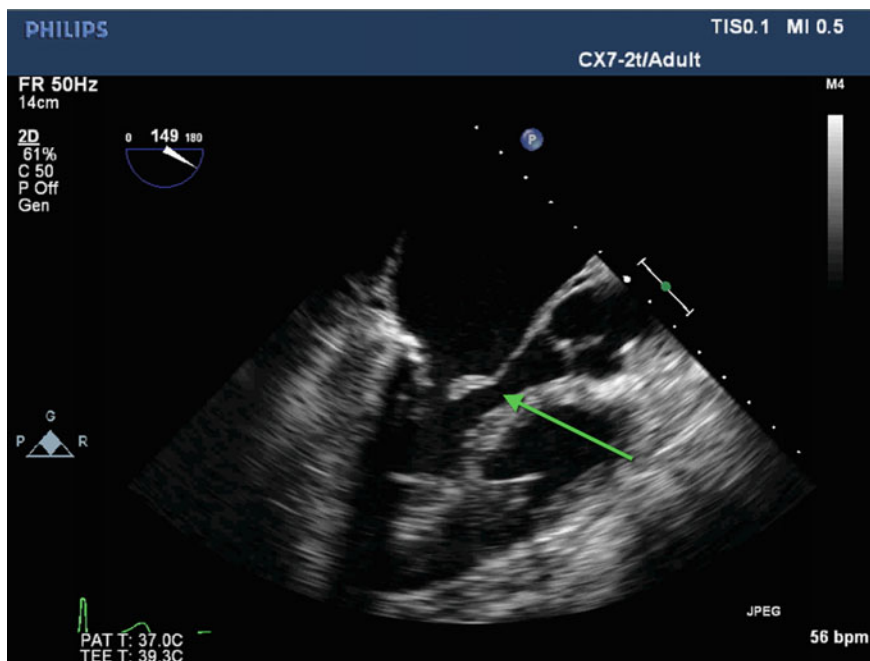


Fig. 6.11 “Hockey stick” deformity (green arrow) in a patient with rheumatic mitral stenosis

Table 6.2 Mitral valve stenosis: quantitative assessment

	Mild	Moderate	Severe
PHT (ms)	100	200	>220
Mean gradient (mmHg)	6	6–10	>10
Valve area ^a (cm ²)	1.6–2.0	1.0–1.5	<1.0

Criteria for severe MS is highlighted in bold

PHT Pressure half time

^aValve area as determined by PHT formula, PISA calculation or planimetry

proximal to the stenotic mitral valve, an area of flow convergence is observed on color flow Doppler as blood accelerates into the narrow orifice. As blood crosses the plane of the valve, a population of high aliasing velocities beyond the limit of detection (Nyquist limit) emerge and are displayed as a region of turbulent flow on the color Doppler map.

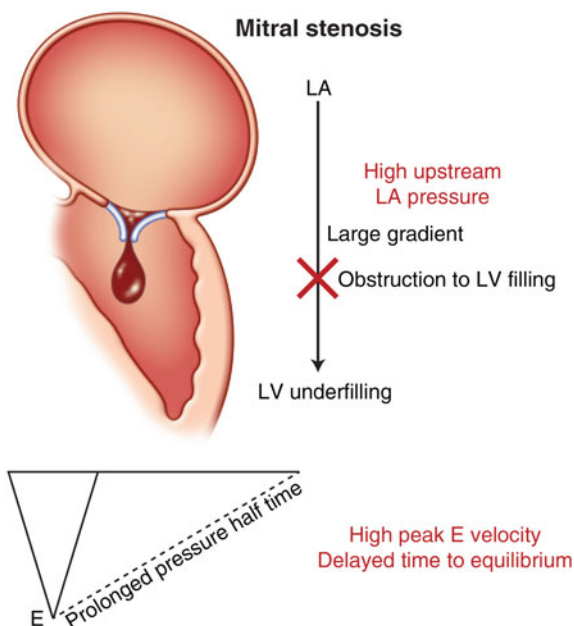
Quantitative Assessment of Mitral Stenosis

The following sections describe the different quantitative echocardiographic assessments of mitral stenosis (Table 6.2).

Pressure Gradients

As the underlying cause of mitral stenosis progresses, an increase in the LA–LV transvalvular gradient develops as flow accelerates across the narrow opening. The pressure differential (ΔP) between the LA and LV is described by the modified Bernoulli's equation or $\Delta P = 4v^2$, where v is the instantaneous peak velocity of blood across the valve and ΔP is the pressure difference or gradient. The ME four chamber and ME LAX views can be used measure the transvalvular gradient across the mitral valve. Using continuous wave Doppler interrogation, it is important to align the sampling cursor parallel to the direction of LV inflow. The resultant transmitral inflow profile and velocity time integral (VTI) describes the observed increase in velocities across the valve and delayed time for the LA and LV pressures to reach equilibrium due to the stenotic orifice. From the transmitral inflow profile, a mean gradient can be determined by tracing the area under the early filling (E-wave) and late filling (A-wave) waves in their entirety (Figs. 6.12 and 6.13a, b). The peak gradient or velocity describes the greatest pressure differential or velocity of the fastest red blood cell of the entire population. More importantly, the mean gradient is a value that represents the average pressure difference or velocity of the entire column of blood moving from the atrium to the ventricle across the stenotic orifice. The mean gradient derived from the VTI or area under the curve is used in grading severity of mitral stenosis [24].

Fig. 6.12 Flow dynamics of mitral stenosis resulting in an elevated peak E-wave velocity and prolonged pressure half time downstream from stenotic orifice



Mitral Valve Area Calculations

Pressure Half Time (PHT)

As blood moves across the stenotic mitral valve, the pressure gradient between the left atrium and ventricle begins to dissipate proportional to the degree of stenosis. Similarly, the maximum peak instantaneous velocity of blood decelerates over time proportional to the severity of MS. The more severe the obstruction to flow, the longer it takes for the pressure in the LA and LV to equilibrate (Fig. 6.12). The pressure half time (PHT) describes the slope or rate at which the atrial and ventricular pressure differential decreases by 50%. The more severe the stenosis, the longer it takes for the LA and LV pressures to equalize and thus, a more prolonged PHT (Figs. 6.12 and 6.13a, b). A PHT measurement as long as 300 ms corresponds to severe MS whereas a normal mitral valve area with an insignificant transvalvular pressure difference exhibits a PHT of ~50 ms. The PHT is inversely proportional to the mitral valve area (MVA) and is defined by the equation

$$\text{MVA}(\text{cm}^2) = 220/\text{PHT} \text{ (milliseconds)}$$

In the ME four chamber or ME LAX view, the PHT is obtained by aligning the Doppler beam parallel to the direction of flow through the MV and using continuous wave Doppler to interrogate LV inflow. The PHT is then measured by taking

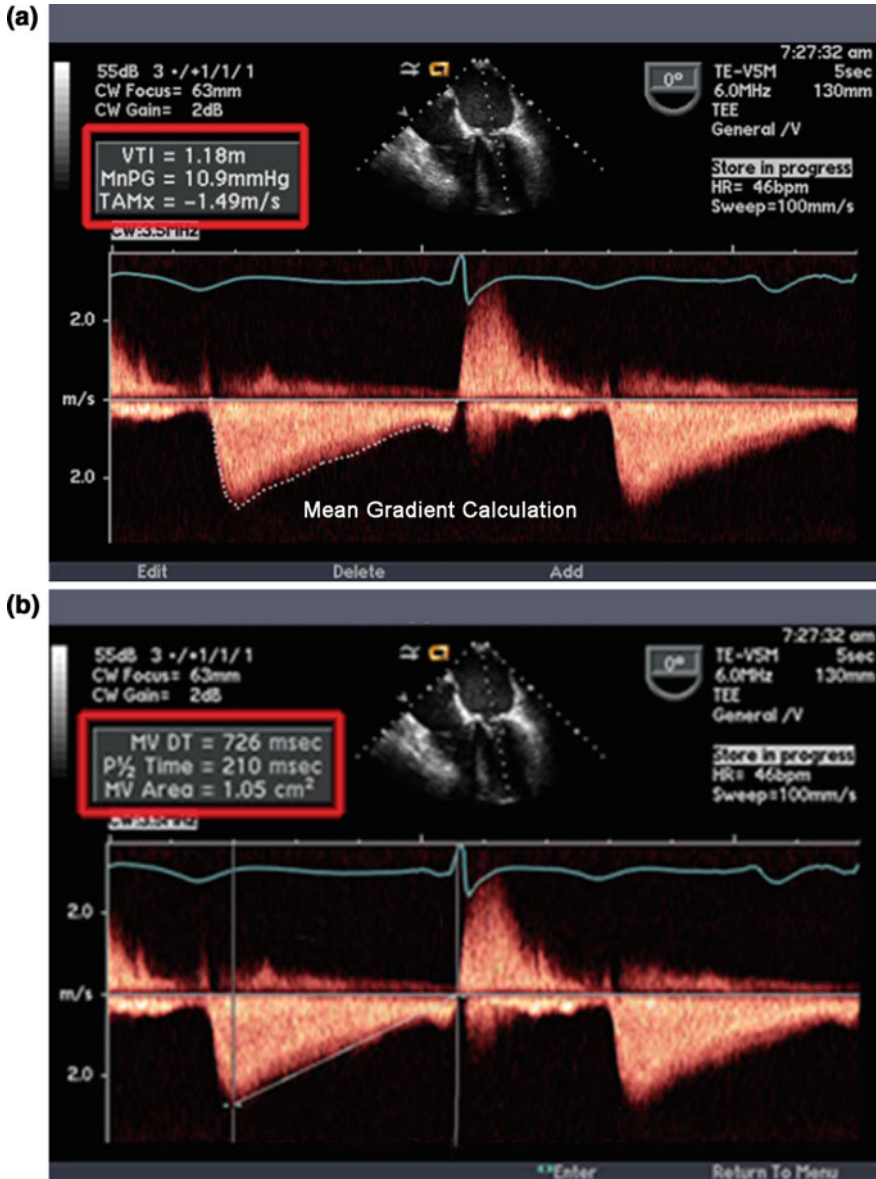


Fig. 6.13 **a** Continuous wave Doppler interrogation across the mitral valve. The mean gradient of the transmitral flow profile is calculated by tracing the entire envelope or velocity time integral. **b** The spectral Doppler profile is characterized by a high velocity E-wave with a prolonged pressure half time or deceleration time, which can be used to calculate the mitral valve area

the peak velocity of the E-wave (early filling) and drawing a caliper along the slope of deceleration, being careful to include the slope that encompasses the peak velocity and the baseline (point of zero velocity). The machine software will extrapolate the PHT in milliseconds and compute a mitral valve area. PHT measurements above 220 ms correspond to severe MS (Figs. 6.12 and 6.13a, b) [3, 24].

Proximal Isovelocity Surface Area (PISA)

Proximal isovelocity surface area (Fig. 6.14) or flow convergence method is an application of the continuity equation to measure the mitral valve area [24, 27]. As blood flow converges upon the stenotic mitral valve, a marked increase in velocity ensues, creating a series of organized hemispheres on the left atrial side of the valve. The border between blue and red on the color flow map defines the boundary between the first isovelocity hemisphere and represents the location of the first aliasing velocity, corresponding to blood traveling faster than the limit of detection (Nyquist limit) on the color flow Doppler scale. The radius of the first isovelocity hemisphere is then carefully measured along with the angle (α) that is formed by both mitral leaflets during diastole. The product of the area of the hemisphere ($2\pi r^2$) and the aliasing velocity on the color flow Doppler scale provides the volumetric flow on the atrial side. The volumetric flow on the atrial side is then multiplied by the angle correction factor, $\alpha/180^\circ$, defined by the angle formed by the mitral leaflets, yielding a more accurate flow measurement. To calculate the mitral valve area, velocity of flow on the ventricular side must be measured by continuous wave Doppler across the mitral valve. In the ME four chamber or ME LAX view, the Doppler beam is positioned parallel to the direction of flow into the LV. The continuous wave Doppler then produces a spectral profile that can be used to

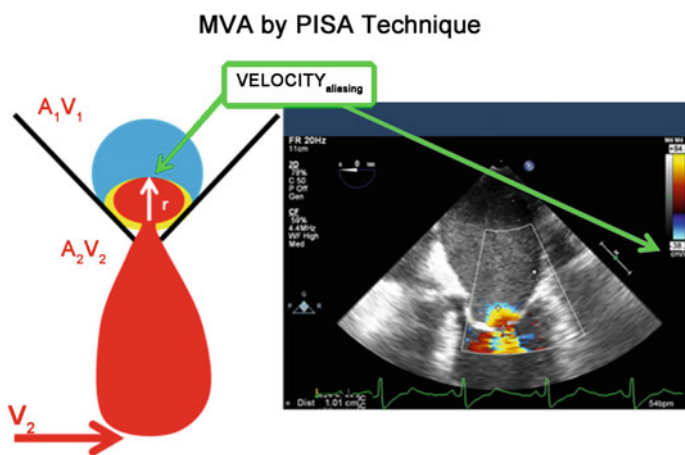


Fig. 6.14 Calculation of mitral valve area by PISA technique

calculate the maximum velocity across the valve. Using the continuity equation where the flow of blood on the atrial side equals the flow on the ventricular side

$$\text{Area}_{\text{hemisphere}} \times \text{Velocity}_{\text{aliasing}} = \text{Area}_{\text{mitral valve}} \times \text{Velocity}_{\text{mitral inflow}};$$

Mitral Valve Area can then be derived as follows:

$$\text{Area}_{\text{mitral valve}} = \alpha/180^\circ \left(\text{Area}_{\text{hemisphere}} \times \text{Velocity}_{\text{aliasing}} / \text{Velocity}_{\text{mitral inflow}} \right).$$

Similar to utilizing PISA for MR, using PISA for MS can be laborious and time-consuming with the potential for magnified errors in measurement of the hemisphere. Therefore measurement of PHT and mean gradients are the mainstay of estimating MS severity with PISA utilized for confirmation.

Planimetry

Planimetry is the direct measurement of the mitral valve area using two-dimensional echocardiography [24]. Trace measurement of the mitral valve area can be achieved using the transgastric basal SAX view. It is important to obtain the best image possible and utilize the freeze function on the machine to capture the valve opening in diastole. An accurate measurement of the valve area can be maximized by advancing or withdrawing the probe in attempt to move the scan plane from a superior position down to the level of the smallest valve opening. If the scan plane measures the opening above the actual orifice, the mitral valve area will be overestimated.

References

1. Silverman ME, Hurst JW. The mitral complex. Interaction of the anatomy, physiology, and pathology of the mitral annulus, mitral valve leaflets, chordae tendineae, and papillary muscles. *Am Heart J.* 1968;76(3):399–418.
2. Sidebotham DA, et al. Intraoperative transesophageal echocardiography for surgical repair of mitral regurgitation. *J Am Soc Echocardiogr.* 2014;27(4):345–66.
3. Sherman SK. Perioperative transesophageal echocardiographic evaluation of the native mitral valve. *Crit Care Med.* 2007;35(8 Suppl):S372–83.
4. Silbiger JJ, Bazaz R. Contemporary insights into the functional anatomy of the mitral valve. *Am Heart J.* 2009;158(6):887–95.
5. Mahmood F, Matyal R. A quantitative approach to the intraoperative echocardiographic assessment of the mitral valve for repair. *Anesth Analg.* 2015;121(1):34–58.
6. Salgo IS, et al. Effect of annular shape on leaflet curvature in reducing mitral leaflet stress. *Circulation.* 2002;106(6):711–7.
7. Silbiger JJ. Anatomy, mechanics, and pathophysiology of the mitral annulus. *Am Heart J.* 2012;164(2):163–76.

8. Mahmood F, et al. Echocardiography derived three-dimensional printing of normal and abnormal mitral annuli. *Ann Card Anaesth*. 2014;17(4):279–83.
9. Padala M, et al. Saddle shape of the mitral annulus reduces systolic strains on the P2 segment of the posterior mitral leaflet. *Ann Thorac Surg*. 2009;88(5):1499–504.
10. Hahn RT, et al. Guidelines for performing a comprehensive transesophageal echocardiographic examination: recommendations from the American Society of Echocardiography and the Society of Cardiovascular Anesthesiologists. *J Am Soc Echocardiogr*. 2013;26(9):921–64.
11. Lambert AS, et al. Improved evaluation of the location and mechanism of mitral valve regurgitation with a systematic transesophageal echocardiography examination. *Anesth Analg*. 1999;88(6):1205–12.
12. Mathew JP, et al. ASE/SCA recommendations and guidelines for continuous quality improvement in perioperative echocardiography. *Anesth Analg*. 2006;103(6):1416–25.
13. Silbiger JJ. Novel pathogenetic mechanisms and structural adaptations in ischemic mitral regurgitation. *J Am Soc Echocardiogr*. 2013;26(10):1107–17.
14. Jiang L, et al. Dynamism of the mitral annulus: a spatial and temporal analysis. *J Cardiothorac Vasc Anesth*. 2014;28(5):1191–7.
15. Mahmood F, et al. Changes in mitral valve annular geometry after repair: saddle-shaped versus flat annuloplasty rings. *Ann Thorac Surg*. 2010;90(4):1212–20.
16. Mahmood F, et al. Mitral annulus: an intraoperative echocardiographic perspective. *J Cardiothorac Vasc Anesth*. 2013;27(6):1355–63.
17. Mahmood F, et al. Intraoperative application of geometric three-dimensional mitral valve assessment package: a feasibility study. *J Cardiothorac Vasc Anesth*. 2008;22(2):292–8.
18. Owais K, et al. Three-dimensional printing of the mitral annulus using echocardiographic data: science fiction or in the operating room next door? *J Cardiothorac Vasc Anesth*. 2014;28(5):1393–6.
19. Khabbaz KR, et al. Dynamic 3-dimensional echocardiographic assessment of mitral annular geometry in patients with functional mitral regurgitation. *Ann Thorac Surg*. 2013;95(1):105–10.
20. Lee AP, et al. Quantitative analysis of mitral valve morphology in mitral valve prolapse with real-time 3-dimensional echocardiography: importance of annular saddle shape in the pathogenesis of mitral regurgitation. *Circulation*. 2013;127(7):832–41.
21. Connell JM, et al. Ischemic mitral regurgitation: mechanisms, intraoperative echocardiographic evaluation, and surgical considerations. *Anesthesiol Clin*. 2013;31(2):281–98.
22. Shakil O, et al. Ischemic mitral regurgitation: an intraoperative echocardiographic perspective. *J Cardiothorac Vasc Anesth*. 2013;27(3):573–85.
23. Shah PM. Current concepts in mitral valve prolapse—diagnosis and management. *J Cardiol*. 2010;56(2):125–33.
24. Wunderlich NC, Beigel R, Siegel RJ. Management of mitral stenosis using 2D and 3D echo-Doppler imaging. *JACC Cardiovasc Imaging*. 2013;6(11):1191–205.
25. Grayburn PA, et al. Multiplane transesophageal echocardiographic assessment of mitral regurgitation by Doppler color flow mapping of the vena contracta. *Am J Cardiol*. 1994;74(9):912–7.
26. Zoghbi WA, et al. Recommendations for evaluation of the severity of native valvular regurgitation with two-dimensional and Doppler echocardiography. *J Am Soc Echocardiogr*. 2003;16(7):777–802.
27. Ashikhmina E, et al. Three-dimensional versus two-dimensional echocardiographic assessment of functional mitral regurgitation proximal isovelocity surface area. *Anesth Analg*. 2015;120(3):534–42.
28. Lambert AS. Proximal isovelocity surface area should be routinely measured in evaluating mitral regurgitation: a core review. *Anesth Analg*. 2007;105(4):940–3.
29. Longo M, et al. Usefulness of transesophageal echocardiography during open heart surgery of mitral stenosis. *J Cardiovasc Surg (Torino)*. 2000;41(3):381–5.

Chapter 7

Aortic Valve

Michael Benggon, MD and Thomas Griffiths, MD

Abstract Echocardiographic evaluation of the aortic valve is not limited to just the valve leaflets itself but also should include the left ventricular outflow tract, sinuses of Valsalva, and the sinotubular junction. Echocardiographic evaluation of any valve pathology should include a thorough two-dimensional examination of the valve and associated anatomic findings, color flow Doppler interrogation, and spectral Doppler analysis. Aortic stenosis is one of the most common cardiac pathologies and can be caused by atherosclerotic thickening over time, congenital bicuspid disease, or rheumatic heart disease. The severity of the stenosis can be assessed by planimetry, spectral Doppler analysis using the continuity equation, mean gradient measurement, and by evaluation of color flow through the valve leaflets. Aortic regurgitation may be caused by root dilatation from vascular or connective tissue disease processes as well as leaflet pathology. Color flow Doppler analysis is a key to determining disease severity through measurement of the vena contracta and jet width to left ventricular outflow diameter. Measurement of the aortic regurgitation pressure half time and determining if there is any reversal of blood flow within the descending aorta will also help to assess disease severity.

Keywords Aortic valve • Aortic • Valve • Aortic stenosis • Aortic regurgitation • Aortic insufficiency

Electronic supplementary material The online version of this chapter (doi:[10.1007/978-3-319-34124-8_7](https://doi.org/10.1007/978-3-319-34124-8_7)) contains supplementary material, which is available to authorized users.

M. Benggon, MD (✉)

Department of Anesthesiology, Loma Linda University, Loma Linda, CA, USA
e-mail: mbenggon@gmail.com

T. Griffiths, MD

Department of Anesthesiology, University of California San Diego,
200 West Arbor Drive MC 7651, San Diego, CA 92103, USA
e-mail: thomaslgriffiths@googlemail.com

Introduction

The aortic valve (AV) is one of two semilunar valves in the heart, the other being the pulmonic valve. The AV allows blood that is ejected from the left ventricle to enter the systemic circulation while preventing reversal of flow back into the left ventricle during diastole. Unlike the atrioventricular valves (mitral and tricuspid valves), the semilunar valves do not have associated chordae tendineae to support their form and rely on fibrous connective tissue to keep their shape. A thorough echocardiographic evaluation of the aortic valve includes evaluation of the left ventricular outflow tract, aortic annulus, the sinuses of Valsalva, the sinotubular junction, proximal ascending aorta, and the valve itself (Fig. 7.1). The structure of the aortic valve is made up of three curved leaflets or cusps, designated by their location in relation to the coronary arteries, i.e., the left coronary cusp, right coronary cusp, and non-coronary cusp (adjacent to the inter-atrial septum). Associated with each cusp is a sinus or concavity that forms the sinuses of Valsalva. The sinuses of Valsalva connect distally to the ascending aorta at the sinotubular junction. The structure of these sinuses function to allow constant blood flow to the coronary arteries while the aortic valve is open, preventing the leaflets from occluding the coronary orifices, and reducing stress to the leaflets [1, 2].

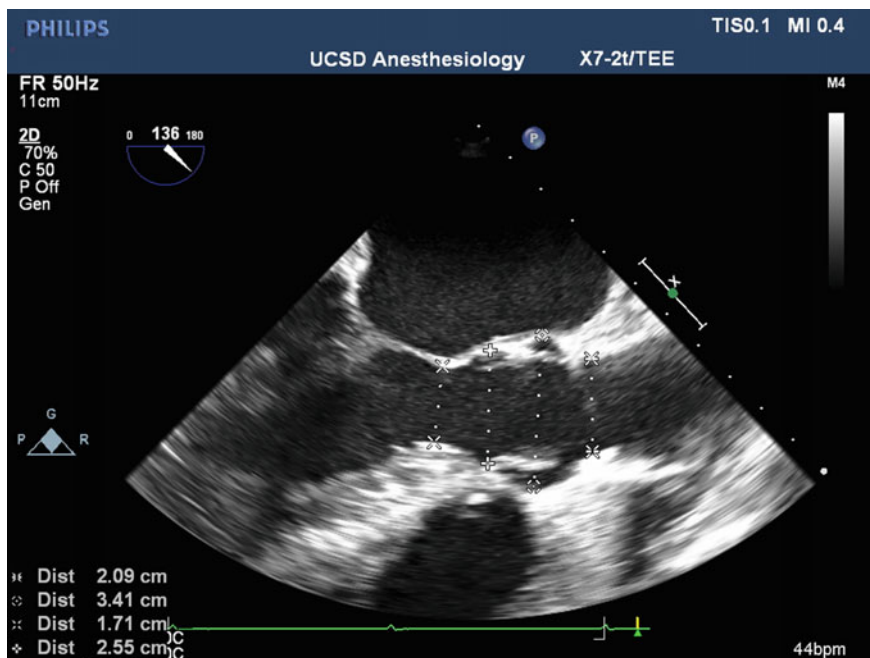


Fig. 7.1 ME AV LAX view: from *left to right*, the measured indices are of the left ventricular outflow tract (LVOT), aortic annulus, sinuses of Valsalva and the sinotubular junction

The left ventricular outflow tract (LVOT) is the portion of the ventricle just proximal to the annulus of the aortic valve made up of the ventricular septum and the fibrous tissue or “intervalvular septum” adjoining the aortic and mitral valves along the left and non-coronary cusps and anterior leaflet, respectively. Dilatation of these proximal or distal areas may cause structural changes to the valve that affect how the three leaflets come together or coapt. Narrowing or stenosis will cause obstruction of blood flow.

Constant high pressure due to the driving force of the left ventricle into the systemic circulation with its own high pressures from vascular resistance causes cellular restructuring after birth which makes the aortic the most durable valve. These same forces can also be detrimental in excess, causing valvular pathology over time.

Aortic Stenosis

Aortic stenosis (AS) is one of the most common cardiac pathologies in the elderly population, second to coronary artery disease. Causes include atherosclerotic thickening of the leaflets, a congenital bicuspid aortic valve, or as a sequelae from rheumatic heart disease. Sclerotic thickening is the most common cause in the elderly population, whereas congenital bicuspid aortic valve stenosis tends to present earlier. Rheumatic heart disease, which usually presents with mitral valve involvement as well, can appear earlier or later in life depending on when the patient was infected. Rheumatic causes of valvular disease are becoming less prevalent in developed countries. Symptoms of AS usually do not occur until the disease is severe and include shortness of breath with exertion, syncope, and chest pain. Once symptomatic, timely replacement of the aortic valve must be undertaken as delay to treatment is associated with a poor prognosis due to rapid disease progression [3].

Restriction of blood flow through the aortic valve increases afterload on the left ventricle. The left ventricle adapts by increasing its wall thickness through added muscle and fibrous tissue. This in turn begins to affect diastolic function as the concentrically hypertrophied ventricle becomes less compliant. Ventricular relaxation during diastole also decreases, further decreasing end-diastolic volumes and increasing end-diastolic pressures (see Chap. 9). This results in cardiac congestion. Higher ejection fractions are required to maintain stroke volume and cardiac output, while compensatory neurohormonal signals such as the renin-angiotensin-aldosterone system mediate increased fluid retention [4]. Increased muscle contraction with decreased relaxation may also lead to angina from ischemia due to prolonged compression of endocardial coronary arteries. The pathway of aortic stenosis is a downward spiral that can be made acutely worse by any number of conditions (e.g., hypovolemia, tachycardia, atrial fibrillation, ischemia, and cardiac depressive agents).

Echocardiographic Evaluation

Aortic Stenosis	
2D	<ul style="list-style-type: none"> • Number of Leaflets (tricuspid vs bicuspid) • Calcification (calcific vs. rheumatic) • Leaflet mobility (restriction systole \pm diastole) • Decreased systolic leaflet opening (assess severity) • Secondary changes (LAE, LVH, Post stenotic dilation)
CFD	<ul style="list-style-type: none"> • Flow acceleration proximal to valve • Turbulent flow distal to valve
Spectral	<ul style="list-style-type: none"> • Peak and mean velocities (gradients) • Aortic Valve Area (continuity equation) • Dimensionless index

LAE left atrial enlargement; *LVH* left ventricular hypertrophy

A good strategy for interrogating the aortic valve with transesophageal echocardiography (TEE) involves a three-step approach:

1. Two-dimensional (2D) inspection of the entire apparatus and associated secondary changes (i.e., ventricular hypertrophy, diastolic dysfunction, left atrial enlargement)
2. Color flow Doppler (CFD) across the valve, and
3. Spectral Doppler (pulsed wave Doppler or continuous wave Doppler) evaluation of blood flow velocities.

Basic perioperative transesophageal echocardiography (PTE) certified practitioners should be able to evaluate the severity of a stenotic valve lesion and “*if the valve lesion is considered severe, or if comprehensive quantification is required to ultimately determine the need for intervention, a consultation with an advanced PTE echocardiographer is necessary to confirm the severity and etiology of the valve pathology.*” Furthermore, prosthetic valves should be assessed by practitioners with advanced PTE certification [5].

Two-Dimensional Assessment

As discussed in Chap. 3, two-dimensional echocardiographic evaluation is best achieved when the structure of interest is placed perpendicular to the ultrasound beam. Therefore, visual inspection of the aortic valve is best obtained in the midesophageal aortic valve long and short axis views (ME AV LAX and ME AV SAX). Two other important views, the transgastric long-axis and deep transgastric long-axis (TG LAX and deep TG LAX), should also be inspected in 2D but due to

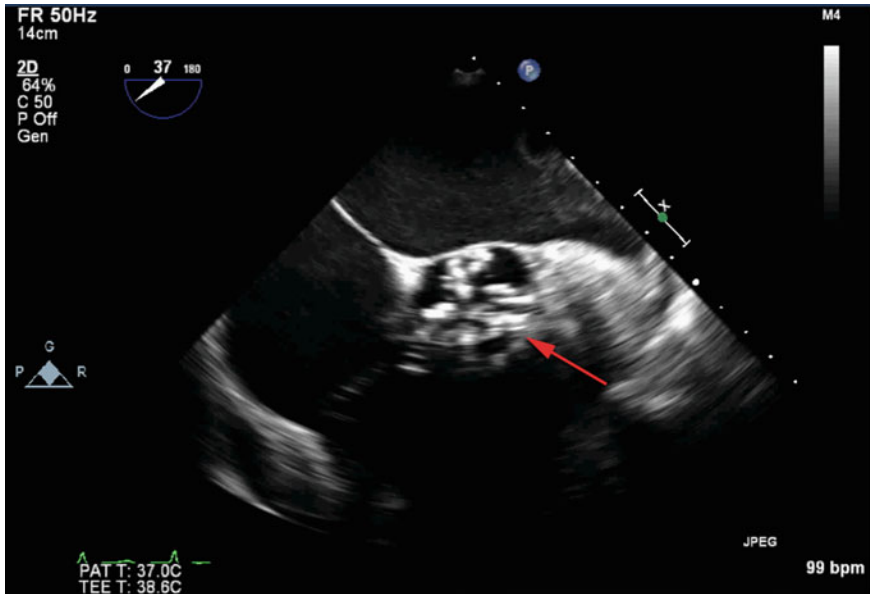


Fig. 7.2 Aortic stenosis: A ME AV SAX view of a severely calcified aortic valve (*red arrow*). Notice the clear distinction of the three leaflets ruling out congenital bicuspid disease. Patient medical history may help to distinguish between senile calcific degeneration and rheumatic disease

their parallel orientation to the ultrasound beam they find more utility in spectral Doppler analysis. The goals of visual inspection include assessing leaflet motion, discerning the location and degree of calcification, and identifying any associated secondary anatomical changes.

In all types of AS, leaflet motion tends to be restrictive with decreased excursion during systole and potentially without appropriate coaptation during diastole. Atherosclerotic or senile calcific degeneration of the valve involves heavy calcification of the entire leaflet, annulus, and may extend through the sinuses of Valsalva to the sinotubular junction (Fig. 7.2; Video 7.1). Congenital bicuspid valves and especially rheumatic valves tend to calcify along the commissures but calcification may become so severe as to be indistinguishable from general atherosclerosis.

Associated anatomic findings in patients with AS are secondary to the change in physiology caused by the stenosis. As mentioned above, left ventricular concentric hypertrophy develops to overcome the increase in afterload. As the disease progresses, diastolic function of the left heart will decrease and indices for assessing diastolic function, such as E to A ratio, E' velocity, E/E' ratio, or pulmonary vein flow will begin to worsen (see Chap. 9). As the diastolic function declines, the left atrium may begin to dilate. As the disease process progresses, left heart failure with decreased ejection fraction resulting in elevated pulmonary artery pressures, and even right heart dilation and dysfunction may occur. Downstream from the valve secondary changes include dilation of the aortic root, termed post-stenotic

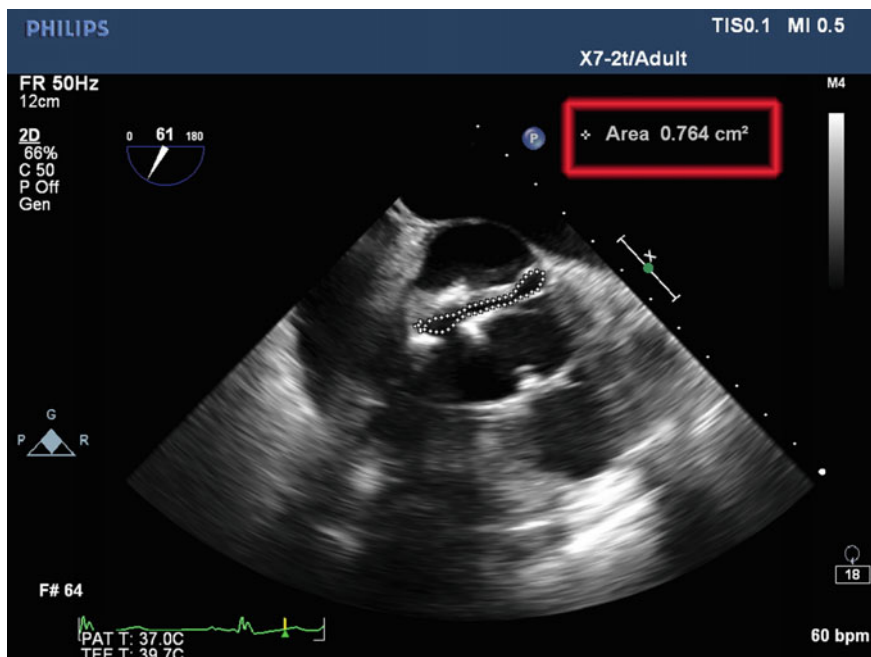


Fig. 7.3 Valve area planimetry: a mid-esophageal aortic valve short axis view of a congenital bicuspid aortic valve during mid to late systole. Using the trace function to outline the ejection orifice at its largest diameter yields an area of 0.764 cm^2 , which constitutes severe aortic stenosis

Table 7.1 Values for grading aortic stenosis severity

	Mild	Moderate	Severe
Valve area (cm^2)	>1.5	1.0–1.5	<1.0
Leaflet separation distance (mm)	>12	<8	<8
Mean gradient (mmHg)	<20	20–40	>40

dilatation. Unlike laminar flow, turbulent flow exerts an outward pressure on the aortic wall and with chronicity leads to aortic dilation.

Using the ME AV SAX view, the area of the aortic valve orifice can be obtained by tracing the perimeter of the leaflet tips during mid to late systole (Fig. 7.3; Video 7.2). However, this can be difficult to visualize with increasing degrees of calcification. Using CFD to identify the narrowest opening between the three leaflets during systole and optimizing tissue echogenicity by turning down the gain can help delineate the orifice. Aortic valve areas of $1.0\text{--}1.5 \text{ cm}^2$ are moderately stenosed, whereas an area less than 1.0 cm^2 is considered severe disease [6] (see Table 7.1).

Two-dimensional views of the valve in the ME AV LAX view, with or without the aid of color flow Doppler, can show the maximum distance between leaflet tips

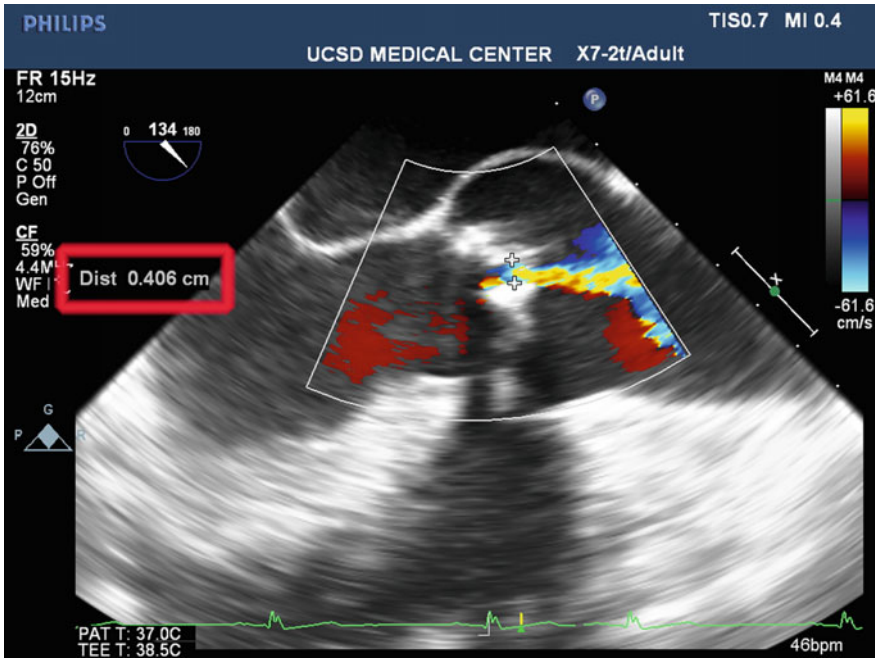


Fig. 7.4 Systolic leaflet tip distance: A ME AV LAX view of maximal leaflet tip separation during systole with the aid of CFD. This distance of 0.406 cm confirms the presence of moderate to severe stenosis

during systole (Fig. 7.4). A distance less than 8 mm is 97 % predictive of severe disease and 100 % predictive of moderate or severe disease, whereas 12 mm or more is 96 % predictive of mild disease or less [7].

Color Flow Doppler (CFD)

Color flow Doppler of the valve may also show flow acceleration in the form of aliasing hemispheres in the LVOT moving toward the stenotic orifice during systole (Fig. 7.5; Video 7.3). While similar to the mitral valve, PISA methods may be employed. However, they are not typically utilized. Instead recognizing the presence of flow acceleration in the LVOT on CFD should alert the echocardiographer that significant stenosis may be present. Due to the high velocity of flow distal to the stenotic valve, CFD will show turbulent flow in the proximal aorta.

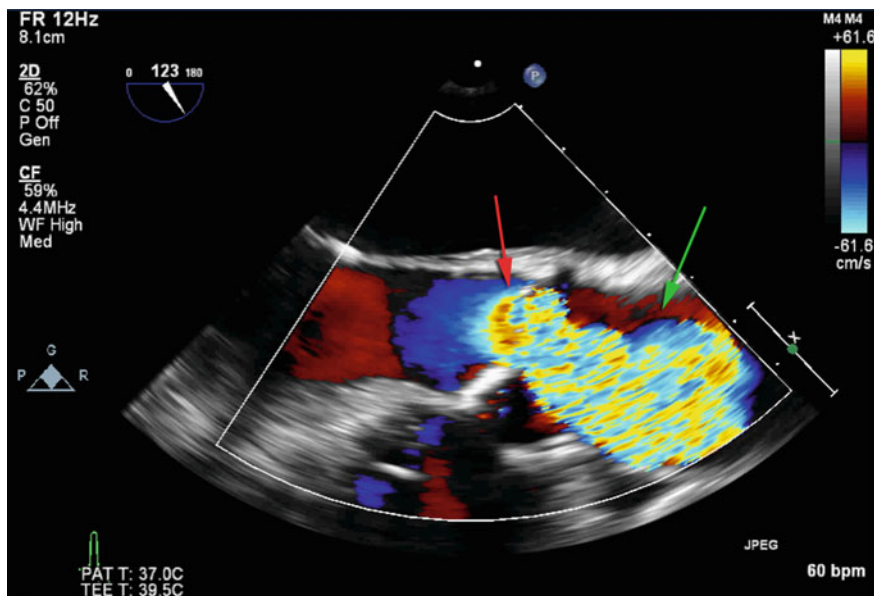


Fig. 7.5 Flow acceleration and turbulence: A ME AV LAX view of flow acceleration in the LVOT as blood flow moves into a stenotic aortic valve orifice. Note the concentric or hemispheric color pattern (*red arrow*). High velocity flow distal to the valve causes a turbulent heterogeneous color pattern indicated by the *green arrow* (vs. a laminar homogenous color pattern in normal flow)

Spectral Doppler

Spectral Doppler assessment of the aortic valve is best obtained in the deep TG LAX and TG LAX views, and is considered the most accurate method for quantifying aortic stenosis echocardiographically. The transgastric views allow the Doppler line of interrogation to be parallel to flow of blood optimizing accurate blood flow velocity measurements. Spectral analysis can then be utilized to estimate the valve area using the continuity equation and the pressure gradient across the valve via the modified Bernoulli equation.

The continuity equation states simply that the volume of blood in a single beat ejected through the LVOT during systole must equal the same volume ejected through the aortic valve orifice during the same single beat. Volumes of blood can be difficult to assess, however, velocity of blood flow through the LVOT and aortic valve can be obtained using pulse and continuous wave Doppler, respectively (Figs. 7.6 and 7.7a). In the deep TG LAX view, the pulse wave Doppler is placed 1 centimeter behind the aortic valve. Using the existing software on the echocardiography machine, the velocity-time integral (VTI) or the integral of the area under the curve of the systolic velocity over time can be calculated (see Chap. 3). The tracing provides the length (cm) that a blood cell travels in one systolic beat in that

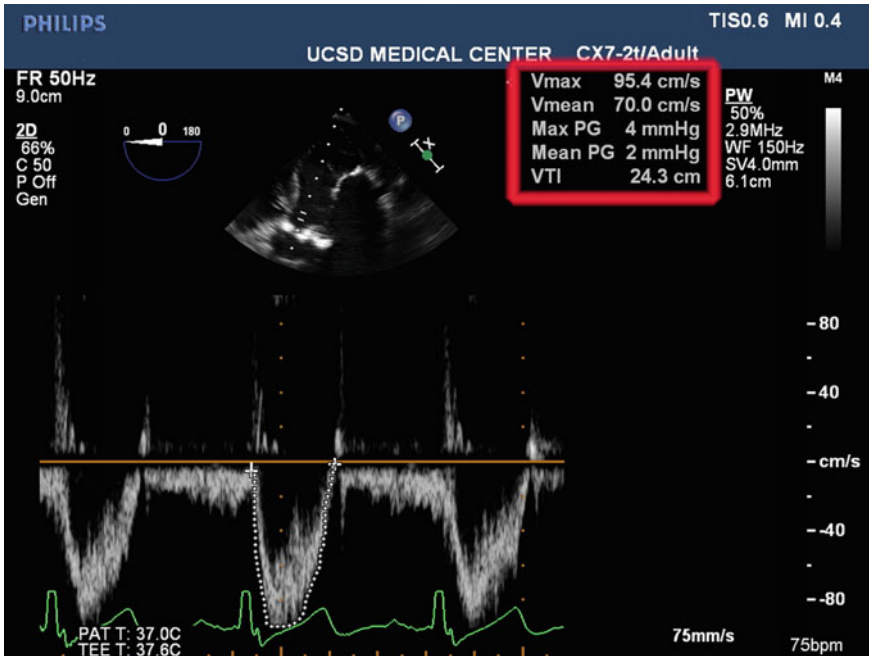
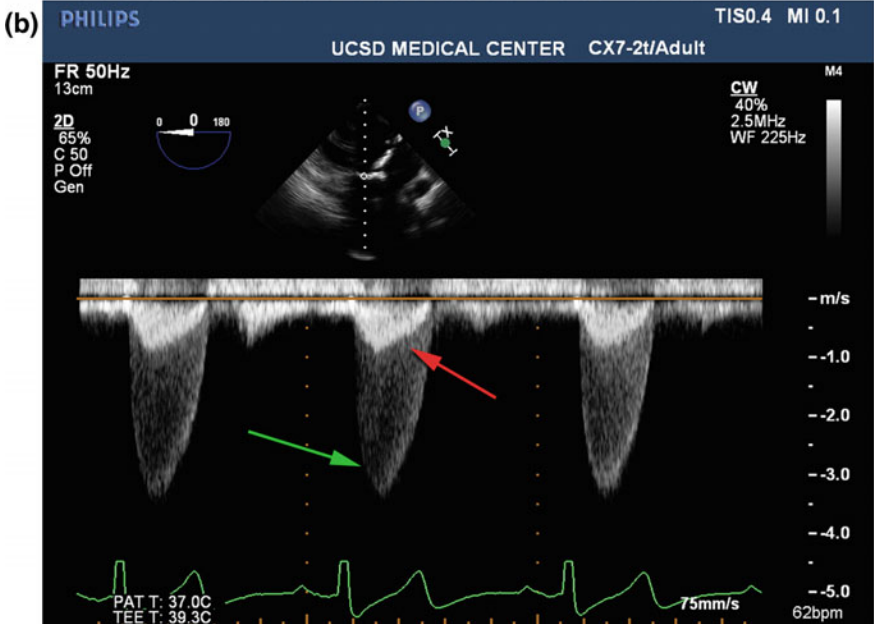
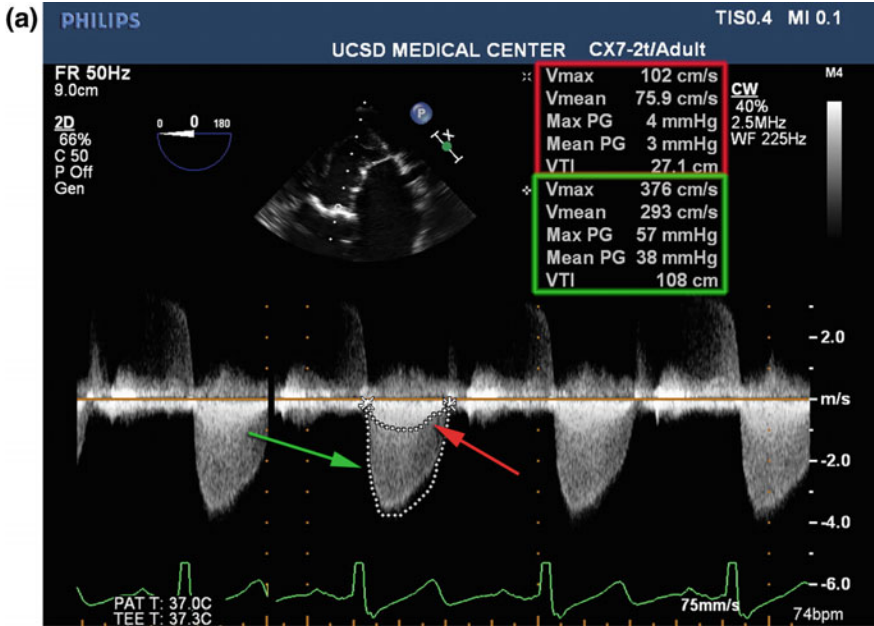


Fig. 7.6 Pulse Wave Doppler of LVOT: A pulse wave Doppler (PWD) measurement of the LVOT one centimeter proximal to the aortic valve at the level of the sample volume (two parallel lines on the cursor). Note that the waveform occurs during systole and has a bright white outline with a black core. The wave is traced from baseline (orange line) and the computer calculates the velocity-time integral (VTI) from the area under the curve

given structure. The LVOT is assumed to be cylindrical in shape and all blood flow traveling though it is laminar (moving in a similar direction at the same speed). The LVOT cross-sectional area (CSA) at the point of pulse wave interrogation can be calculated using πr^2 . The volume of a cylinder of blood that moves uniformly through that space can be calculated by multiplying the cross-sectional area by the velocity-time integral (or cross-sectional area x length). According to the continuity equation principle of “volume in equals volume out,” this cylindrical volume of blood must also pass through the aortic valve during systole. Using the deep TG LAX view or the TG LAX view, the VTI of the aortic valve is measured using continuous wave Doppler and the area of the aortic valve orifice can be calculated as follows:

$$\begin{aligned}
 \text{LVOT volume}_{\text{systole}} &= \text{Aortic valve orifice volume}_{\text{systole}} \\
 \text{LVOT}_{\text{CSA}} \times \text{LVOT}_{\text{VTI}} &= \text{Aortic valve orifice area} \times \text{Aortic valve}_{\text{VTI}} \\
 \text{Aortic valve orifice area} &= (\text{LVOT}_{\text{CSA}} \times \text{LVOT}_{\text{VTI}}) / \text{Aortic valve}_{\text{VTI}}
 \end{aligned}$$



◀ **Fig. 7.7** Continuous wave doppler of aortic valve: **a** A continuous wave Doppler (CWD) measurement of the aortic valve during systole. Since the valve orifice is the narrowest area along the Doppler line of interrogation, a tracing of the outer perimeter of the wave is assumed to represent the VTI at that level (*green arrow*). Note that the echocardiographer also traced a smaller waveform within the larger wave, representing the LVOT VTI (*red arrow*). This is the “double envelope” profile that can be seen with aortic stenosis. **b** A CWD profile of a patient with aortic stenosis. The *green arrow* indicates the AV envelope while the *red arrow* indicates the LVOT envelope

An hour glass is a simple example of the conservation of mass principle involved. Sand proximal to the central orifice moves in a large volume slowly, whereas sand in the narrowest part moves very quickly though the same volume crosses this portion over a fixed time as it moves through the proximal wider area during the same time.

The above described technique utilizes VTI measurements (LVOT and AV) derived from two separate cardiac beats. While this approach to aortic valve area (AVA) is valid, it does assume that the stroke volume does not change beat to beat. This may prove false in the setting of arrhythmias (i.e., atrial fibrillation) or stroke volume changes (i.e., positive pressure ventilation). Therefore, the double envelope technique allows the determination of LVOT and AV VTIs from a singular beat. When a CWD profile in a deep TG LAX view is obtained in an aortic stenosis patient, the profile may display two overlapping “envelopes”. Continuous wave Doppler measures all velocities along its line of interrogation (i.e., range ambiguous). The bulk of velocities measured is traveling slower and make up the brighter inner envelope representing the LVOT velocities. The velocities begin to accelerate and spread out when traversing the stenotic aortic valve. Therefore, the lighter shaded larger envelope represents the AV VTI (Fig. 7.7b). Obtaining both VTI measurements from a single beat removes the variability of stroke volume changes between two different beats.

One potential drawback of the continuity equation is the estimation of the LVOT area. This involves the assumption that the LVOT is circular (which may also be ellipsoid or trapezoidal) as well as the squaring of the radial measurement. Therefore, any error in the measurement becomes significantly expanded and propagated, yielding potentially inaccurate AV areas. An attempt to eliminate this measurement error is the dimensionless index, which is simply a ratio of the LVOT VTI to the AV VTI. A low ratio (less than 0.25) indicates significant velocity differences between the LVOT and AV and represents severe AS.

The modified Bernoulli equation eliminates negligible variables from the original formula in the clinical setting of echocardiography to come up with a simple method of determining change of pressure across a fixed orifice. The simplified equation, $\text{change in pressure} = 4(\text{velocity})^2$, can easily determine the peak pressure gradient across the aortic valve using continuous wave Doppler in a Deep TG LAX or TG LAX view to determine the peak velocity. Mean pressure gradients, which evaluate the average gradient across the valve throughout systole, provide a better trend of disease severity [8]. When tracing a velocity-time profile, the ultrasound

software provides peak velocity and gradient, mean velocity and gradient as well as the VTI discussed previously. Mean aortic valve gradients of 20–40 mmHg denote moderate stenosis, whereas <20 mmHg is mild disease [6] (Table 7.1).

While a peak or mean gradient is less time consuming and does provide a quick glimpse into the severity of aortic stenosis, care must be taken in patients with a reduced stroke volume (e.g., low contractility or hypovolemia). The low stroke volume or low pressure generated from the left ventricle will be reflected in low gradients despite the presence of significant aortic stenosis, thereby underestimating the degree of AS. In this setting the continuity equation is preferred as the reduction in stroke volume and pressure will be reflected in both sides of the equation (the LVOT and AV).

Aortic Regurgitation

As discussed previously, the aortic valve function involves not simply the valve leaflets themselves but also the surrounding structures of the LVOT, aortic valve annulus, sinuses of Valsalva and the proximal ascending aorta. Defects in any of these structures may lead to aortic valve incompetency [9]. When evaluating the cause of aortic incompetency, the etiology can typically be placed into one of three groups:

1. **Aortic Root Dilatation:** Examples of conditions that can cause enlargement of the aortic root include connective tissue disorders (Ehlers–Danlos, Marfan’s, Loey–Dietz), ascending aortic aneurysms, aortitis, and dissections. With enlargement of the aortic root, the cusps of the valve can also be pulled outward, increasing the overall diameter of the valve preventing coaptation of the leaflets. This typically produces a centrally regurgitant jet.
2. **Excessive Cusp Motion:** Flail leaflets that fail to coapt above the annular plane are unable to participate in valve closure and lead to incompetency. These jets tend to be eccentric in nature.
3. **Cusp Integrity:** Heavy calcium deposition, fibrosis, rheumatic heart disease, bicuspid valves, and endocarditis can all cause the integrity of the valve to be breached. The resultant regurgitant jet therefore can be central or eccentric.

Valvular lesions that from the first two groups have the potential of valvular repair, while category three often requires valve replacement.

During evaluation of the aortic valve, care must be taken to note the current hemodynamic state of the patient (i.e., hemodynamic changes of general anesthesia). Similar to the evaluation of the mitral valve, changes in preload, afterload, and contractility can dramatically change the appearance of regurgitant aortic jets. These changes may not give a true representation of disease severity that patients suffer during their normal physiologic hemodynamic state.

Echocardiographic Evaluation

Aortic Regurgitation

2D	<ul style="list-style-type: none"> • Number of Leaflets (tricuspid vs. bicuspid) • Leaflet structure and mobility (calcification, prolapse, flail, perforation, malcoapt) • Surrounding Pathology: Endocarditis (vegetation), Aortic Dissection • Measurements (LVOT, AV Annulus, Sinuses of Valsalva, STJ) • Secondary changes (Eccentric LV Hypertrophy)
CFD	<ul style="list-style-type: none"> • Diastolic turbulent flow • Vena Contracta and Jet Width: LVOT Diameter ratio
Spectral	<ul style="list-style-type: none"> • Pressure Half Time • Deceleration Slope • Diastolic flow reversal (descending thoracic aorta)

LVOT left ventricular outflow tract; *AV* aortic valve; *STJ* sinotubular junction; *LV* left ventricle

Two-Dimensional Assessment

A simple 2-D evaluation will give an overall impression of the valve and supporting structural integrity as well as to categorize the mechanism of regurgitation. Vegetations, flail leaflets, enlarged roots, heavy calcifications, valvular leaflet restrictions, or aortic dissections are among the rapidly identified pathologies using 2-D echo. Observing a malcoaptation in two dimensions alerts the echocardiographer to aortic regurgitation (AR) before even instituting CFD (Fig. 7.8; Video 7.4). Inspection of the valve initially in the ME AV SAX and ME AV LAX views can aid in alluding to a mechanism. Measurements of the LVOT diameter, AV annulus, sinuses of Valsalva, and sinotubular junction can help to ascertain the influence of an enlarged root on valvular function. Leaflet structure and mobility is a key in identifying the role of calcification and restricted leaflet motion (both systole and diastole) versus leaflet destruction and prolapse in the setting of vegetations and endocarditis. Lastly, inspection of the aortic root for aortic dissection flaps is important due to the prognostic implications of a rapid diagnosis (see Chap. 10). Therefore, while the severity of aortic regurgitation rests on CFD and spectral Doppler interrogation, 2D evaluation provides key insight into mechanisms.

Similar to other valvular lesions, secondary anatomical changes may occur in the presence of AR. The chronicity of AR will often dictate such changes. Acute AR

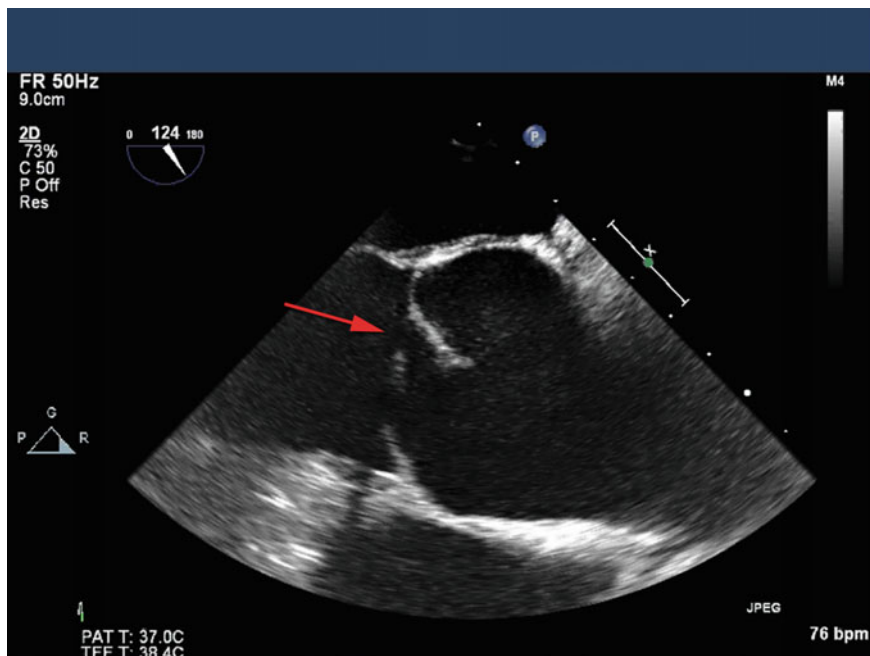


Fig. 7.8 Malcoaptation: A ME AV LAX view in a patient with bicuspid aortic valve disease and a dilated annulus and aortic root. The diastolic image shows a failure of coaptation (*red arrow*)

does not provide the time needed for the LV to accommodate the significant volume overload and may present with LV systolic dysfunction. Chronic AR may be associated with LV dilation and eccentric hypertrophy to accommodate the volume overload with an enlarged stroke volume.

Color Flow Doppler

Color flow Doppler is again most useful in the short and long axis of the aortic valve. Simply placing the CFD box over the aortic valve and adjusting the view to show the point of leaflet coaptation can identify regurgitant lesions (Fig. 7.9; Video 7.5). Once a lesion is identified, as with all valves, quantification of its severity into mild, moderate, or severe should be determined.

Quantification of Aortic Regurgitation

Vena Contracta

The term vena contracta is derived from Latin with vena = blood vessel and contracta = violation. The vena contracta “is the narrowest flow of a regurgitant jet immediately downstream from the convergence region” (Fig. 7.10) [10]. Measuring a vena contracta is a simple and quick method to estimate the severity of aortic regurgitation. The probe is finely adjusted until the largest regurgitant jet cross the

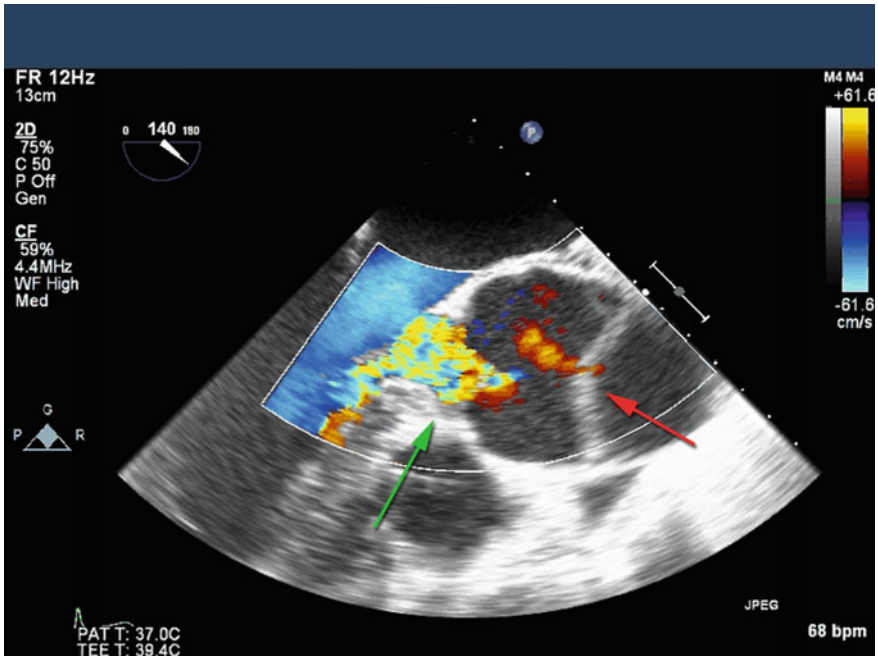


Fig. 7.9 Aortic Regurgitation: A ME AV LAX view in a patient with an ascending aortic dissection and severe aortic regurgitation. The red arrow indicates the intimal flap (flow is seen in the intimal tear). The green arrow indicates the severe aortic regurgitation with flow filling the LVOT during diastole

AV plane is obtained and the image is then acquired. The diastolic phase of the acquired image can then be examined to isolate the largest jet. The neck of the jet at its narrowest point as it crosses the aortic valve is then measured. A diameter below 0.3 mm is mild, 0.3–0.6 mm is graded as moderate and measurements above 0.6 mm is considered severe regurgitation. Importantly, a vena contracta is a relatively load independent measurement which is a valuable characteristic to this quantitative modality.

Jet Width to LVOT Diameter

Jet width to LVOT diameter is another easily deployed quantitative measure of aortic regurgitation. Similar to the measurement of a vena contracta, the regurgitant jet is optimized to find the largest regurgitant flow back into the LVOT. Motion Mode (M-Mode) is a basic function on all echocardiography machines that displays temporal changes of a single echo beam over time. The M-Mode beam should be directed so it images approximately one centimeter into the LVOT from the aortic valve. The size of the jet can then be measured in relation to the width of the LVOT. A regurgitant jet that occupies between 25–65 % of the LVOT is deemed moderate in severity. A jet size sitting below or above this measurement is deemed mild and severe, respectively (Fig. 7.11).

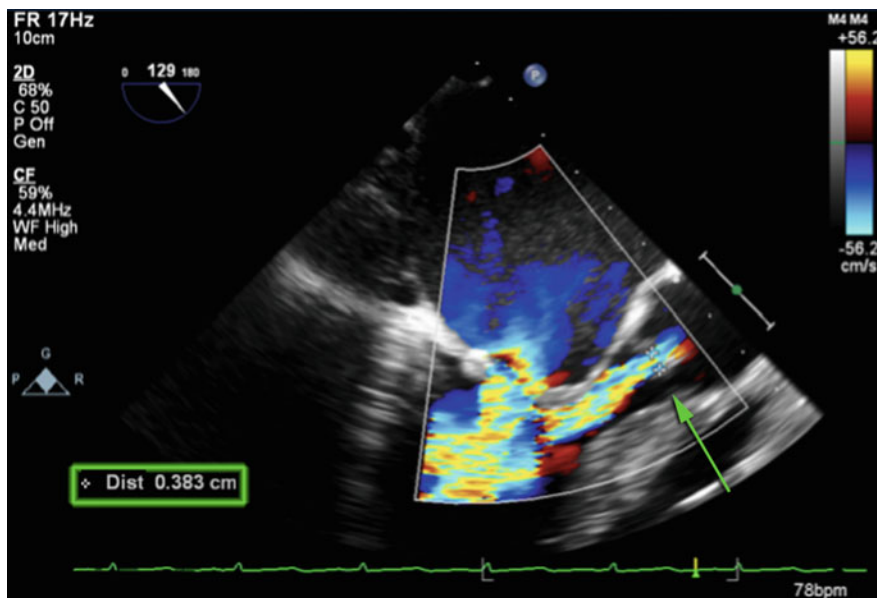


Fig. 7.10 Vena Contracta: The ME AV LAX view with a color flow Doppler box over the mitral and aortic valves. Regurgitant flow can be seen entering the left ventricle. A caliper measurement (green arrow) is seen measuring the jet as it crosses the aortic valve showing a distance of 0.38 cm (moderate severity)

Spectral Doppler

Pulse wave Doppler and continuous wave Doppler can both be utilized to further quantify the severity of aortic regurgitation. These methodologies are complementary to CFD severity techniques. Like any clinical diagnosis, it is a culmination of findings to determine severity as opposed to one single result.

Aortic Valve Pressure Half Time (PHT)

The principle of aortic valve pressure half time, as its name suggests, is to quantify the period of time it takes for the pressure differential between the left ventricle and aorta to decrease by half. This is analogous to the PHT utilized in mitral valve stenosis (see Chap. 6). From the deep TG LAX view, a continuous wave Doppler signal can be aligned to the jet entering the LVOT from a regurgitant lesion. The slope of the regurgitant jet from its peak velocity to the end of its decay is traced (Fig. 7.12). The AR PHT is then calculated by the included ultrasound software, providing a time value in milliseconds. A larger opening in the aortic valve (worse aortic regurgitation) will be noted by a more rapid equilibration of pressures between the aorta and the LVOT. Moderate aortic regurgitation is indicated by a time of 200–500 ms. Values on either side of this are severe (<200 ms) or mild (>500 ms) (see Table 7.2). Similarly the slope of the deceleration line can infer the degree of AR severity. The steeper the slope the more severe the AR, such that

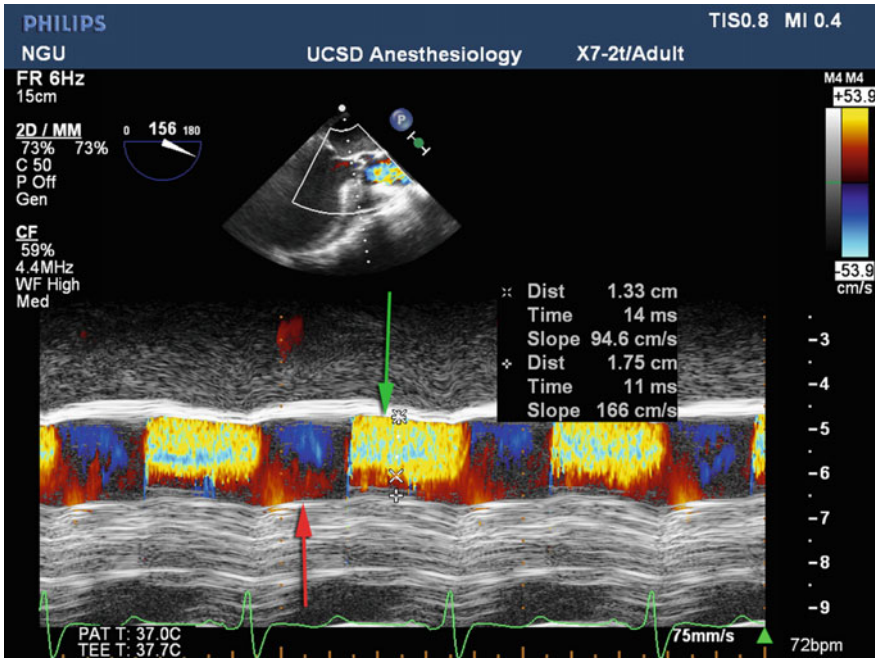


Fig. 7.11 Jet Width to LVOT Diameter: M-Mode of an echo beam one centimeter from the aortic valve into the LVOT. Note the EKG confirming the jet is in diastole. Measurements identify a LVOT jet width of 1.33 cm, LVOT diameter of 1.75 cm and a ratio of jet to outflow tract of 76 % indicating severe regurgitation

values greater than 3 meters per second indicate severe AR while values greater than 2 m/s indicate moderate AR.

Descending Aorta Reversal of Flow

Determining the direction of flow in the descending aorta can help to confirm the severity of aortic regurgitation. In a normal patient, aortic flow in the descending thoracic aorta should be antegrade during systolic ejection as well as during the diastolic runoff. If reversal of flow in the descending thoracic aorta during diastole is identified, aortic insufficiency is confirmed. The further from the aorta valve that the flow reversal is detected the more severe the aortic regurgitation such that detection of reversal in the lower descending aorta suggests severe regurgitation. However conversely, the absence of reversal of flow does not rule out a severe regurgitant lesion. Moderate regurgitant lesions may have reversal in the proximal descending aorta while mild regurgitant lesions typically will not have any reversal of flow within the descending aorta.

In order to make this assessment of the diastolic flow, a long-axis view of the descending aorta is obtained. A pulsed wave Doppler beam is then aligned as parallel to flow as possible. A severely incompetent valve will produce holodiastolic flow reversal (Fig. 7.13).

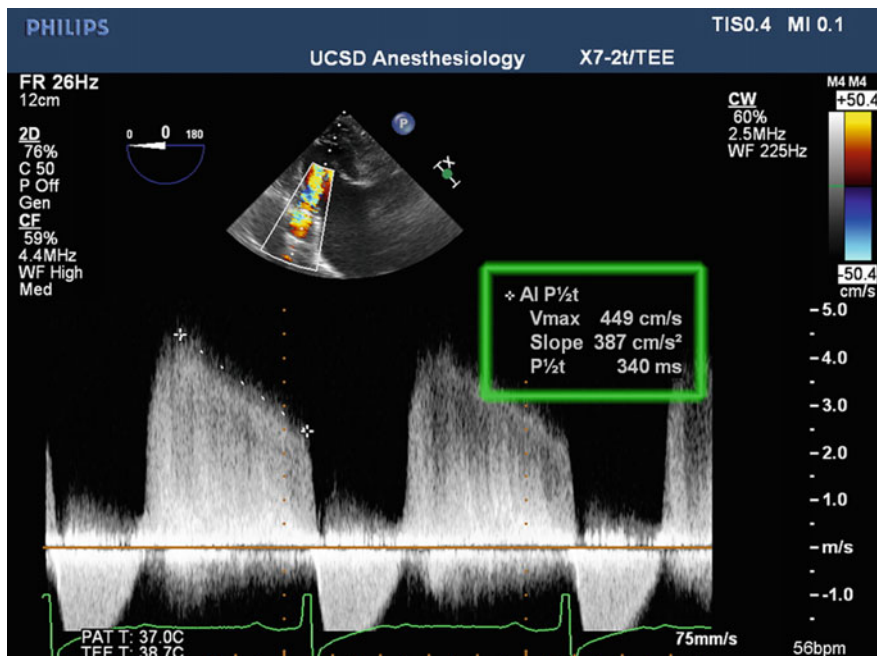


Fig. 7.12 Aortic valve pressure half time: a deep TG LAX view is obtained to align the continuous wave Doppler beam parallel to the flow into the LVOT. The peak velocity (V_{max}) of the regurgitation is the starting point for the measurement of the jet’s pressure decay. The PHT is then calculated –340 ms (moderate aortic regurgitation)

Table 7.2 Values for grading aortic regurgitation severity

	Mild	Moderate	Severe
Vena contracta (mm)	<0.2	0.2–0.6	>0.6
Jet width: LVOT diameter ratio (%)	<25	25–65	>65
PHT (ms)	>500	200–500	<200

LVOT left ventricular outflow tract; PHT pressure half time

Conclusion

The aortic valve is an integral cardiac structure allowing the ejection of blood to the aorta while maintaining a gradient during diastole to provide diastolic runoff and prevent reflux of blood back into the left ventricle. Dysfunction in the form of stenosis leads to a hinderance of systolic ejection, hypertrophy of the left ventricle and eventual heart failure, while dysfunction in the form of regurgitation may occur from multiple mechanisms and may lead to eccentric hypertrophy and congestive

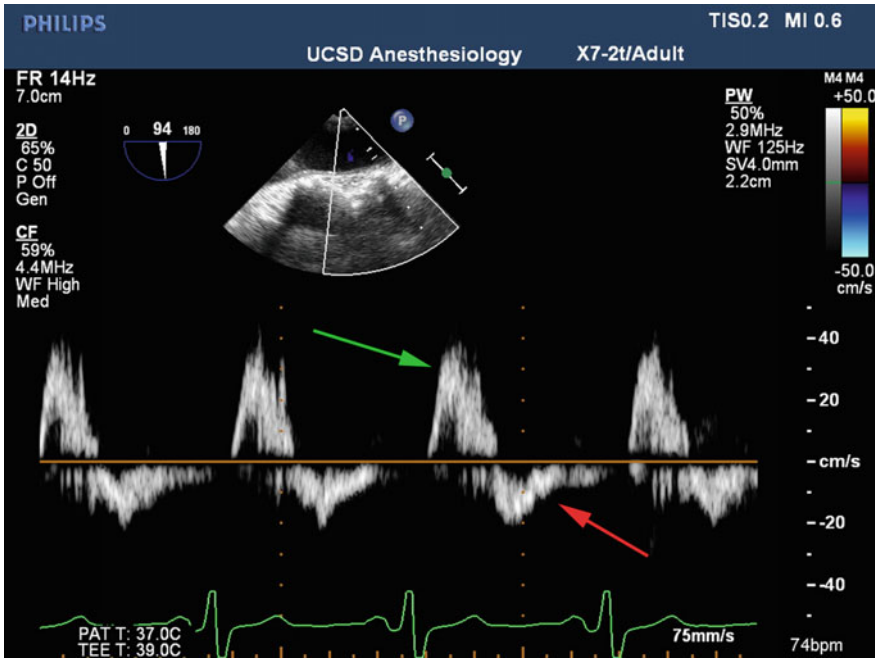


Fig. 7.13 Descending aorta reversal of flow: a long axis of the descending aorta is obtained, and a pulse wave Doppler beam is placed within the aorta. The waveform demonstrates normal systolic forward flow (*green arrow*), however holodiastolic flow reversal (*red arrow*) is noted indicative of severe aortic regurgitation

heart failure. Echocardiography via two-dimensional, color flow Doppler, and spectral Doppler plays a key role in the diagnosis and management of such patients.

References

1. Bellhouse BJ, Bellhouse FH. Mechanism of closure of the aortic valve. *Nature* 1968;217:86–87.
2. Tribouilloy CM, et al. *Circulation*. 2000;102:558–64.
3. Horstkotte D, Loogen F. The natural history of aortic valve stenosis. *Eur Heart J* 1988;9(Suppl E):57–64.
4. Nadir MA, Wei L, Elder D, Libianto R, Lim T, et al. Impact of renin-angiotensin system blockade therapy on outcome in aortic stenosis. *J Am Coll Cardiol*. 2011;58(6):570–6.
5. Reeves ST, Finley AC, Skubas NJ, Swaminathan M, Whitley WS, Glas KE, et al. Basic perioperative transesophageal echocardiography examination: a consensus statement of the American society of echocardiography and the Society of cardiovascular anesthesiologists. *J Am Soc Echocardiogr*. 2013;26:443–56.
6. Baumgartner H, Hung J, Bermejo J, Chambers JB, Evangelista A, Griffin BP, et al. Echocardiographic assessment of valve stenosis: EAE/ASE recommendations for clinical practice. *J Am Soc Echocardiogr*. 2009;22(1):1–23.

7. Godley RW, Green D, Dillon JC, Rogers EW, Feigenbaum H, Weyman AE. Reliability of two-dimensional echocardiography in assessing the severity of valvular aortic stenosis. *Chest*. 1981;79:657–62.
8. Lindman B, Bonow R, Otto C. Current management of calcific aortic stenosis. *Circ Res*. 2013;113:223–37.
9. Bekeredjian R, Grayburn P. Valvular heart disease: aortic regurgitation. *Circulation*. 2005;112:125–34.
10. Lancellotti P, Tribouilloy C, et al. European association of echocardiography recommendations for the assessment of valvular regurgitation. Part 1: aortic and pulmonary regurgitation (native valve disease). *Eur J Echocardiogr*. 2010;11(3):223–244.

Chapter 8

The Right Heart

Dalia Banks, MD, FASE

Abstract Historically, clinical and research efforts have primarily focused on the left ventricle. However, relatively recent identification that evidence of right heart dysfunction increases the perioperative morbidity and mortality of patients undergoing both cardiac and noncardiac surgery has brought the echocardiographic evaluation of the right heart into the spotlight. This chapter serves to identify the unique concerns when evaluating echocardiographically the complex geometry and physiology of the right heart as well as its unique adaptive properties in response to acute and chronic afterload increases. Both anatomical assessments and quantitative methods of evaluating right ventricular function will be discussed. Transesophageal echocardiography therefore plays a key role in the identification and management of those patients at risk for right heart dysfunction.

Keywords Right ventricle • Right atrium • Pulmonary hypertension • Pulmonary embolism • Tricuspid regurgitation • Pulmonary artery

Introduction

The right ventricle (RV) historically has been overlooked and viewed as less important than the left heart. However, recently there has been considerable interest in understanding the function of the right ventricle. Right ventricular dysfunction has been associated with increased morbidity and mortality within both cardiac and

Electronic supplementary material The online version of this chapter (doi:[10.1007/978-3-319-34124-8_8](https://doi.org/10.1007/978-3-319-34124-8_8)) contains supplementary material, which is available to authorized users.

D. Banks, MD, FASE (✉)
Department of Anesthesiology, University of California San Diego,
9300 Campus Point Drive, MC 7651, La Jolla, San Diego, CA 92037, USA
e-mail: dabanks@ucsd.edu

noncardiac surgical arenas. The main function of the RV is to enhance venous return by accommodating systemic return into a low-pressure chamber and subsequently transit blood to the left heart via the low-pressure pulmonary circuit. Recognition of right heart dysfunction due to acute pathology such as pulmonary embolism or chronic pathology such as pulmonary hypertension is key to perioperative management. Transesophageal echocardiography (TEE) plays a significant role both in the identification and quantification of perioperative right heart dysfunction.

Right Ventricle Structure and Function

The RV forms the major portion of the anterior surface of the heart immediately behind the sternum, while the inferior border of the RV abuts the diaphragm. The right ventricle is an asymmetric crescent-shaped chamber that is wrapped around the right and anteroseptal side of the left ventricle (LV). In healthy individuals, RV dimensions are roughly two-thirds the size of LV dimensions. The RV is generally separated into three portions: inflow, apical, and outflow. These distinct regions are separated by a series of encircling muscular bands. The inflow portion is trabeculated and consists of the tricuspid valve, chordae tendinae, and papillary muscles. The apical portion is also a muscular portion connecting the inflow to the smooth-surfaced outflow tract. The outflow region therefore contains the smooth myocardial outflow tract and pulmonic valve [1, 2].

The encircling muscular bands include four individual bands, however the moderator band is most important to the echocardiographer. The moderator band extends from the base of the anterior papillary muscle near the ventricular free wall to the ventricular septum. When it becomes prominent from right ventricular hypertrophy, the moderator band may be mistaken for a thrombus or intracavitary mass [3, 4].

The RV wall motion is complex, characterized by a peristaltic-like motion. Contraction is sequential, beginning with the inlet portion contracting toward the apex and ending with the infundibulum. RV longitudinal shortening occurs mainly during the ejection phase of the cardiac cycle, while circumferential motion occurs mainly during the isovolumic contraction phase [5, 6].

The RV is mostly supplied by the right coronary artery (RCA) with the posterior descending artery (PDA) supplying one-third to two-third of the RV septum. The left anterior descending artery (LAD) may supply a portion of the apex, while branches off of the RCA, the acute marginal arteries, supply the RV free wall. Lastly, in the majority of patients, the RCA supplies perfusion to the atrioventricular (AV) node and sinoatrial (SA) node.

The RV provides a similar stroke volume as the LV, however with 25 % of the stroke work due to the low-pressure, high-compliance circuit in the pulmonary circulation [7]. As a result, the wall thickness of the RV is half the size of LV wall, making the RV a much more compliant chamber. The right and left ventricles share

the interventricular septum (IVS) and are enclosed within the same pericardial sac. Therefore, ventricular interdependence exists. The IVS contributes to both LV and RV function, is responsible for approximately one-third of the RV stroke work under normal conditions, and is a major determinant of overall RV performance [8–10]. Normally the IVS is shifted toward the RV free wall (concave toward the LV) during systole and diastole, contributing to RV ejection. However, this relationship is changed in conditions that lead to an increase in RV pressure or volume overload, shifting the septum paradoxically toward the LV, altering LV geometry, resulting in decreased LV preload and low cardiac output [11].

Transesophageal Echocardiographic Views for Evaluation of the Right Ventricle

Qualitative evaluation of the RV should allow the examiner to answer five questions as illustrated in Table 8.1. As described in Chap. 2, there are several views that focus on evaluation of the right heart. They are briefly outlined below.

Midesophageal four-chamber—A midesophageal (ME) view with a multiplane angle of 0–20° allows for evaluation of RV chamber size, function, and anatomical variants [12, 13]. From a standard ME four-chamber view, turning the probe to the right (clockwise) allows imaging of the right atrium (RA), right ventricle, tricuspid valve (TV), as well as the interatrial and interventricular septums. This view is the most utilized view to assess the right heart.

ME RV inflow–outflow view—Placing the right heart in the center of the imaging sector and increasing the multiplane angle to 60–90° will develop the ME RV inflow–outflow view. This view demonstrates the “wrapping” nature of the RA, RV, and pulmonary artery (PA) in relation to the left heart. Assessment of the RA, TV, RV free wall, RV outflow tract, pulmonic valve (PV), and main PA can be accomplished in this view. With an image of both the TV and PV, this view is used to help guide placement of the pulmonary artery catheter as well as estimate RV systolic pressure.

ME bicaval view—From the ME RV inflow–outflow view, increasing the multiplane angle to 90–110° and turning the probe to the right develops the ME bicaval view. This view displays the LA, RA, and the interatrial septum. In the

Table 8.1 Outline of echocardiographic evaluation of the right heart

Echocardiographic evaluation of the RV should allow the examiner to answer the following five questions
1. What is the RV Shape?
2. What is the RV area relative to LV area?
3. What is the RV free wall thickness?
4. How is the RV free wall motion?
5. What is the interventricular septal motion?

standard bicaval view, the SVC and IVC, as well as the right atrial appendage, are in view. Turning of the probe slightly left (counterclockwise) or increasing the multiplane angle by 10–20° will bring the tricuspid valve and coronary sinus in view. This adjustment results in the modified bicaval view [2, 12].

ME ascending aortic short axis view—This view demonstrates the relation of the main and right PA to the ascending aorta and SVC, and proves useful in identifying PA dilatation and PA thrombus, as well as confirming the position of a properly placed PA catheter.

Transgastric (TG) midpapillary short axis view—With a rightward probe rotation from a standard TG midpapillary short axis view, an image of the crescent-shaped RV is developed. Again, the anterolateral position of the RV in relation to the left ventricle (LV) is noted.

TG RV inflow view—Increasing the multiplane angle to 90° from the prior view yields the TG RV inflow view. This view shows a “two-chamber” view of the right heart with a focus on the tricuspid valve and the subvalvular apparatus, as well as the right ventricular free wall.

Physiology of the Right Heart: Adaptations to Pulmonary Hypertension

The pulmonary circulation is normally a low-pressure and low-resistance circuit in comparison to the systemic circulation. The normal systolic, diastolic, and mean pulmonary artery pressure (PAP) are 22, 10, and 15 mmHg, respectively. The pulmonary vascular resistance (PVR) is normally 0.9–1.4 Wood units, or about 90–120 dynes sec cm^{-5} . Pulmonary hypertension (PH) is generally defined as a mean PAP of greater than 25 mmHg, or a PVR greater than 300 dynes sec cm^{-5} . A mean PAP greater than 50 mmHg or a PVR greater than 600 dynes sec cm^{-5} is considered severe PH. The PVR is important because it represents the afterload of the right ventricle (the pressure encountered during ejection), and therefore, affects RV function and cardiac output.

Emphasis on PH classification began in 1973 at the World Health Organization conference and since then, has undergone multiple changes as the appreciation of the disease and treatment of PH has evolved, resulting in five distinct subgroups of patients sharing specific features [13–15] (Table 8.2). The effects on the RV in response to pulmonary hypertension are readily identified on echocardiography. The adaptations are generally categorized as RV dilation in response to volume overload (inability to properly move the volume through the pulmonary circuit) and RV hypertrophy in response to the increase afterload (inability to eject a proper stroke volume due to increased resistance). Both of these adaptations, when progressive, lead to RV dysfunction. Additionally, septal wall motion may become abnormal with a deviation toward the left heart, further contributing to RV dysfunction. An echocardiographic evaluation with particular focus on the right side of the heart allows both the identification as well as quantification of RV dysfunction.

Table 8.2 Classification of pulmonary hypertension

Definition pulmonary hypertension (PH)	Clinical group(s)
Precapillary: MPAP > 25 mmHg PCWP < 15 mmHg	Group I: Pulmonary arterial Hypertension (PAH) and other subtypes of PAH Group III: World Respiratory disease and hypoxemia Group IV: Chronic thromboembolic pulmonary hypertension (CTEPH) Group V: Miscellaneous causes
Postcapillary: MPAP > 25 mmHg PCWP > 15 mmHg	Group II: Left heart disease

Adapted from McLaughlin et al. [16], Bossone et al. [17]. Mean pulmonary artery pressure (MPAP); Pulmonary capillary wedge pressure (PCWP)

Right Ventricular Enlargement

The normally thin-walled, crescent-shaped RV allows the RV to be highly compliant, accommodating a large increase in preload to maintain a normal stroke volume in the early stages of RV dysfunction. Consequently, the initial primary compensatory mechanism of RV dysfunction often is dilatation that is usually well tolerated. With progressive dilatation, the ability to maintain a normal stroke volume is lost. Qualitative visual measures are typically used to assess RV chamber size in the ME four-chamber view. RV size normally occupies two-thirds of the cross-sectional area in comparison to LV area. Additionally, the LV typically forms the cardiac apex in this view. With mild enlargement, the RV increases in size to greater than two-thirds of the LV cross-sectional area; with moderate enlargement, the RV apex includes both the RV and LV and the cross-sectional areas are equal; while with severe enlargement, the RV apex completely forms the cardiac apex, and the cross-sectional area of the RV exceeds that of the LV (Fig. 8.1; Video 8.1).

Additionally two-dimensional measurements of the RV in the ME four-chamber view can be utilized to assess RV size. The RV basal dimension [measure of the width of the TV annulus in the ME four-chamber view] ranges from 2 to 2.8 cm with 4.0 cm as the reference limit of a severely dilated annulus [18]. Longitudinal measurements from the tricuspid valve plane to the RV apex range from 7.1 to 7.9 cm, with a 9.2 cm measurement indicating a severely dilated RV [19, 20].

Right Ventricular Hypertrophy

Echocardiographic evaluation of RV wall thickness may also serve to evaluate global RV performance because conditions of RV pressure overload cause

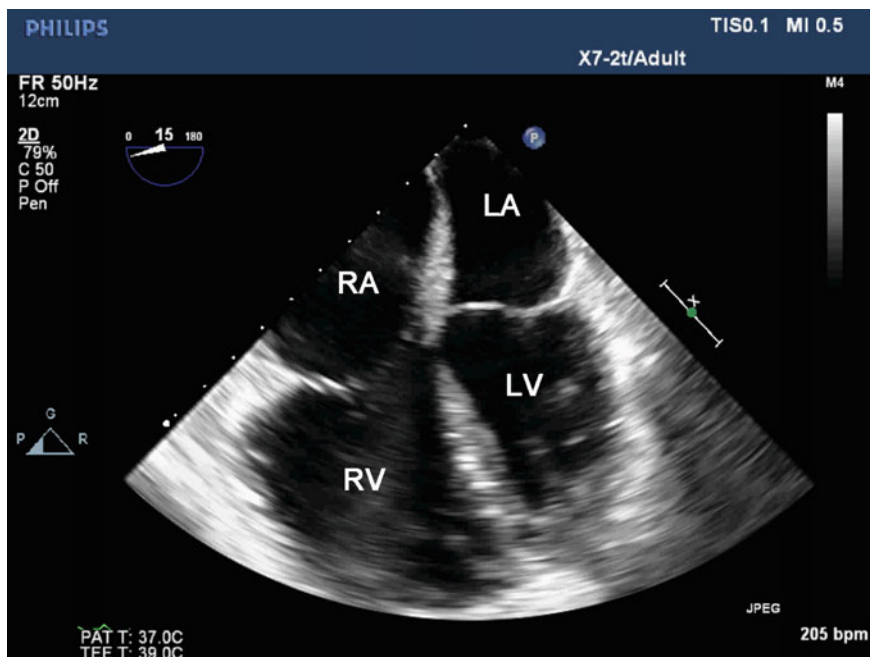


Fig. 8.1 A mid-esophageal four-chamber view of a patient with pulmonary hypertension and severe right ventricular enlargement. Note that the size of the right ventricle (RV) exceeds that of the left ventricle (LV) and the apex of the heart appears to be formed by the RV. RA right atrium; LA left atrium

compensatory right ventricular hypertrophy (RVH). This increase in RV myocardial mass is an effort to maintain cardiac output in the presence of increased PVR.

TEE evaluation of RV wall thickness typically assesses the lateral RV free wall thickness. Normally, the RV is thin-walled with RV free wall thickness (RVWT) approximately half the wall thickness of the LV, measuring <5 mm at end-diastole. RVH may be diagnosed when the RVWT is >5 mm, while RVWT exceeding 10 mm is considered severe hypertrophy (Fig. 8.2). The best views to measure the RV free wall are in the ME four-chamber, ME RV inflow–outflow, or TG RV inflow views. Measurements of RVWT occur during myocardial relaxation (diastole) and must exclude the epicardial fat layer. Additionally, the moderator band is usually more prominent in patients with RV hypertrophy and is often visualized near the RV apex (Fig. 8.3; Video 8.2).

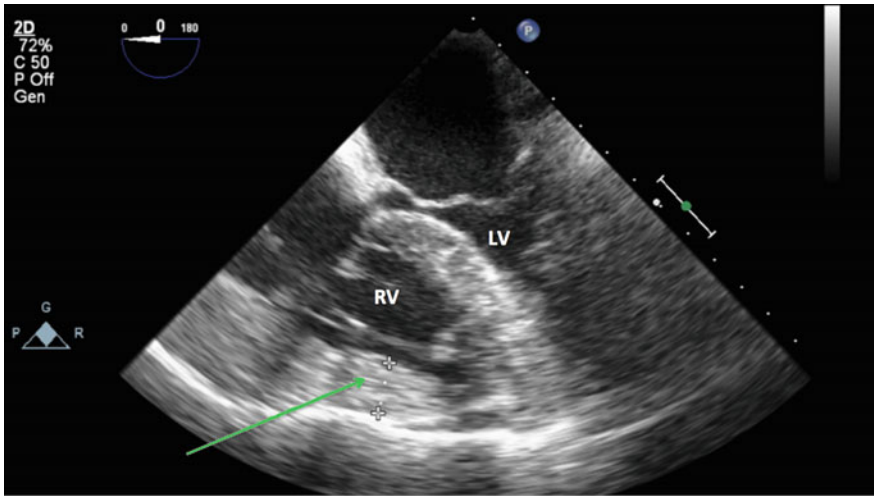


Fig. 8.2 A midesophageal four-chamber view of a patient with chronic pulmonary hypertension and resultant right ventricular hypertrophy (*green arrow*)

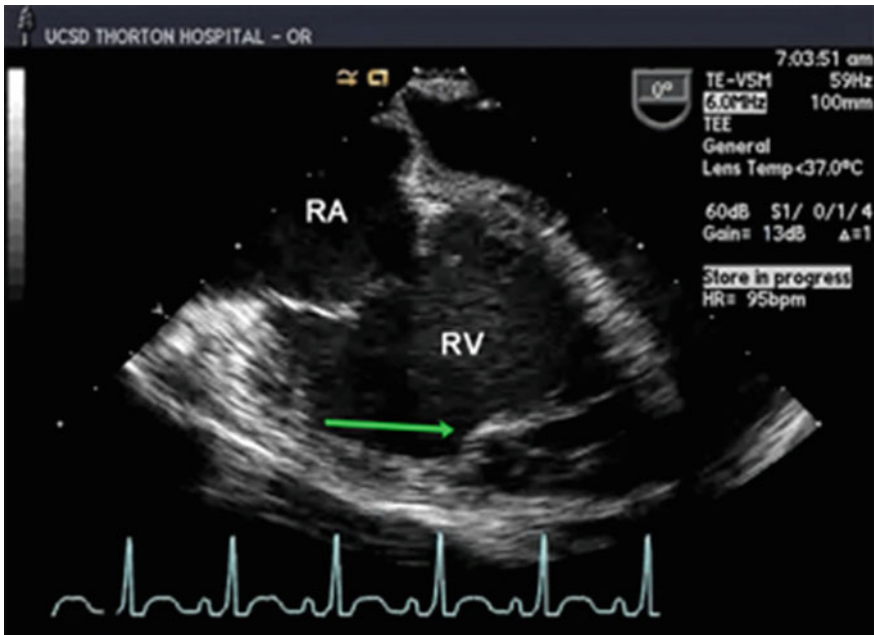


Fig. 8.3 A midesophageal four-chamber view of a patient with severe right ventricular and right atrial enlargement. A prominent moderator band (*green arrow*) is present

Quantitative Assessment of Right Ventricular Function

Right ventricular dysfunction	
2D	<ul style="list-style-type: none"> • Right Atrial Enlargement • Right Ventricular Enlargement and/or hypertrophy • IAS/IVS shifted toward the left heart • Underfilled LA and LV • Decreased TAPSE (M-mode) • Decreased FAC
CFD	<ul style="list-style-type: none"> • Tricuspid regurgitation
Spectral	<ul style="list-style-type: none"> • TDI: Tricuspid Annular Velocity (S') • PASP Estimation • Hepatic Vein confirmation of TR

IAS Interatrial septum; *IVS* Interventricular septum; *LA* Left atrium; *LV* Left ventricle; *TAPSE* Tricuspid annular plane systolic excursion; *FAC* Fractional area of change; *TDI* Tissue Doppler imaging; *PASP* Pulmonary artery systolic pressure; *TR* Tricuspid regurgitation

A quantitative evaluation of RV global function is more difficult to achieve owing to its more complex shape [19–21]. Unlike the shape of the LV which allows some geometrical assumptions (e.g., Simpson’s method of discs), the shape of the RV is complicated as evidenced by its triangular shape in the ME four-chamber view, “wrap around” nature in the ME RV inflow–outflow view, and crescent shape in the TG midpapillary short axis view. Additionally, contraction of the RV differs from the LV’s concentric and “piston-like” longitudinal contraction. The RV contracts in a peristaltic-like manner from the base toward the apex and subsequently the outflow tract. The major contributor to RV ejection is the basal contraction, and therefore constitutes a basis for several methods of quantitative RV analysis. This complex shape and differing contraction has necessitated surrogate parameters to be developed and subsequently validated for RV systolic function.

Tricuspid Annular Plane Systolic Excursion (TAPSE)

TAPSE measures the longitudinal movement of the tricuspid annulus toward the apex during systole. Again the basal contraction of the RV is a large contributor to RV ejection; therefore TAPSE is a single measurement that extrapolates and estimates global RV function. Normal TAPSE measurement is greater than 17 mm, therefore, TAPSE values <17 mm are suggestive of RV systolic dysfunction [18]. While often obtained as a visual estimate in noncardiac surgery, measurement of

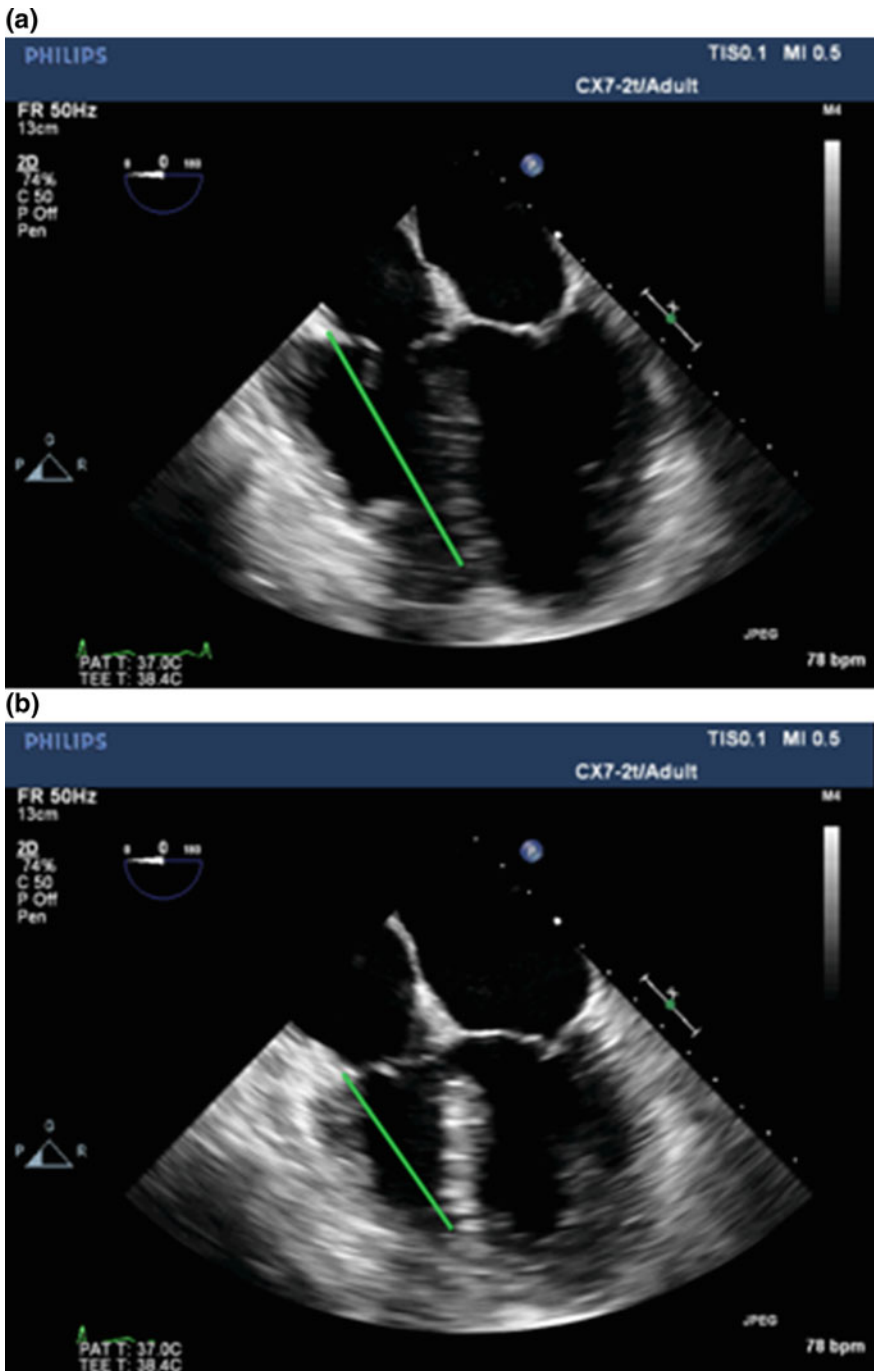


Fig. 8.4 **a** A midesophageal four-chamber view with a *green line* depicting measurement of the distance from the tricuspid annulus to the apex in diastole. **b** A systolic frame from the same patient with a *green line* depicting the distance from the tricuspid annulus to the apex. TAPSE is calculated as the difference of these two measurements

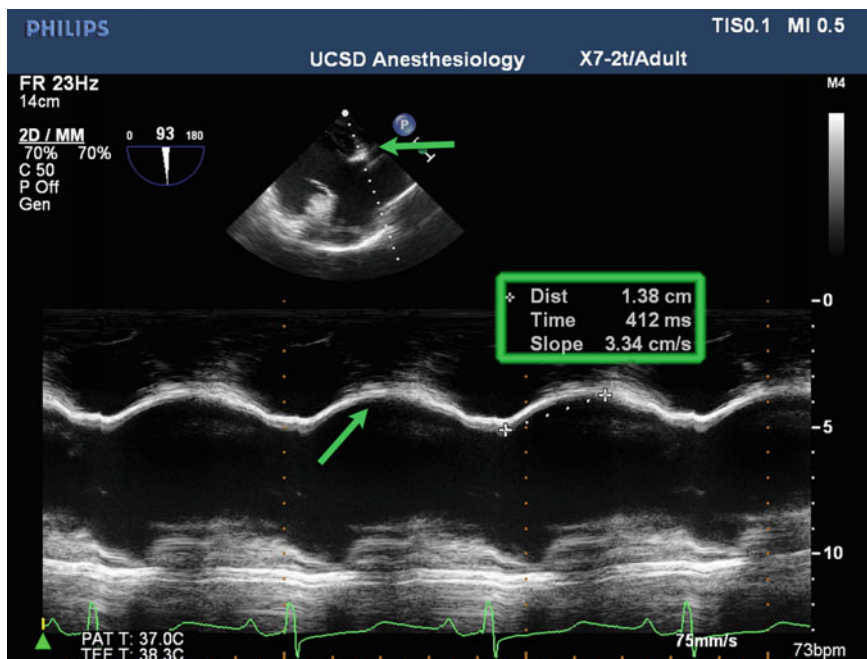


Fig. 8.5 An M-mode analysis of the lateral tricuspid annular motion in a modified transgastric right ventricular inflow view. The *green arrow* on the 2D image depicts the tricuspid annular motion on the M-mode display. TAPSE is easily measured by the movement of the annulus between diastole and systole

TAPSE involves measuring along the RV long axis from the lateral tricuspid annulus to the apex of the RV at end-diastole and end-systole [2] (Fig. 8.4a, b). The difference in measurements constitutes the TAPSE.

Some of the major limitations of TAPSE include oblique imaging of the RV (TV motion is often not aligned to the TEE ultrasound signal) and poor endocardial delineation; both can yield inaccurate measurements. Transthoracic echocardiography, in an apical four-chamber view, allows the alignment of the TV annulus to the echo plane and the use of M-mode to quantify TV motion. The use of a modified TG RV inflow view (deeper insertion of the TEE probe and an increase of the multiplane angle by 10–20°) can provide a less oblique angle of TV motion to the ultrasound probe, allowing the use of M-mode echocardiography (Fig. 8.5).

RV Fractional Area of Change (RV FAC)

RV fractional area of change is analogous to LV fractional area of change (see Chap. 4), and also serves as a surrogate measure of right ventricular ejection fraction (RV EF). TEE assessment of RV FAC is commonly performed in the ME four-chamber view and is the percentage change in ventricular area between systole and diastole with a normal value of >35 %. While a RV FAC <35 % indicates RV dysfunction, values lower than 17 % for RV FAC are suggestive of severe RV dysfunction [18]. Right ventricular FAC is obtained by tracing the RV endocardium both in systole and diastole from the annulus, along the free wall to the apex, and then back to the annulus along the IVS. Care must be taken to exclude trabeculations while tracing the RV area (Fig. 8.6a, b). This measurement correlates well with RV EF by cardiac magnetic resonance imaging (MRI) [22] Fractional area change (FAC) is calculated as follows:

$$\text{FAC} = (\text{End Diastolic Area} - \text{End Systolic Area}) / \text{End Diastolic Area} \times 100$$

Tissue Doppler Imaging

Tissue Doppler Imaging (TDI) is a mode of Doppler imaging that utilizes a filter that removes high velocity, low intensity signals (i.e., blood) and focuses on low velocity, high intensity signals (i.e., myocardium). When applied to the RV, measurement of the velocity of the basal RV free wall allows a determination of peak systolic velocity (S'). After initiation of TDI, a pulsed wave Doppler beam is placed at the basal RV free wall (near the TV annulus) in either a ME four-chamber view or a modified TG RV inflow view [23]. Attention to alignment of the motion of the myocardium to the ultrasound probe is the key to prevent an underestimation (Fig. 8.7) An RV S' measurement less than 9.5 cm/s is suggestive of abnormal RV function [2]. Peak systolic velocity has been demonstrated to correlate well to RV EF as determined by cardiac MRI [21, 23].

Right Ventricular Myocardial Performance Index (MPI)

The myocardial performance index, also known as the Tei Index, is a global estimate of both systolic and diastolic cardiac performance of the RV during both ejecting and nonejecting periods. While not routinely utilized in noncardiac surgery, MPI remains a validated method for assessing RV function. Right ventricular MPI is defined as the ratio of the total isovolumic time (isovolumetric relaxation time and isovolumetric contraction time) divided by ejection time (ET) [24, 25].

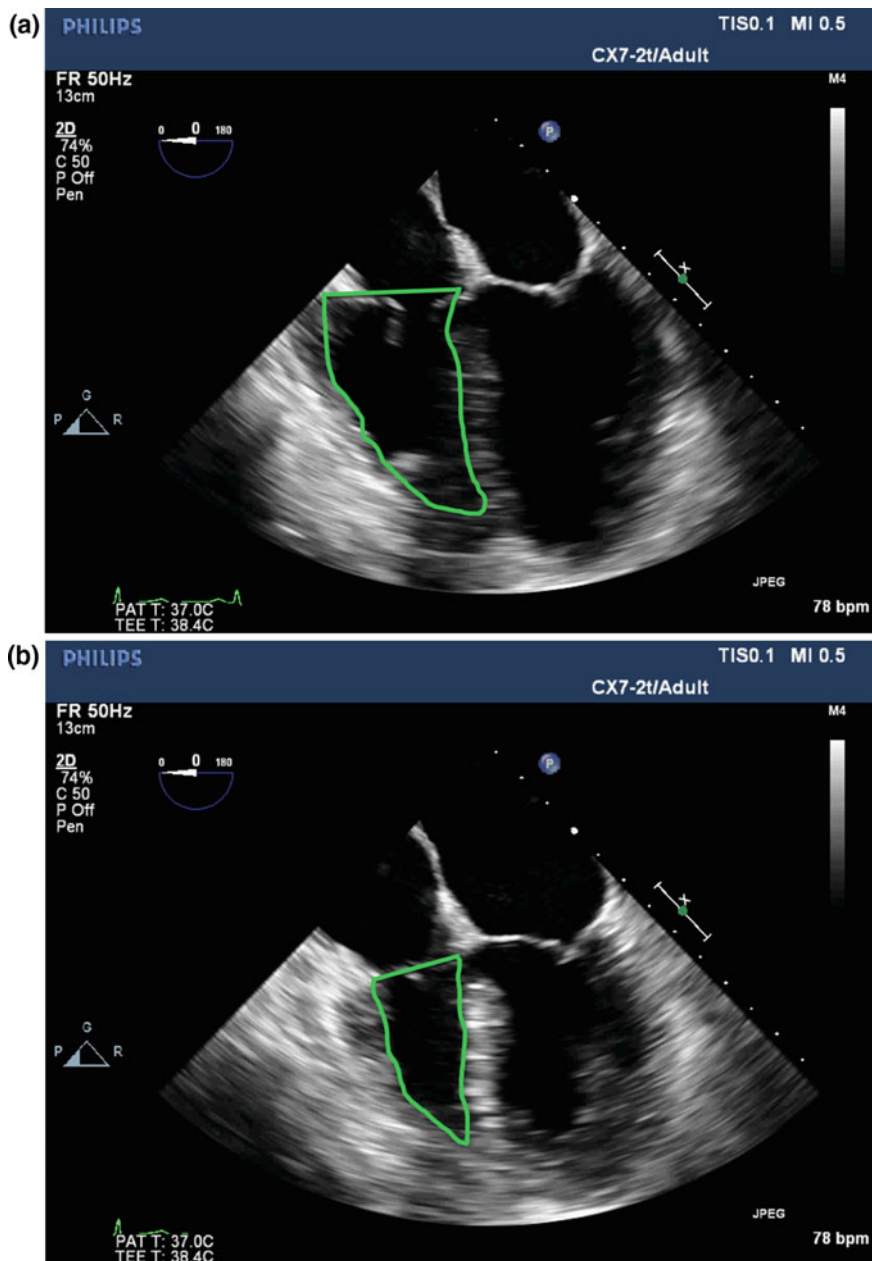


Fig. 8.6 **a** A mid-esophageal four-chamber view with a *green* tracing outlining the right ventricular area in a diastolic frame. **b** Systolic frame from the same patient with a *green* tracing outlining the right ventricular area. FAC is calculated as $(RV \text{ Diastolic Area} - RV \text{ Systolic Area}) / RV \text{ Diastolic Area} \times 100$

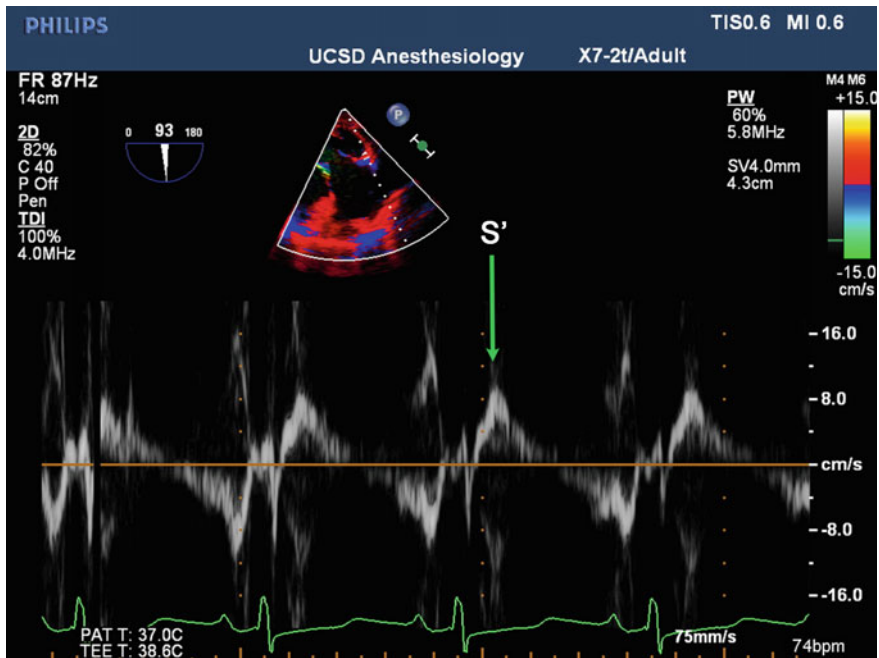


Fig. 8.7 Pulsed wave tissue Doppler imaging of the basal right ventricular myocardium in a modified transgastric right ventricular inflow view. Peak tricuspid annular velocity (S') is identified by the *green arrow*

$$MPI = (IVRT + IVCT)/ET$$

The index has been shown to correlate with symptoms and survival and has a prognostic value in patients with primary pulmonary hypertension [26]. Two methods may be utilized to obtain RV-MPI including one based on pulsed wave Doppler of the transtricuspid flow and pulmonic ejection and another method based on tissue Doppler imaging of the tricuspid annular motion.

Evaluation of the Shape and Motion of the IVS to Assess Global RV Function

Evaluation of RV geometry serves as a qualitative method to assess for global RV dysfunction. In the TG midpapillary short axis view, the RV often appears crescent shaped due to the high LV pressure, causing the IVS to bulge into the lower pressured RV. However, when RV dysfunction ensues, the compensatory RV dilation results in flattening of septum and loss of the natural crescent shape of the RV, yielding a “D-shaped” left ventricular chamber [21] (Fig. 8.8; Video 8.3).

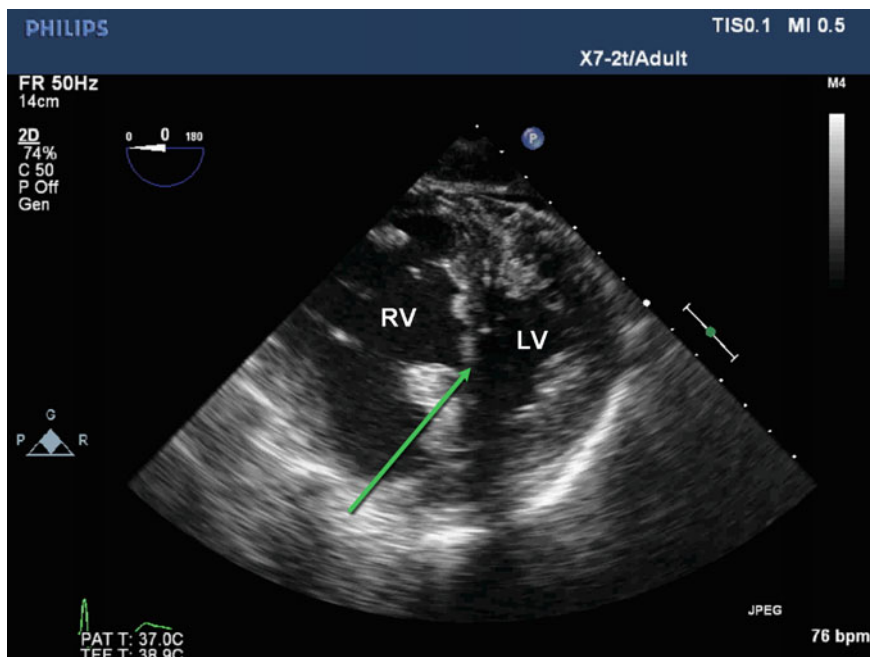


Fig. 8.8 Transgastric midpapillary short axis view in a patient with right ventricular failure. Note the shifted interventricular septum (*green arrow*), which results in a “D-shaped” left ventricle. The presence of the shifted septum at end-diastole indicates right ventricle (RV) volume overload whereas at end-systole indicates RV pressure overload

Although RV volume overload and RV pressure overload may occur concomitantly, they may also occur separately. The timing of the septal flattening can allude to the presence of RV volume overload versus pressure overload. With RV volume overload, the RV volume is largest at end-diastole, which corresponds to the time of peak diastolic overfilling (septal flattening at end-diastole). This is opposed to RV pressure overload where septal flattening occurs at end-systole corresponding to when RV systolic afterload is at its peak (i.e., the time when RV pressure is the highest).

Eccentricity index (EI) is an echocardiographic index for measuring the LV dimensions to differentiate RV volume overload from RV pressure overload [27]. It is the ratio of LV minor axis (anterior-to-inferior) to its perpendicular axis (septal-to-lateral) using the TG midpapillary short axis view. In normal individuals, the LV is round in systole and diastole and the EI has a value of 1. EI value is greater than 1 when the LV is D-shaped during end-systole in pressure overload, whereas in volume overload it is greater than 1 during end-diastole. A high EI is an important echocardiographic predictor of mortality in pulmonary arterial hypertension.

Right Atrium Adaptation to Chronic Right Ventricular Pressure Overload

In chronic right ventricular pressure overload, the right atrium adapts to support active atrial contribution to RV filling, leading to increased atrial distensibility, and functioning as a reservoir to support the cardiac output. These compensatory changes play an important role in maintaining cardiac output in the face of increased RV diastolic stiffness during chronic RV pressure overload [28, 29]. The normal RA upper reference limit is 4.4 cm and 5.3 cm for major (base to TV annulus) and minor (septal-to-lateral) axis dimensions, respectively. With chronic pulmonary hypertension, the RV dilation results in a dilated tricuspid valve annulus with significant tricuspid regurgitation leading to further RA dilatation.

Interatrial Septum Position also serves as an indicator of right heart function. With RV failure, the high right-sided pressure is transmitted to the RA, leading to increasing RA pressure and shifting of the interatrial septum toward the LA. This is usually more apparent in the ME four-chamber, ME RV inflow–outflow, or ME bicaval views as septal bowing toward the left atrium throughout the cardiac cycle can be appreciated (Fig. 8.9; Video 8.4). In patient populations where RA pressures exceed left atrial pressures, there is an increased incidence of patent foramen ovale

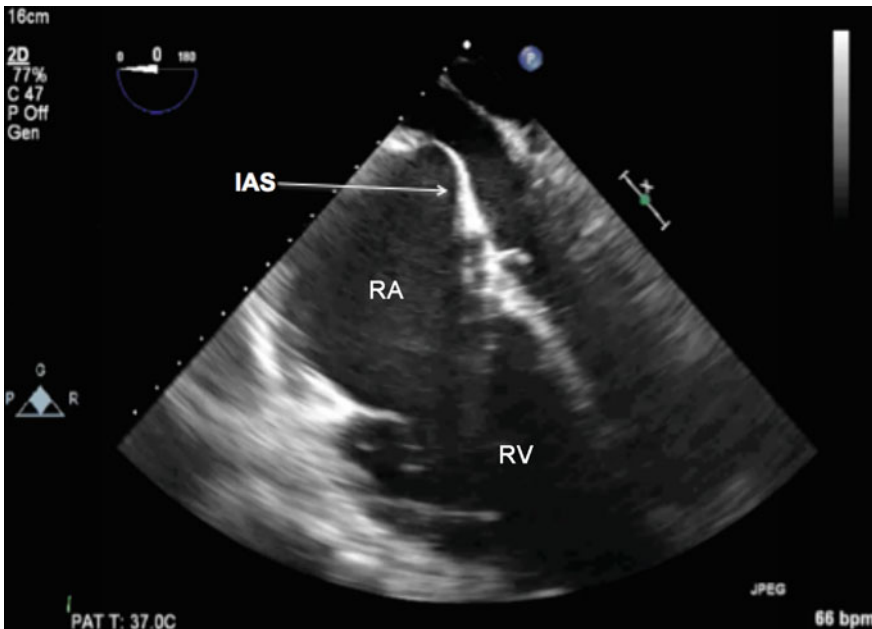


Fig. 8.9 Midesophageal four-chamber view in a patient with significant right atrial (RA) dilation and high right atrial pressure, noted by a shifted interatrial septum (IAS) toward the left atrium. RV right ventricle

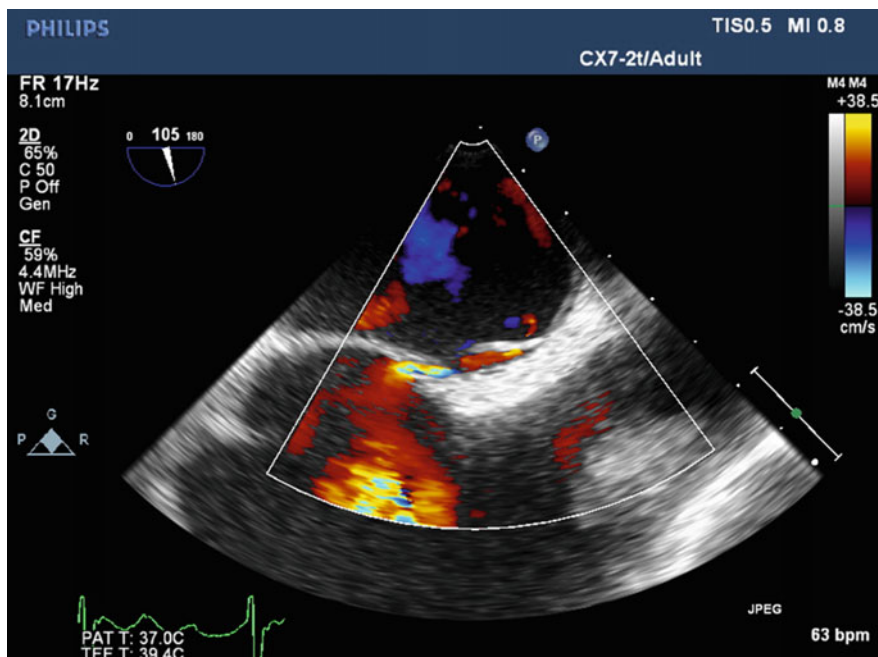


Fig. 8.10 Midesophageal bicaval view in a patient with a patent foramen ovale and right-to-left flow on color flow Doppler

(PFO) compared to the estimated 25 % of the adult population. This can lead to clinically significant right-to-left intracardiac shunting [18]. The shunting may be detected with echocardiography using color flow Doppler or agitated saline, most commonly in the ME bicaval view (Fig. 8.10; Video 8.5).

Tricuspid Regurgitation

For many years, the tricuspid valve (TV) was mostly ignored, and only in recent years has the TV claimed deserved attention. In the majority of patients who have “functional” TR, increased pulmonary and right ventricular pressures lead to RV dilation and subsequent TV annular dilation and leaflet tenting. The result is worsening regurgitation as the valve leaflets are unable to coapt during systole [30]. In this scenario, the tricuspid leaflets are morphologically without any pathology but do not coapt adequately. With RV systolic failure, the diastolic pressure rises and the interventricular septum shifts toward the LV during diastole, which in turn will raise left ventricular diastolic pressure, further aggravating the TR [31]. Therefore, any patient with a history of PH or evidence of right heart dysfunction

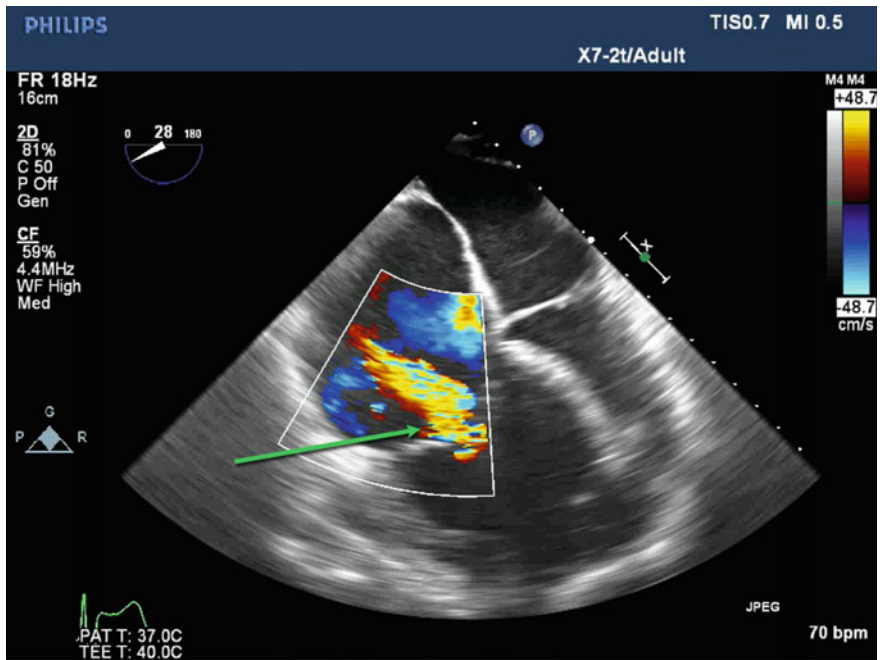


Fig. 8.11 Midesophageal four-chamber view demonstrating severe tricuspid regurgitation (*green arrow*) in a patient with a severely dilated right atrium and right ventricle

deserves an echocardiographic evaluation of the tricuspid valve morphology and evaluation for the causes of TR.

The trileaflet tricuspid valve is composed of the anterior leaflet, which is the largest, the posterior leaflet, and the septal leaflet. Several echocardiographic views are used to visualize the tricuspid valve, including the ME four-chamber, ME RV inflow–outflow, and modified ME bicaval views, as well as TG midpapillary short axis view of the RV and TG RV inflow view. There are several methods to assess the severity of TR; however, the most frequently used modality in the assessment of TR is the vena contracta measurement, with a value greater than >0.7 cm indicative of severe TR (Fig. 8.11; Video 8.6). Additionally, a confirmatory method is pulsed wave Doppler evaluation of the hepatic vein flow pattern. Evaluation of hepatic vein flow when evaluating TR is analogous to evaluating pulmonary vein flow when evaluating mitral regurgitation (MR). Similarly, systolic hepatic flow reversal is specific to severe TR, while blunting of forward systolic flow indicates moderate TR [18] (Fig. 8.12). To image the hepatic veins, perform a rightward probe rotation from the transgastric midpapillary short axis view until the liver is centered; subsequent omniplane rotation may be necessary to obtain a hepatic vein with a parallel orientation to the probe.

The presence of tricuspid regurgitation opens the opportunity to estimate the degree of pulmonary hypertension. As described in Chap. 3, utilizing the simplified

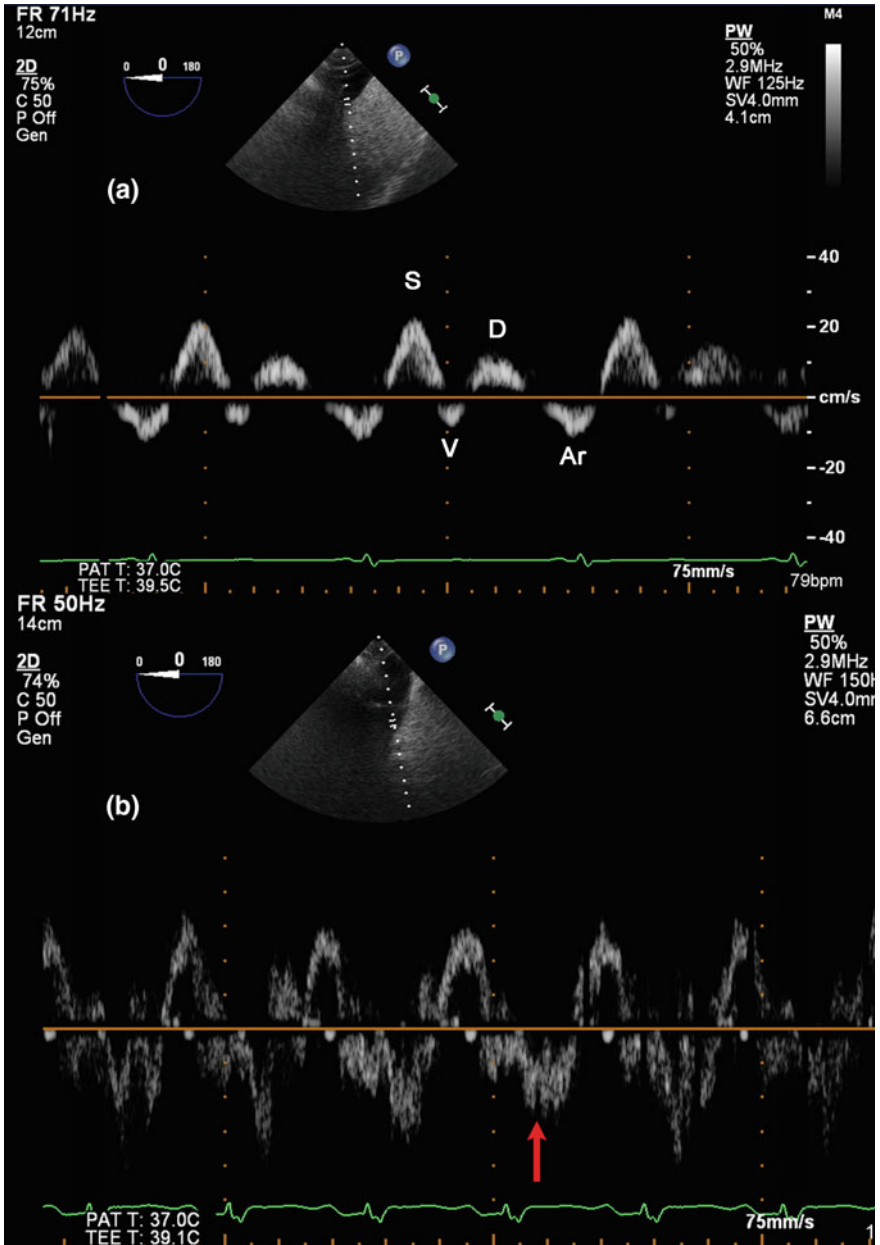


Fig. 8.12 Pulsed wave Doppler of hepatic vein flow. The *top panel* (a) demonstrates normal hepatic vein flow with positive systolic (S) and diastolic (D) waves, and brief negative atrial (Ar) wave and variably present V wave. The *bottom panel* (b) demonstrates systolic flow reversal confirming severe tricuspid regurgitation

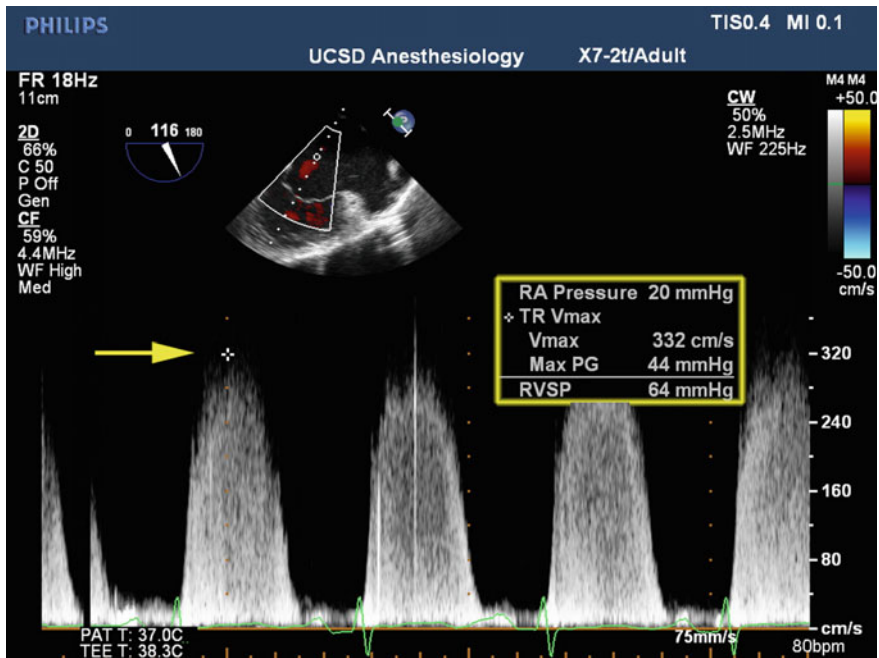


Fig. 8.13 Continuous wave Doppler of the tricuspid regurgitation jet in a modified bicaval view. Applying the modified Bernoulli equation to the peak TR jet (yellow arrow) yields an estimation of right ventricular and pulmonary arterial systolic pressure

Bernoulli equation ($\Delta P = 4v^2$) the *pulmonary artery systolic pressure (PASP)* can be calculated from the peak velocity of the TR jet using continuous wave Doppler. The peak TR velocity reflects the pressure gradient between the RV and the RA, and when added to central venous pressure provides an estimate of right ventricular systolic pressure and PASP. Commonly utilized views for measurement of PASP are the ME RV inflow–outflow view and ME modified bicaval view (Fig. 8.13).

$$PASP = 4(\text{TR Jet Velocity}^2) + \text{estimated RAP}$$

Pulmonary Artery

With long-standing pulmonary hypertension, the chronically increased pressure within the pulmonary artery will cause dilation beyond the normal diameter of 2.1 cm. Commonly utilized views to evaluate the main pulmonary artery (PA) are the ME ascending aortic short axis or UE aortic arch short axis views (Fig. 8.14). A view of the main pulmonary artery allows measurement of RV *cardiac output (CO)* which serves as a load-dependent index of global RV systolic function. The

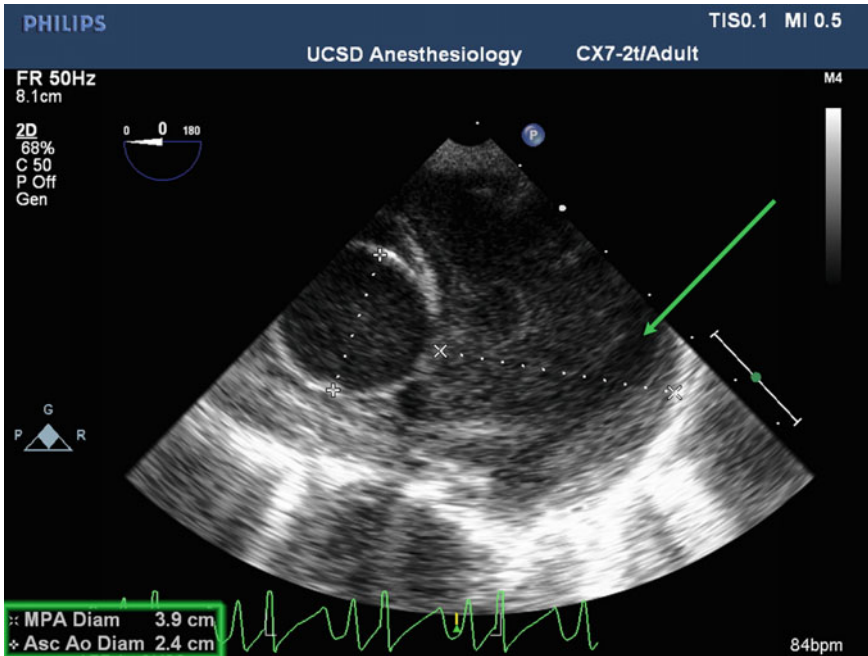


Fig. 8.14 Midesophageal ascending aortic short axis view with slight leftward probe rotation demonstrates significant pulmonary artery dilation (*green arrow*)

right-sided stroke volume can be calculated using pulsed wave Doppler in the ME ascending aortic short axis or UE aortic arch short axis views to obtain the right ventricular outflow tract (RVOT) or PA velocity time integral and the RVOT or PA diameter, respectively [32]. Doppler-derived RV CO provides a method to detect right-sided cardiac output despite the presence of significant TR.

$$RVCO = \left[0.785 \times (RVOT_{\text{diameter}})^2 \times VTI_{RVOT} \right] \times HR$$

Echocardiographic Findings in Acute Pulmonary Embolism

Pulmonary embolism (PE) is a potentially fatal condition with mortality ranging from 40 to 80 % within 2 h of onset [33]. An acute PE causes a sudden increase in RV afterload, resulting in RV dilation and dysfunction. The acute pressure increase also displaces the IVS, further contributing to RV failure. Both the decreased right-sided cardiac output and the septal shift lead to underfilling of the LV. Massive PE should be considered with the onset of unexplainable severe and sudden hypoxia or hypotension.

The most common echocardiographic findings in acute pulmonary embolism are RV dilatation and RV dysfunction, with preservation of the motility of the apex in some cases (McConnell's sign) (see Chap. 11). 90 % of patients with a large pulmonary embolism will develop ventricular hypokinesis [34]. Other signs are dilatation of the inferior vena cava with lack of collapse during inspiration, IVS flattening, and paradoxical systolic motion suggesting right ventricular pressure overload, and pulmonary artery dilatation together with tricuspid or pulmonary regurgitation. Patients with an acute PE will have marked prolongation of the isovolumic contraction time and isovolumic relaxation time, resulting in an increased RV-MPI over LV-MPI, which helps to differentiate chronic versus acute pulmonary hypertension of PE. With an acute PE, there is no time for the LV to adapt and therefore, the LV-MPI does not increase [35]. While observing an acutely dilated and dysfunctional right heart is suggestive of a pulmonary embolism, it is not entirely a specific or diagnostic finding. Observation of thromboembolic material in the right heart (thrombus-in-transit), either in the RA, RV, or PA, is a diagnostic finding (Fig. 8.15; Video 8.7). However, the contrary holds true: observation of a normal-sized RA and RV with normal RV function renders the diagnosis of pulmonary embolism unlikely. A thorough echocardiography exam is

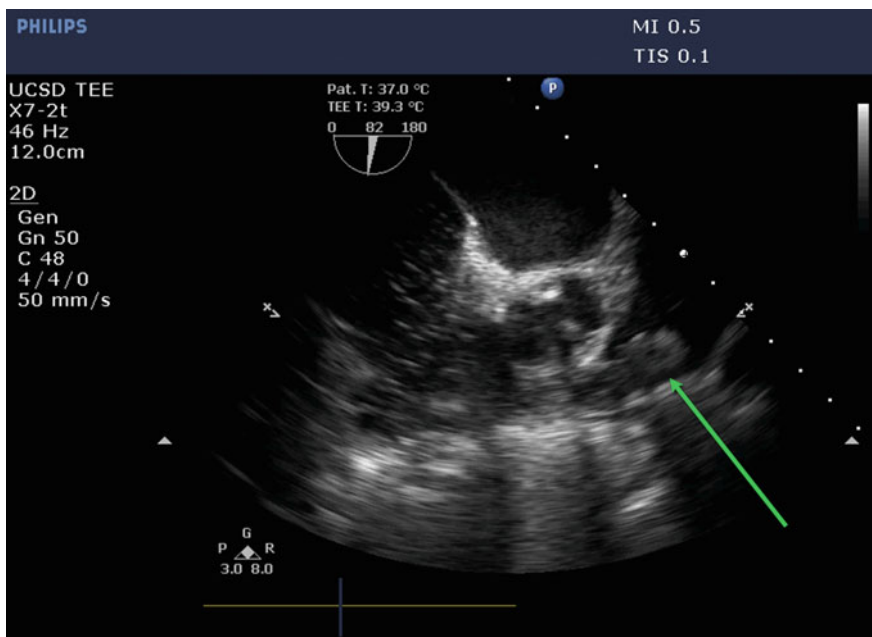


Fig. 8.15 Midesophageal RV inflow–outflow view demonstrating a thrombus-in-transit (*green arrow*) in a patient experiencing a pulmonary embolism

therefore imperative to observe the effects of acutely increased pulmonary afterload as well as to directly visualize embolized thrombi within the right heart chambers and the pulmonary arteries [36].

Conclusion

For many years, the left ventricular physiology overshadowed the study of the right ventricle. Only recently physicians have recognized the importance of right-sided function. With advances in echocardiography, new opportunities have emerged for studying the RV and its effects on patient outcomes. TEE is a helpful tool for the clinician who faces acutely ill patients and can help in the treatment of these patients. In the perioperative setting, echocardiography is able to determine which patient is at highest risk of an adverse outcome by means of evaluation and management of RV failure.

References

1. Hahn RT, Abraham T, Adams MS, et al. Guidelines for performing a comprehensive transesophageal echocardiographic examination: recommendations from the American Society of Echocardiography and the Society of Cardiovascular Anesthesiologists. *J Am Soc Echocardiogr.* 2013;26:921–64.
2. Rudski LG, Lai WW, Afilalo J, et al. Guidelines for the echocardiographic assessment of the right heart in adults: a report from the American Society of Echocardiography endorsed by the European Association of Echocardiography, a registered branch of the European Society of Cardiology, and the Canadian Society of Echocardiography. *J Am Soc Echocardiogr.* 2010;23:685–713; quiz 86–8.
3. Ho SY, Nihoyannopoulos P. Anatomy, echocardiography, and normal right ventricular dimensions. *Heart.* 2006;92(Suppl 1):i2–13.
4. Farb A, Burke AP, Virmani R. Anatomy and pathology of the right ventricle (including acquired tricuspid and pulmonic valve disease). *Cardiol Clin.* 1992;10(1–21):5.
5. Dell'Italia LJ. The right ventricle: anatomy, physiology, and clinical importance. *Curr Probl Cardiol.* 1991;16:653–720.
6. Jiang L, Wieggers S, Weyman A. Right Ventricle. In: Weyman A, editor. *Principles and practice of echocardiography.* 2nd ed. Philadelphia: Lea & Febiger; 1994. p. 901–21.
7. Lee FA. Hemodynamics of the right ventricle in normal and disease states. *Cardiol Clin.* 1992;10:59–67.
8. Kaul S. The interventricular septum in health and disease. *Am Heart J.* 1986;112:568–81.
9. Lindqvist P, Mømer S, Karp K, Waldenström A. New aspects of septal function by using 1-dimensional strain and strain rate imaging. *J Am Soc Echocardiogr.* 2006;19:1345–9.
10. Klima U, Guerrero JL, Vlahakes GJ. Contribution of the interventricular septum to maximal right ventricular function. *Eur J Cardiothorac Surg.* 1998;14:250–5.
11. Santamore WP, Dell'Italia LJ. Ventricular interdependence: significant left ventricular contributions to right ventricular systolic function. *Prog Cardiovasc Dis.* 1998;40:289–308.
12. Horton KD. Assessment of the right ventricle by echocardiography: a primer for cardiac sonographers. *J Am Soc Echocardiogr.* 2009;22:776–92.

13. Simonneau D, Gatzoulis M, Adatia I, et al. Updated Clinical Classification of Pulmonary Hypertension. *J Am Coll Cardiol*. 2013;62:D34–41.
14. Galie N, Hoeper MM, Humbert M, et al. ESC committee for practice guidelines (CPG). Guidelines for the diagnosis and treatment of pulmonary hypertension: the task force for the diagnosis and treatment of pulmonary hypertension of the European society of cardiology (ESC) and the European respiratory society (ERS), endorsed by the international society of heart and lung transplantation (ISHLT). *Eur Heart J*. 2009;30:2493–537.
15. Dadfarmay S, Berkowitz R, Kim B, et al. Differentiating pulmonary arterial and pulmonary venous hypertension and the implications for therapy. *Congest Heart Fail*. 2010;16:287–91.
16. McLaughlin V, Langer A, Tan M, et al. Contemporary trends in the diagnosis and management of pulmonary arterial hypertension. *CHEST*. 2013;143(2):324–32.
17. Bossone E, D'Andrea A, D'Alto M, et al. Echocardiography in pulmonary arterial hypertension from diagnosis to prognosis. *J Am Soc Echocardiogr*. 2013;26:1–14.
18. Lang RM, Badano LP, Mor-Avi V, et al. Recommendations for cardiac chamber quantification by echocardiography in adults: an update from the American society of echocardiography and the European association of cardiovascular imaging. *J Am Soc Echocardiogr*. 2015;28:1–39.
19. Lindqvist P, Calcutteea A, Henein M. Echocardiography in the assessment of right heart function. *Eur J Echocardiogr* 2008;9:225–34.
20. Samad BA, Alam M, Jensen-Urstad K. Prognostic impact of right ventricular involvement as assessed by tricuspid annular motion in patients with acute myocardial infarction. *Am J Cardiol*. 2002;90:778–81.
21. Cacciapuoti F. Echocardiographic evaluation of right heart function and pulmonary vascular bed. *Int J Cardiovasc Imaging*. 2009;25:689–97.
22. Anavekar NS, Gerson D, Skali H, Kwong RY, Yucel EK, Solomon SD. Two-dimensional assessment of right ventricular function: an echocardiographic-MRI correlative study. *Echocardiography*. 2007;24:452–6.
23. Pavlicek M, Wahl A, Rutz T, et al. Right ventricular systolic function assessment: rank of echocardiographic methods vs. cardiac magnetic resonance imaging. *Eur J Echocardiogr*. 2011;12:871–80.
24. Tei C, Ling LH, Hodge DO, et al. New index of combined systolic and diastolic myocardial performance: a simple and reproducible measure of cardiac function—A study in normals and dilated cardiomyopathy. *J Cardiol*. 1995;26:357–66.
25. Tei C, Dujardin KS, Hodge DO, et al. Doppler echocardiographic index for assessment of global right ventricular function. *J Am Soc Echocardiogr*. 1996;9:838–47.
26. Karnati PK, et al. Myocardial performance index correlates well with right ventricular ejection fraction measured by nuclear ventriculography. *Echocardiography*. 2008;25:381–5.
27. Ryan T, Petrovic O, Dillon JC, et al. An echocardiographic index for separation of right ventricular volume and pressure overload. *J Am Coll Cardiol*. 1985;5(4):918–27.
28. Gaynor SL, Maniar HS, Bloch JB, et al. Right atrial and ventricular adaptation to chronic right ventricular pressure overload. *circulation*. 2005;112 Suppl I:I-212–218.
29. Banks DA, Pretorius GV, Kerr KM, et al. Pulmonary endarterectomy: part I. Pathophysiology, clinical manifestations, and diagnostic evaluation of chronic thromboembolic pulmonary hypertension. *Semin Cardiothorac Vasc Anesth*. 2014 Jun 22. Pii:1089253214536621.
30. Badano LP, Muraru D, Enriquez-Sarano M. Assessment of functional Tricuspid Regurgitation. *Eur Heart J*. 2013 Jan 9.
31. Antunes MJ, Barlow JB. Management of tricuspid valve regurgitation. *Heart*. 2007;93:271–6.
32. Maslow A, Comunale ME, Haering JM, Watkins J. Pulsed wave Doppler measurement of cardiac output from the right ventricular outflow tract. *Anesth Analg*. 1996;83:466–71.
33. Lualdi JC, Goldhaber SZ. Right ventricular dysfunction after acute pulmonary embolism: pathophysiologic factors, detection, and therapeutic implications. *Am Heart J*. 1995;130:1276.

34. Mookadam F, Jiamsripong P, Goel R, et al. Critical appraisal on the utility of echocardiography in the management of acute pulmonary embolism. *Cardiol Rev.* 2010 Jan–Feb; 18(1):29–37.
35. Hsiao SH, Lee CY, Chang SM, et al. Pulmonary embolism and right heart function: insights from myocardial Doppler tissue imaging. *J Am Soc Echocardiogr.* 2006;19:822–88.
36. Cohen R, Loarte P, Navarro V, et al. Echocardiographic findings in pulmonary embolism: an important guide for the management of the patient. *World J Cardiovas Dis.* 2012;2:161–4.

Chapter 9

Diastology

Liem Nguyen, MD and Neal Gerstein, MD

Abstract Echocardiography can be used in real time to guide fluid responsiveness and assess the results of hemodynamic interventions perioperatively. Diastology, the assessment of intraoperative cardiac filling, can be studied by echocardiography using pulse-wave Doppler modalities. The speed at which blood enters a given chamber can be used to derive and estimate chamber pressures. There are two main properties that govern filling in a specific chamber. The first is the ability for the chamber to relax or drop its pressure. The second property is the ability of the chamber to maintain its compliance as filling proceeds. Filling abnormalities can be detected on echocardiography, yielding a spectrum of filling patterns that characterize the various stages of diastolic dysfunction.

Keywords Diastology · Diastolic dysfunction · Diastole · Cardiac filling · Pulse-wave doppler · Transmitral inflow · Pulmonary venous flow · Tissue doppler index

Introduction

In its simplest form, the study of diastolic function by echocardiography is a means to measure the speed at which blood moves or travels through the heart during diastole [1–5]. The pulse-wave Doppler serves as a “radar detector” as it measures the speed of blood moving through a given chamber. Information on the velocity of blood allows the echocardiographer to derive or estimate pressures, thus providing a means to measure the relationship between pressure and volume in a specific chamber of the heart [e.g., left atrium (LA) or left ventricle (LV)] [1, 4]. Beat to beat data on how the heart fills enables the anesthesiologist to optimize the determinants of stroke volume and thus, cardiac

L. Nguyen, MD (✉)

Department of Anesthesiology, University of California San Diego, 9300 Campus Point Drive #7651, San Diego, CA 92037-7651, USA
e-mail: liem@ucsd.edu

N. Gerstein, MD

Department of Anesthesiology, University of New Mexico, 2211 Lomas Blvd NE, Albuquerque, NM 87106, USA
e-mail: ngerstein@gmail.com

performance. The importance of understanding diastolic filling comes down to the most basic of concepts: *if the heart cannot fill adequately, it cannot eject adequately.*

There are two distinct properties that govern the normal filling of the heart. The first prerequisite to normal filling is an adequate drop or fall in pressure in the downstream receiving chamber (e.g., pressure drop in the LA or LV) as a result of the heart's intrinsic ability to relax. The pressure drop establishes the gradient necessary to drive blood downhill through the heart. The second property that governs normal adequate filling is the ability for the heart to fill with volume and simultaneously maintain a relatively low filling pressure. The heart's pressure response to increasing volume is referred to as compliance ($\Delta V/\Delta P$). Together, the heart's ability to relax (adequate pressure drop) and remain compliant (maintain low pressures despite high volumes) are the two main properties that regulate adequate filling. It is the presence of inadequate relaxation and/or poor compliance that characterizes the onset of impaired filling. The hallmark of diastolic dysfunction is therefore a result of the inability of the heart to relax and/or remain compliant [1, 4].

The echocardiographer uses the pulse-wave Doppler to detect changes or deviations from normal blood velocity, indicating the presence of an abnormal filling process. Using Doppler echocardiography, the anesthesiologist may be able to identify a shift from a normal filling state to an abnormal filling state. This data can then be used to determine how to improve and correct the filling abnormality [4, 5].

Phases of Diastole

There are four main phases of diastole (Fig. 9.1): Isovolumetric relaxation (IVRT), early rapid filling, diastasis, and atrial contraction [1, 2, 6].

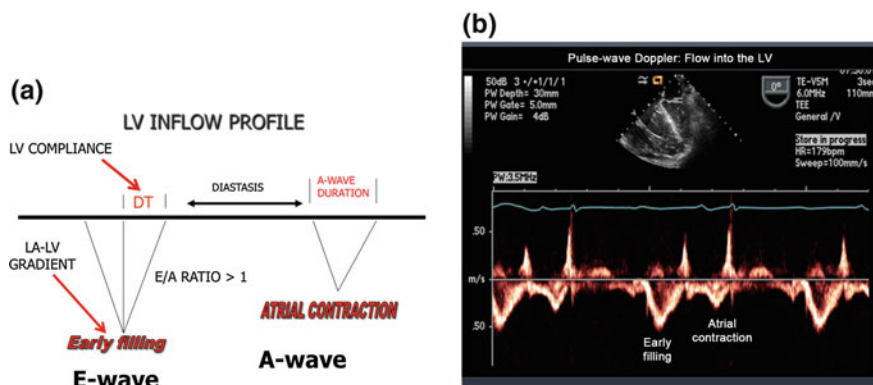


Fig. 9.1 **a** Diagram of a normal transmitral inflow profile. After IVRT, the mitral valve opens and early filling (E-wave) commences, followed by a period of pressure equalization (diastasis), ending with atrial contraction (A-wave). The peak E-wave velocity is proportional to the LA–LV gradient while the deceleration time (DT) is dependent on LV compliance. **b** Pulse-wave Doppler of normal transmitral inflow. The profile is obtained by placing the point of interrogation just below the mitral leaflet tips and utilizing pulse-wave Doppler echocardiography

1. Isovolumetric relaxation

The start of IVRT corresponds to the onset of aortic valve closure. With both the tricuspid and mitral valves closed, the chamber pressure in both ventricles fall, creating a gradient to pull blood downward into the receiving ventricle when the atrioventricular valves are open in the next phase of diastole. This active phase of relaxation is energetically consuming, with the inactivation of the contractile apparatus driven by sequestration of Ca^{2+} ions into the sarcoplasmic reticulum. The pressure drop in the ventricle is the prerequisite for establishing an adequate atrial-ventricular pressure gradient for normal filling [1, 2].

2. Early rapid filling

As the tricuspid and mitral valves open, early filling of the ventricle commences as blood is pulled downward into the downstream chamber. Pulse-wave Doppler interrogation of the blood flowing into the ventricle produces the characteristic E-wave (velocity of the early filling wave) on the LV or right ventricle (RV) inflow profile (Fig. 9.1). The peak E-wave velocity is primarily dependent on the LA–LV gradient. The LA–LV gradient is a function of the large pressure drop in the LV during the IVRT phase, and *not* a result of a rise in LA pressure. The deceleration time (DT) is the time it takes for the atrial and ventricular pressure to equilibrate and is predicated upon the volume–pressure relationship or compliance ($\Delta V/\Delta P$) of the downstream receiving ventricle. That is, the DT is the time for the peak velocity (E-wave) of blood moving into the ventricle to reach zero [1, 4].

3. Diastasis

Diastasis marks the period in which the atrium and ventricle are in equilibrium with very little flow moving into either chamber. This period is often truncated or shortened during higher heart rates (shorter time in diastole) and is more prolonged during lower heart rates.

4. Atrial contraction

Atrial contraction (A-wave) occurs at the latter stage of diastole and corresponds to the p-wave on the electrocardiogram. The atrial contraction or “atrial kick” mechanism transiently increases the atrial pressure and generates a “push” of blood into the receiving ventricle. The velocity of blood being “pushed” downward into the ventricle is described by the peak A-wave velocity. Diastole is finally complete when the atrioventricular valves close [1, 4].

Assessment of Chamber Filling: Pulse-Wave Doppler Echocardiography

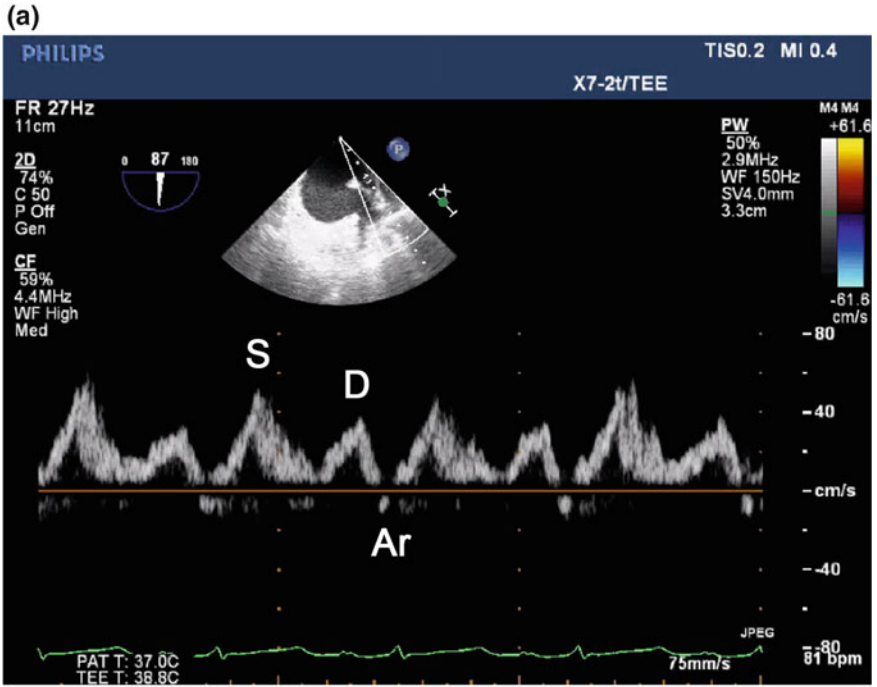
Transmitral Inflow: Measuring Flow into the Left Ventricle

The LV or transmitral inflow profile (Fig. 9.1) is obtained with pulse-wave Doppler echocardiography by setting the point of interrogation just below the leaflet tips of

the mitral valve in the midesophageal 4-chamber view at zero degrees [1, 2, 4, 6]. This modality measures the velocity of blood traveling from the left atrium to the ventricle during the early filling phase of diastole. In other words, it is a measurement of how fast blood enters the LV. The speed at which blood enters the LV is primarily dependent on the LA–LV gradient (Fig. 9.1), which under normal conditions is a result of LV relaxation. As in any Doppler assessment, it is essential to align the pulse-wave Doppler parallel to the direction of blood flow to obtain the most accurate results. The normal LV filling pattern (Fig. 9.1) is described by a higher velocity E-wave (early filling), a period of diastasis (equilibrium), and a lower velocity A-wave (atrial contraction and late filling). The higher velocity E-wave is a consequence of the larger LA–LV gradient during the initial mitral valve opening. By contrast, at late diastole, the gradient between the LA–LV gradient is smaller due to the almost filled LV (from the early filling phase), resulting in a lower velocity A-wave. The end result is an E-wave velocity that is ~ 1.5 times greater than the A-wave velocity or E/A ratio of $\sim 1.5:1.0$. The DT marks the time for the peak E-velocity to reach baseline (zero velocity) and defines the time it takes for the LA and LV pressures to equilibrate. The DT mathematically describes how long the early filling occurs before diastasis begins and is a measure of LV compliance (Fig. 9.1). A short DT signifies a truncated filling period where the mitral valve opens and flow ceases quickly due to rapid atrial–ventricular pressure equilibration often from poor ventricular compliance. Normal deceleration times indicate that the early filling occurs longer and may represent adequate ventricular filling and compliance [1, 4, 5].

Pulmonary Venous Flow: Measuring Flow into the Left Atrium

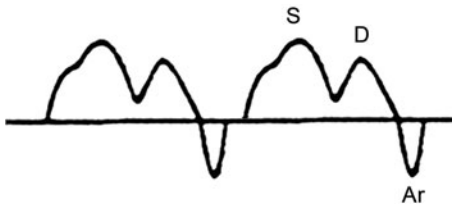
LA inflow or pulmonary venous flow can be measured by placing the pulse-wave Doppler point of interrogation into the left or right upper pulmonary vein [1, 2, 6]. The point of interrogation is placed approximately one centimeter into the pulmonary vein near the entry point of the left atrium. The resulting velocity profile (Fig. 9.2) consists of higher velocity systolic wave (S-wave) and lower velocity diastolic wave (D-wave). The higher velocity S-wave is a result of active left atrial relaxation promoting a larger gradient for forward flow from the pulmonary veins into the left atrium during early systole. As the mitral valve opens during early diastole, forward flow from the pulmonary veins travels downhill into the LA and eventually into the LV, corresponding to the D-wave on the LA inflow profile. The higher velocity S-wave is often affected by either the inability of the left atrium to relax adequately and/or an increase in left atrial pressure. Accordingly, a blunted or reduced S-wave velocity is often a marker of an abnormality of left atrial relaxation and/or compliance (Fig. 9.2) [4].



(b) LEFT ATRIAL FILLING

SYSTOLIC WAVE AND DIASTOLIC WAVE

S-wave Dominant



(c) LEFT ATRIAL FILLING

DIASTOLIC DOMINANCE SYSTOLIC BLUNTING

D-wave Dominant



Fig. 9.2 **a** Left atrial filling or pulmonary vein flow profile obtained by placing point of interrogation ~1 cm into the left upper pulmonary vein near the entry of the left atrium. **b** Left atrial filling or pulmonary vein flow profile consists of a higher velocity and more dominant systolic (S-wave) component and a lower velocity diastolic (D-wave) component. **c** The blunted S-wave velocity is a result of a poor left atrial relaxation and/or a rise in LA pressure

Tissue Doppler Imaging: Measuring the Velocity of Myocardial Tissue

During the first stage of diastole, IVRT results in a net drop in LV pressure creating a downhill pressure gradient. During this period of LV relaxation, the lateral aspect of the mitral annulus and atrial myocardium moves upward (the LV is “snapping open”). The direction, movement, and velocity of the atrial myocardium-mitral annulus can be measured using tissue Doppler imaging [1, 4, 7, 8]. Tissue Doppler imaging is a mode of spectral Doppler with the filter simply reversed. Doppler evaluation of blood flow utilizes a filter to remove slow moving bright echoes (i.e., tissue) to focus on fast moving low echoes (i.e., blood). Tissue Doppler inverses the filter to focus on the velocity of slower moving bright echoes, the tissue velocity and filters out the faster moving lower echoes, the blood. Analogous to measuring the velocity of blood moving across the mitral valve, pulsed-wave tissue Doppler interrogation can be utilized to measure the velocity of myocardial tissue, or specifically, the translational movement of the atrial myocardium or mitral annulus during diastole.

The tissue Doppler profile (Fig. 9.3) of the lateral mitral annulus-atrial myocardium is described by two positive deflections, a positive signal in early diastole,

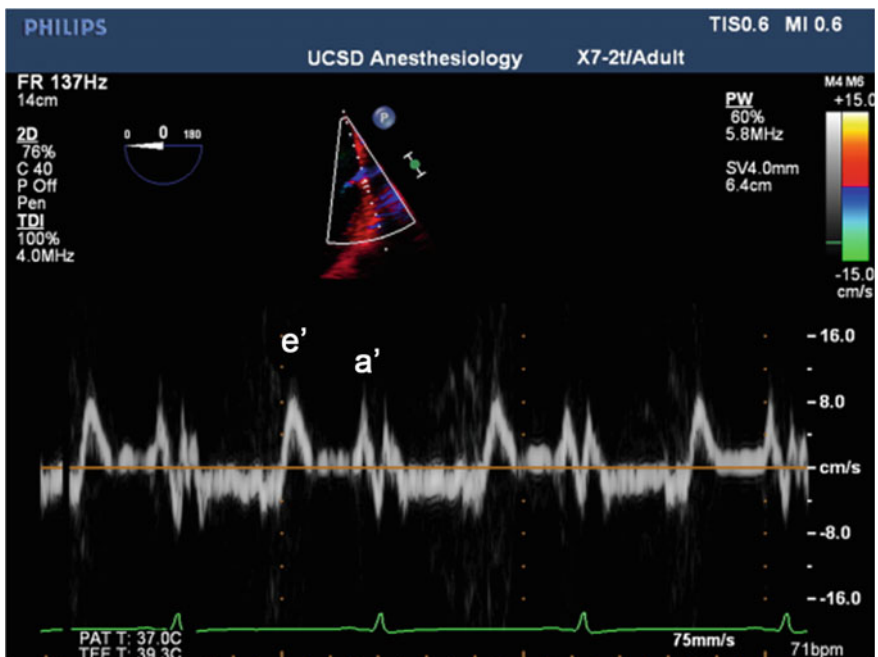


Fig. 9.3 Tissue doppler interrogation measuring the upward velocity of the atrial myocardium and mitral annulus during diastole. The e'-wave corresponds to ascension of the atrial myocardium and mitral annulus during IVRT. The a'-wave corresponds to movement of the myocardium just before atrial contraction

carrying the designation of e' (e prime), and another wave in late diastole with the designation of a' (a prime). The onset of the e' -wave occurs just before the mitral valve opens and represents the rate of relaxation of the myocardium during the isovolumetric relaxation period (IVRT). The e' -wave velocity is therefore an index of myocardial relaxation. The tissue Doppler e' -wave velocity (normally $\sim 10\text{--}12$ cm/s) is much lower than the LV inflow E-wave velocity ($\sim 50\text{--}100$ cm/s) of blood during early diastole, with a normal E/e' ratio of ≤ 8 [7]. An e' -wave velocity of less than 10 cm/s is abnormal and suggests that impaired myocardial relaxation is present [7]. The a' -wave represents upward motion of the atrial myocardium and lateral annulus just before atrial contraction [1, 4].

Stages of Diastolic Dysfunction: From Mild to Severe Dysfunction (Table 9.1)

Diastolic Dysfunction	
2D	<ul style="list-style-type: none"> • Left Ventricular Hypertrophy • Left Atrial Enlargement • Secondary right heart dysfunction from pHTN
CFD	<ul style="list-style-type: none"> • Typically not utilized
Spectral	<ul style="list-style-type: none"> • Assess severity <ul style="list-style-type: none"> – PWD: Mitral Inflow – PWD: Pulmonary Venous Inflow – TDI: Mitral Annular Velocity

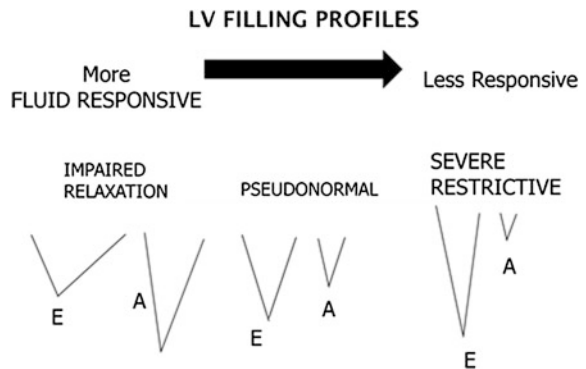
pHTN Pulmonary hypertension, *PWD* Pulsed-wave Doppler, *TDI* Tissue Doppler imaging

The term diastolic dysfunction encompasses a spectrum of abnormal filling stages of increasing severity (Fig. 9.4) [1, 2, 4, 6]. On the other hand, the term diastolic heart failure describes a state of decompensation due to diastolic dysfunction as a result of redistribution of fluid into the pulmonary venous system despite a normal ejection fraction [3, 4]. At the left side of the spectrum, the mildest stage of diastolic dysfunction is designated as *impaired relaxation*, which is characterized by the inability of the ventricle to adequately relax or drop its pressure. The next stage of the spectrum is designated as *pseudonormalization*, which is a moderate or intermediate stage of diastolic dysfunction characterized by the presence of *impaired relaxation* and a compensatory elevation in left atrial pressure. The final and most severe stage of diastolic dysfunction is referred to as the *restrictive* form. The *restrictive form* is manifested by the presence of impaired relaxation, elevated LA pressures, and elevated LV pressures (from poor compliance) [1, 4, 5].

Table 9.1 Stages of diastolic dysfunction

	Normal	Impaired relaxation	Pseudo-normalization	Restrictive
ECG				
Mitral inflow				
Pulmonary venous doppler				
Tissue doppler imaging				
E/e'	$e' > 10$	$E/e' < 8$	$E/e' = 9-12$	$E/e' > 13$
LAP	NI	NI	↑	↑

Fig. 9.4 The spectrum of diastolic dysfunction



Impaired Relaxation

The inability of the LV to relax marks the first stage of diastolic dysfunction and is referred to as *impaired relaxation* [1, 4, 6]. In this mild form of diastolic dysfunction, isolated impaired relaxation of the ventricle is present in the setting of

normal LA and LV compliance. Due to a smaller drop in LV pressure (smaller $\Delta P/\Delta T$), the LA–LV gradient is decreased leading to a reduction in the velocity and amount of blood moving into the ventricle during early filling (reduced E-wave velocity). As less blood fills the LV during the early filling phase, more volume is left in the LA during diastasis. The increased residual LA volume leads to a larger LA–LV gradient during late diastole, corresponding to a higher A-wave velocity and greater dependence on atrial contraction ($\sim 30\text{--}40\%$ contribution vs. $\sim 20\text{--}30\%$) for adequate filling. In the earliest stage of diastolic dysfunction, impaired LV relaxation results in a *decrease* in the E-wave velocity and an *increase* in the A-wave velocity (E/A ratio <1 or E to A reversal, Fig. 9.4).

Pulsed-wave tissue Doppler interrogation of patients with *impaired relaxation* generally show reduced myocardial tissue velocity signals (<10 cm/s) of the lateral mitral annulus or atrial myocardium. This corresponds with an impaired ability of the atrial myocardium-mitral annulus to move upward during LV relaxation. However, since the LA pressures are normal in *impaired relaxation*, the velocity of blood flowing into the LA remains normal, as evidenced by a normal left atrial inflow pattern (S-wave dominant, Fig. 9.2). In summary, impaired relaxation is characterized by a *decreased* E-wave velocity, *increased* A-wave velocity, abnormal tissue Doppler velocities (<10 cm/s), in the presence of normal LA and LV compliance [1, 4].

Pseudonormalization: Impaired Relaxation and Elevated LA Pressure

The moderate or intermediate stage of diastolic dysfunction can be simplified by superimposing the presence of elevated left atrial pressures onto a background of poor LV relaxation. This defines the transition of the *impaired relaxation* stage to the next stage of diastolic dysfunction, designated as *pseudonormal*. The increase in left atrial pressure in the setting of impaired relaxation generates a reduction or blunting of the S-wave velocity ($S_{\text{velocity}} < D_{\text{velocity}}$) in the left atrial inflow (pulmonary venous flow) Doppler profile. As a result of poor left atrial relaxation and/or a rise in LA pressure, the pressure gradient dictating forward flow from the pulmonary veins into the left atrium is reduced, yielding a diastolic (D-wave) dominant profile (Fig. 9.2) [1, 4]. The additional increase in LA pressures (larger LA–LV gradient) in the setting of impaired relaxation ($E < A$) produces an increase in the E-wave velocity, resulting in reversal and therefore, normalization of the E and A transmitral velocities ($E > A$). The resulting “pseudonormal” $E > A$ pattern and systolic blunting of the left atrial inflow profile are the defining characteristics of this intermediate stage of diastolic dysfunction. Furthermore, as the *pseudonormal* stage combines impaired relaxation and the presence of elevated LA pressures, tissue Doppler interrogation of the atrial myocardium and mitral annulus is abnormal (<10 cm/s), consistent with an LV relaxation defect. In summary, the

pseudonormal stage of diastolic dysfunction is an intermediate stage characterized by impaired relaxation and elevated LA pressures. Accordingly, the distinguishing features of the *pseudonormal* stage are the presence of abnormal myocardial velocities (<10 cm/s) and blunted S-wave velocities (diastolic dominance) on tissue Doppler imaging and left atrial inflow, respectively [1, 4].

Restrictive: Impaired Relaxation, Poor LV Compliance, Elevated LA and LV Pressures

The progression from *pseudonormal* to the most severe or *restrictive* stage of diastolic dysfunction is marked by the addition of poor LV compliance on the background of impaired relaxation and elevated LA pressures. The *restrictive* stage features the addition of a stiff and noncompliant LV in the setting of already present impaired relaxation and high LA pressures [1, 4, 6]. Marked elevations in LV pressure from poor LV compliance result in restricted LV filling and a major redistribution of volume to the left atrium. The large left atrial volume thus provides the basis for pulmonary venous congestion and symptomatic diastolic heart failure. Marked elevations in LA volume and pressure generate a much larger LA–LV gradient and faster E-wave velocity ($E \gg A$) during early filling compared to normal (Fig. 9.4). In addition, as the pressure in the LA rapidly increases, the mitral valve is forced open before the LV can adequately relax. The velocity of blood moving into the LV is very fast as the elevated LA pressure forces the mitral valve open and pushes blood downstream into the LV. However, the overall volume of filling is extremely restricted as the LV pressures rise abruptly and rapidly equalize with the LA, generating a very short DT (time from peak E-wave velocity to zero). The end result is a small and quick “pulse” of volume that is delivered to the LV as the filling rapidly begins and ends during the early filling phase. After a period of diastasis, the elevated LV pressures are not conducive to late filling, resulting in a very small or negligible A-wave velocity during atrial contraction. This provides the basis for the unique pattern of a very fast E-wave, low velocity A-wave ($E \gg A$, or $E/A > 2$), and short DT ($DT < 150$) on the LV inflow or transmitral profile (Fig. 9.4) [1, 4, 6].

Clinical Implications of Diastolic Dysfunction: Real-Time Measurements

Pulsed wave Doppler allows the echocardiographer to measure the velocity of blood moving into a given chamber. This is the main clinical value of diastology. It confers the echocardiographer the ability to evaluate how the heart fills and responds to volume on a beat-to-beat basis [9]. This modality allows the clinician to identify which patients are at risk of developing heart failure [4], providing the

foundation to optimize hemodynamics and cardiac performance in high risk patients [4, 10]. For example, in patients with impaired relaxation (i.e., E/A reversal or E/A ratio <1) and normal LA and LV pressures, the A-wave, or “atrial kick” component plays a larger role in LV filling compared to a normal profile. An increase in left atrial pressure with fluid therapy will therefore improve LV filling. Taken together, this early stage of diastolic dysfunction may be improved by maintaining a slow sinus rhythm, allowing more time for the LV to relax and fill, and by gentle administration of fluid to increase the LA–LV gradient [4]. Medications that may enhance LV relaxation such as milrinone, nitroglycerin, or levosimendan may also improve the relaxation abnormality and augment LV filling [4, 11–13]. On the other end of the spectrum, patients with a severe restrictive pattern with poor compliance and marked elevations in LA and LV pressures display a fixed end diastolic volume and stroke volume. In this case, slower heart rates may actually compromise cardiac output, whereas relative tachycardia may be more beneficial [1, 4]. Additionally, the elevated left ventricular end diastolic pressure (LVEDP) observed in patients with a restrictive pattern may necessitate an equivalent rise in aortic pressure to optimize coronary perfusion. Judicial use of diuretics may also be warranted as marked elevations in LA and LV pressure portends a greater risk of developing heart failure. Patients with a restrictive pattern may therefore benefit from relative tachycardia, higher aortic pressures, and avoiding further increases in LA or LV pressure [4]. The dynamic spectrum of diastolic dysfunction can be appreciated in the operating room (Fig. 9.4) [4, 7–10]. A patient with a pseudonormal pattern of filling may be pushed to the right of the spectrum and progress to a restrictive form following a fluid bolus, sudden decrease in coronary perfusion pressure, or acute onset valvular regurgitation. On the other hand, a patient with a restrictive pattern may improve and move to the left of the spectrum after hemodynamic optimization with diuretic therapy, careful initiation of inotropic therapy, and an increase in coronary perfusion pressure. Patients demonstrating impaired relaxation may benefit from slight increases in LA pressure and are therefore more fluid responsive compared to pseudonormal or restrictive patterns (Fig. 9.4). An impaired relaxation pattern may be moved to the left of the spectrum by the administration of nitroglycerin or a lusitropic agent to improve relaxation and b-blockers to increase diastolic filling by maximizing early filling and atrial kick [4].

Doppler analysis of flow into the left ventricle or left atrium can also be individually performed to estimate changes in LV or LA filling pressures to optimize intraoperative hemodynamics as well. Using this approach, targeting a specific filling abnormality can be exploited to optimize cardiac output in real time (Fig. 9.5) [4, 9, 10]. By taking serial measurements of the velocity of blood moving into the left ventricle and obtaining an LV inflow profile before and after a therapeutic intervention, the clinician can track changes in the peak E-wave velocity, A-wave velocity, or deceleration times. For example, if the DT shortens after multiple fluid boluses, this suggests a right shift (Fig. 9.4) to a less fluid responsive state or less compliant portion of the Starling curve. Similarly, flow into the left atrium and the left atrial inflow profile can detect changes in left atrial pressure after

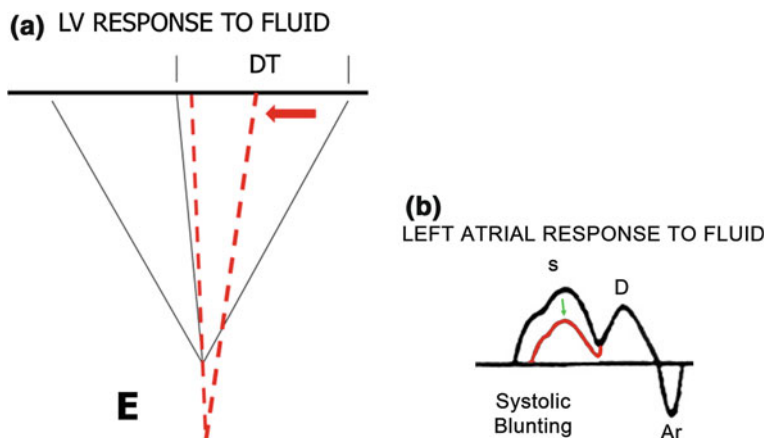


Fig. 9.5 **a** LV inflow profile at baseline (*black line*) and after a fluid challenge (*red dashed line*) demonstrating an increase in the peak E-wave velocity and shortening of the DT, corresponding to an increase in LA pressure and poor LV compliance. **b** LA inflow profile before (*black line*) and after (*red line*) a fluid challenge demonstrating systolic blunting and an increase in LA pressure

fluid administration. A normal left atrial inflow pattern exhibiting an S-wave dominant pattern ($S > D$) indicates normal left atrial pressures. If the S-wave begins to blunt and a D-wave dominant pattern ($S < D$) emerges after a fluid bolus, a rise in left atrial pressure is the likely cause of the change in the left atrial inflow profile (Fig. 9.5). A sudden increase in LA pressures signifies a shift to a less fluid responsive state and carries a greater risk of pulmonary congestion [9, 10].

The use of intraoperative echocardiography assisted hemodynamic management may confer additional advantages when compared to traditional static indices of chamber filling pressures [9, 10, 14]. One of the main advantages of intraoperative echocardiography is the ability to estimate the filling pressures of the left side of the heart and combine the data with stroke volume measurements by echocardiography or by other modalities [9, 10, 14]. The other main advantage of Doppler echocardiography is the ability to easily and repeatedly measure flow velocities and chamber pressures in real time. In a few studies, dynamic markers of LA and LV filling by echocardiography have been shown to be a viable alternative to conventional catheter-based techniques to measure intracardiac filling pressures. The use of intraoperative echocardiography-guided hemodynamic management was shown to reduce the amount of overall fluid administration when compared to the control group in one study [9]. At present, the ability to monitor dynamic indices of cardiac performance in real time to optimize hemodynamics is thoroughly lacking. With further study, spectral Doppler ultrasound has the potential to be an excellent dynamic cardiovascular monitor.

References

1. Nicoara A, Swaminathan M. Diastolic dysfunction, diagnostic and perioperative management in cardiac surgery. *Curr Opin Anaesthesiol*. 2015;28(1):60–6.
2. Nicoara A, Whitener G, Swaminathan M. Perioperative diastolic dysfunction: a comprehensive approach to assessment by transesophageal echocardiography. *Semin Cardiothorac Vasc Anesth*. 2013;18(2):218–36.
3. Mahmood F, Matyal R. Assessment of perioperative diastolic function and dysfunction. *Int Anesthesiol Clin*. 2008;46(2):51–62.
4. Mahmood F, Jainandunsing J, Matyal R. A practical approach to echocardiographic assessment of perioperative diastolic dysfunction. *J Cardiothorac Vasc Anesth*. 2012;26(6):1115–23.
5. Matyal R, et al. Perioperative assessment of diastolic dysfunction. *Anesth Analg*. 2011;113(3):449–72.
6. Groban L, Dolinski SY. Transesophageal echocardiographic evaluation of diastolic function. *Chest*. 2005;128(5):3652–63.
7. Swaminathan M, et al. Utility of a simple algorithm to grade diastolic dysfunction and predict outcome after coronary artery bypass graft surgery. *Ann Thorac Surg*. 2011;91(6):1844–50.
8. Matyal R, et al. Perioperative diastolic dysfunction during vascular surgery and its association with postoperative outcome. *J Vasc Surg*. 2009;50(1):70–6.
9. Shillcutt SK, et al. Echocardiography-based hemodynamic management of left ventricular diastolic dysfunction: a feasibility and safety study. *Echocardiography*. 2014;31(10):1189–98.
10. Lattik R, et al. Mitral Doppler indices are superior to two-dimensional echocardiographic and hemodynamic variables in predicting responsiveness of cardiac output to a rapid intravenous infusion of colloid. *Anesth Analg*. 2002;94(5):1092–9 (table of contents).
11. Axelsson B, et al. Milrinone improves diastolic function in coronary artery bypass surgery as assessed by acoustic quantification and peak filling rate: a prospective randomized study. *J Cardiothorac Vasc Anesth*. 2010;24(2):244–9.
12. Lobato EB, Gravenstein N, Martin TD. Milrinone, not epinephrine, improves left ventricular compliance after cardiopulmonary bypass. *J Cardiothorac Vasc Anesth*. 2000;14(4):374–7.
13. Malik V, et al. Effect of levosimendan on diastolic function in patients undergoing coronary artery bypass grafting: a comparative study. *J Cardiovasc Pharmacol*. 2015;66(2):141–7.
14. Porter TR, et al. Guidelines for the use of echocardiography as a monitor for therapeutic intervention in adults: a report from the American Society of Echocardiography. *J Am Soc Echocardiogr*. 2015;28(1):40–56.

Chapter 10

Thoracic Aorta

Timothy M. Maus, MD, FASE

Abstract The close proximity of the esophagus to the thoracic aorta provides an excellent imaging opportunity. Transesophageal echocardiography (TEE) serves an important role in several important pathologies including aortic dissection, aortic aneurysms, aortic atheromatous disease, and aortic trauma. A thorough understanding of the use of TEE in evaluating the thoracic aorta including normal and pathologic presentations is essential to the basic perioperative echocardiographer. However, knowledge of the limitations of the modality is also key to appropriate patient management and preventing mismanagement.

Keywords Thoracic aorta • Aortic dissection • Aortic aneurysm • Atheromatous disease • Plaque • Blunt aortic trauma

Introduction

Basic perioperative transesophageal echocardiography (TEE) guidelines suggest that knowledge of echocardiographic manifestations of lesions of the great vessels is a necessary training objective. Therefore, a thorough understanding of the use of TEE in evaluating the thoracic aorta including normal and pathologic presentations is essential to the basic perioperative echocardiographer. This chapter will review the essential views for evaluating the thoracic aorta, including potential pitfalls and

Electronic supplementary material The online version of this chapter (doi:[10.1007/978-3-319-34124-8_10](https://doi.org/10.1007/978-3-319-34124-8_10)) contains supplementary material, which is available to authorized users.

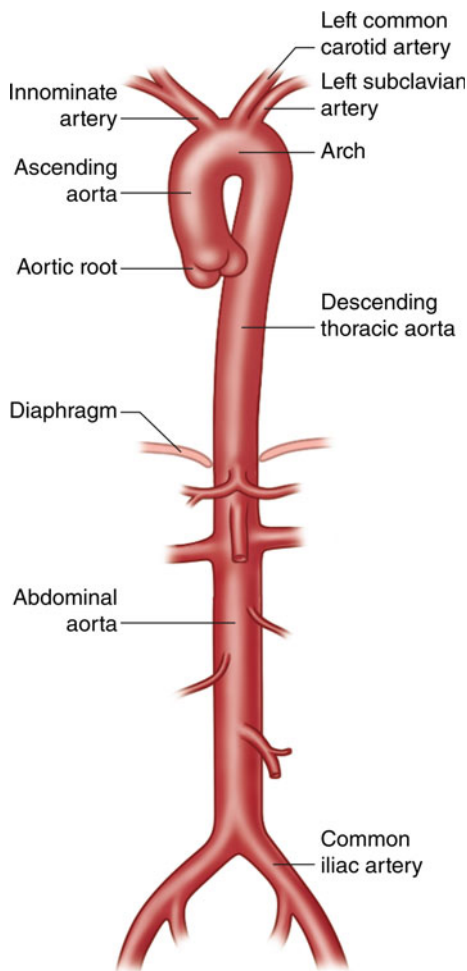
T.M. Maus, MD, FASE (✉)
Department of Anesthesiology, University of California San Diego,
9300 Campus Point Drive #7651, San Diego, CA 92037, USA
e-mail: tmaus@ucsd.edu

review the major aortic pathologies of aortic dissection, aortic aneurysms, aortic atheromatous disease, and thoracic aortic trauma.

TEE: Aortic Views

The immediate proximity of the esophagus to the thoracic aorta allows excellent imaging and superior subsequent detection of disease states. The aorta is a three-layered structure, with intimal, medial, and adventitial layers, that extends from the heart immediately beyond the aortic valve through the transverse aortic arch and descends towards the lower extremity vessel branches. It is described as having five anatomical sections (Fig. 10.1):

Fig. 10.1 Diagram of the entire aortic vascular system include its five anatomical components: 1 aortic root; 2 tubular ascending aorta; 3 aortic arch; 4 descending thoracic aorta; 5 abdominal thoracic aorta



1. Aortic root which extends from the aortic valve to the sinotubular junction (which connects the root to the ascending tubular aorta). The aortic root contains three sinuses of Valsalva, two of which contain the left and right coronary artery ostia.
2. Tubular ascending aorta which extends from the sinotubular junction to the aortic arch.
3. Aortic arch which is the transverse portion of the aorta with typically three great vessel branches: innominate artery, left common carotid, and left subclavian artery.
4. Descending thoracic aorta which extends from the left subclavian artery takeoff to the diaphragm.
5. Abdominal thoracic aorta which continues from the diaphragm to the lower extremity branch points.

As described above, the proximity of the esophagus to the aorta provides excellent views, however, limitations do exist. Because the trachea and left main bronchus are interposed between the esophagus and aorta creating significant air-related artifact, imaging of the distal ascending aorta and proximal arch is often challenging or impossible (Fig. 10.2). Alternative echocardiographic approaches to imaging this region include transthoracic echocardiography (TTE), epiaortic imaging intraoperatively with an opened chest or the use of saline-filled balloons placed in the trachea. However, each of these techniques is beyond the scope of this text.

The relationship of the esophagus to the aorta changes from cranial to caudal. The esophagus is posterior to the aorta at the cranial aspect near the arch, however, the structures twist on themselves such that the esophagus is anterior to the aorta at the gastroesophageal junction. This makes description and location of pathology difficult because the echocardiographic imaging demonstrates a normally circular shape throughout the entire descending thoracic aorta (Fig. 10.3). The anterior, posterior or lateral nature of a lesion thus cannot be accurately identified. Lastly, when entering the stomach, the probe enters the intraperitoneal space, while the aorta continues into the retroperitoneal space. Therefore, the probe is no longer opposing tissue near the aorta and thus, the abdominal aorta is not consistently imaged.

Fig. 10.2 Diagram of the distal ascending aorta, aortic arch, and proximal descending thoracic aorta including its anterior relationship to the esophagus with the trachea interposed

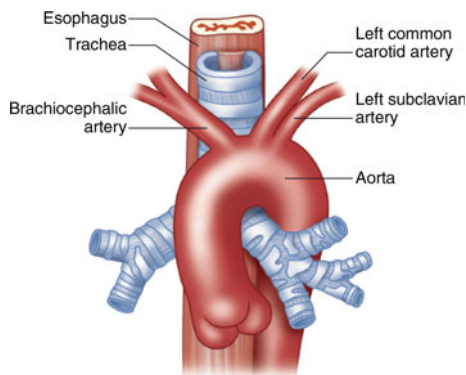
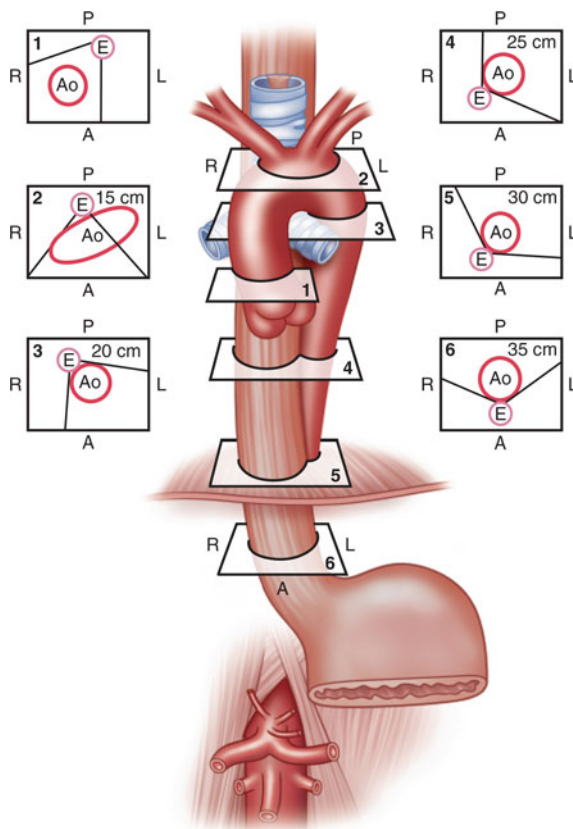
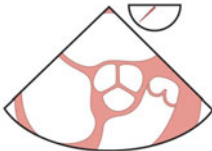

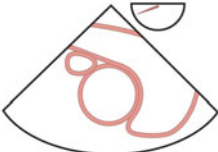

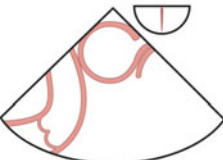
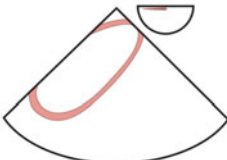
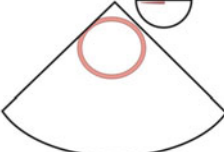
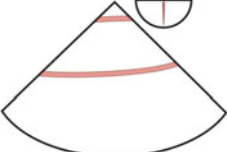


Fig. 10.3 Diagram of the thoracic aorta in relation to the esophagus. Note when cephalad the esophagus is positioned posterior to the aorta, however, when moving caudally the esophagus moves to an anterior position relative to the descending thoracic aorta. (E, esophagus)



The TEE views of the aorta can largely be separated into a short and long axis view of each segment of the visible thoracic aorta (Table 10.1). When discussing the thoracic aorta, one must consider the aortic valve as disease of the aorta may affect the aortic valve and vice versa. The short and long axis views of the aortic valve provide an opportunity to evaluate the number, quality, and function of leaflets, to make appropriate measurements of the left ventricular outflow tract (LVOT), aortic valve annulus, and sinotubular junction, as well as to identify pathology such as aortic dissection or aneurysmal disease. The addition of color flow Doppler aids in the detection of valvular dysfunction. Withdrawing and advancing the probe at zero and ninety degrees of multiplane allows the short and long axis examination, respectively, of the tubular ascending aorta. Obtaining the aortic arch views is easily obtained by rotating the echocardiography probe to the left until the circle shaped descending thoracic aorta is identified and subsequently withdrawing the probe until the oval shaped long axis of the aortic arch is obtained. Increasing the multiplane angle to ninety degrees develops the short axis of the aortic arch. Of note, most commonly the left subclavian artery takeoff is identified on the right side of the screen with the innominate vein noted distally. The left subclavian artery takeoff is

Table 10.1 Transesophageal aortic views

Structure	Short axis	Long axis
Aortic valve	 <p>ME AV SAX</p>	 <p>ME AV LAX</p>
Ascending aorta	 <p>ME asc aortic SAX</p>	 <p>ME asc aortic LAX</p>
Aortic arch	 <p>UE aortic arch SAX</p>	 <p>UE aortic arch LAX</p>
Descending aorta	 <p>Desc aortic SAX</p>	 <p>Desc aortic LAX</p>

an important structure for location identification in the descending aorta. As described above, determining location of pathology in the descending aorta is difficult. Therefore, most commonly the distance from the left subclavian artery takeoff to the pathology is used to communicate location. This technique is also utilized to properly place an intra-aortic balloon pump (IABP) within 1–2 cm distal to the left subclavian. Advancing the probe in both a zero and ninety degree multiplane develops the short and long axis views of the descending thoracic aorta, respectively.

Aortic Dissection

Aortic Dissection

2D	<ul style="list-style-type: none"> • Large undulating mobile flap within aortic lumen • Ensure flap not due to imaging artifact • Differentiate true versus false lumen • SEC or Thrombus in false lumen • Presence of Pericardial or Pleural effusion • Coronary Artery Involvement (Wall Motion Abnormality)
CFD	<ul style="list-style-type: none"> • Differential flow patterns (true lumen = laminar; false lumen = sluggish) • Presence of Aortic Insufficiency
Spectral	<ul style="list-style-type: none"> • Evaluation of Aortic Insufficiency

Aortic dissection is typified by bleeding within the medial layer of the aorta, most commonly due to intimal tearing and separation. Propagation of bleeding within this layer separates the intima from the surrounding adventitial layer, yielding the classically identified dual lumen appearance. The true lumen contains blood within the natural aortic lumen while the false lumen is created by the force of blood ejecting through the intimal tear into the medial layer and contained by the adventitial layer.

This pathology carries a significant risk of morbidity and mortality with a 1–2 % increased mortality per hour until definitive treatment [1]. Therefore, prompt diagnosis is of the utmost concern. Patients at risk for developing an aortic dissection include those with long standing hypertension, smoking, and connective tissue disorders [2]. Common associated diseases include Marfan’s syndrome, Ehlers–Danlos syndrome, bicuspid aortic valve, and coarctation of the aorta.

Two classification systems exist for classifying aortic dissections, DeBakey and Stanford [1]. The Stanford system nicely separates involvement of the ascending aorta into Stanford A, which is a surgical emergency, while Stanford B involves the descending thoracic aorta below the left subclavian artery takeoff. Stanford B dissections without complicating ischemia (paralysis, mesenteric ischemia, etc.) are often treated medically. The DeBakey system divides aortic dissections into three types: Type 1 involves the ascending and descending aorta, Type 2 involves the ascending aorta only, while Type 3 involves only the descending aorta below the left subclavian artery takeoff.

As mentioned above, prompt diagnosis is of paramount importance in such patients to reduce morbidity and mortality. The historical gold standard involves angiography and the demonstration of contrast exiting the true lumen into the false lumen. The time consuming process and increased risk of contrast-induced nephropathy has reduced this practice, being replaced by Helical CT and MRI. The downside of each of these modalities is the continued need for patient transport as well as being potentially time consuming. TEE provides a mobile modality with excellent sensitivity and specificity in the detection of aortic dissections. Shiga et al.

demonstrated that TEE has a sensitivity of 98 % and specificity of 95 % and is comparable to helical CT or MRI [3]. Therefore, patients who are hemodynamically unstable and unable to be transported to an imaging suite may be evaluated by TEE in the emergency room, intensive care unit or operating room.

The echocardiographic approach to an aortic dissection involves confirming the presence and the location of a dissection flap as well as potentially identifying intimal tear entry/exit sites, differentiating true versus false lumen, and identifying complicating pathologies such as aortic insufficiency, pericardial and pleural effusions, coronary artery involvement and ventricular dysfunction. Of note, the current basic perioperative TEE consensus statement suggests that in the setting of complex pathology such as an aortic dissection, appropriate consultation with an advanced echocardiographer or other imaging modality is indicated [4].

Dissection Flap Identification

Identification of the intimal flap is the cornerstone of the aortic dissection diagnosis. Typically the intimal flap is noted as a thin, undulating mobile structure that is entirely contained within the lumen of the aorta. Multiple multiplane angles should be utilized to ensure that there is a flap present, representing the separation of the true from false lumens (Figs. 10.4 and 10.5; Videos 10.1 and 10.2). With the cardiac cycle, systolic ejection into the aortic lumen causes true lumen expansion while delayed entry of blood through the intimal tear into the false lumen causes delayed filling with sluggish or no flow. This cycling of expansion leads to the

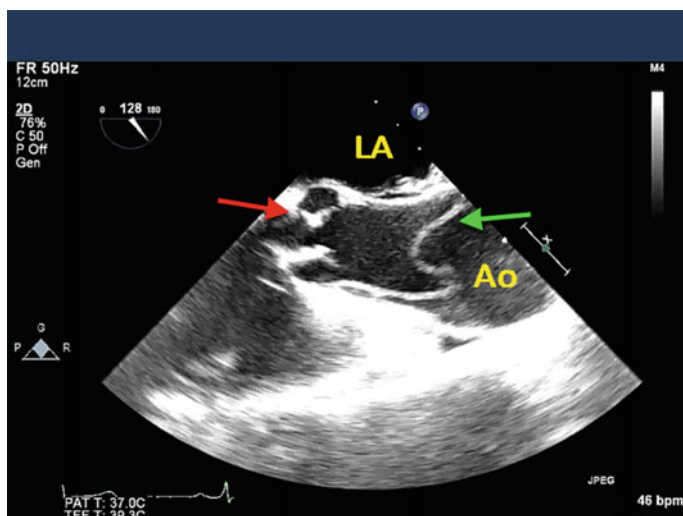


Fig. 10.4 Midesophageal aortic valve long axis view with the probe slightly withdrawn to demonstrate more of the tubular ascending aorta. The *red arrow* points to a calcified aortic valve while a *green arrow* indicates the undulating intimal flap within the aortic lumen (LA left atrium; Ao Aorta)

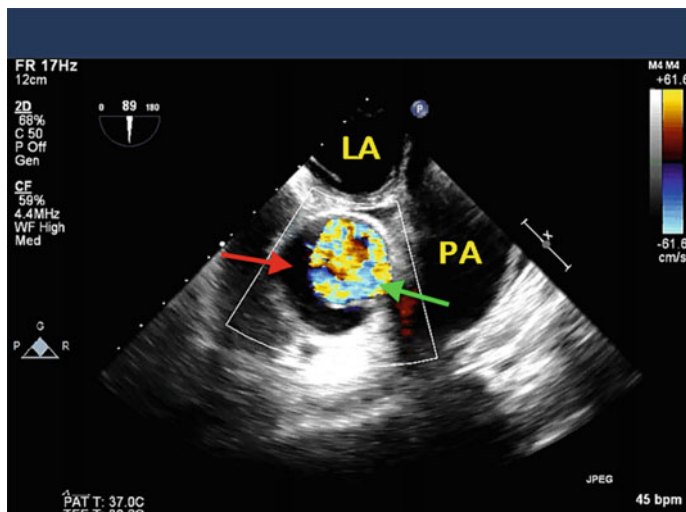


Fig. 10.5 Midesophageal view of ascending aorta developed by a slow withdrawal of the probe from an aortic valve short axis. The *green arrow* points to a true lumen with noted rapid early systolic flow while the *red arrow* indicates the false lumen with little to no flow demonstrated on color flow Doppler (LA left atrium; PA main pulmonary artery)

undulating mobile appearance of the intimal flap. Discussed below, the differential flow patterns may be detected with color flow Doppler to aid in identifying true versus false lumens. In addition to identifying the presence of the intimal flap, describing the location and extent of the dissection is important. Location within the ascending aorta or aortic arch denotes a surgical emergency. Dissection through adjacent structures or branches such as the coronary arteries, great vessels, or aortic valves may also necessitate prompt surgical repair.

Echocardiography may also identify not just the presence of an intimal flap but also the intimal tear site. The tear displays as an opening or communication in the intimal flap with color flow Doppler documenting the presence of flow from the true to the false lumen (Fig. 10.6; Video 10.3). When a tear site is identified in the ascending aorta near the aortic valve, flow may be bidirectional between the true and false lumens because of pressure differentials near the aortic valve during systole and diastole. During systolic ejection, flow and pressure is higher in the true lumen with flow from true to false lumen through the tear site. During diastole, particularly with associated aortic insufficiency, the pressure is temporarily higher in the false lumen with a return of flow to the true lumen (Fig. 10.7; Video 10.4).

Care must be taken when diagnosing intimal flaps as imaging artifacts which, particularly in the ascending aorta, may appear as linear densities within the aortic lumen. Side lobe artifacts involve weak ultrasound beams emanating off axis from the main imaging plane and returning from strong reflectors to the ultrasound probe. A not infrequent occurrence is a side lobe reflection from an off-plane central line or pulmonary artery catheter displayed as a linear echogenic density in the ascending aorta

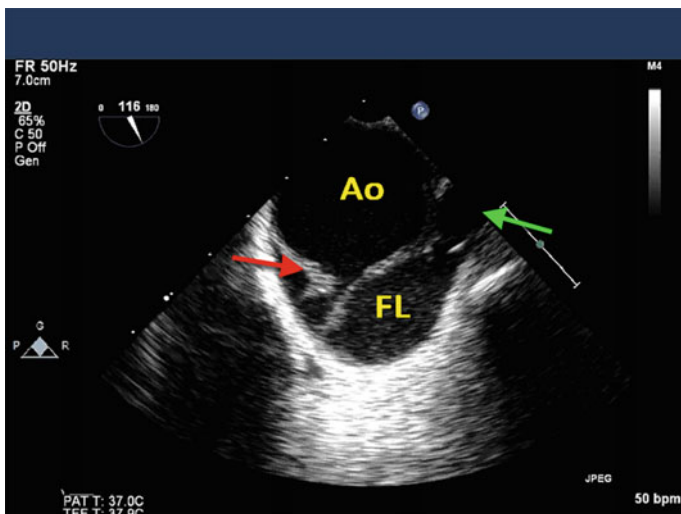


Fig. 10.6 Upper esophageal aortic arch short axis view in a patient with an acute aortic arch dissection. The *red arrow* points to the tear site in the intimal flap. The *green arrow* indicates the left subclavian artery takeoff which branches from the false lumen and has compromised flow (Ao Aorta; FL False Lumen)

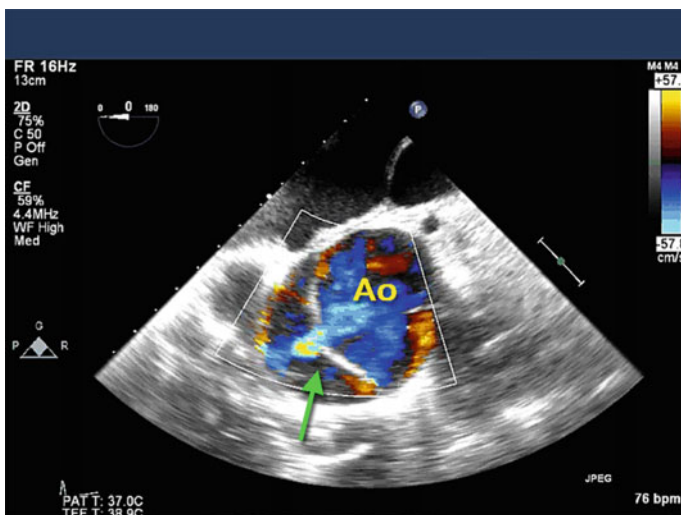


Fig. 10.7 Midesophageal ascending aortic short axis view in a patient with an ascending aortic dissection. The *green arrow* indicates the tear site in the intimal flap with systolic flow demonstrated from the true lumen into the false lumen (Ao ascending aorta)

in the midesophageal ascending aortic short axis view (Fig. 10.8; Video 10.5a, b). Again it is emphasized that except in emergency situations, current consensus statement suggests that a basic echocardiographer consult an advanced echocardiographer when evaluating aortic dissections to confirm the diagnosis.

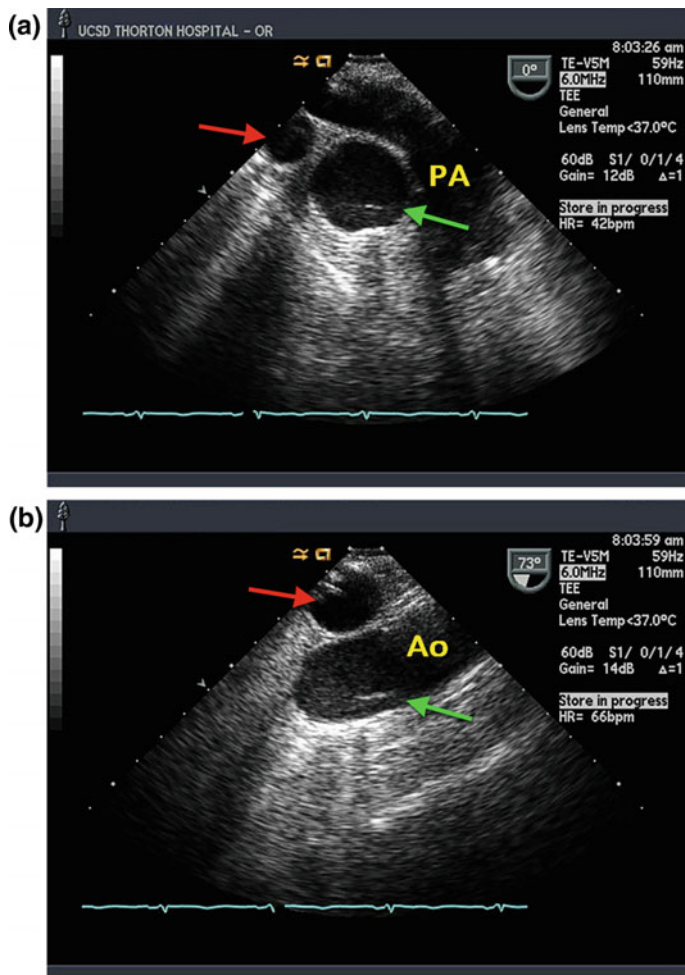


Fig. 10.8 **a** Midesophageal ascending aortic short axis view in a patient with a side lobe artifact. The *red arrow* indicates the superior vena cava. The *green arrow* indicates a side lobe artifact from a large out of plane specular reflector such as a central line or pulmonary artery catheter. This linear density in the ascending aorta may be confused with an aortic dissection. **b** Midesophageal ascending aortic long axis view of the same patient. The *red arrow* points to the right PA which contains a PA catheter. The *green arrow* points to a side lobe artifact which may be confused for an aortic dissection (*Ao* Ascending Aorta; *PA* pulmonary artery)

Differentiating True from False Lumens

The ability to differentiate true from false lumens serves to confirm the presence of an aortic dissection, rule out imaging artifacts, and in the case of aortic surgery, allow the confirmation of surgical repair (lack of false lumen flow post repair). There are several characteristics of true and false lumens that are fairly common: size, shape, systolic motion, and type or presence of flow (Table 10.2).

Table 10.2 Echocardiographic differentiation of aortic dissection true and false lumens

True lumen	False lumen
Smaller	Larger
Round	Irregular
Systolic expansion	Systolic compression
Early laminar flow	Late turbulent flow
	+/- Spontaneous contrast
	+/- Thrombus

On two-dimensional echocardiography, the true lumen is often the smaller and round shaped lumen while the false lumen tends to be the larger, irregular shaped structure. The larger false lumen is often crescentic (“moon-like”) with concavity towards the true lumen. Systolic motion, as described above, involves the expansion of the true lumen with systolic ejection. Since the false lumen has delayed flow, the structure will compress during systole (Fig. 10.9; Video 10.6a, b). M-mode echocardiography may aid in identifying which structure is expanding during the systolic portion of the cardiac cycle. Lastly, color flow Doppler may be useful in differentiating where true lumens have early systolic laminar flow while false lumens have late systolic turbulent flow. False lumens contain such sluggish flow that spontaneous echo contrast or frank thrombus may be identified.

Identifying Complicating Pathologies

The proximity of the aorta to several other anatomical structures as well as the dependency of the branch vessels on an intact aorta allow an aortic dissection to wreak havoc beyond just the damaged vessel itself. An advantage of TEE over other modalities includes its ability to evaluate surrounding structures and the effect of a dissection on those structures. As described above, the aortic valve is intimately connected to the aorta such that an aortic dissection may yield significant aortic valve dysfunction (Fig. 10.10; Video 10.7a, b). There are several mechanisms by which an ascending dissection may cause aortic insufficiency, such as the mobile flap itself impeding valve closure or the large false lumen causing annular dilation or distortion and subsequent malcoaptation. A detailed evaluation of the mechanism is important in determining the need for concomitant valve replacement during aortic surgery, however this analysis is beyond the scope of this text.

In a normal state, the three layers of the aortic wall (intima, media, adventitia) contain the blood within the aortic lumen. During an aortic dissection, blood in the false lumen is now only contained by the adventitial layer, allowing a transudative process to leak into the surrounding spaces, such as the pericardial or left pleural space. An inflammatory component also appears to play a role in the development of pleural effusions [5]. Pericardial effusions are noted as an echolucent area surrounding the heart or great vessels in nearly any view but commonly the midesophageal four

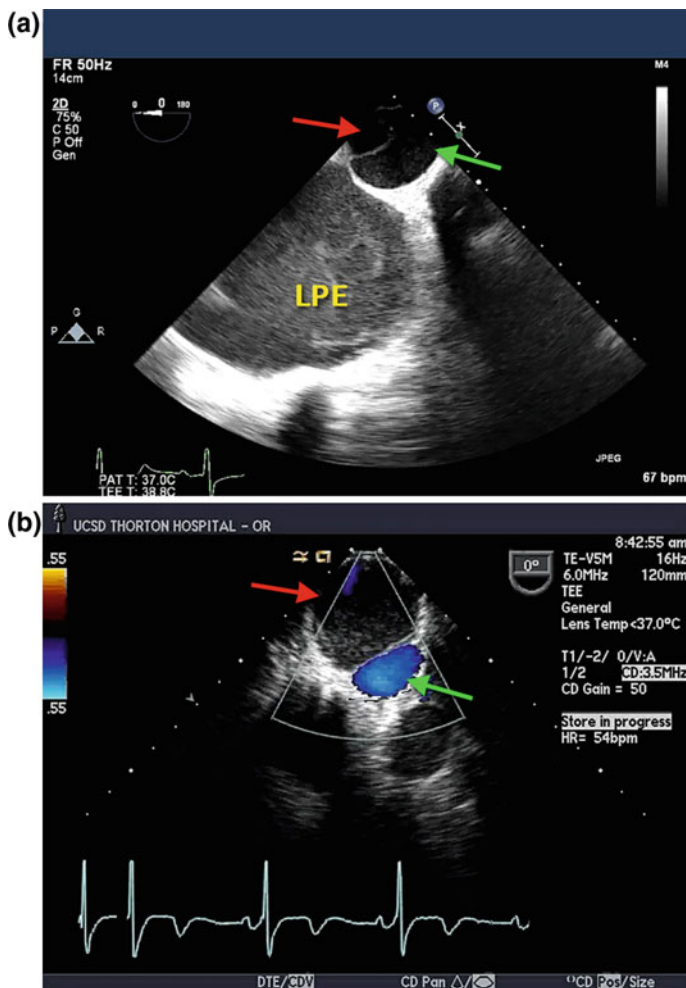


Fig. 10.9 **a** Descending thoracic aortic short axis view in a patient with an aortic dissection. The *red arrow* indicates the true lumen. The *green arrow* indicates the false lumen which contains spontaneous echo contrast. Note the large left sided pleural effusion (LPE). **b** Descending thoracic aortic short axis view with color flow Doppler in a separate patient with an aortic dissection. The *green arrow* indicates laminar flow in the true lumen and the *red arrow* indicates the false lumen with sluggish flow

chamber or transgastric short axis views. Determining tamponade physiology is discussed in the Rescue Echo chapter (See Chap. 12). Left sided pleural effusions are noted as an echolucent area anterior to the descending thoracic aorta in the descending aortic short axis view (Fig. 10.11; Video 10.8). Another process can yield pericardial or pleural effusions, however, with often more dramatic clinical presentations. Frank rupture of the dissection into the pericardial or pleural space causes a hemorrhagic effusion, rapid accumulation of blood, and significant hemodynamic deterioration.

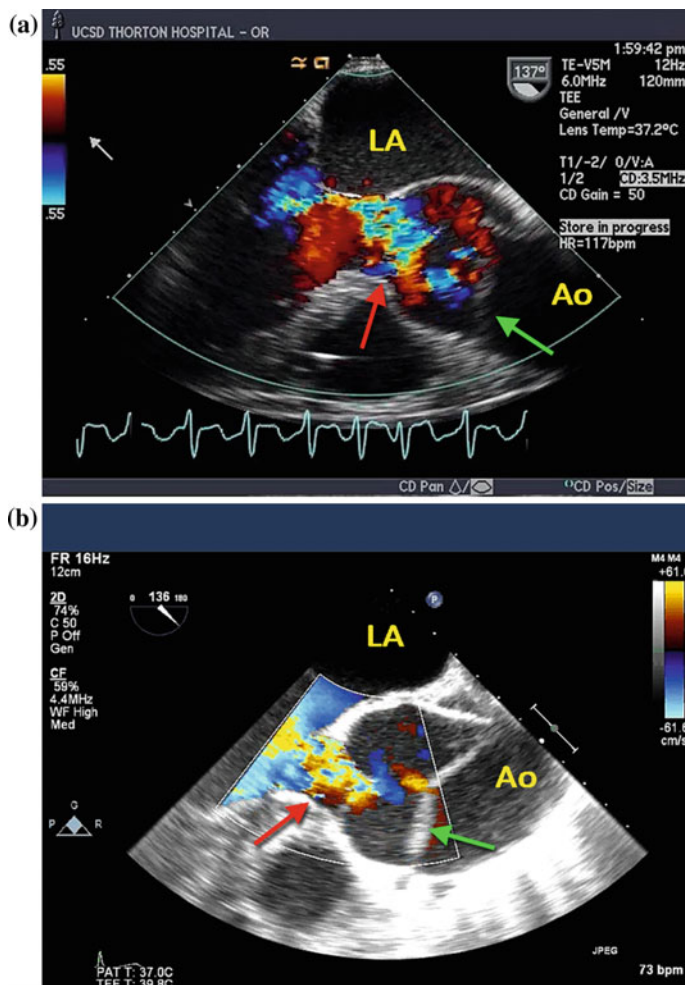


Fig. 10.10 **a** Midesophageal aortic valve long axis view in a patient with an ascending aortic dissection. The *green arrow* indicates the intimal flap located near the sinotubular junction while the *red arrow* indicates associated severe aortic insufficiency. **b** Midesophageal aortic valve long axis view in a separate patient with an ascending aortic dissection. The *green arrow* indicates the intimal flap located near the sinotubular junction. Note the intimal tear with diastolic flow reversing back into the true lumen from the false lumen. The *red arrow* indicates associated severe aortic insufficiency (LA left atrium; Ao Ascending Aorta)

During evaluation of an ascending aortic dissection that is approaching the aortic root, concern must exist for dissection through the ostium of the main coronary arteries. The aortic root contains three sinuses of Valsalva, two of which contain coronary arteries (left and right). A proximal dissection through a coronary ostium and resultant reduction of its blood supply may result in significant ischemia or frank infarction. An evaluation for wall motion abnormalities is essential if coronary involvement is suspected (Fig. 10.12; Video 10.9a, b).

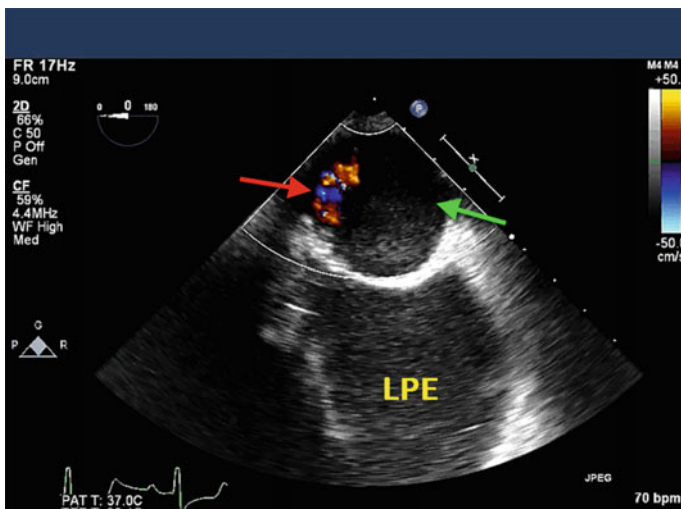


Fig. 10.11 Descending thoracic aortic short axis view with color flow Doppler in a patient with an aortic dissection and a large left pleural effusion (LPE). The *red arrow* indicates the true lumen; the *green arrow* notes the false lumen

Lastly, aortic dissections may result in ventricular dysfunction through two major mechanisms. As previously described, acute ischemia may result in wall motion abnormalities and frank RV or LV dysfunction. In another fashion, acute aortic insufficiency causes abrupt volume overload to a ventricle that has not had the time to dilate and adapt to the volume overload (as in chronic aortic insufficiency). Therefore, an evaluation of biventricular function is imperative in the setting of ascending aortic dissections.

Aortic Aneurysms

Aortic Aneurysm	
2D	<ul style="list-style-type: none"> Evidence of aortic dilation (linear measurements) Branch involvement Aortic Root Involvement (Aortic Valve malcoaptation)
CFD	<ul style="list-style-type: none"> Presence of Aortic Insufficiency
Spectral	<ul style="list-style-type: none"> Evaluation of Aortic Insufficiency

Aortic dilation refers to the enlargement of the aortic vessel beyond the upper limits of normal. Normal adult thoracic aortic are approximately 3.5 to 4.0 cm for the aortic root, less than 3.0 cm for the ascending aorta and descending thoracic aorta.

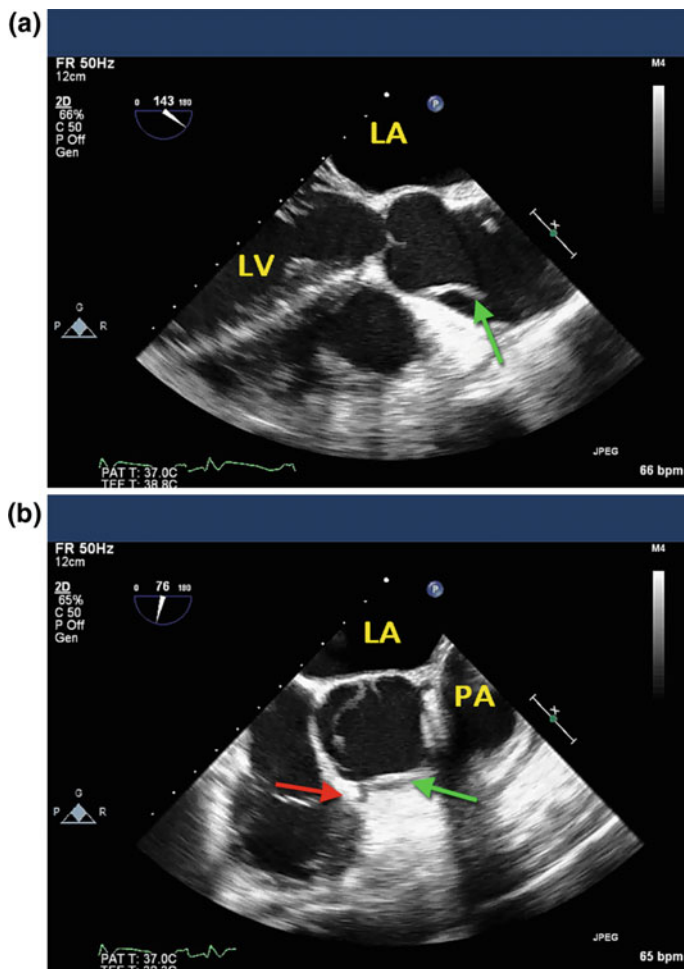


Fig. 10.12 **a** Midesophageal aortic valve long axis view in a patient with an ascending aortic dissection. The *green arrow* indicates the intimal flap located near the sinotubular junction and extending into the right sinus of Valsalva. **b** Midesophageal aortic valve short axis view in the same patient. The *green arrow* indicates the intimal flap located abutted the right coronary ostium (indicated by the *red arrow*) (LA left atrium; LV left ventricle; PA pulmonary artery)

Additionally, there is variability between genders at each segment (Root, Ascending, Mid-descending and Diaphragmatic) [6]. An aneurysm is classically described as a dilated segment of all three layers of an arterial wall with a vessel size that is beyond 150 % of its normal size. Surgical repair is considered as the aorta dilates beyond 4.5–5.5 cm taking into consideration the patients history and risk factors [6]. Again, the close relationship of the esophagus to the aorta allows excellent imaging of dilated and aneurysmal segments of the aorta. However, TEE does not carry the same potency in diagnosis as it does in the setting of acute aortic dissection. In the setting of aortic aneurysms, proper surgical planning is essential

to successful treatment and relies on preoperative imaging. Proper identification of tortuosity, anterior spinal arteries including the artery of Adamkiewicz, and branch vessels may help guide management of cardiopulmonary bypass and neuroprotection strategies. TEE, however, still plays a role in the intraoperative management and in the setting of an unstable patient with an aneurysm rupture.

The echocardiographic approach to a patient with an aneurysm is similar to that of a dissection and includes determining the location and extent of disease as well as identifying coexisting pathologies. Measurements in multiple planes may be helpful to identify the degree and extent of the aneurysm. In the setting of ascending aortic aneurysms, measurement of the aortic valve annulus and sinotubular junction may aid in assessing both the aneurysm and potential aortic valve involvement (Fig. 10.13). Care must be undertaken as proper cross-sectional measurements may be difficult in the setting of tortuosity.

Coexisting pathology with aortic aneurysms most often relate to the aorta's intimate structural relationship to the aortic valve. In the setting of aortic stenosis, the resultant post-stenotic turbulent flow in the ascending aorta leads to altered hemodynamics and a continued outward pressure. This results in post-stenotic aortic dilatation that may halt after aortic valve replacement in calcific aortic stenosis [7]. Bicuspid aortic valve disease may also progress towards aortic stenosis with attendant aortic dilatation. However, despite aortic valve replacement, aortic dilatation may continue in these patients. In addition, another group of bicuspid aortic valve patients may present with annular dilation and aortic insufficiency without stenosis, potentially necessitating replacement of both the valve and

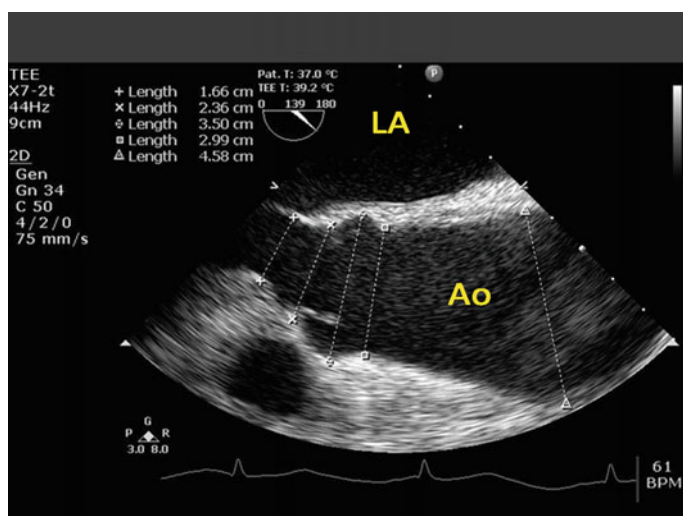


Fig. 10.13 Midesophageal aortic valve long axis view in a patient with an ascending aortic aneurysm. Measurements of the left ventricular outflow tract, aortic annulus, sinuses of Valsalva, sinotubular junction, and ascending aorta note the presence of an ascending aortic aneurysm without significant involvement of the aortic root (LA left atrium; Ao Ascending Aorta)

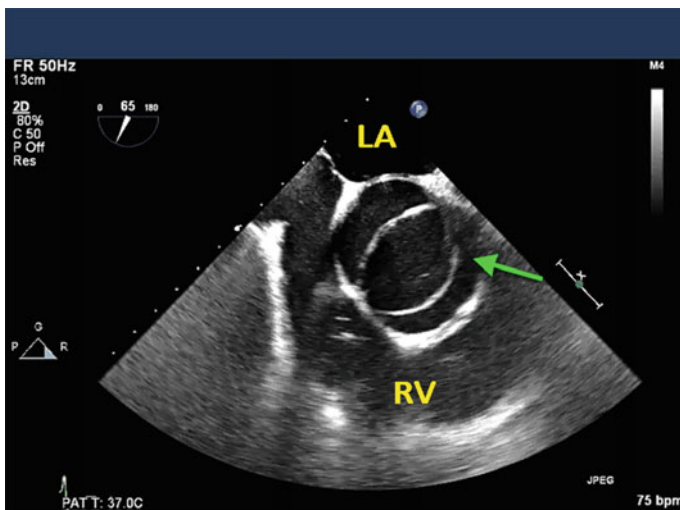


Fig. 10.14 Midesophageal aortic valve short axis view in a patient with a bicuspid valve and ascending aortic aneurysm. The *green arrow* indicates the bicuspid valve with a unified right and left coronary cusp. Note the dilated annulus (LA left atrium; RV right ventricle)

ascending aorta (Fig. 10.14; Video 10.10). Finally, the dilated aorta itself may have an impact on aortic valve function. As the aortic valve is crown shaped with attachments near the annulus at the base and the sinotubular junction at the top, dilation of the root may result in malcoaptation of the aortic valve leaflets and subsequent aortic regurgitation (Fig. 10.15; Video 10.11).

Aortic Atheroma

TEE is very sensitive to the detection of aortic atheromatous disease and the presence of such plaque carries significant patient risk. When the atheromatous disease is noted to be greater than or equal to 4 mm in thickness, it is associated with increased risk of all vascular events including stroke, myocardial infarction, peripheral embolism and death [1]. The transesophageal echocardiographic imaging approach includes noting severity, location, as well as mobility of atheromas (Figs. 10.16 and 10.17; Video 10.12a, b). The grading of atheromatous disease is displayed in Table 10.3. In the setting of interventional vascular procedures, the presence of severe atheromatous disease including plaque mobility should be communicated to the surgical team to prevent inadvertent embolization.

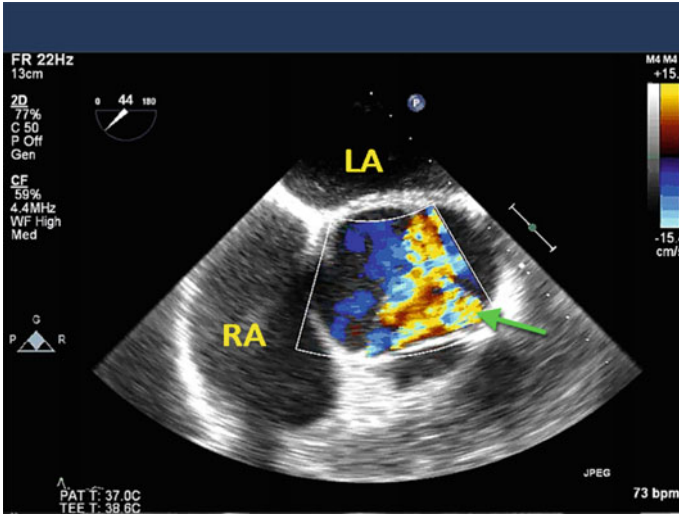


Fig. 10.15 Midesophageal aortic valve short axis view with color flow Doppler in a patient with an ascending aortic aneurysm. The *green arrow* indicates the significant aortic insufficiency from the associated dilated annulus and ascending aortic aneurysm (LA left atrium; RA right atrium)

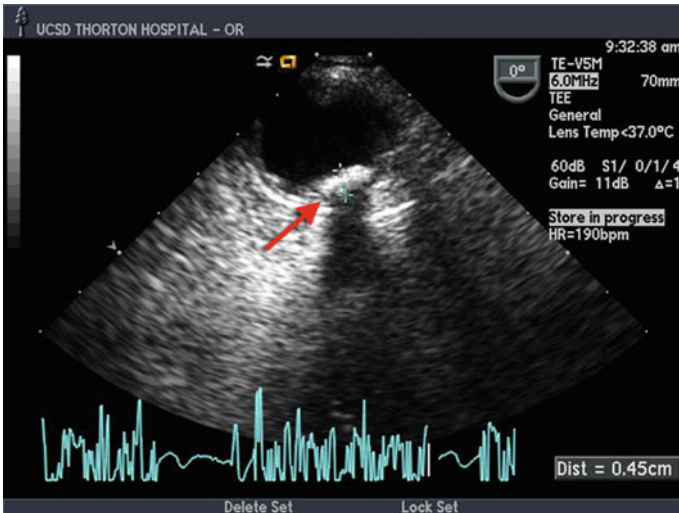


Fig. 10.16 Descending thoracic aorta short axis view demonstrating aortic atheroma measuring 4.5 cm, Grade III disease (*red arrow*)

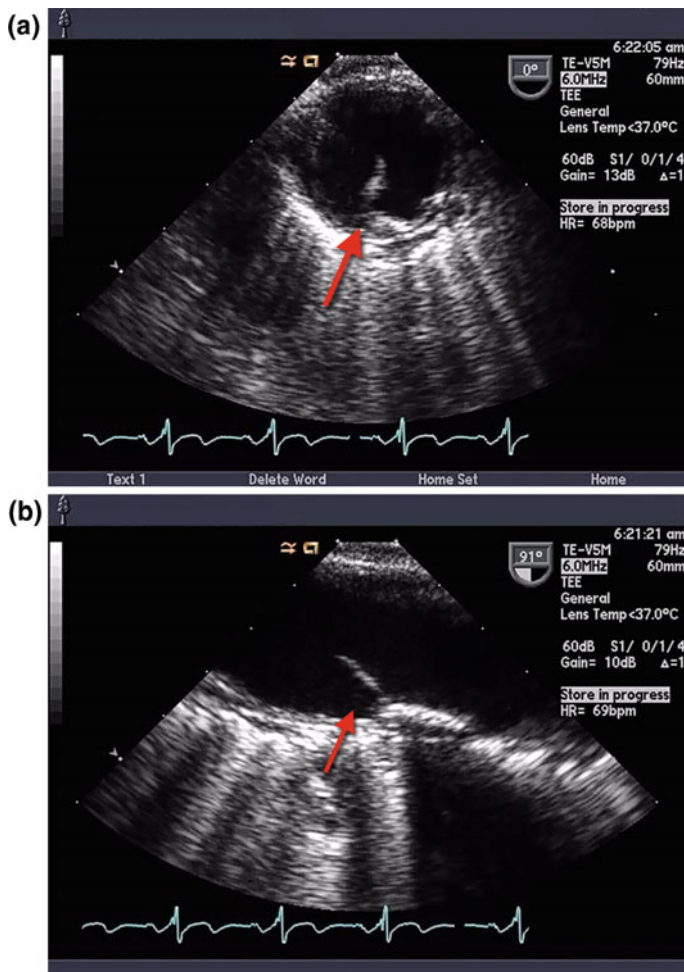


Fig. 10.17 **a** Descending thoracic aortic short axis view demonstrating complex atheromatous disease. The *red arrow* indicates a large pedunculated mobile portion extending into the aortic lumen. **b** Descending thoracic aortic long axis view of the same patient. The *red arrow* again points to the pedunculated mobile portion of the atheroma

Table 10.3 Echocardiographic grading of atheromatous disease

Grade	Description
1	Normal aorta; minimal intimal thickening
2	Extensive intimal thickening
3	Calcified aortic plaque less than 5 mm
4	Calcified aortic plaque greater than 5 mm
5	Mobile atheroma or ulcerated plaque

Thoracic Aortic Trauma

The thoracic aorta has both relatively fixed and mobile portions. The junctions of these portions are often the site of injury in blunt aortic injury, mostly commonly the aortic isthmus (immediately distal to the left subclavian artery) and the ascending aorta (immediately distal to the aortic valve). The most common mechanism for this type of injury is a rapid deceleration which transmits the sheer force between the relatively fixed and mobile portions. This usually involves damage to the aortic intima with potential damage through the media and adventitia including complete aortic transection [8].

Echocardiographically, aortic trauma may share characteristics of a spontaneous aortic dissection. However, on examination of a traumatic aortic injury, the medial flap tends to be thicker in appearance, the lesion is more often isolated without propagation, and there may be the presence of an abnormal aortic contour, an aortic pseudoaneurysm, or a crescentic shaped intramural hematoma. A complete evaluation of the thoracic aorta in this setting should be in consultation with an advanced echocardiographer or confirmed with an alternative imaging technique.

Conclusion

TEE is an excellent monitor for the diagnosis of several aortic pathologies, albeit with some limitations. Knowledge of these limitations allows this modality to be utilized in the setting of aortic dissection, aneurysm, atheroma, and trauma. The basic echocardiographer should have a sound understanding of thoracic aortic imaging with TEE.

References

1. Khalil A, Helmy T, Porembka DT. Aortic pathology: aortic trauma, debris, dissection, and aneurysm. *Crit Care Med*. 2007;35:S392–400.
2. Nienaber CA, Clough RE. Management of acute aortic dissection. *Lancet*. 2015;385:800–11.
3. Shiga T, Wajima Z, Apfel CC, Inoue T, Ohe Y. Diagnostic accuracy of transesophageal echocardiography, helical computed tomography, and magnetic resonance imaging for suspected thoracic aortic dissection: systematic review and meta-analysis. *Arch Intern Med*. 2006;166:1350–6.
4. Reeves ST, Finley AC, Skubas NJ, et al. Basic perioperative transesophageal echocardiography examination: a consensus statement of the American society of echocardiography and the society of cardiovascular anesthesiologists. *J Am Soc Echocardiogr*. 2013;26:443–56.
5. Hata N, Tanaka K, Imaizumi T, et al. Clinical significance of pleural effusion in acute aortic dissection. *Chest*. 2002;121:825–30.
6. Hiratzka LF, Bakris GL, Beckman JA, et al. ACCF/AHA/AATS/ACR/ASA/SCA/SCAI/SIR/STS/SVM guidelines for the diagnosis and management of patients with thoracic aortic disease. A report of the American College of Cardiology Foundation/American Heart association

- task force on practice guidelines, American Association for thoracic surgery, American College of Radiology, American Stroke Association, Society of Cardiovascular Anesthesiologists, Society for Cardiovascular Angiography and Interventions, Society of Interventional Radiology, Society of Thoracic Surgeons, and Society for Vascular Medicine. *J Am Coll Cardiol.* 2010;55:e27–129.
7. Wilton E, Jahangiri M. Post-stenotic aortic dilatation. *J Cardiothorac Surg.* 2006;1:7.
 8. Goldstein SA, Evangelista A, Abbara S, et al. Multimodality imaging of diseases of the thoracic aorta in adults: from the American society of echocardiography and the european association of cardiovascular imaging: endorsed by the society of cardiovascular computed tomography and society for cardiovascular magnetic resonance. *J Am Soc Echocardiogr.* 2015;28:119–82.

Chapter 11

Rescue Echocardiography

Byron Fergerson, MD and Joshua Zimmerman, MD, FASE

Abstract Current recommendations include the use of transesophageal echocardiography (TEE) for acute, persistent, unexplained hypotension. Perioperative transesophageal echocardiography is well suited to assess for the etiology of acute hemodynamic instability as it provides information on multiple aspects of cardiovascular physiology, from contractility and valvular function to volume status and intracardiac pressures. Its portable and relatively noninvasive nature allows quick diagnosis and rapid implementation of therapy in unstable patients. A rapid, qualitative assessment of the hemodynamic event, or “eyeballing”, is the cornerstone to rescue echocardiography. Rescue echocardiography is a process, not an event, where a qualitative estimation of the abnormality followed by reevaluation after the intervention is suggested. This chapter describes this process of rapid diagnosis, intervention, and reevaluation and highlights several key and common causes of perioperative hemodynamic instability.

Keywords Rescue echocardiography • Hemodynamic instability • Transesophageal echocardiography • Hypotension • Valvular disease • Ventricular dysfunction • Hypovolemia • Tamponade

Electronic supplementary material The online version of this chapter (doi:[10.1007/978-3-319-34124-8_11](https://doi.org/10.1007/978-3-319-34124-8_11)) contains supplementary material, which is available to authorized users.

B. Fergerson, MD (✉)
Department of Anesthesiology, University of California San Diego,
200 W Arbor Drive MC #8770, San Diego, CA 92103, USA
e-mail: bfergerson@ucsd.edu; byronfergerson@gmail.com

J. Zimmerman, MD, FASE
Department of Anesthesiology, University of Utah,
30 N 1900 E, Salt Lake City, UT 84132, USA
e-mail: Joshua.Zimmerman@hsc.utah.edu

The American Society of Echocardiography (ASE) recommends the use of transesophageal echocardiography (TEE) for acute, persistent, unexplained hypotension [1]. Transesophageal echocardiography is well suited to assess for the etiology of acute hemodynamic instability as it provides information on multiple aspects of cardiovascular physiology, from contractility and valvular function to volume status and intracardiac pressures. There are several other key advantages as well. It is portable, relatively noninvasive, and provides a qualitative picture of the hemodynamic event. A rapid, qualitative assessment of the hemodynamic event, or “eyeballing”, is the cornerstone to rescue echocardiography. A detailed quantitative analysis of cardiovascular function is neither feasible nor necessary in the emergent setting. Grasping the overarching hemodynamic picture, performing an intervention, and reassessing the hemodynamics is the most practical and effective use of TEE. A qualitative analysis is also significantly easier to learn [2].

Unfortunately, there is a paucity of data on the use of TEE in the setting of hemodynamic instability in the perioperative period. Markin et al. looked retrospectively at 364 rescue echocardiograms performed on cardiac and noncardiac cases throughout the perioperative period [3]. Anesthetic management was changed in more than half of the patients evaluated by TEE with no echo-related complications. Interestingly, there was a change in surgical management in 7 % of the cases.

Time is of the essence in rescue echocardiography as the etiology of the instability must be rapidly diagnosed and acted upon. There are 28 recommended views in the most recently published comprehensive TEE exam, many of which are redundant. Redundancy is valuable in general because it allows for visualization of structures from multiple angles. It is not, however, conducive to brevity. For this reason, a condensed examination is suggested. The “rescue exam” presented in this chapter is a modification of the 11 cross-sectional views recommended by the ASE and Society of Cardiovascular Anesthesiologists (SCA) for the basic TEE exam [4]. The primary differences are the order of the views and the use of spectral Doppler. Spectral Doppler is vital to delineate between certain causes of hemodynamic instability and thus is included in this exam. The rescue exam is short but covers the majority of clinically relevant pathologies. In addition, performing the same exam every time minimizes distraction. The rescue exam is listed in Table 11.1, beginning in the mid-esophagus and ending in the stomach for ease of use. Similar protocols have been studied and used effectively [3, 5, 6]. In agreement with the ASE and SCA [4], it is suggested to perform and store the limited exam in its entirety before focusing on segments specific to the area of interest.

It is important to note that rescue echocardiography is a process, not an event. The cardiovascular system is complex and dynamic, potentially changing on a beat-to-beat basis. What may be considered an appropriate intervention one minute, may not be appropriate the next. It may be difficult to discern the precise cause of the cardiovascular abnormality. In addition, it is possible that multiple abnormalities are present. Similar to Markin et al. [3], a qualitative estimation—a “best guess”—of the abnormality followed by reevaluation after the intervention is suggested. If parameters improve, one should continue the intervention. If they do not improve or worsen, an alternate diagnosis should be sought.

Table 11.1 Recommended limited TEE exam

-
1. Mid-esophageal AV SAX
 2. Mid-esophageal AV LAX
 - Measurement of LVOT diameter
 3. Mid-esophageal bicaval
 4. Mid-esophageal RV inflow/outflow
 5. Mid-esophageal 4 chamber
 - With and without CFD on the TV and MV
 6. Mid-esophageal 2 chamber
 7. Mid-esophageal LV LAX
 8. Transgastric midpapillary LV SAX
 9. Deep transgastric LAX
 - PWD of LVOT
 - Calculation of stroke volume
 10. Descending aorta SAX
-

AV Aortic valve; *SAX* Short axis; *LAX* Long axis; *CFD* Color flow Doppler; *TV* Tricuspid valve; *MV* Mitral valve; *PWD* Pulse wave Doppler; *RV* Right ventricle; *LV* Left ventricle; *LVOT* Left ventricular outflow tract; *TG* Transgastric

The most common causes of hemodynamic instability will be reviewed: acute valvular and aortic pathology, tamponade, RV dysfunction, pulmonary embolism, hypovolemia, low afterload, and LV hypo- and hypercontractility.

Acute Valvular and Aortic Pathology

The echocardiographic assessments of valvular and aortic pathology (specifically dissection and traumatic rupture) are discussed elsewhere in the text and will be mentioned only briefly here (see Chaps. 7 and 10). Acute valvular dysfunction is most likely to occur on left-sided structures [7]. Endocarditis is the most common cause of acute regurgitation. Other potential causes include trauma, aortic dissection, and left ventricular ischemia. Evaluation of valvular regurgitation in the acute setting should be limited to a rapid, qualitative assessment as quantitative measures may be inaccurate [7]. Color flow Doppler (CFD) is the primary modality for a visual assessment of the regurgitant jet focusing primarily on the vena contracta. New onset or a change in chronic regurgitation is more valuable than grading the severity. Keep in mind that the regurgitation may be a manifestation of changes in ventricular function and loading conditions induced by another cardiac abnormality.

Regarding aortic dissection, as discussed in Chap. 10, TEE is as reliable as helical computed tomography and magnetic resonance imaging in diagnosing or ruling out a dissection [8]. The diagnosis of dissection is based on the detection of an intimal flap that divides the aorta into true and false lumens [9]. The lumens are best delineated through CFD. TEE is also valuable in assessing for the intimal tear, intramural hematomas [10], and penetrating ulcers [11].

Cardiac Tamponade

Cardiac Tamponade

2D	<ul style="list-style-type: none"> • Echolucent space between heart and pericardium (may be loculated) • Effusion >2cm are severe • Chamber Collapse (RA – Systolic; RV – Diastolic)
CFD	• Typically not utilized
Spectral	• >10% respiratory variation in LVOT VTI

RA = right atrium; RV = right ventricle; LVOT = left ventricular outflow tract; VTI = velocity time integral

Pericardial effusions with associated tamponade physiology are extremely dangerous under general anesthesia. Rapid diagnosis and intervention is necessary making echocardiography, with its portability and accuracy, the diagnostic modality of choice. Acute effusions are generally due to trauma or ischemia, but must also be considered in the setting of inflammation, infection, malignancy, and renal and hepatic failure. Pericardial effusions are seen as darkened areas between

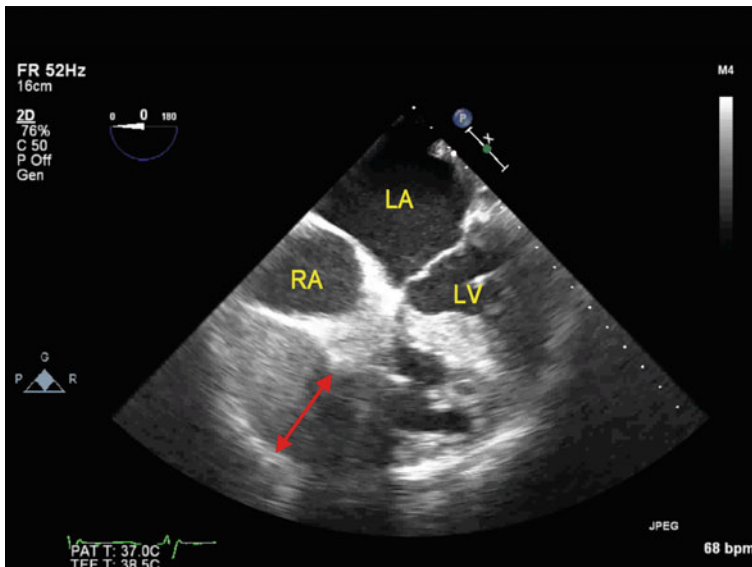


Fig. 11.1 Mid-esophageal four-chamber view demonstrating an acute pericardial effusion following percutaneous transvenous lead extraction. Double-headed red arrow indicates the pericardial effusion. LA Left Atrium; LV Left Ventricle; RA Right Atrium

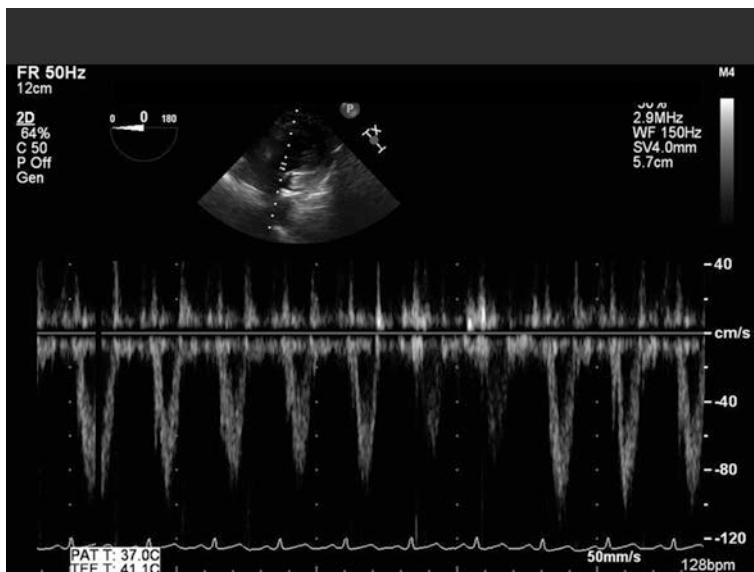


Fig. 11.2 Deep transgastric long axis view with pulse wave Doppler placed in the left ventricular outflow tract showing respiratory variability

the heart and the parietal layer of the pericardium (Fig. 11.1; Video 11.1). An effusion may be identified in nearly any mid-esophageal or transgastric view. Effusions measuring less than 1 cm are considered small; 1–2 cm are considered moderate; and >2 cm are considered large. Visualization of an effusion does not necessarily mean there is tamponade physiology. The pericardium can become quite distensible in the setting of a chronic effusion and thus, have a limited effect on intracardiac pressures and filling. However, in the case of extreme hemodynamic instability, a large pericardial effusion should be considered to cause cardiac tamponade regardless of the results of the continuing study (i.e., chamber collapse or spectral Doppler findings). A pericardial effusion can be contained within a loculation making it difficult to locate. The localized pressure exerted on the heart in this situation can still cause cardiac tamponade.

Echocardiographic diagnosis of cardiac tamponade is based on both two-dimensional and spectral Doppler findings. The normal respiratory variation in LV stroke volume (SV) seen during mechanical ventilation is exaggerated in the setting of tamponade physiology with SV increasing on inspiration and decreasing on expiration (see below for a detailed discussion of the physiology of this variation). The variation can be detected by pulse wave Doppler interrogation of the left ventricular outflow tract in the deep transgastric view using a sweep speed of 25–50 mm/sec (Fig. 11.2). Sweep speed indicates how fast the spectral Doppler refreshes on the screen (a lower speed allows the visualization of more beats per

Table 11.2 Respiratory variation in LV outflow in the setting of tamponade

	Mechanical ventilation	
	Inspiration	Expiration
LV Outflow	↑	↓

screen). A respiratory variation greater than 10 % in the LV outflow tract is one of the initial echocardiographic signs of cardiac tamponade (Table 11.2).

Further fluid accumulation in the pericardial space will soon cause the pericardial pressure to exceed right atrial (RA) pressure. This will be visualized as a late diastolic collapse of the RA which will extend into systole (Fig. 11.3; Video 11.2). The mid-esophageal RV inflow/outflow and the mid-esophageal four chamber are the best views to visualize this. As the pericardial pressure increases further, the RV will begin to collapse in diastole. The RV outflow tract is most likely to collapse and thus the preferred view is the RV inflow–outflow. The thicker left-sided structures are less likely to collapse. When left-sided collapse is seen, this portends a bad outcome. Once the diagnosis is established, echocardiography can be a useful adjunct to guide needle placement during a pericardiocentesis [12]. Table 11.3 outlines the two-dimensional manifestations of tamponade.

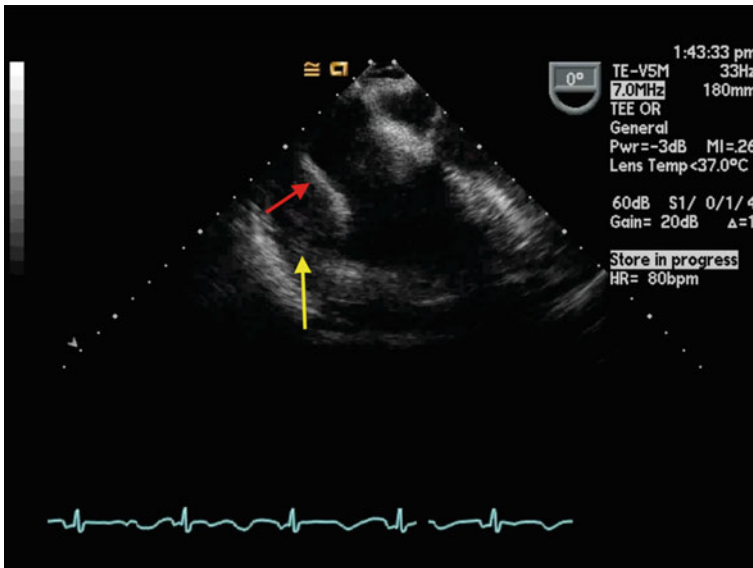


Fig. 11.3 Mid-esophageal four-chamber view with right atrial collapse in the setting of a pericardial effusion indicating tamponade physiology. *Red arrow* indicates right atrial systolic free wall collapse. *Yellow arrow* indicates the pericardial effusion

Table 11.3 Two dimensional manifestations of cardiac tamponade

	Systole		Diastole	
	Normal	Tamponade	Normal	Tamponade
RA	Expansion	Compression	Contraction	Contraction
RV	Contraction	Contraction	Expansion	Compression

RA Right Atrium; RV Right Ventricle

Right Ventricular Dysfunction

Right Ventricular Dysfunction	
2D	<ul style="list-style-type: none"> • RA & RV Size (RV should be 2/3 size of LV) • Encroachment of RV into LV • “D-shaped” LV (flattened septum) • Reduced TAPSE
CFD	<ul style="list-style-type: none"> • New or worsened TR (dilated annulus)
Spectral	<ul style="list-style-type: none"> • PASP estimation

RA = right atrium; RV = right ventricle; LV = left ventricle; TAPSE = tricuspid annular plane systolic excursion; TR = tricuspid regurgitation

Right ventricular failure (please also see Chap. 8) is the inability of the RV to provide adequate blood flow to the LV in the setting of a normal central venous pressure. RV failure in cardiac and noncardiac surgeries has a very high mortality [13]. Potential causes of RV failure are numerous but generally involve RV contractile dysfunction in association with acute elevations in pulmonary artery pressures [14]. The anatomy of the RV is complex making echocardiographic assessment very difficult [15]. For this reason, we suggest performing a qualitative assessment in the emergent setting. A qualitative assessment of RV function is as good as MRI at detecting dysfunction [16]. Evaluation begins with inspection of right-sided chambers looking for dilation of the RV and RA. Mid-esophageal four-chamber, RV inflow–outflow, bicaval as well as transgastric midpapillary short axis views are helpful in evaluating the right heart. Encroachment into the left side with right-to-left bowing of the interatrial septum (Fig. 11.4; Video 11.3) and/or a “D-shaped” intraventricular septum seen in the transgastric midpapillary short axis view (Fig. 11.5; Video 11.4) indicate elevated right-sided pressures. RV contractility can then be assessed by looking for regional wall motion abnormalities. In addition, one can qualitatively evaluate the distance the tricuspid annulus moves down in systole (tricuspid annular systolic excursion or TAPSE) [17] (Fig. 11.6). A reduced TAPSE less than 17 mm suggests RV dysfunction [18]. Lastly, new onset or worsening of chronic tricuspid regurgitation may indicate either RV contractile dysfunction or annular dilation.

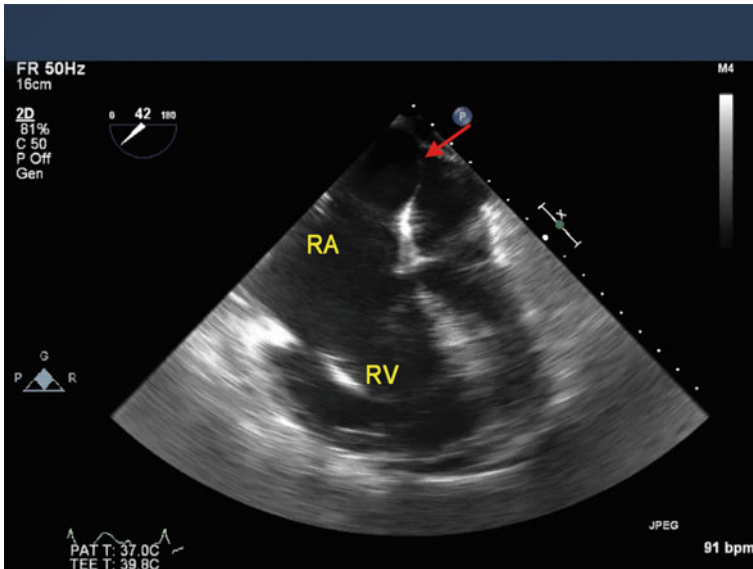


Fig. 11.4 Mid-esophageal four-chamber view of a patient with right heart failure. The *red arrow* indicates the atrial septal bowing due to high right atrial pressure. RA Right Atrium; RV Right Ventricle

Pulmonary Embolism

Pulmonary Embolism

2D	<ul style="list-style-type: none"> • Evidence of RV Failure • Dilated RA and RV • Evidence of thromboembolic material in right heart (Main or Right PA) • McConnell’s sign – hypokinetic RV with normal RV apical function
CFD	<ul style="list-style-type: none"> • New or worsened TR (dilated annulus)
Spectral	<ul style="list-style-type: none"> • PASP estimation

RA = right atrium; RV = right ventricle; TR = tricuspid regurgitation

Early diagnosis and treatment can reduce the mortality associated with a pulmonary embolism (PE) tenfold [19]. Although TEE can help guide both diagnosis and management, it is not the gold standard [20]. Echocardiography has a high specificity and a low sensitivity (90 and 56 % respectively) [21]. Risk factors associated with PE are listed in Table 11.4.

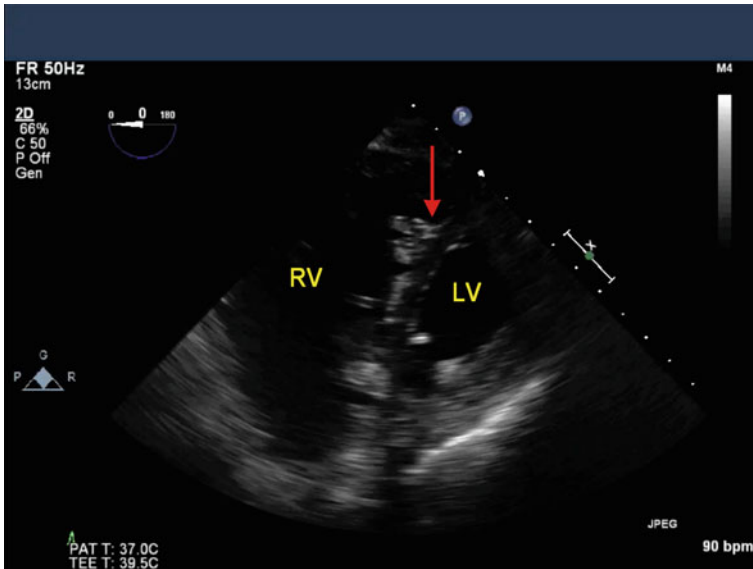


Fig. 11.5 Transgastric midpapillary short axis view revealing a “D” shaped interventricular septum secondary to right ventricular failure. *Red arrow* indicates flattened interventricular septum. *RV* Right Ventricle; *LV* Left Ventricle

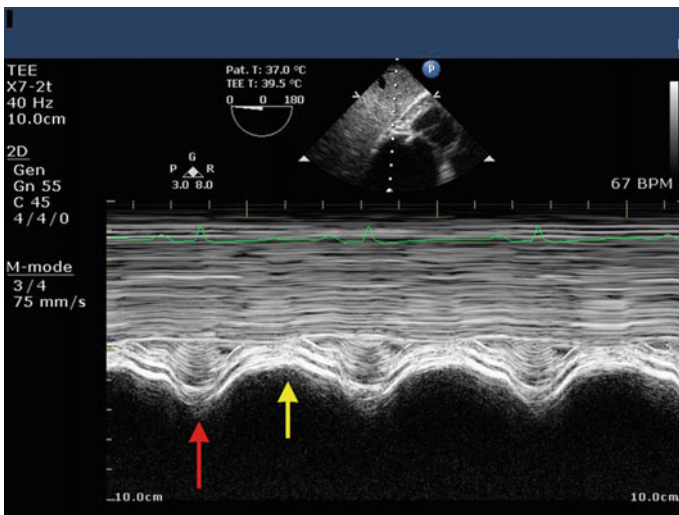


Fig. 11.6 Example of tricuspid annular plane systolic excursion (TAPSE) using M-mode imaging of the tricuspid annulus in the transgastric right ventricular inflow view. *Red arrow* indicates tricuspid annulus in diastole, while the *yellow arrow* indicates the tricuspid annulus in systole. The difference in position is the TAPSE measurement

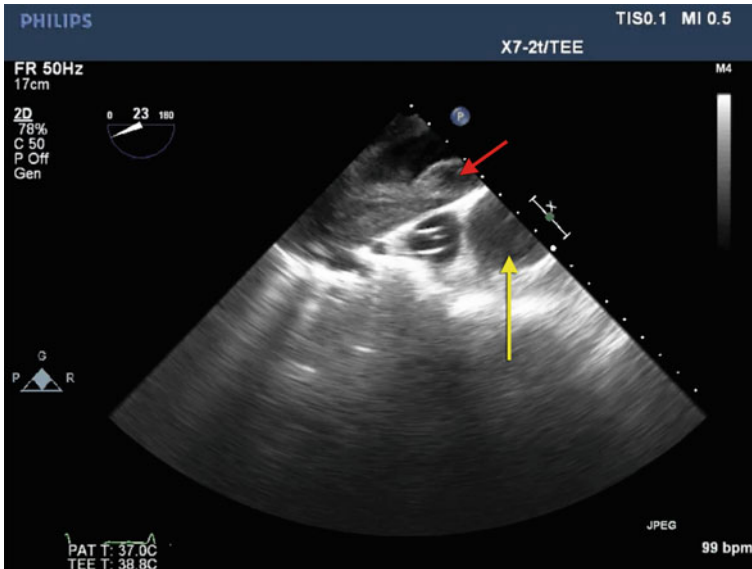


Fig. 11.7 Mid-esophageal ascending aortic short axis view with slight probe rotation to the right. Thrombus noted in the right pulmonary artery (*red arrow*). *Yellow arrow* indicates the ascending aorta in short axis

Table 11.4 Risk factors associated with pulmonary embolism

-
- Malignancy
 - Prolonged immobilization
 - Obesity
 - Tobacco use
 - Medications particularly
 - Oral contraceptives
 - Hormone replacement therapy
 - Antipsychotics
 - General Surgery particularly
 - Hip fractures
 - Acute spinal cord injuries
 - Trauma
-

A thrombus can be found anywhere on the right side from the vena cavae to the pulmonary artery (PA) and can be seen in over 80 % of cases (Fig. 11.7; Video 11.5). The ideal views to assess for thrombus include the mid-esophageal bicaval, RV inflow–outflow, and ascending aorta short axis. The main and right PAs can be seen by withdrawal of the probe to the high esophagus until a cross section of the ascending aorta is obtained. The left PA, on the other hand, is often obscured by the tracheobronchial tree.

Although a thrombus visualized in a right-sided cardiac structure is pathognomonic of PE, right ventricular wall motion abnormalities are the most common echocardiographic findings [20]. The extent of RV dysfunction correlates with the clot burden [22, 23] and overall mortality [24–26]. McConnell et al. showed that a hypokinetic RV free wall and a normal to hyperdynamic apex has a sensitivity of 77 % and a specificity of 94 % in predicting a PE [27]. Subsequent studies, however, have found a reduced sensitivity and specificity [28]. Structural and inflammatory changes in the LV associated with a PE as well as reduced coronary perfusion from loss of SV can lead to LV dysfunction. A low LV ejection fraction is an independent predictor of mortality in the setting of acute PE [24].

Left Ventricular Dysfunction

Left Ventricular Dysfunction	
2D	<u>Regional</u> • Wall Motion Abnormalities (Thickening and Excursion) <u>Global</u> • FAC or EF • LV or LA dilation • SEC <u>LVOTO</u> • Movement of anterior MV leaflet during systole (SAM) • Hyperdynamic, hypovolemic LV
CFD	<u>Regional / Global</u> • New or worsened MR (dilated annulus vs papillary dysfunction) <u>LVOTO</u> • New anterior MR jet from anterior MV displacement into LVOT (SAM) Aliasing in LVOT
Spectral	<u>Regional / Global</u> • Decreased SV or CO (calculated from LVOT) <u>LVOTO</u> • “Dagger” shaped – late peaking high velocity CWD profile

FAC = Fractional Area of Change; *EF* = Ejection Fraction; *LV* = left ventricle; *LA* = left atrium; *SEC* = spontaneous echo contrast; *SAM* = systolic anterior motion; *MR* = mitral regurgitation; *MV* = mitral valve; *LVOT* = left ventricular outflow tract; *SV* = stroke volume; *CO* = cardiac output; *CWD* = continuous wave Doppler; *LVOTO* = Left Ventricular Outflow Tract Obstruction

Echocardiography is an excellent tool for the diagnosis and management of LV dysfunction, particularly in the setting of myocardial ischemia. Segmental wall thickening less than 30 % suggests myocardial ischemia and can manifest within seconds making it an earlier marker of ischemia than ECG changes [29–31]. Acute ischemia is distinguished from chronic by a change in segmental wall motion from

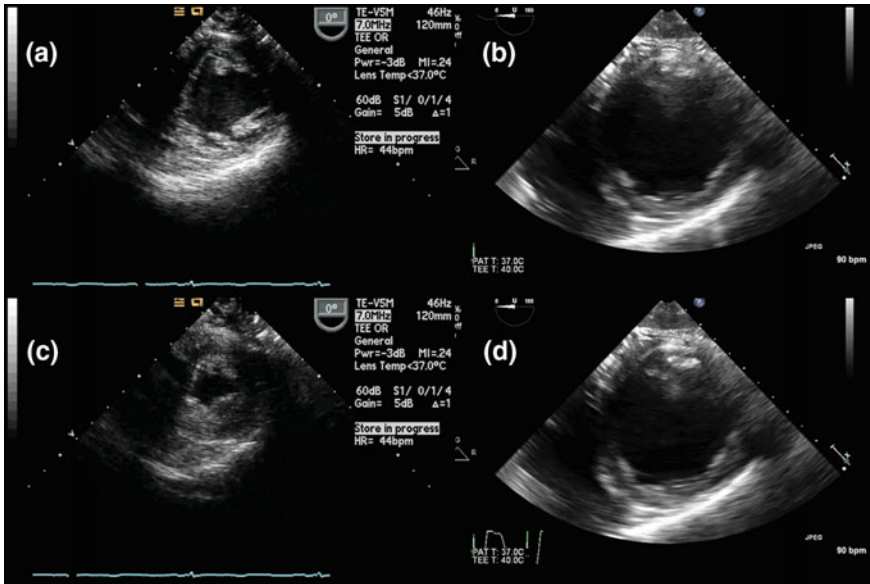


Fig. 11.8 Comparison of normal versus poor ejection fraction using the transgastric midpapillary short axis view. **a** and **c** are the diastolic and systolic frames, respectively, of a patient with normal systolic function. **b** and **d** are the diastolic and systolic frames, respectively, of a patient with grossly abnormal systolic function

baseline by two grades (i.e., from normal to severe hypokinesia) in two or more segments (Video 11.6) [32]. Stress, inflammation, and catecholamine excess associated with acute illness can also cause secondary cardiomyopathies and LV dysfunction [33]. Sepsis-induced cardiomyopathy [33] and stress-induced cardiomyopathy, also known as Takotsubo cardiomyopathy, [34] are relatively common causes of nonischemic LV dysfunction. Regardless of etiology, the echocardiographic manifestations of LV dysfunction are similar.

In keeping with the concept of a qualitative echocardiographic assessment in the setting of hemodynamic instability, the SCA recommends an estimation of the LV ejection fraction when assessing who may benefit from inotropic therapy [4]. Visual estimation, or “eyeballing”, has been found to be as good as Simpson’s biplane method [35] and 3D echocardiography [36] and requires only approximately 20 studies to become proficient [37]. The transgastric midpapillary short axis (SAX) view is the primary view used for assessing LV contractility (Fig. 11.8; Video 11.7). A reduced fractional area change (FAC), which is the comparison of the end-diastolic area (EDA) and end-systolic area (ESA), indicates poor LV function. An FAC is calculated by using the equation $(LVEDA - LVESA) / LVEDA$ with normal values being approximately the same as those for EF (Fig. 11.9; Video 11.8) [38]. It is important to note, however, that with regional dysfunction, the transgastric midpapillary short axis view may miss significant pathology in the basal and apical segments [39]. A brief assessment of the LV in the

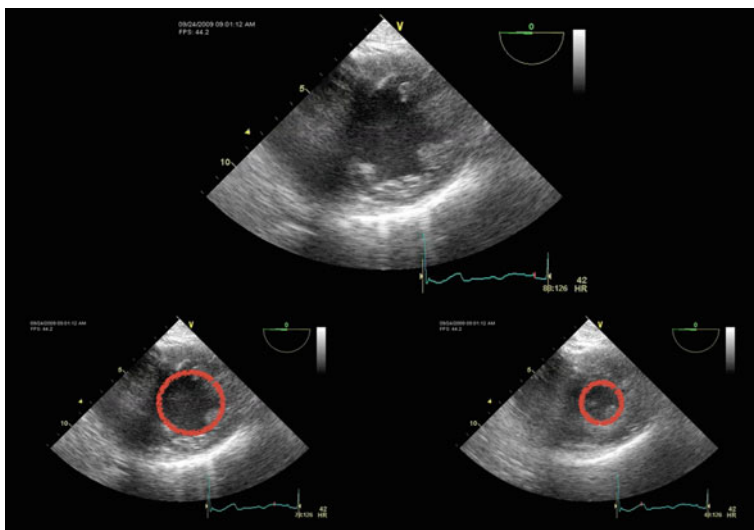


Fig. 11.9 Example of how to calculate left ventricular fractional area change. The image on the *top* is the transgastric short axis. The image on the *bottom left* is a rough estimate of the end-diastolic area. The image on the *bottom right* is a rough estimate of the end-systolic area. Fractional area change is then a percentage change between the two areas

four-chamber, two-chamber, and long axis views looking for segmental wall motion abnormalities will aid in diagnosis. Particular attention should be paid to the apex as it contributes a significant portion of the overall EF (Video 11.9).

Left ventricular hypercontractility resulting in dynamic left ventricular outflow tract obstruction (LVOTO) may also cause hemodynamic instability and must be considered in patients with risk factors whose hemodynamics worsen with inotropic support. LVOTO can occur in many pathophysiologic settings (Table 11.5). LVOTO likely results from localized increases in flow velocity during ejection due to a narrow LVOT. This results in the anterior mitral leaflet and chordae being

Table 11.5 Pathophysiologic settings associated with left ventricular outflow tract obstruction

-
- Hypertrophic cardiomyopathy
 - Hypertension [56]
 - Type 1 diabetes [57]
 - Myocardial ischemia [58, 59]
 - Pheochromocytoma [60]
 - Takotsubo cardiomyopathy [61, 62]
 - Valvular replacements and repairs [63, 64]
 - Catecholamine administration [65, 66]
-

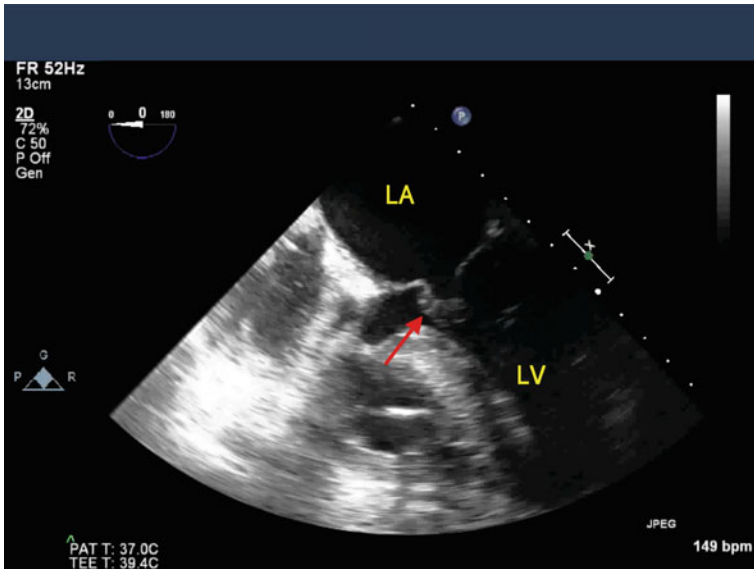


Fig. 11.10 Midesophageal four-chamber view in systole of a patient with left ventricular outflow tract obstruction. Note the anterior mitral leaflet contacting the septum (*Red Arrow*). LA Left Atrium; LV Left Ventricle

drawn toward the septum [40, 41], causing mid-to-late systolic mitral regurgitation and LVOT obstruction. It is often possible to see movement of the anterior leaflet of the MV toward the upper septum in the ME Four Chamber or ME LAX views (Fig. 11.10; Video 11.10). Color flow Doppler (CFD) may show an anteriorly directed MR jet as well as turbulent flow in the LVOT. A “dagger” shaped spectral Doppler pattern in the LVOT is the hallmark echocardiographic finding in LVOTO. Obstruction occurs late in systole because it takes time for the blood to generate enough velocity to draw in the mitral apparatus via Venturi effect. This dynamic property of the obstruction yields a late peaking continuous wave Doppler (CWD) pattern producing a “dagger” shape (Fig. 11.11). This profile shape is distinctly different from the fixed obstruction of aortic valve stenosis (see Chap. 7). The peak velocity of the wave will be high consistent with an elevated pressure gradient.

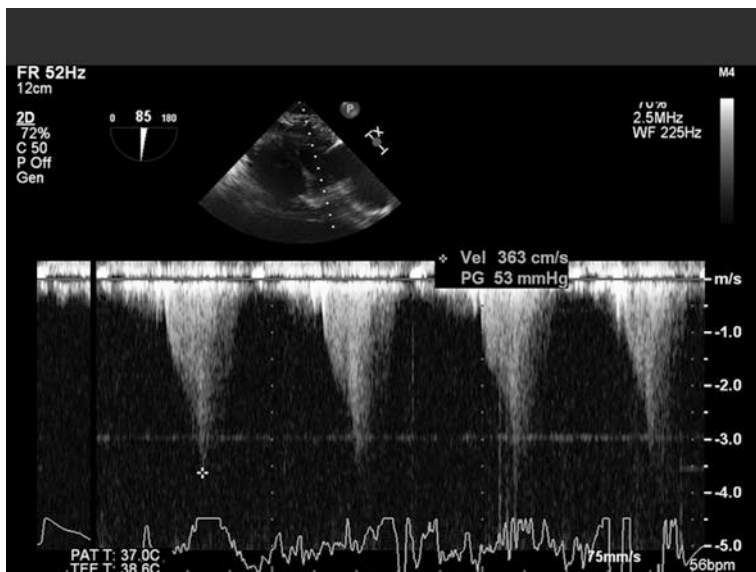


Fig. 11.11 Pulse wave Doppler in the left ventricular outflow tract revealing a “dagger” shaped wave consistent with dynamic outflow obstruction

Hypovolemia

Hypovolemia	
2D	<ul style="list-style-type: none"> • Small end-diastolic area / Small end-systolic area • Hyperdynamic LV
CFD	<ul style="list-style-type: none"> • Typically not utilized
Spectral	<ul style="list-style-type: none"> • Decreased SV or CO (calculated from LVOT) • Respiratory variation of peak LVOT velocity > 12 %

LV = left ventricle; *SV* = stroke volume; *CO* = cardiac output; *LVOT* = left ventricular outflow tract

The transgastric midpapillary short axis view has been shown to be a reasonable view for estimating ventricular volume by assessments of the LV end-diastolic (LVEDA) and end-systolic (LVESA) areas [42–44]. A euvoletic patient has a “normal” LVEDA, whereas the LVEDA of a hypovolemic patient is often reduced because of a reduced expansion (Fig. 11.12; Video 11.11). Normal value ranges for LVEDA is 8–14 cm² [45]. Several studies have confirmed the correlation between LV volume and LVEDA [46–49], although at varying strengths of correlation.

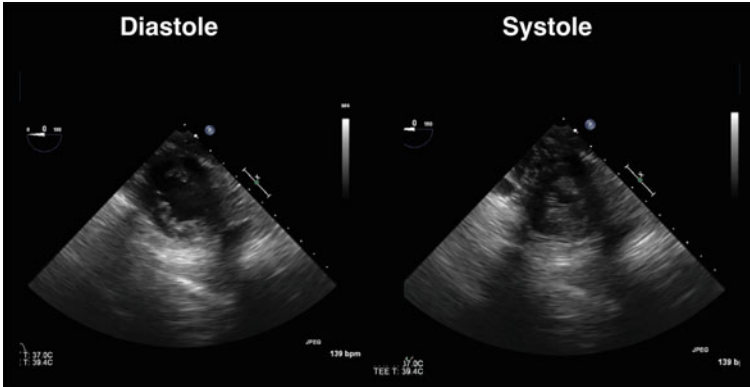


Fig. 11.12 Diastolic and Systolic frames from a transgastric midpapillary short axis view in the setting of hypovolemia. Note the small end-diastolic and end-systolic areas

The LVESA reflects the end point of the LV ejection fraction (EF). A hypovolemic patient who starts off with a reduced LV diastolic volume (and thus a reduced LVEDA) will end with a reduced systolic volume (and thus reduced LVESA). A correlation between a reduced LVEDA and hypovolemia has also been established [50]. Evaluation of the LVEDA and LVESA aid in qualitatively assessing volume status but often require further evaluation to confirm.

A reduced stroke volume (SV) in the setting of a normal or hyperdynamic LV strongly suggests hypovolemia as a cause of hypotension. Calculation of stroke volume assumes a cylindrical LVOT. The area of the cylinder is determined by measuring the LVOT diameter and using the following equation:

$$\text{Area} = D^2 \times 0.785$$

The LVOT diameter is usually measured in the mid-esophageal long axis view approximately 5 mm proximal to the aortic valve (Fig. 11.13). Small inaccuracies in measuring the diameter can introduce significant errors in the overall calculations since the diameter is squared. For this reason it is important to use the same LVOT diameter annular measurement for all subsequent calculations when performing serial SV measurements.

The length of the cylinder is determined by calculating the average distance a red blood cell travels in the LVOT during ejection, also called the stroke distance. Using the deep transgastric view, the pulse wave Doppler cursor is placed in the LVOT and a systolic waveform is obtained. The waveform is the velocities (i.e., speed and direction) of the red blood cells in the LVOT over time. The stroke distance, also called the velocity time integral (VTI), is obtained by tracing the Doppler wave (Fig. 11.14). To better understand this concept, consider a car traveling 50 miles an hour for 2 h. Figure 11.15 illustrates this data plotted on a graph with velocity on the Y-axis and time on the X-axis. The area of the rectangle

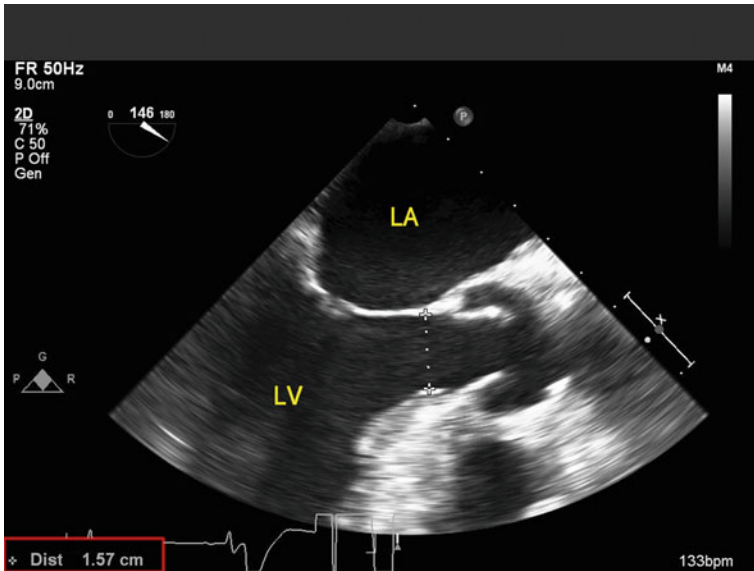


Fig. 11.13 Example of how to measure the diameter of the left ventricular outflow tract in the mid-esophageal long axis view. LA Left Atrium; LV Left Ventricle

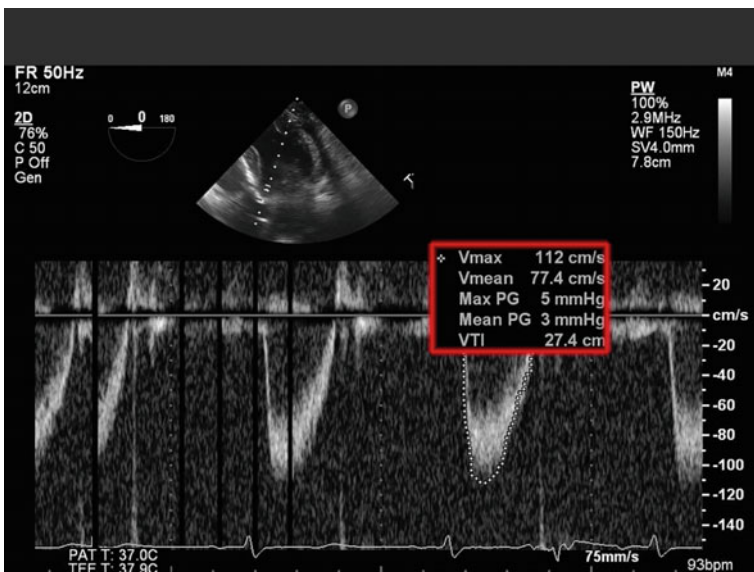


Fig. 11.14 Spectral profile from pulse wave Doppler placed in the left ventricular outflow tract in a Deep transgastric long axis view. Tracing the profile provides the velocity time integral (stroke distance)

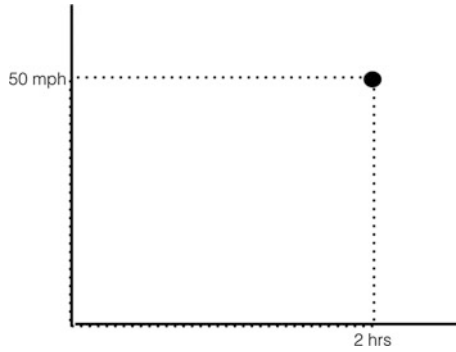


Fig. 11.15 Area under the curve for a time/velocity graph

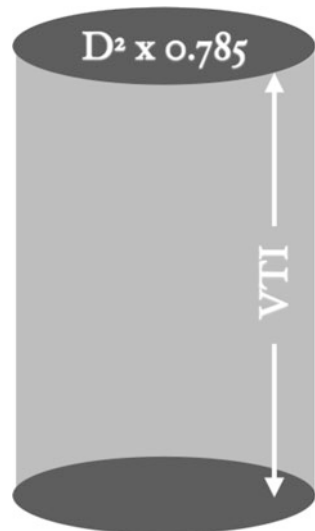
created by these measurements yields a distance (i.e., $50 \text{ mph} \times 2 \text{ h} = 100 \text{ miles}$). The VTI is similar to this calculation in that it is the area under the curve of red blood cell velocities over time. In this case, the velocities are represented by centimeters per second, the time by seconds, and the VTI by centimeters.

The overall equation for determining the SV is the following (Fig. 11.16):

$$SV = D^2 \times 0.785 \times VTI$$

Cardiac output (CO) can then be calculated by multiplying SV by the heart rate (HR). This method of stroke volume calculation is the recommended method for determining CO by the American Society of Echocardiography [51].

Fig. 11.16 LVOT stroke volume calculation (Area of LVOT \times Stroke Distance)



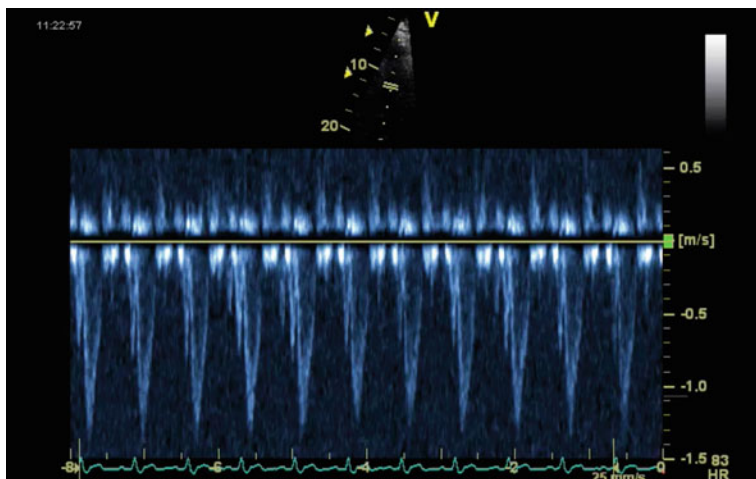


Fig. 11.17 Pulse wave Doppler in the left ventricular outflow tract showing minimal change in velocity with respiration

In addition to a static calculation of SV, volume status can be determined by dynamic changes in SV with respiration. Dynamic indices assess fluid responsiveness, which is the effect of a change in preload on SV [52]. Positive pressure insufflation pushes blood out of the lungs into the LV augmenting LV SV. At the same time, the positive intrathoracic pressure reduces RV preload and increases RV afterload thus reducing RV stroke volume. After several beats, the reduced RV stroke volume results in a reduced LV preload and reduced LV SV. These changes are exaggerated when the ventricles are on the steep part of the Frank–Starling curve with the magnitude of this variation predicting fluid responsiveness. Pulse wave Doppler interrogation of the LVOT over time has been shown to accurately assess these changes in SV and thus predict fluid responsiveness [53] (Fig. 11.17). One can use the following equation to quantitatively determine fluid responsiveness [54]:

$$\Delta V_{\text{peak}}(\%) = 100 \times (V_{\text{max}} - V_{\text{min}}) / [(V_{\text{max}} + V_{\text{min}}) / 2]$$

V_{min} represents the minimum velocity in the LVOT and V_{max} the maximum velocity. A ΔV_{peak} of 12 % or greater indicates volume responsiveness with a sensitivity of 100 % and specificity of 89 %. Such a calculation is impractical in the emergent setting. A visual estimate of the respiratory variation is often adequate (normal LVOT variation is <15 %).

Low Afterload

Low Afterload	
2D	<ul style="list-style-type: none"> • Normal end-diastolic area / Small end-systolic area • Hyperdynamic LV
CFD	<ul style="list-style-type: none"> • Typically not utilized
Spectral	<ul style="list-style-type: none"> • Elevated SV or CO (calculated from LVOT)

LV = left ventricle; *SV* = stroke volume; *CO* = cardiac output; *LVOT* = left ventricular outflow tract

Theoretically, the LVEDA and LVESA, typically measured in the transgastric midpapillary short axis view, can also help determine if the patient has a low afterload. A euvolemic patient should have a normal LVEDA regardless of afterload. If the afterload is low, the EF should increase which manifests as a small LVESA. Therefore, a euvolemic patient with a low afterload should have a normal LVEDA but a reduced LVESA (Fig. 11.18; Video 11.12). In contrast, a hypovolemic patient with a normal afterload should have a reduced LVEDA and LVESA. Table 11.6 compares LVEDAs and LVESAs in hypovolemia and low afterload. Unfortunately, a direct relationship between a low afterload and a normal LVEDA with a low LVESA has not been established in the literature, only suggested [50, 55]. A qualitative assessment of the LVEDA and LVESA can therefore only suggest hypovolemia or low afterload. Further confirmation by way of calculating the stroke volume, as described above, is often necessary. The stroke volume

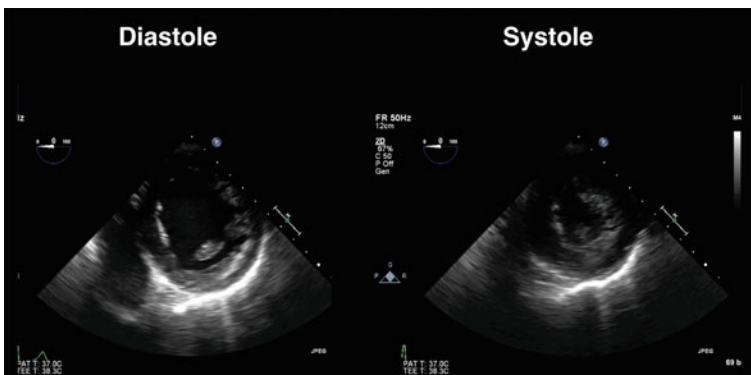


Fig. 11.18 Transgastric midpapillary short axis view with evidence of low afterload (small end-systolic area and normal end-diastolic area)

Table 11.6 Left ventricular end-diastolic and systolic areas in the setting of hypovolemia and low afterload

	LVEDA	LVESA
Normal	NI	NI
Low afterload	NI	Reduced
Hypovolemia	Reduced	Reduced

LVEDA Left Ventricular end-diastolic area; *LVESA* Left ventricular end-systolic area; *NI* Normal

should be elevated in the setting of a low afterload and reduced in the setting of hypovolemia.

Conclusion

Echocardiography is extremely useful to the perioperative physician in assessing the cause of hemodynamic instability, aiding in both diagnosis and management. It is the diagnostic tool of choice owing to its portability and ease of use. Not only does TEE help identify etiology, it also allows the practitioner to follow the effects of an intervention and make changes if necessary.

References

1. American Society of A, Society of Cardiovascular Anesthesiologists Task Force on Transesophageal E. Practice guidelines for perioperative transesophageal echocardiography. An updated report by the American Society of Anesthesiologists and the Society of Cardiovascular Anesthesiologists Task Force on Transesophageal Echocardiography. *Anesthesiology*. 2010;112(5):1084–96.
2. Price S, Ilper H, Uddin S, et al. Peri-resuscitation echocardiography: training the novice practitioner. *Resuscitation*. 2010;81(11):1534–9.
3. Markin NW, Gmelch BS, Griffie MJ, Holmberg TJ, Morgan DE, Zimmerman JM. A review of 364 perioperative rescue echocardiograms: findings of an anesthesiologist-staffed perioperative echocardiography service. *J Cardiothorac Vasc Anesth*. 2015;29(1):82–8.
4. Reeves ST, Finley AC, Skubas NJ, et al. Basic perioperative transesophageal echocardiography examination. *Anesth Analg*. 2013;117(3):543–58.
5. Miller JP, Lambert AS, Shapiro WA, Russell IA, Schiller NB, Cahalan MK. The Adequacy of Basic Intraoperative Transesophageal Echocardiography Performed by Experienced Anesthesiologists. *Anesthesia and Analgesia*. 2001:1103–10.
6. Shillcutt SK, Markin NW, Montzingo CR, Brakke TR. Use of rapid “rescue” perioperative echocardiography to improve outcomes after hemodynamic instability in noncardiac surgical patients. *J Cardiothorac Vasc Anesth*. 2012;26(3):362–70.
7. Stout KK, Verrier ED. Acute valvular regurgitation. *Circulation*. 2009;119(25):3232–41.
8. Shiga T, Wajima Zi, Apfel CC, Inoue T, Ohe Y. Diagnostic accuracy of transesophageal echocardiography, helical computed tomography, and magnetic resonance imaging for suspected thoracic aortic dissection. *Arch Intern Med*. 2006;166(13):1350.

9. Evangelista A, Flachskampf FA, Erbel R, et al. Echocardiography in aortic diseases: EAE recommendations for clinical practice. *Eur J Echocardiogr.* 2010;11(8):645–58.
10. Erbel R, Oelert H, Meyer J, et al. Effect of medical and surgical therapy on aortic dissection evaluated by transesophageal echocardiography. Implications for prognosis and therapy. The european cooperative study group on echocardiography. *Circulation.* 1993;87(5):1604–15.
11. Vilacosta I, San Román JA, Aragoncillo P, et al. Penetrating atherosclerotic aortic ulcer: documentation by transesophageal echocardiography. *J Am Coll Cardiol.* 1998;32(1):83–9.
12. Salem K, Mulji A, Lonn E. Echocardiographically guided pericardiocentesis—The gold standard for the management of pericardial effusion and cardiac tamponade. *Can J Cardiol.* 1999;15(11):1251–5.
13. Denault AY, Haddad F, Jacobsohn E, Deschamps A. Perioperative right ventricular dysfunction. *Curr Opin Anaesthesiol.* 2013;26(1):71–81.
14. Zochios V. Does β_2 -agonist use improve survival in critically ill patients with acute respiratory distress syndrome? In: *Reducing mortality in critically ill patients.* Springer Science+Business Media; 2015. pp. 103–9.
15. Sheehan F, Redington A. The right ventricle: anatomy, physiology and clinical imaging. *Heart.* 2008;94(11):1510–5.
16. Drake D, Gupta R, Lloyd SG, Gupta H. Right ventricular function assessment: comparison of geometric and visual method to short-axis slice summation method. *Echocardiography.* 2007;24(10):1013–9.
17. Lang RM, Bierig M, Devereux RB, et al. Recommendations for chamber quantification: a report from the american society of echocardiography's guidelines and standards committee and the chamber quantification writing group, developed in conjunction with the european association of echocardiography, a branch of the European society of cardiology. *J Am Soc Echocardiogr.* 2005;18(12):1440–63.
18. Lang RM, Badano LP, Mor-Avi V, et al. Recommendations for cardiac chamber quantification by echocardiography in adults: an update from the American Society of Echocardiography and the European Association of Cardiovascular Imaging. *J Am Soc Echocardiogr.* 2015;28(1):1–39, e14.
19. Tapson VF. Acute pulmonary embolism. *N Engl J Med.* 2008;358(10):1037–52.
20. Visnjevac O, Pourafkari L, Nader ND. Role of perioperative monitoring in diagnosis of massive intraoperative cardiopulmonary embolism. *J Cardiovasc Thorac Res.* 2014;6(3):141–5.
21. Miniati M, Monti S, Pratali L, et al. Value of transthoracic echocardiography in the diagnosis of pulmonary embolism: results of a prospective study in unselected patients. *Am J Med.* 2001;110(7):528–35.
22. Kjaergaard J, Schaadt BK, Lund JO, Hassager C. Quantification of right ventricular function in acute pulmonary embolism: relation to extent of pulmonary perfusion defects. *Eur J Echocardiogr.* 2008;9(5):641–5.
23. Ribeiro A, Juhlin-Dannfelt A, Brodin L-Å, Holmgren A, Jorfeldt L. Pulmonary embolism: relation between the degree of right ventricle overload and the extent of perfusion defects. *Am Heart J.* 1998;135(5):868–74.
24. Kjaergaard J, Schaadt BK, Lund JO, Hassager C. Prognostic importance of quantitative echocardiographic evaluation in patients suspected of first non-massive pulmonary embolism. *Eur J Echocardiogr.* 2009;10(1):89–95.
25. Ribeiro A, Lindmarker P, Juhlin-Dannfelt A, Johnsson H, Jorfeldt L. Echocardiography Doppler in pulmonary embolism: right ventricular dysfunction as a predictor of mortality rate. *Am Heart J.* 1997;134(3):479–87.
26. Sanchez O, Trinquart L, Colombet I, et al. Prognostic value of right ventricular dysfunction in patients with haemodynamically stable pulmonary embolism: a systematic review. *Eur Heart J.* 2008;29(12):1569–77.
27. McConnell MV, Solomon SD, Rayan ME, Come PC, Goldhaber SZ, Lee RT. Regional right ventricular dysfunction detected by echocardiography in acute pulmonary embolism. *Am J Cardiol.* 1996;78(4):469–73.

28. Lodato JA, Ward RP, Lang RM. Echocardiographic predictors of pulmonary embolism in patients referred for helical CT. *Echocardiography*. 2008;25(6):584–90.
29. Hauser AM, Gangadharan V, Ramos RG, Gordon S, Timmis GC, Dudlets P. Sequence of mechanical, electrocardiographic and clinical effects of repeated coronary artery occlusion in human beings: echocardiographic observations during coronary angioplasty. *J Am Coll Cardiol*. 1985;5(2):193–7.
30. Wohlgeleit D, Cleman M, Highman HA, et al. Regional myocardial dysfunction during coronary angioplasty: evaluation by two-dimensional echocardiography and 12 lead electrocardiography. *J Am Coll Cardiol*. 1986;7(6):1245–54.
31. Seeberger MD, Skarvan K, Buser P, et al. Dobutamine stress echocardiography to detect inducible demand ischemia in anesthetized patients with coronary artery disease. *Anesthesiology*. 1998;88(5):1233–9.
32. Wang J, Filipovic M, Rudzitis A, et al. Transesophageal echocardiography for monitoring segmental wall motion during off-pump coronary artery bypass surgery. *Anesth Analg*. 2004;99(4):965–73.
33. Romero-Bermejo FJ, Ruiz-Bailen M, Gil-Cebrian J, Huertos-Ranchal MJ. Sepsis-induced Cardiomyopathy. *CCR*. 2011;7(3):163–83.
34. Chockalingam A. Acute left ventricular dysfunction in the critically ill. *Chest*. 2010;138(1):198.
35. Gudmundsson P, Rydberg E, Winter R, Willenheimer R. Visually estimated left ventricular ejection fraction by echocardiography is closely correlated with formal quantitative methods. *Int J Cardiol*. 2005;101(2):209–12.
36. Shahgaldi K, Gudmundsson P, Manouras A, Brodin L-Å, Winter R. Visually estimated ejection fraction by two dimensional and triplane echocardiography is closely correlated with quantitative ejection fraction by real-time three dimensional echocardiography. *Cardiovasc Ultrasound*. 2009;7(1):41.
37. Akinboboye O, Sumner J, Gopal A, et al. Visual estimation of ejection fraction by two-dimensional echocardiography: the learning curve. *Clin Cardiol*. 1995;18(12):726–9.
38. Skarvan K, Lambert A, Filipovic M, Seeberger M. Reference values for left ventricular function in subjects under general anaesthesia and controlled ventilation assessed by two-dimensional transesophageal echocardiography. *Eur J Anaesthesiol*. 2001;18(11):713–22.
39. Rouine-Rapp K, Ionescu P, Balea M, Foster E, Cahalan MK. Detection of intraoperative segmental wall-motion abnormalities by transesophageal echocardiography. *Anesth Analg*. 1996;83(6):1141–8.
40. Sherrid MV, Gunsburg DZ, Moldenhauer S, Pearle G. Systolic anterior motion begins at low left ventricular outflow tract velocity in obstructive hypertrophic cardiomyopathy. *J Am Coll Cardiol*. 2000;36(4):1344–54.
41. Wigle ED, Rakowski H, Kimball BP, Williams WG. Hypertrophic cardiomyopathy: clinical spectrum and treatment. *Circulation*. 1995;92(7):1680–92.
42. Clements FM, Harpole DH, Quill T, Jones RH, McCann RL. Estimation of left ventricular volume and ejection fraction by two-dimensional transoesophageal echocardiography: comparison of short axis imaging and simultaneous radionuclide angiography. *Br J Anaesth*. 1990;64(3):331–6.
43. Ryan T, Burwash I, Lu J, et al. The agreement between ventricular volumes and ejection fraction by transesophageal echocardiography or a combined radionuclear and thermodilution technique in patients after coronary artery surgery. *J Cardiothorac Vasc Anesth*. 1996;10(3):323–8.
44. Schmidlin D, Jenni R, Schmid ER. Transesophageal echocardiographic area and doppler flow velocity measurements: comparison with hemodynamic changes in coronary artery bypass surgery. *J Cardiothorac Vasc Anesth*. 1999;13(2):143–9.
45. Roysse CF. Ultrasound-guided haemodynamic state assessment. *Best Pract Res Clin Anaesthesiol*. 2009;23(3):273–83.

46. Cheung AT, Savino JS, Weiss SJ, Aukburg SJ, Berlin JA. Echocardiographic and hemodynamic indexes of left ventricular preload in patients with normal and abnormal ventricular function. *Anesthesiology*. 1994;81(2):376–87.
47. Greim CA, Roewer N, Apfel C, Laux G, am Esch JS. Relation of echocardiographic preload indices to stroke volume in critically ill patients with normal and low cardiac index. *Intensive Care Medicine*. 1997;23(4):411–6.
48. Swenson JD, Bull D, Stringham J. Subjective assessment of left ventricular preload using transesophageal echocardiography: corresponding pulmonary artery occlusion pressures. *J Cardiothorac Vasc Anesth*. 2001;15(5):580–3.
49. Tousignant CP, Walsh F, Mazer CD. The use of transesophageal echocardiography for preload assessment in critically ill patients. *Anesth Analg*. 2000;90(2):351.
50. Leung JM, Levine EH. Left ventricular end-systolic cavity obliteration as an estimate of intraoperative hypovolemia. *Anesthesiology*. 1994;81(5):1102–9.
51. Quiñones MA, Otto CM, Stoddard M, Waggoner A, Zoghbi WA. Recommendations for quantification of Doppler echocardiography: a report from the Doppler quantification task force of the nomenclature and standards committee of the American Society of Echocardiography. *J Am Soc Echocardiogr*. 2002;15(2):167–84.
52. Michard F, Teboul JL. Using heart-lung interactions to assess fluid responsiveness during mechanical ventilation. *Crit Care*. 2000;4(5):282–9.
53. Renner J, Broch O, Gruenewald M, et al. Non-invasive prediction of fluid responsiveness in infants using pleth variability index. *Anaesthesia*. 2011;66(7):582–9.
54. Feissel M. Respiratory changes in aortic blood velocity as an indicator of fluid responsiveness in ventilated patients with septic shock. *Chest*. 2001;119(3):867–73.
55. van Daele MERM, Trouwborst A, van Woerkens LCSM, Tenbrinck R, Fraser AG, Roelandt JRTC. Transesophageal echocardiographic monitoring of preoperative acute hypervolemic hemodilution. *Anesthesiology*. 1994;81(3):602–9.
56. Doi YL, Deanfield JE, McKenna WJ, Dargie HJ, Oakley CM, Goodwin JF. Echocardiographic differentiation of hypertensive heart disease and hypertrophic cardiomyopathy. *Heart*. 1980;44(4):395–400.
57. Maraud L, Gin H, Roudaut R, Aubertin J, Bricaud H. Echocardiographic study of left ventricular function in type 1 diabetes mellitus: hypersensitivity of β -adrenergic stimulation. *Diabetes Research and Clinical Practice*. 1991;11(3):161–8.
58. Hrovatin E, Piazza R, Pavan D, et al. Dynamic left ventricular outflow tract obstruction in the setting of acute anterior myocardial infarction: a serious and potentially fatal complication? *Echocardiography*. 2002;19(6):449–55.
59. Haley JH, Sinak LJ, Tajik AJ, Ommen SR, Oh JK. Dynamic left ventricular outflow tract obstruction in acute coronary syndromes: an important cause of new systolic murmur and cardiogenic shock. *Mayo Clinic Proceedings*. 1999;74(9):901–6.
60. GÖLbasi Z, Sakalli M, ÇİÇEK D, Aydogdu S. Dynamic left ventricular outflow tract obstruction in a patient with pheochromocytoma. *Jpn Heart J*. 1999;40(6):831–5.
61. Chandrasegaram MD, Celermajer DS, Wilson MK. Apical ballooning syndrome complicated by acute severe mitral regurgitation with left ventricular outflow obstruction—case report. *J Cardiothorac Surg*. 2007;2:14.
62. Brunetti ND, Ieva R, Rossi G, et al. Ventricular outflow tract obstruction, systolic anterior motion and acute mitral regurgitation in Tako-Tsubo syndrome. *Int J Cardiol*. 2008;127(3):e152–7.
63. Jebara VA, Mihaileanu S, Acar C, et al. Left ventricular outflow tract obstruction after mitral valve repair. Results of the sliding leaflet technique. *Circulation*. 1993;88(5 Pt 2):II30–34.
64. Aurigemma G, Battista S, Orsinelli D, Sweeney A, Pape L, Cuenoud H. Abnormal left ventricular intracavitary flow acceleration in patients undergoing aortic valve replacement for aortic stenosis. A marker for high postoperative morbidity and mortality. *Circulation*. 1992;86(3):926–36.

65. Auer J, Berent R, Weber T, Lamm G, Eber B. Catecholamine therapy inducing dynamic left ventricular outflow tract obstruction. *Int J Cardiol.* 2005;101(2):325–8.
66. Mingo S, Benedicto A, Jimenez MC, Pérez MA, Montero M. Dynamic left ventricular outflow tract obstruction secondary to catecholamine excess in a normal ventricle. *Int J Cardiol.* 2006;112(3):393–6.

Chapter 12

Imaging Artifacts and Common Misdiagnoses

Brett Cronin, MD

Abstract The ability to identify imaging artifacts and normal anatomic variants commonly encountered during a TEE exam can be as important as identifying normal anatomy and function. Lack of knowledge regarding these anatomic structures and imaging artifacts can result in misdiagnoses and adverse effects for patients. Anatomic variants commonly encountered in a TEE exam include Lambl's Excrescences, Eustachian Valve, Chiari Network, Moderator Band, Crista Terminalis, Nodules of Arantius, and the Coumadin Ridge. Imaging artifacts that result from the violation of the basic assumptions of ultrasound physics include Dropout, Acoustic Shadowing, Side Lobes, Reverberation, and Mirroring. The focus of this chapter will be the identification of the aforementioned anatomic variants/imaging artifacts and the general techniques the echocardiographer can utilize to distinguish them from pathology.

Keywords Echocardiography • Transesophageal echocardiography • Artifacts • Normal anatomic variants • Misdiagnoses • Pitfalls

The ability to identify artifacts and normal anatomic variants commonly encountered during a transesophageal echocardiography (TEE) exam can be as important as identifying normal anatomy and function. In fact, the American Society of Echocardiography (ASE) recognizes the importance of this skill in the objectives for basic perioperative transesophageal (PTE) training [1]. Lack of knowledge

Electronic supplementary material The online version of this chapter (doi:[10.1007/978-3-319-34124-8_12](https://doi.org/10.1007/978-3-319-34124-8_12)) contains supplementary material, which is available to authorized users.

B. Cronin, MD (✉)

Department of Anesthesiology, University of California San Diego,
200 W Arbor Drive MC #8770, San Diego, CA 92103, USA
e-mail: bcronin@ucsd.edu

regarding these common anatomic structures and artifacts can result in misdiagnoses and adverse effects for patients.

The following does not represent an all-encompassing list but rather focuses on the appearance of the artifacts and normal anatomic variants commonly encountered in a perioperative TEE exam.

Normal Anatomic Variants and Misdiagnoses

A major principle of echocardiography is the identification of pathology which requires recognition of diseased states as well as normal anatomic states. This can occasionally be complicated by misdiagnosis of a normal anatomical variant as actual pathology. Many of these variants described below are inappropriately diagnosed as thrombi, masses, or foreign bodies. A thorough understanding of common anatomical variants is essential to reduce the opportunity for misdiagnosis and potentially inappropriate therapy. These anatomical variants are categorized below based upon the common physical location of the anatomical variant (Table 12.1).

Epicardial Fat (Location—Pericardium)

Echocardiographers often monitor for the development of pericardial effusions intraoperatively with TEE. Epicardial fat may be confused for a pericardial effusion given its location and presentation as an echolucent area between the right ventricle (RV) and the pericardium (Fig. 12.1; Video 12.1). However, epicardial fat has a non-homogeneous, textured appearance that can be distinguished from a pericardial effusion by altering the gain and examining the area of interest in multiple imaging planes [2]. In addition epicardial fat does not cause hemodynamic compromise, chamber compression or Doppler changes suggestive of tamponade physiology (see Chap. 11).

Table 12.1 Commonly identified normal anatomic variants (by location)

Right atrium	<ul style="list-style-type: none"> • Eustachian Valve • Chiari network • Crista terminalis
Right ventricle	<ul style="list-style-type: none"> • Moderator band
Left atrium	<ul style="list-style-type: none"> • Coumadin ridge
Aortic valve	<ul style="list-style-type: none"> • Nodules of arantius • Lambl's excrescences • Papillary fibroelastoma
Pericardium	<ul style="list-style-type: none"> • Pericardial fat

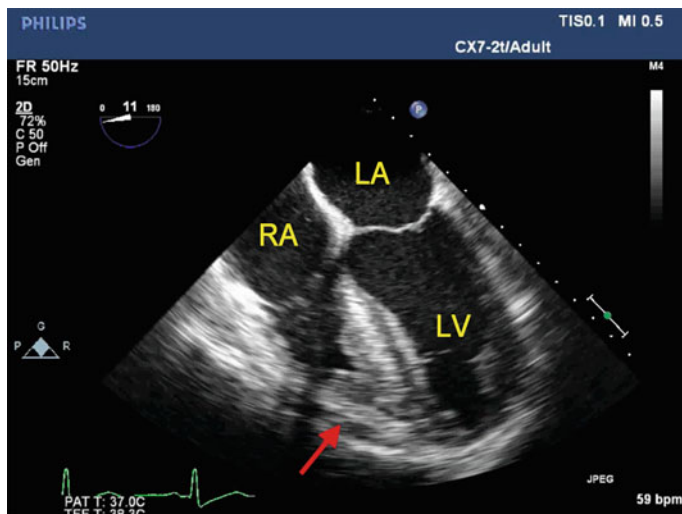


Fig. 12.1 Mid-esophageal four chamber view at end systole. Epicardial fat is present (*red arrow*) between the *right ventricular* lateral wall and the pericardium. RA right atrium; LA left atrium; LV left ventricle

Eustachian Valve (Location—Right Atrium)

The Eustachian valve is an embryologic remnant whose purpose in utero was to shunt oxygenated blood from the inferior vena cava through the right atrium (RA) to the left atrium (LA). If this tissue fails to completely regress after birth, the remnant is termed the Eustachian valve and is easily identified echocardiographically. The valve can be found in adults in the mid-esophageal (ME) bicaval view at the junction of the inferior vena cava (IVC) and RA (Fig. 12.2; Video 12.2) [3]. Its appearance is a linear echogenic structure emanating from the IVC/RA junction and may be confused as thrombus or tumor. Rarely thrombus or vegetations may be attached to the Eustachian valve.

Chiari Network (Location—Right Atrium)

While a Chiari network shares its origin with the Eustachian valve, it is not simply a longer variant. A Chiari network refers to an inferiorly located, mobile, and heavily fenestrated structure in the RA (Fig. 12.3; Video 12.3). Echocardiographically it appears as a mobile undulating flap extending from the RA and IVC junction. Its mobility often leads to misdiagnosis as a vegetation or thrombus. In addition, Chiari networks are associated with patent foramen ovale and atrial septal aneurysms [3].

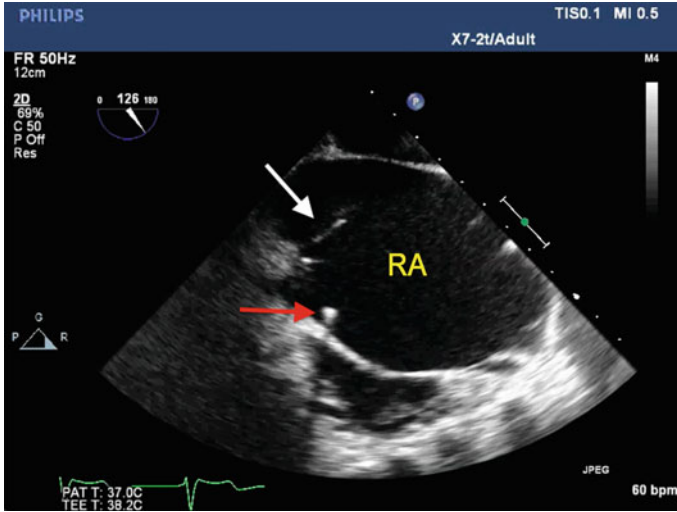


Fig. 12.2 Mid-esophageal bicaval view demonstrating a Eustachian valve at the junction of the inferior vena cava and RA (*white arrow*). A pulmonary artery catheter (*red arrow*), which is seen in cross section, is also directed towards the area of the tricuspid valve. RA right atrium

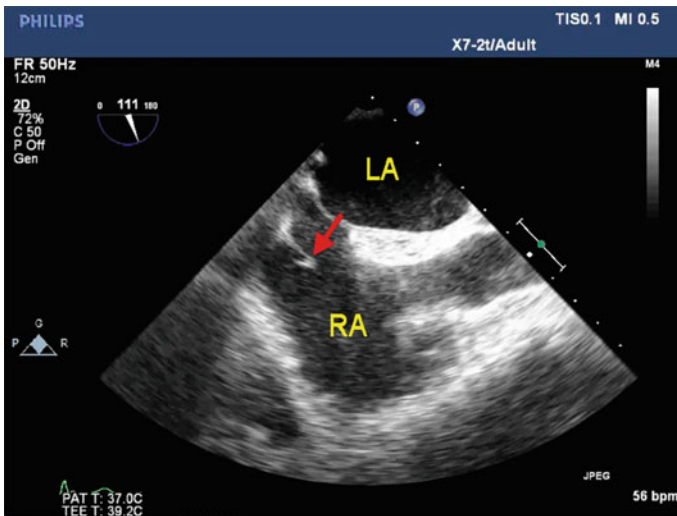


Fig. 12.3 Mid-esophageal bicaval view. A thin, filamentous, and mobile Chiari network (*red arrow*) is present at the junction of the inferior vena cava and RA. RA right atrium; LA left atrium

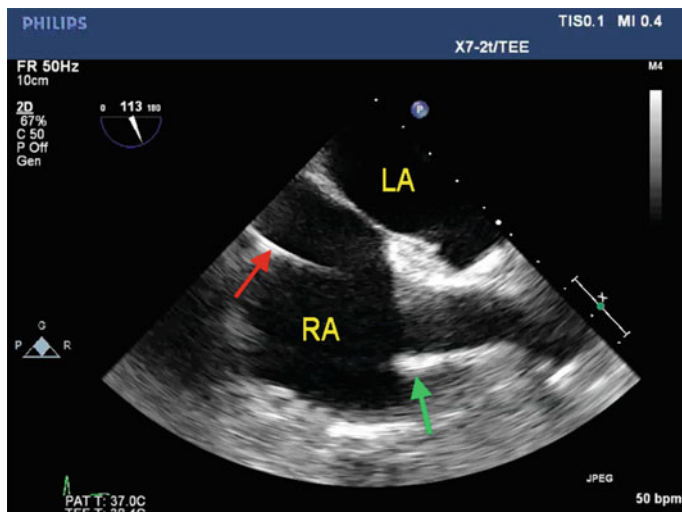


Fig. 12.4 Mid-esophageal bicaval view demonstrating a prominent crista terminalis (*green arrow*) at the superior portion of the right atrium near the superior vena cava and right atrial junction. A pulmonary artery catheter (*red arrow*) is also visualized traversing the RA toward the tricuspid valve. RA right atrium; LA left atrium

Crista Terminalis (Location—Right Atrium)

The crista terminalis is a smooth fibromuscular ridge located in the right atrium, which separates the smooth right atrium from the more trabeculated right atrial appendage (Fig. 12.4; Video 12.4). Echocardiographically it is commonly identified at the SVC and RA junction in a ME bicaval view. Its appearance ranges from a ridge to pedunculated mass of tissue and may be mistaken for tumor or thrombus [3]. The superior portion of the crista terminalis also contains the sinoatrial node and has been implicated as the origin of atrial arrhythmias [4].

Moderator Band (Location—Right Ventricle)

Also known as septomarginal trabecula, the moderator band, one of the encircling muscular bands of the RV, functions as a conduction path from the right bundle branch to the RV free wall. The band can become quite prominent in cases of chronic RV pressure overload (e.g., chronic pulmonary hypertension), becoming mistaken for tumor or an in-transit thromboembolism. In addition to examination in multiple views, the diagnosis of a moderator band is more likely if it moves with the cardiac cycle and the adjacent wall motion is normal (Fig. 12.5; Video 12.5) [5].

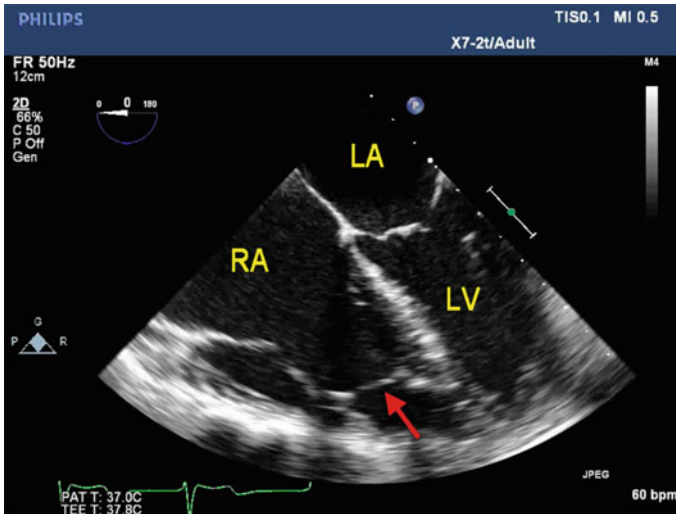


Fig. 12.5 Mid-esophageal four chamber view at end diastole. A moderator band (*red arrow*) is seen connecting the interventricular septum to the anterior papillary muscle in the distal half of the ventricle. *RA* right atrium; *LA* left atrium; *LV* left ventricle

Lambl's Excrescences (Location—Aortic Valve)

Lambl's excrescences are typically identified on the aortic valve (AV) and originate as small, thin projections on the endocardial surface at the site of valve closure (Fig. 12.6; Video 12.6). Histologically Lambl's excrescences are thin pieces of fibrous tissue covered by a layer of endothelial cells [6]. While patients with Lambl's excrescences are usually asymptomatic these small filiform (threadlike) fronds can embolize. Therefore, patients who suffer from multiple cerebrovascular accidents may be offered treatment in the form of anticoagulation or resection [7].

Papillary Fibroelastoma (Location—Aortic Valve)

Cardiac papillary fibroelastomas are benign tumors that are typically attached to the aortic valve, although they may be found on other valves. On echocardiography, fibroelastomas appear as mobile, pedunculated masses along the line of valve closure, as opposed to the linear "strand" of a Lambl's excrescence (Fig. 12.7a, b; Video 12.7a, b). Fibroelastomas are slow growing and are more gelatinous in appearance than Lambl's excrescences [8]. Given their propensity to embolize, these masses often require surgical resection.

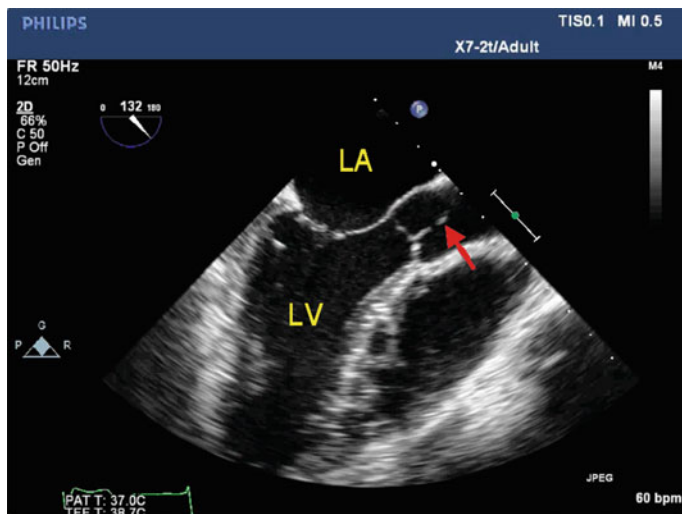


Fig. 12.6 Mid-esophageal long axis view in diastole demonstrating Lambert's excrescences (*red arrow*) present on the AV extending to the level of the sinotubular junction. See associated video online to observe the classic appearance and movement of these relatively small structures. *LA* left atrium; *LV* left ventricle

Nodules of Arantius (Location—Aortic Valve)

Nodules of Arantius are thickened central areas on the AV cusps (Fig. 12.8; Video 12.8). The role of these nodules is not clear; however, it has been theorized that they have a protective role in reducing the stress on the coapting surfaces. In contrast, aortic regurgitation has been attributed to the fibrosis and hypertrophy of the nodules of Arantius in isolated patients [6].

Coumadin Ridge (Location—Left Atrium)

The Coumadin ridge, also known as the Ligament of Marshall, describes the muscular ridge located between the left upper pulmonary vein and left atrial appendage, commonly identified in a mid-esophageal two chamber view (Fig. 12.9; Video 12.9). This structure may be quite prominent and therefore derives its name from its frequent misdiagnosis for left atrial thrombus and the need for anticoagulation.

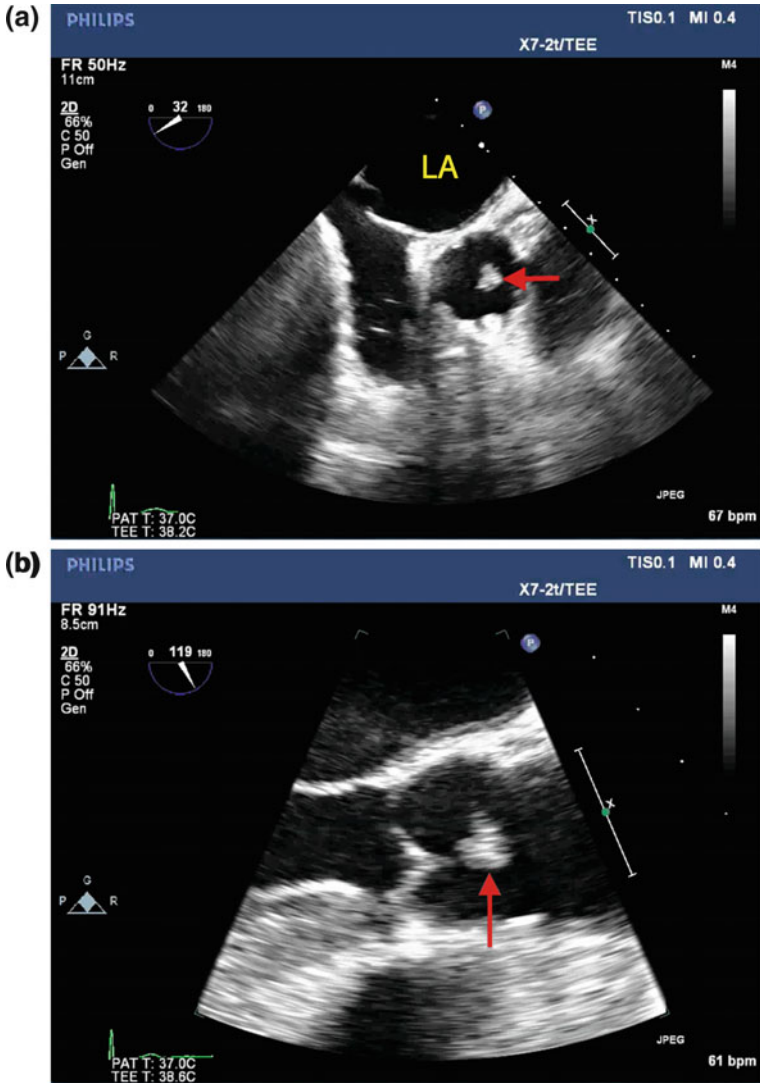


Fig. 12.7 **a** Mid-esophageal aortic valve short axis view with the probe slightly withdrawn demonstrating a papillary fibroelastoma (*red arrow*) attached to the aortic valve. **b** A zoomed in mid-esophageal AV long axis view of the same patient demonstrates the pedunculated mass attached near the coaptation line of the aortic valve. The pedunculated mass is consistent with a papillary fibroelastoma (*red arrow*)

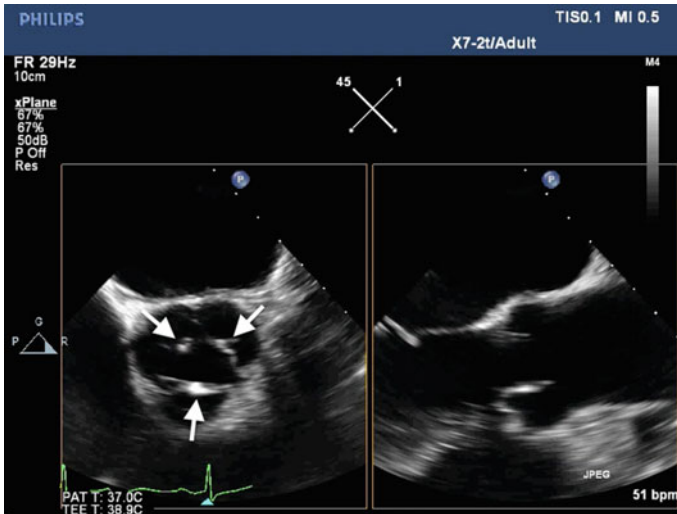


Fig. 12.8 Simultaneous mid-esophageal AV short axis and long axis views demonstrating Nodules of Arantius (*white arrows*) that are present on the center of all three AV cusps

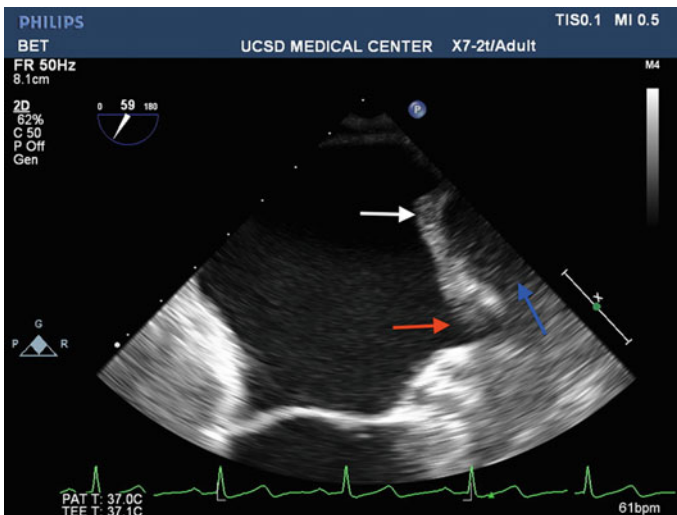


Fig. 12.9 Mid-esophageal commissural view (depth decreased). The Coumadin ridge (*white arrow*) separates the left upper pulmonary vein (*blue arrow*) from the left atrial appendage (*red arrow*)

Artifacts

Imaging artifacts result from violations of assumptions about the physics of ultrasounds. The following assumptions are made when generating ultrasound images:

1. Sound waves travel in straight lines to the reflecting surface and back.
2. Sound travels at exactly 1540 m/sec.
3. Only structures along the central axis of the ultrasound beam reflect sound waves back to the probe to generate images.

While these assumptions generally hold true, artifacts are generated when one or more of these assumptions are violated [9, 10].

Dropout

Image generation is optimal when the object of interest is perpendicular to the ultrasound beam. Reflections are suboptimal when the area of interest is parallel to the ultrasound beam. Without a surface perpendicular to the beam, there is a lack of ultrasound reflection back towards the probe. This results in an echolucent area that should not otherwise be echolucent. Transgastric short axis imaging often has dropout along the septal and lateral walls due to the parallel orientation to the ultrasound beam (Fig. 12.10; Video 12.10). Alternative views, which place the area

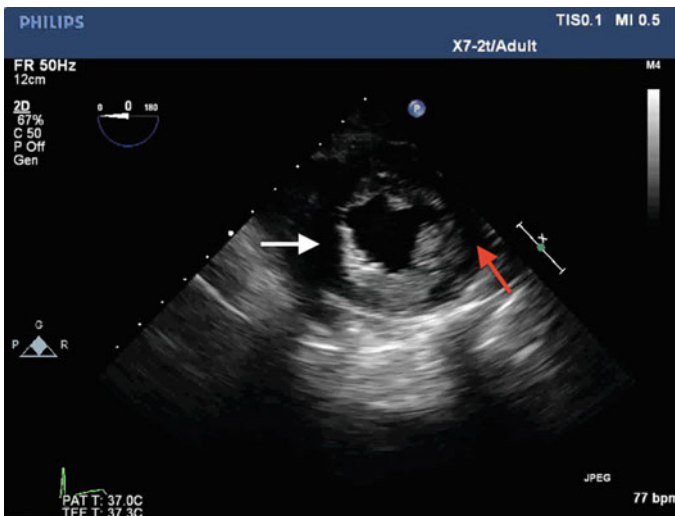


Fig. 12.10 Transgastric midpapillary SAX view. Hypo or anechoic areas of the septal (*white arrow*) and lateral walls (*red arrow*) represent imaging dropout, common in the TG SAX view

of interest perpendicular to the ultrasound beams should be utilized to overcome imaging “dropout.”

Acoustic Shadowing

Acoustic shadowing results from the reflection of ultrasound waves by a structure with large acoustic impedance. The strong reflector—typically a prosthetic valve, catheter, or heavy calcification—reflects a large proportion of the ultrasound waves and thus blocks distal propagation of the ultrasound beam (Fig. 12.11; Video 12.11). This results in hypoechoic areas and an inability to image the far field [10].

Side Lobe

Side lobe artifacts are generated when diverging side beams, which are weaker than the central beam, encounter a strong reflector. The reflections are perceived by the ultrasound probe as being generated by the primary, central beam and display an incorrect echogenic structure within the imaging plane. (Figure 12.12; Video 12.12).

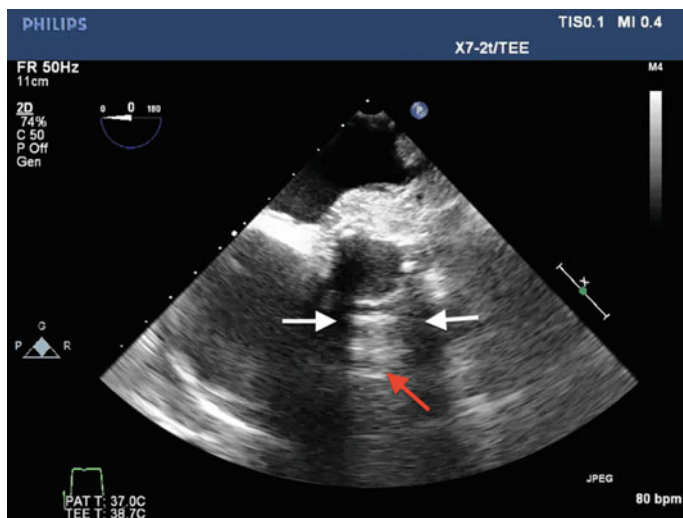


Fig. 12.11 Mid-esophageal AV SAX (modified angle of interrogation) in a patient with a bioprosthetic aortic valve replacement. The prosthetic aortic valve creates a shadowing artifact (white arrows) which obscures visualization of the RV. In addition, a ring down or comet tail artifact (red arrow), which is generated by the closely spaced annular ring and ascending aorta, is also present. Acoustic shadowing and ring down artifacts can both result in inadequate imaging distal to the reflecting structure(s)

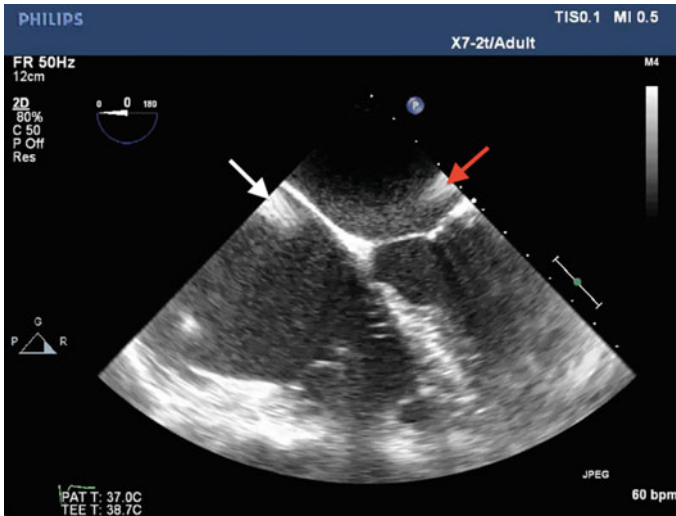


Fig. 12.12 Mid-esophageal four chamber view demonstrating side lobe artifacts and inappropriately high gain settings, which result in echogenic artifacts in the RA near the interatrial septum (*white arrow*) and LA above the lateral mitral annulus (*red arrow*)

Side lobe artifacts are typically curvilinear artifacts that maintain a constant depth along a sector arc [10]. Commonly, a strong reflector, such as an out-of-plane pulmonary artery catheter, may reflect enough ultrasound energy back to the probe to generate a linear density that displays within the aortic lumen in a mid-esophageal ascending aortic short axis view. This artifact may easily be confused for an ascending aortic dissection. Noting that the artifact crosses tissue planes, beats “out of sync” with the surrounding tissues and is not present in multiple imaging planes suggest that the linear density is an artifact and not a dissection.

Reverberation

A reverberation artifact is described as a “step ladder” artifact that appears at equally spaced distances along a scan line (Fig. 12.13; Video 12.13). The artifact is generated by the ultrasound energy bouncing back and forth between two objects multiple times before returning to the ultrasound probe. The ricocheting of the ultrasound energy between the objects and subsequently returning to the probe is displayed as a series of ultrasound densities at equally spaced intervals away from the image apex. Objects that often cause this artifact include tracheal rings, calcified aortic walls, or even the ultrasound transducer itself. Decreasing the gain or utilizing alternative imaging planes may be helpful when this artifact is encountered [10].

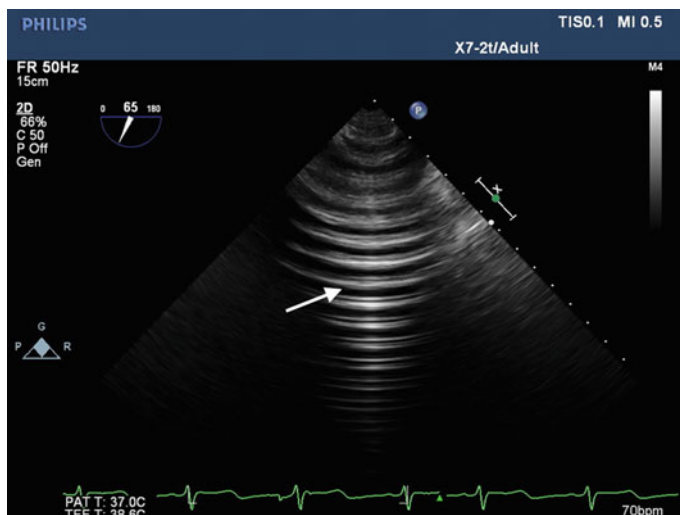


Fig. 12.13 An upper esophageal view withdrawn from the ascending aortic views encountering tracheal rings. A reverberation artifact (*white arrow*) is generated by the tracheal rings, demonstrating repeating artifacts at evenly spaced intervals

Mirroring

Mirroring artifacts have a similar mechanism to reverberation artifacts. A strong reflector, such as a calcific aortic wall will ricochet the ultrasound energy between the two aortic walls prior to returning the ultrasound energy to the ultrasound probe. The increased transit time results in a duplicate or mirror image of the structure being displayed just distal to the real object (Fig. 12.14; Video 12.14). Interestingly, color flow Doppler information is also mirrored demonstrating flow in the “mirrored” structure. This can lead to a misdiagnosis of the true and false lumens of an aortic dissection. Mirror artifacts are commonly encountered when imaging the arch of the aorta and the descending aorta.

Avoiding Pitfalls

In order to distinguish between anatomic variants or imaging artifacts and true pathology, the echocardiographer must utilize all information at their disposal. This includes not only a detailed knowledge of cardiac anatomy but also surgical and clinical correlation (i.e., discussion with the surgeon and a full patient history) [11]. Additional evidence that a structure may be an artifact includes its adherence to the path of a scanning arc, continuance through a clearly identifiable solid structure, or disappearance in alternative views. Proper image acquisition (e.g., gain, focus, and

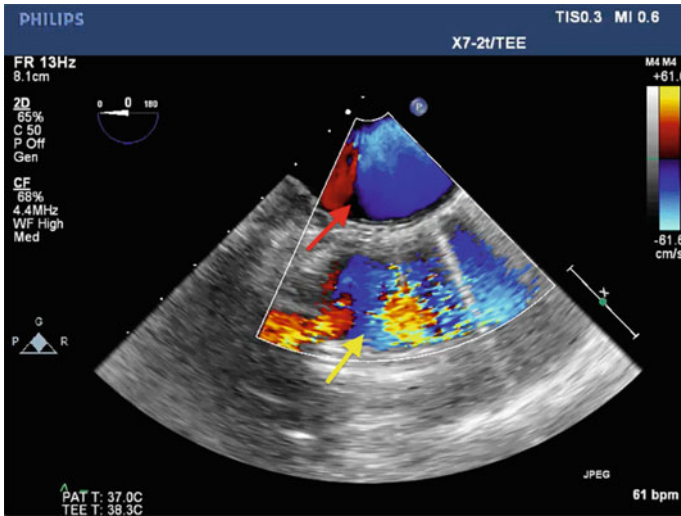


Fig. 12.14 Descending aortic view demonstrating mirroring artifacts that can occur in both two dimensional imaging and color flow Doppler imaging. A mirroring artifact (*yellow arrow*) of the true aorta (*red arrow*) is displayed here with CFD

gastric de-airing, etc.) can eliminate many artifacts or clarify an area of interest. If the diagnosis is still in question, the echocardiographer should consider utilizing echo contrast or additional imaging modalities (e.g., computed tomography, fluoroscopy, etc.) [12].

References

1. Reeves ST, Finley AC, Skubas NJ, et al. Basic Perioperative transesophageal echocardiography examination: a consensus statement of the american society of echocardiography and the society of cardiovascular anesthesiologists. *J Am Soc Echocardiogr.* 2013;26(5):443–56.
2. Najib MQ, Ganji JL, Raizada A, Panse PM, Chaliki HP. Epicardial fat can mimic pericardial effusion on transesophageal echocardiogram. *Eur J Echocardiogr.* 2011;12(10):804.
3. Tan CO, Harley I. Perioperative transesophageal echocardiographic assessment of the right heart and associated structures: a comprehensive update and technical report. *J Cardiothorac Vasc Anesth.* 2014;28(4):1100–21.
4. George A, Parameswaran A, Nekkanti R, Lurito K, Movahed A. Normal anatomic variants on transthoracic echocardiogram. *Echocardiography.* 2009;26(9):1109–17.
5. Keren A, Billingham ME, Popp RL. Echocardiographic recognition and implications of ventricular hypertrophic trabeculations and aberrant bands. *Circulation.* 1984;70(5):836–42.
6. Dumaswala B, Dumaswala K, Hsiung MC, et al. Incremental value of three-dimensional transesophageal echocardiography over two-dimensional transesophageal echocardiography in the assessment of lambl’s excrescences and nodules of arantius on the aortic valve. *Echocardiography.* 2013;30(8):967–75.

7. Aziz F, Baciewicz FA Jr. Lambl's excrescences: review and recommendations. *Tex Heart Inst J.* 2007;34(3):366–8.
8. Hakim FA, Aryal MR, Pandit A, et al. Papillary fibroelastoma of the pulmonary valve—A systematic review. *Echocardiography.* 2013;31(2):234–40.
9. Aldrich JE. Basic physics of ultrasound imaging. *Crit Care Med.* 2007;35(Suppl):S131–7.
10. Pamnani A, Skubas NJ. Imaging artifacts during transesophageal echocardiography. *Anesth Analg.* 2014;118(3):516–20.
11. Cronin B, Nguyen L, Manecke G, Pretorius V, Banks D, Maus T. Foreign body located intraoperatively using transesophageal echocardiography. *J Cardiothorac Vasc Anesth.* 2014;28(3):852–3.
12. Apostolidou I, Krishnan K, Keith V, Madlon-Kay R. Contrast echocardiography to differentiate artifact from left atrial thrombus. *Anesth Analg.* 2012;114(4):742–5.

Chapter 13

Adult Congenital Heart Disease

Swapnil Khoche, MBBS

Abstract The increasing number of patients with either uncorrected or repaired congenital cardiac lesions is on the rise, likely reflective of improvements in care and detection. With more patients surviving well into adulthood, they often present for non-cardiac surgery. Echocardiography remains central to the detection, and aids in both surgical and device-based correction. It can also provide important prognostic information and quantify the effects (from the lesion) on ventricular function, pulmonary and systemic flow, etc. It is important for the beginner and intermediate practitioner to familiarize himself/herself with basic lesions encountered in adulthood, the echocardiographic techniques used to further identify and evaluate each condition, and the associated conditions that need to be sought and ruled out.

Keywords TEE for congenital heart disease • Ventricular septal defect • Atrial septal defect • Patent foramen ovale • Bubble study • Dilated coronary sinus • Persistent left SVC • PDA • Device closure • Tetralogy of fallot

Introduction

With the advancement of technology, transesophageal echocardiography (TEE) has quickly become invaluable in pediatric congenital heart surgery, both as a diagnostic tool and to assess repair [1]. Patients with congenital heart disease (CHD) are now

Electronic supplementary material The online version of this chapter (doi:[10.1007/978-3-319-34124-8_13](https://doi.org/10.1007/978-3-319-34124-8_13)) contains supplementary material, which is available to authorized users.

S. Khoche, MBBS (✉)
Department of Anesthesiology, University of California San Diego,
200 W Arbor Drive MC #7651, San Diego, CA 92103, USA
e-mail: skhoche@ucsd.edu

surviving longer, and will ultimately need further anesthesia for non-cardiac and cardiac procedures [2]. Echocardiography has remained the cornerstone of diagnosing and managing these conditions. The basic perioperative transesophageal echocardiography (PTE) examination consensus statement recommends that a physician trained in basic perioperative TEE uses the exam to identify simple congenital heart disease lesions as a potential cause for right to left or left to right shunts [3]. Complex lesions are beyond the scope of the basic echocardiographer and if suspected, consultation with an advanced PTE echocardiographer or another diagnostic technique is warranted. Perioperatively, TEE provides real-time monitoring of ventricular filling, myocardial performance, and identification of intracardiac shunting, in addition to optimization of hemodynamic management strategies. A brief outline of the major congenital cardiac lesions and their echocardiographic correlates is provided here. The bicuspid aortic valve, which is the most common congenital heart lesion seen in adulthood, is discussed separately in Chap. 7.

Atrial Septal Defect (ASD)

ASDs comprise 7–8 % of all congenital heart disease and thus, are relatively common, either in combination with other lesions, or by themselves. Its location and size, which are related to its embryonic origin, often determine the magnitude of its hemodynamic effects. Due to the proximity of the left atrium to the probe, TEE results in excellent imaging of the interatrial septum (IAS), and is superior to TTE in this respect.

A patent foramen ovale (PFO), present in up to 27 % of population, can cause an intracardiac shunt if right atrial pressure exceeds the left atrial pressure [4]. Although a PFO represents a possible communication between the atria, it is technically not considered an ASD as there is no actual defect or tissue missing. Identification of a PFO may be accomplished through the use of color flow Doppler (CFD). While the flow through a PFO may be small, lowering the aliasing velocity (Nyquist limit) on CFD may help to identify the lower flow (Fig. 13.1; Video 13.1). As well, an agitated saline study with identification of “microbubbles” moving across the foramen during a Valsalva maneuver can help identify a PFO. The use of a Valsalva maneuver is important as the release of the Valsalva maneuver temporarily increases right atrial pressure in comparison to left atrial pressure, thereby exacerbating the shunt and visualizing the interatrial septal crossing of the agitated saline [4] (Fig. 13.2; Video 13.2).

The defects or gaps truly classified as ASDs involve some degree of absent tissue, allowing the potential for various degrees of intracardiac shunting. The ASDs are subdivided based upon their location, which relates to the defect during embryologic development. The subdivided defects are described below (Fig. 13.3):

1. Ostium secundum ASD:

It is the most common ASD (approximately 70 %), and generally occurs in the area contained in the limbus of the fossa ovalis [5]. During embryologic

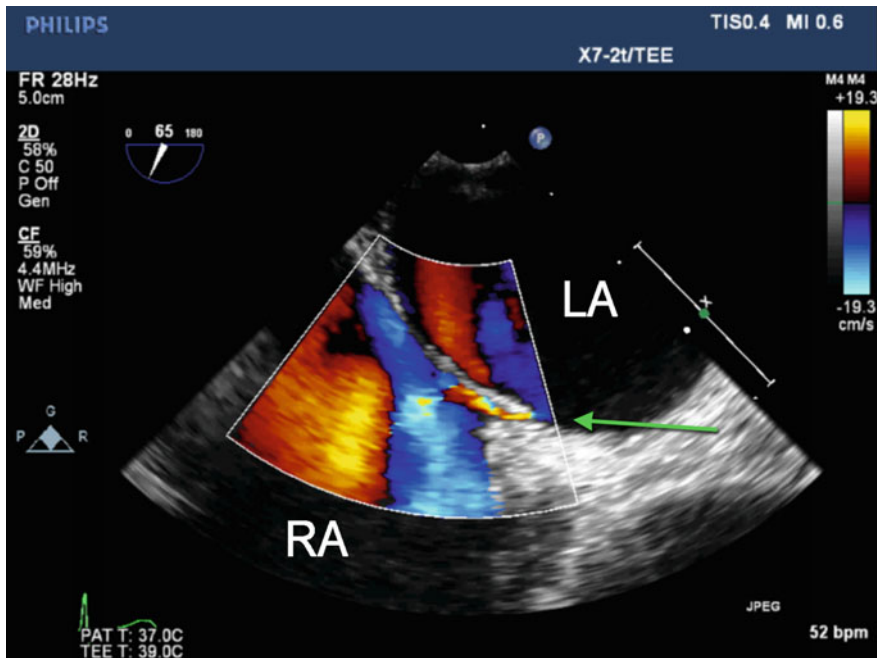


Fig. 13.1 Midesophageal view of interatrial septum with color flow Doppler. The *green arrow* indicates a *left to right* shunt across a patent foramen ovale (PFO). LA left atrium; RA right atrium

development, the septum primum grows toward the atrioventricular canal. An ostium develops centrally (termed the ostium secundum) which allows oxygenated blood in utero to cross the interatrial septum. Subsequently, a septum secundum develops to cover this ostium yet still allows flow through as the foramen ovale. After birth, with the increase in left atrial pressure from increased pulmonary blood flow, the foramen ovale is functionally pushed closed. Fusion of the two septums finalizes the process, leaving a fossa ovalis. A defective closure of the ostium secundum leads to the ostium secundum ASD (Fig. 13.4; Video 13.3). It may be circular in shape or may be a series of fenestrations associated with an aneurysmal interatrial septum.

2. Ostium Primum ASD:

These defects are the second most common type of ASD (approximately 20 %) and occur in the inferior and anterior portion of the IAS, near the AV valves. This defect generally represents the smallest degree of an atrioventricular canal defect. Ostium primum ASDs have been associated with Down's syndrome (Trisomy 21). During embryologic development, the septum primum develops in the direction of the atrioventricular valves, leaving the ostium primum to be developed by the endocardial cushion. Failure of this closure leaves the ostium primum atrial septal defect (Fig. 13.5; Video 13.4). As the endocardial cushion

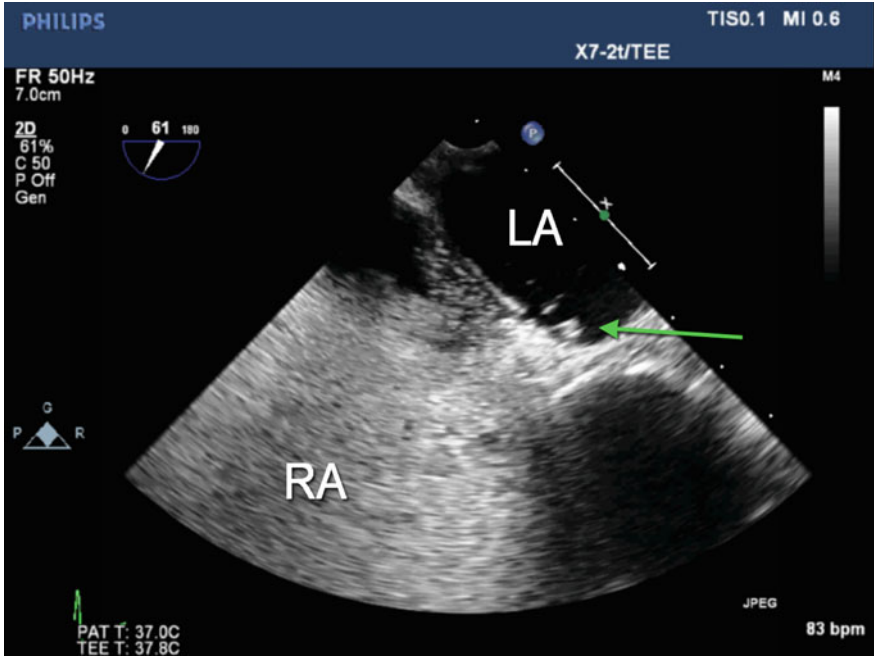


Fig. 13.2 Midesophageal view of interatrial septum during agitated saline injection. *Green arrow* indicates transseptal flow of agitated saline from right atrium (RA) to left atrium (LA)

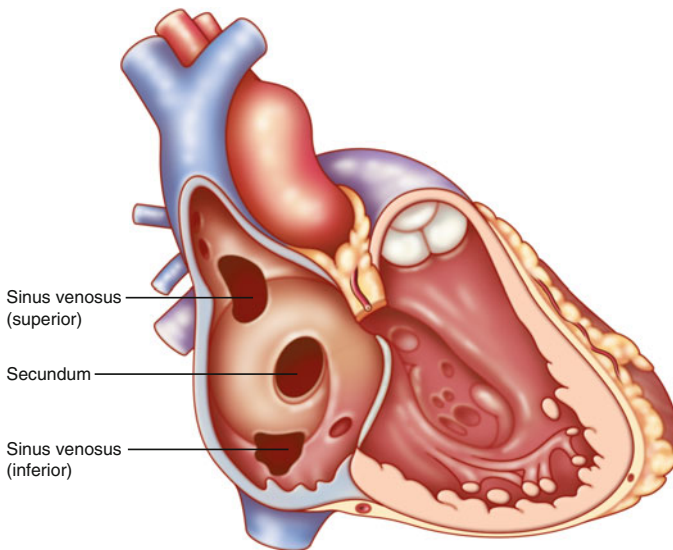


Fig. 13.3 Diagram of interatrial septum from the perspective of the right atrium and right ventricle

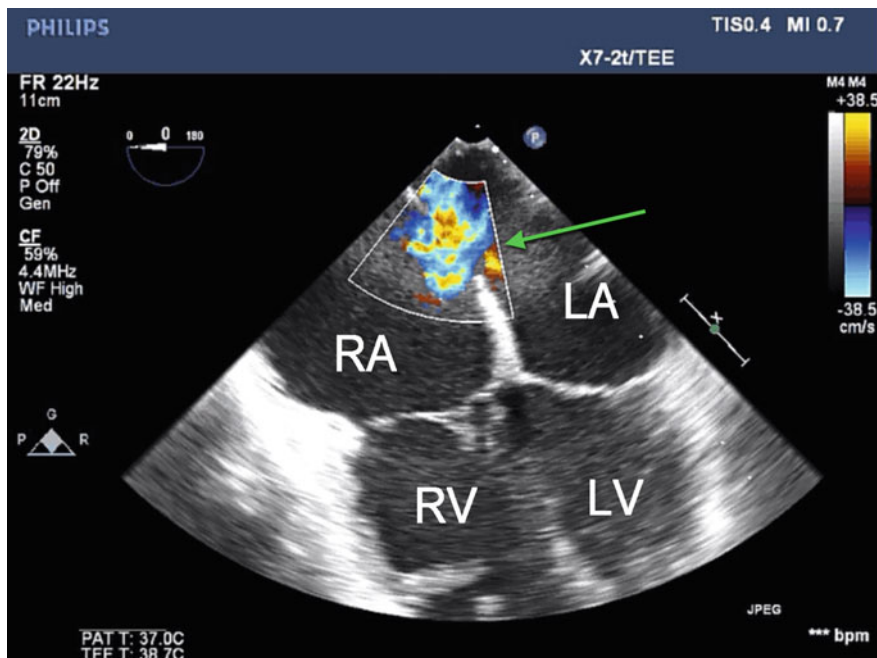


Fig. 13.4 Midesophageal four chamber view demonstrating an ostium secundum ASD (*green arrow*) with left to right flow noted on color flow Doppler. RA right atrium; LA left atrium; RV right ventricle; LV left ventricle

is also involved in the development of the atrioventricular valves, ostium primum defects can be associated with a cleft in the anterior mitral leaflet.

3. Sinus Venosus ASD:

This defect represents an atrial communication adjacent to the attachment of either the superior or inferior vena cavae, and results in the respective vena cava overriding the defect. Sinus venosus defects account for about 8 % of all ASDs [5]. Embryologically, the vena cavae are derived from the sinus venosus. Abnormal resorption of the sinus venosus leads to a defect between the cavae and the left atrium (Fig. 13.6; Video 13.5). The defect is often associated with partial anomalous pulmonary venous return (i.e., anomalous right upper pulmonary vein draining into the right atrium).

4. Coronary sinus ASD (unroofed coronary sinus):

These rare defects (<1 %) result from a partial or complete defect in the separation between the LA and the coronary sinus, resulting in “unroofing”, and causing communication between the right and the left atria.

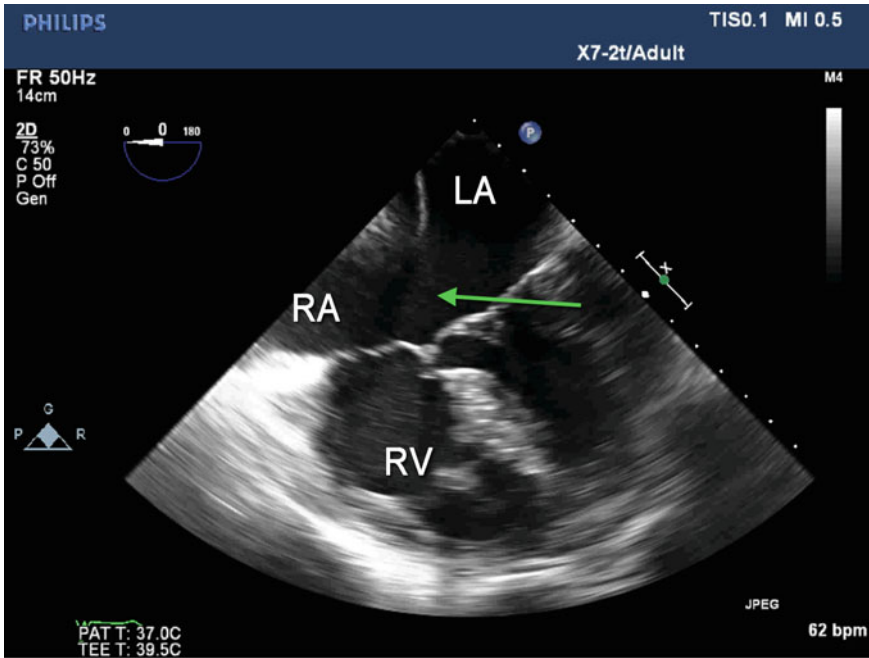


Fig. 13.5 Midesophageal four chamber view demonstrating an ostium primum ASD (green arrow). RA right atrium; LA left atrium; RV right ventricle

Echocardiographic Examination for ASDs

Atrial Septal Defects

2D	<ul style="list-style-type: none"> • Echogenic defect of tissue in interatrial septum <ul style="list-style-type: none"> – Secundum—ME Four Chamber or Bicaval Views – Primum—ME Four Chamber View – Unroofed Coronary Sinus—Difficult to visualize on 2D • Associated Findings <ul style="list-style-type: none"> – Cleft Anterior Mitral Leaflet (Primum) – Anomalous Pulmonary Venous Return (Sinus Venosus) – Atrial Enlargement – Ventricular dilation
CFD	<ul style="list-style-type: none"> • Interatrial flow – note directionality <ul style="list-style-type: none"> – May or may not be turbulent (dependent on ASD size)
Spectral	<ul style="list-style-type: none"> • Calculate Pulmonary to Systemic Flow Ratio (Qp:Qs)

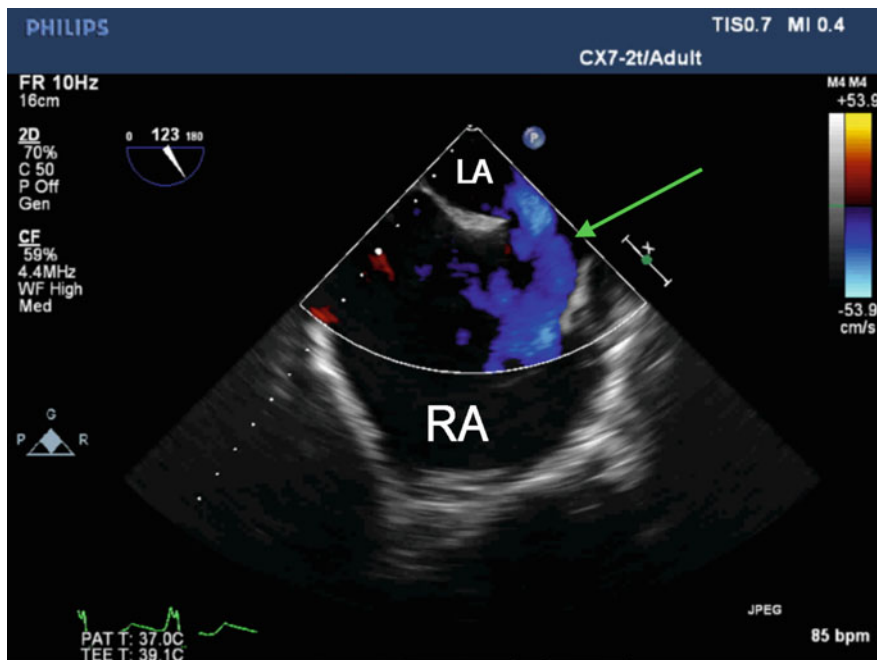


Fig. 13.6 Midesophageal bicaval view in a patient with a superior sinus venosus ASD and a grossly dilated right atrium (RA). The *green arrow* indicates left to right flow from the left atrium (LA) to the RA near the superior vena cava and RA junction

The midesophageal (ME) four chamber view can interrogate the majority of the interatrial septum, though probe withdrawal and insertion may be required for superiorly and inferiorly located ostium secundum defects as well as sinus venosus defects. Advancing the probe to the AV groove allows detection of ostium primum defects, evaluation of the coronary sinus, and Doppler evaluation of atrioventricular valves. Rotation of the probe to right and left is recommended to thoroughly interrogate the area. The ME Aortic Valve SAX or ME right ventricular inflow-outflow views can also be used to evaluate the septum, tricuspid valve (TV), and pulmonic valve (PV). In addition, these views can be used to quantify the tricuspid regurgitation, estimate pulmonary artery systolic pressure (PASP) as well as RV function, and search for abnormalities of venous return. The ME bicaval view provides a good cross-sectional display of the septum (superior to inferior), aligns the Doppler beam perpendicular to the septum, and is also an excellent view for agitated saline studies. This view is not particularly suited for detection of ostium primum defects, but can be modified by clockwise or counterclockwise rotation and omniplane manipulation to detect and evaluate all other ASDs. The transgastric mid-papillary SAX views can be used to detect flattening of the interventricular septum and help diagnose RV pressure or volume overload (see

Chap. 8). While beyond the scope of this textbook, TEE, especially 3D TEE, can be invaluable during device closure of ASDs by identifying the site and size of the defect, evaluating adequacy of the tissue ring around the defect (generally 5 mm) to hold the device, and follow the deployment of the device in real time.

Ventricular Septal Defect (VSD)

VSDs account for approximately 10 % of all adults with congenital heart disease, and can occur isolated or in association with other disorders. The ventricular septum can be divided into four components, each with its distinct morphology: Membranous, Inlet, Trabecular (muscular), Outlet [6] (Fig. 13.7). VSDs follow similar nomenclature, but can span more than one segment. Spontaneous closure is more likely for VSDs of the membranous or muscular type.

The most common of the four subtypes is the perimembranous VSD, occurring in 75–80 % of all VSDs. This defect is found in the membranous portion of the septum beneath the tricuspid valve and allows a connection to the left ventricular outflow tract (LVOT) immediately beneath the aortic valve [6]. It is best seen in the ME right ventricular inflow-outflow or ME aortic valve SAX views (Fig. 13.8; Video 13.6). Associated aneurysm of the membranous septum or accessory tricuspid tissue may be visualized. Perimembranous defects that occur high in the

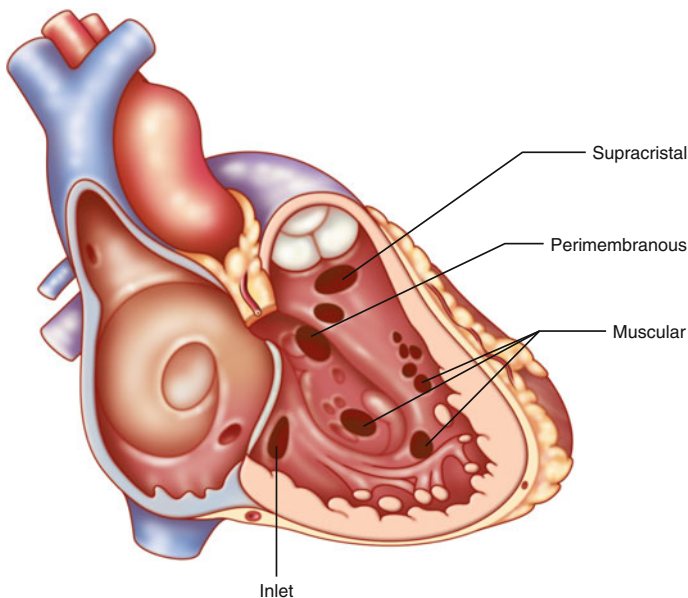


Fig. 13.7 Diagram of the interventricular septum from the perspective of the right atrium and right ventricle

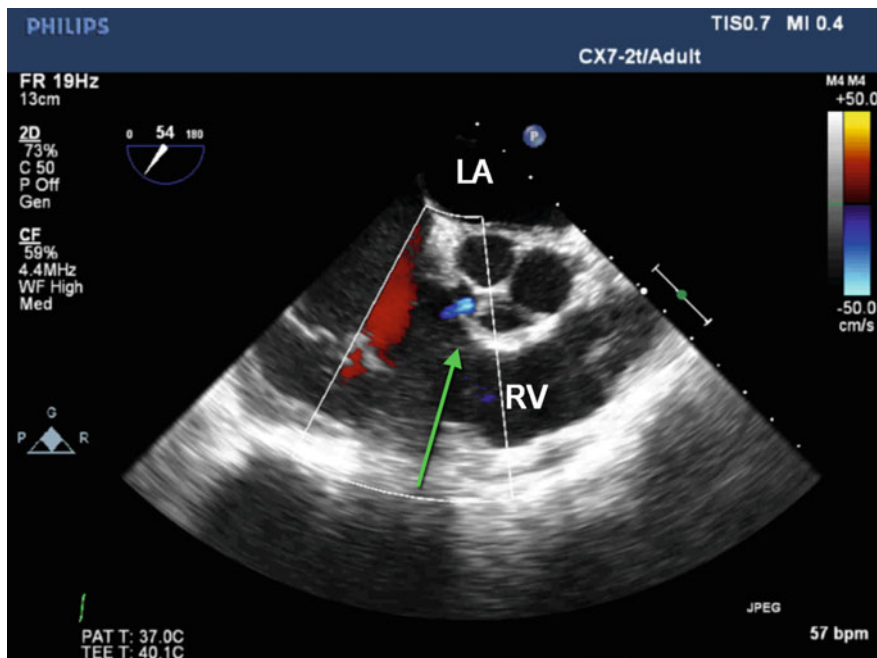


Fig. 13.8 Midesophageal right ventricular inflow-outflow view in a patient with a perimembranous ventricular septal defect (VSD) indicated by the green arrow. LA left atrium; RV right ventricle

LVOT can result in aortic regurgitation due to cusp herniation through the defect (most commonly the right coronary cusp).

Inlet VSDs, also part of the endocardial cushion defect spectrum, are located in the posterior portion of the interventricular septum immediately below the atrioventricular valves (mitral and tricuspid valves) [6]. Echocardiographically, these two valves tend to be located at the same level, however the normal insertion of the tricuspid valve is typically a few millimeters distal. These defects are large and generally do not close spontaneously. Multiple configurations of the atrioventricular valves can occur, the details of which are outside the scope of this text. Endocardial cushion defects represent defects in the separation of the right and the left heart chambers, and can have complete absence of the septa, one common atrioventricular valve, and an ostium primum ASD, among other abnormalities.

Muscular defects, approximately 5–20 % of all VSDs, occur centrally or apically in the trabecular portion, and can have multiple openings (“swiss cheese” appearance). Apical VSDs may occur after myocardial infarctions [7]. Color flow Doppler is invaluable to detect multiple defects in the muscular septum.

Outlet VSDs are also known by several terms: suprasternal, infundibular, doubly committed, or subarterial VSDs. Irrespective of the nomenclature used, they occur in the region just below the aortic and pulmonic valves and can have associated

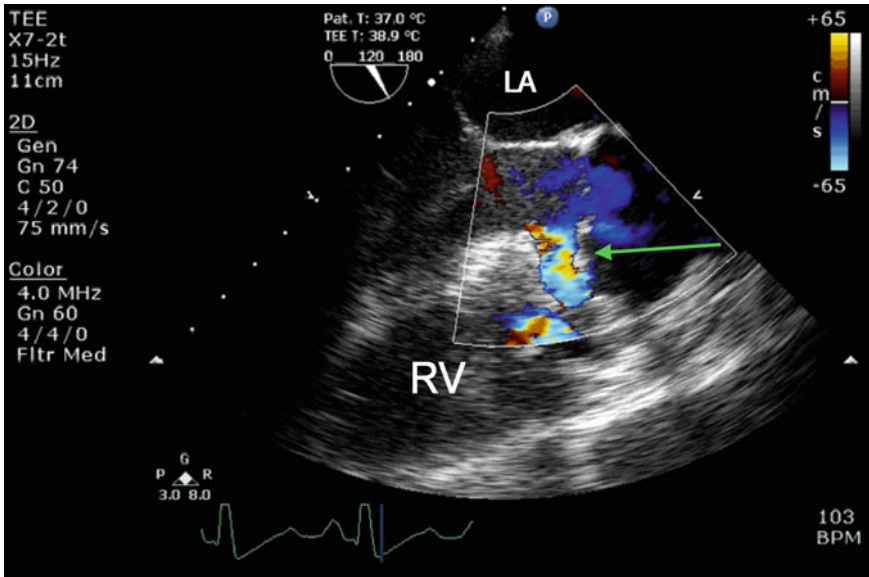


Fig. 13.9 Midesophageal aortic valve long-axis view in a patient with an outlet VSD (*green arrow*). LA left atrium; RV right ventricle

aortic insufficiency (related to the herniation of the right coronary cusp). Interrogation of the outflow tracts side by side, done as a modification of the ME aortic valve LAX view or the ME right ventricular inflow-outflow view, is used to detect these defects (Fig. 13.9; Video 13.7).

Echocardiographic Examination of VSDs

Ventricular Septal Defects	
2D	<ul style="list-style-type: none"> • Echogenic defect of tissue in interventricular septum <ul style="list-style-type: none"> – ME Four Chamber View (Muscular and Inlet) – ME AV SAX View (Perimembranous and Outlet) • Associated Findings <ul style="list-style-type: none"> – Atrial Enlargement – Ventricular dilation
CFD	<ul style="list-style-type: none"> • Presence of Interventricular flow <ul style="list-style-type: none"> – May or may not be turbulent (dependent on VSD size)
Spectral	<ul style="list-style-type: none"> • Calculate Pulmonary to Systemic Flow Ratio (Qp:Qs) • Estimate Pulmonary Arterial Systolic Pressure (TR Jet)

The complexity of the interventricular septum requires multiple views as well as rotation and use of the omniplane angle at nonstandard imaging planes. The ME four chamber, ME aortic valve short axis and long axis, ME RV inflow-outflow and deep transgastric long axis views are recommended for a focused interrogation. Apart from number, size, location, and nature of defects, other pertinent findings to look for include: additional congenital heart disease, aortic valve abnormalities, signs of RV pressure and volume overload, and its functional consequence. Doppler interrogation can quantify the nature and magnitude of the intracardiac shunt, estimate valvular regurgitation, and estimate PA systolic pressure (see Chap. 3).

High velocity through the defect as evidenced by Doppler interrogation is indicative of a restrictive shunt whereas low, nonturbulent flow denotes a nonrestrictive defect. Generally, a nonrestrictive defect indicates a more severe lesion [8, 9]. The ratio of pulmonary to systemic blood flow (Q_p/Q_s) should be measured since it has diagnostic and therapeutic implications. A high Q_p/Q_s indicates that there is a significant left to right shunt which may eventually lead to pulmonary overcirculation and Eisenmenger's syndrome. A low Q_p/Q_s is indicative of a right to left shunt.

Persistent Left Superior Vena Cava (SVC)

Approximately 0.5 % of the population has a persistent left SVC, which drains into the coronary sinus 90 % of the time. It is uncommonly associated with an absent right SVC. In embryologic development there are two superior vena cavae. Normally the left-sided SVC regresses with blood from the internal jugular (IJ) and left subclavian returning to the heart via the innominate vein. In the setting of a persistent left SVC, the left IJ and subclavian typically return blood flow to the heart via the left SVC into the coronary sinus. In its presence, central venous cannulation and pacemakers can take an abnormal orientation. In cardiac surgery, retrograde cardioplegia can be ineffective and venous cannulation strategies may need to be adjusted.

The coronary sinus (CS) can be imaged by advancing the probe from a ME four chamber view, in a modified bicaval view or in the posterior AV groove in the ME two chamber view. Dilation of the coronary sinus (>10 mm in diameter) should arouse suspicion for a persistent left SVC (Fig. 13.10; Video 13.8). Other causes such as elevated right atrial pressures from heart failure, atresia, or stenosis of the ostium or a coronary artery fistula to the CS need to be ruled out. The suspicion can then be confirmed with injection of agitated saline into the left upper extremity and resultant coronary sinus opacification. A large coronary sinus and its drainage into the right atrium have been mistaken for an ASD in some patients, and this makes thorough imaging essential [10].

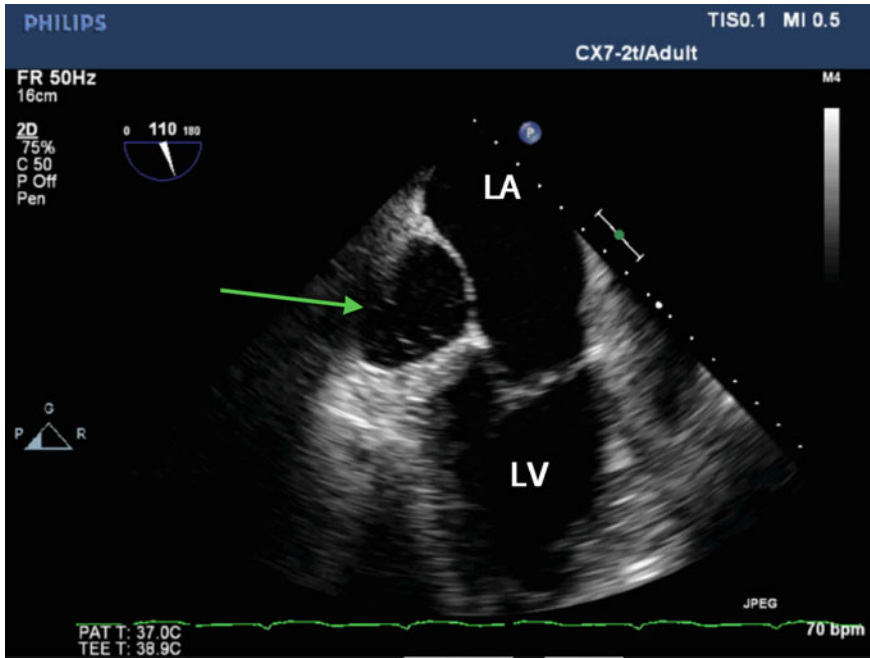


Fig. 13.10 Midesophageal two chamber view with the dilated coronary sinus in cross section to the posterior aspect of the top of the left ventricle. Agitated saline injected into the left arm has resulted in “microbubbles” within the dilated coronary sinus confirming a persistent left superior vena cava

Patent Ductus Arteriosus (PDA)/Aorticopulmonary Window

The ductus arteriosus is a vascular communication between the proximal descending aorta and the main or the left pulmonary artery in its roof. It closes spontaneously after birth but can persist into adulthood in rare cases, causing a left to right shunt. It is usually a coincidental finding picked up due to a murmur that leads to an echocardiography exam [11]. Echocardiography is helpful to not only diagnose the lesion, but also to evaluate the shunt magnitude and volume load, estimate pulmonary artery pressures, and identify associated cardiac pathology. Some patients may present with endarteritis (endocarditis of the ductus), which is responsible for almost half of the deaths in adult patients with a PDA [12]. The pulmonary side of the ductus is more commonly the site of infection. The patent ductus can be closed either surgically or often with a transcatheter device with excellent results. Upper esophageal views have been used to visualize a PDA, with nonstandard orientation of the omniplane angles. Since the connection between the aortic isthmus and the main pulmonary artery hides behind the left main bronchus,

it is often difficult to visualize with TEE. The demonstration of flow abnormality in the pulmonary artery using color flow Doppler is excellent supportive evidence but not diagnostic by itself of a PDA. Proper parallel alignment of the Doppler beam with the flow is even more difficult. It is important to note the FiO_2 during the shunt calculation since hyperoxia leads to reduction in PA pressures and an increase in the shunt [12]. The aorticopulmonary window represents a more proximal communication between the ascending aorta and the pulmonary artery, and can be easier to pick up on TEE. Hemodynamic consequences tend to be similar to a PDA.

Tetralogy of Fallot (ToF)

Tetralogy of Fallot	
2D	<ul style="list-style-type: none"> • Pulmonic Stenosis <ul style="list-style-type: none"> – Narrowed RVOT in ME RV inflow-outflow view • Right Ventricular Hypertrophy <ul style="list-style-type: none"> – Measure in ME Four Chamber view • Overriding Aorta <ul style="list-style-type: none"> – Observed in ME LAX view • Ventricular Septal Defect <ul style="list-style-type: none"> – Typical Perimembranous VSD in ME AV SAX View
CFD	<ul style="list-style-type: none"> • Presence of Interventricular flow <ul style="list-style-type: none"> – May or may not be turbulent (dependent on VSD size) • Turbulence in RVOT / Pulmonary Artery
Spectral	<ul style="list-style-type: none"> • Calculate Pulmonary to Systemic Flow Ratio ($Q_p:Q_s$) • Estimate Pulmonary Arterial Systolic Pressure (TR Jet)

Classic ToF patients manifest a VSD, pulmonic stenosis, an overriding aorta, and RV hypertrophy. Addition of an ASD makes it a pentalogy (present in about a third of cases). Multiple other congenital cardiac lesions can accompany a ToF, such as a right aortic arch, systemic venous abnormalities, and LVOT obstruction among others. Most patients require surgery early due to the cyanosis and right to left shunt, and thus patients that survive into adulthood generally have little RV obstruction. The goals of echocardiography should include (apart from confirming the diagnosis): quantification of the RV obstruction, VSD shunt magnitude and direction, and detection of associated anomalies.

The large, perimembranous VSD is best seen in the ME aortic valve LAX or SAX views. The defect is located between the right and the non-coronary cusps of the aortic valve. This generally permits shunt interrogation by Doppler (either color flow or spectral). The entire septum should be carefully interrogated to rule out additional defects. The ME aortic valve LAX view can also demonstrate the aortic override, which can be variable in presentation. In the post-repair adult, the repair of

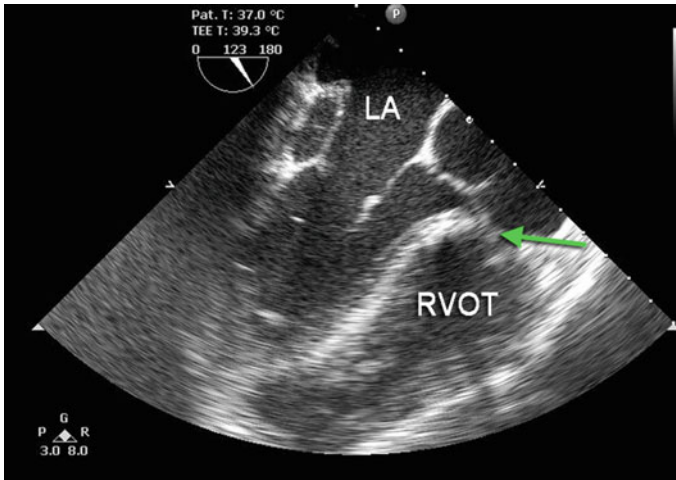


Fig. 13.11 Midesophageal long-axis view in a patient with tetralogy of fallot s/p VSD repair. Note the overriding aorta (*green arrow*) that remains and the evidence of right ventricular hypertrophy. Incidentally there is a dilated coronary sinus in this patient that was a persistent left-sided superior vena cava. LA left atrium; RVOT right ventricular outflow tract

the VSD using a patch still permits identification of the override (Fig. 13.11; Video 13.9). Involvement of the aortic valve, either as part of the primary lesion or during repair needs to be carefully ruled out.

Manipulation of the omniplane angle from either the ME aortic valve LAX or ME right ventricular inflow-outflow view can be used to interrogate the RV outflow tract. Obstruction is suggested (using color flow Doppler) by the presence of aliasing and turbulence in the RVOT. RV wall thickness can be measured in the ME right ventricular inflow-outflow to quantify the hypertrophy while transgastric views can be used to examine the RVOT. These views can help detect abnormalities of the pulmonic valve, if present. Interrogation of the RV outflow and the pulmonary artery with two-dimensional echocardiography, color flow Doppler, and spectral Doppler is helpful after repair since stenosis can persist and indeed, even worsen as the patient continues to grow into adulthood. After repair, left and right ventricular outflow obstruction and valvular regurgitation remain as the focus. Assessment of RV systolic pressure, size, and function is vital to the exam. Tricuspid and pulmonic regurgitation is not uncommon, and their quantification can be useful for future comparison.

Conclusion

With more congenital heart disease patients now surviving longer, it is likely that these patients will ultimately need further anesthesia for non-cardiac and cardiac procedures. Echocardiography has remained the cornerstone of diagnosing and managing these conditions. The basic perioperative echocardiographer should be familiar with and able to recognize simple congenital heart lesions. Complex lesions should involve consultation with an advanced echocardiographer. Perioperatively, TEE provides useful information about the real-time monitoring of ventricular filling, myocardial performance, and identification of intracardiac shunting, in addition to optimization of hemodynamic management strategies.

References

1. Miller-Hance WC, Russell IA. Intraoperative and Postoperative Transesophageal Echocardiography in Congenital Heart Disease. In: Wong PC, Miller-Hance WC (eds) Transesophageal echocardiography for congenital heart disease (internet). Springer, London; 2014. 2015. p. 383–97. Available from: http://link.springer.com/chapter/10.1007/978-1-84800-064-3_15.
2. Webb G, Mulder BJ, Aboulhosn J, Daniels CJ, Elizari MA, Hong G, et al. The care of adults with congenital heart disease across the globe: current assessment and future perspective: a position statement from the International Society for Adult Congenital Heart Disease (ISACHD). *Int J Cardiol.* (Internet). 2015. Available from: <http://www.sciencedirect.com/science/article/pii/S016752731500964X>.
3. Reeves ST, Finley AC, Skubas NJ, Swaminathan M, Whitley WS, Glas KE, et al. Basic perioperative transesophageal echocardiography examination: a consensus statement of the American Society of Echocardiography and the Society of Cardiovascular Anesthesiologists. *J Am Soc Echocardiogr.* 2013;26(5):443–56.
4. Hara H, Virmani R, Ladich E, Mackey-Bojack S, Titus J, Reisman M, et al. Patent foramen ovale: current pathology, pathophysiology, and clinical status. *J Am Coll Cardiol.* 2005;46(9):1768–76.
5. Craig RJ, Selzer A. Natural history and prognosis of atrial septal defect. *Circulation.* 1968;37(5):805–15.
6. Minette MS, Sahn DJ. Ventricular septal defects. *Circulation.* 2006;114(20):2190–7.
7. Kamran M, Attari M, Webber G. Ventricular septal defect complicating an acute myocardial infarction. *Circulation.* 2005;112(22):e337–8.
8. Ishii M, Hashino K, Eto G, Tsutsumi T, Himeno W, Sugahara Y, et al. Quantitative assessment of severity of ventricular septal defect by three-dimensional reconstruction of color doppler-imaged vena contracta and flow convergence region. *Circulation.* 2001;103(5):664–9.
9. Backer CL, Winters RC, Zales VR, Takami H, Muster AJ, Benson DWJ, et al. Restrictive ventricular septal defect: How small is too small to close? *Ann Thorac Surg.* 56(5):1014–9.
10. Sarodia BD, Stoller JK. Persistent left superior vena cava: case report and literature review. *Respir Care.* 2000;45(4):411–6.
11. Wiyono SA, Witsenburg M, de Jaegere PPT, Roos-Hesslink JW. Patent ductus arteriosus in adults. *Neth Heart J.* 2008;16(7–8):255–9.
12. Rigby ML. Closure of a large patent ductus arteriosus in adults: first do no harm. *Heart.* 2007;93(4):417–8.

Part III
Surface Ultrasound

Chapter 14

Transthoracic Echocardiography: The Basic Views

Sonia Nhieu, MD

Abstract Bedside transthoracic echocardiography (TTE) is a valuable, noninvasive, point-of-care diagnostic tool that can be used for cardiac evaluation of symptomatic or hemodynamically unstable patients. Use of TTE in the perioperative setting, emergency medicine or critical care patient population can provide new objective data and guide clinical management. The increasing availability of TTE and minimal training required to become competent makes the bedside TTE examination complementary to TEE.

Keywords Transthoracic echocardiography • Cardiac ultrasound • Basic views • Bedside transthoracic echocardiography (TTE) • Noninvasive

Abbreviations

TTE	Transthoracic echocardiography
TEE	Transesophageal echocardiography
LV	Left ventricle
FOCUS	Focused cardiac ultrasound
ASE	American Society of Echocardiography
ACEP	American College of Emergency Physicians
PEA	Pulseless electrical activity
LAX	Long axis
LA	Left atrium

Electronic supplementary material The online version of this chapter (doi:[10.1007/978-3-319-34124-8_14](https://doi.org/10.1007/978-3-319-34124-8_14)) contains supplementary material, which is available to authorized users.

S. Nhieu, MD (✉)
Division of Cardiovascular Anesthesiology and Critical Care,
Texas Heart Institute at Baylor St. Luke's Medical Center,
6720 Bertner Ave. MC1-226, Houston, TX 77030, USA
e-mail: sonia.nhieu@gmail.com

LVOT	Left ventricular outflow tract
RV	Right ventricle
SAX	Short axis
IVC	Inferior vena cava

Bedside transthoracic echocardiography (TTE) is an increasingly used, noninvasive diagnostic tool for cardiac evaluation of symptomatic and hemodynamically unstable patients. With minimal training in image acquisition and interpretation, intensivists can use bedside TTE to estimate global left ventricular (LV) function with reasonable accuracy [1]. In addition, the information obtained from a focused cardiac ultrasound (FOCUS) examination can guide management in the critically ill patient until a formal echocardiographic examination can be completed. The American Society of Echocardiography (ASE) and American College of Emergency Physicians (ACEP) emphasize the important role of FOCUS in patient care and its complementary role to comprehensive echocardiography [2].

For patients with undifferentiated hypotension, the primary advantage of bedside TTE is to distinguish cardiogenic shock from shock of other causes [2]. Hand-held echocardiography may also be used in the management of cardiac arrest for the evaluation of reversible causes [3]. Furthermore, using bedside echocardiography to distinguish between true pulseless electrical activity (PEA) and “pseudo-PEA,” in which the patients have echocardiographic evidence of cardiac motion without palpable pulses, can change outcomes [2, 3]. Patients with “pseudo-PEA” arrest had better prognoses as they had potentially treatable causes that could be identified by TTE [4]. Other time-sensitive evaluations that can be completed with bedside TTE include assessment for pericardial effusion, relative chamber size, global cardiac systolic function, and volume status.

This chapter is not intended to be a comprehensive review of TTE. Instead, the goal of this chapter is to provide a brief overview of how to acquire the basic TTE views and recognize abnormalities that may cause hemodynamic instability. As discussed in Chap. 11, evaluating the hemodynamically unstable patient focuses on identifying gross abnormalities on echocardiography and implementing correctional action. Noting small minutiae of findings is typically not the cause of significant hemodynamic disturbances. A formal echocardiographic evaluation may be indicated to follow up and/or confirm preliminary findings.

Basic TTE Views

When introducing TTE imaging into a practice, many practitioners have the sense that this modality is a difficult endeavor to learn. However, when transitioning to TTE imaging from a knowledge base of transesophageal echocardiography (TEE), the echocardiographer can envision that the ultrasound physics, cardiac structures,

and cardiac physiology are unchanged. Although the approach to the heart, “the windows,” is different, the views are often very similar. For example, the parasternal long-axis view images the same structures as the midesophageal (ME) long-axis view; the image is simply “turned” on its side. Once the echocardiographer gathers confidence in the image acquisition, the interpretation of the images is essentially unchanged.

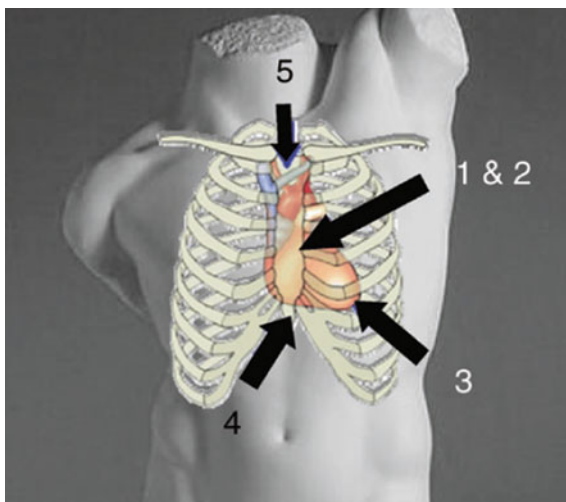
Unlike transesophageal imaging where the esophagus remains in close position to the heart despite patient position or respiration, transthoracic imaging requires interaction of the patient for optimal views. The optimal patient position for transthoracic imaging depends upon the specific imaging window and desired view. Parasternal and apically located views often utilize the left lateral decubitus (LLD) position with the patient’s left arm extended above the head. The purpose of this position is to allow the heart to be located nearest the chest wall due to gravity. Raising the left arm also increases the intercostal distance, decreasing shadowing from the ribs. However, this is not always possible in critically ill or perioperative patients and compromises may be necessary. Subcostal views often benefit from the patient remaining supine and therefore offer an alternative window in patients who are unable to be optimally positioned. In addition, image clarity will vary with respirations as the probe on the chest wall moves toward and away from the heart. The addition of air-filled lungs between the probe and cardiac structures will often obscure the image appearance. Therefore, timing of ventilation through patient breath holding can aid in obtaining improved images.

Parasternal Long-Axis (LAX) View

The basic TTE examination begins with the parasternal LAX view and proceeds in a clockwise fashion (Fig. 14.1). With the ultrasound indicator (notch or light

Fig. 14.1 Probe placement on chest wall for windows to basic transthoracic views.

1 parasternal long-axis view;
2 parasternal short-axis view;
3 apical four-chamber view;
4 subcostal view;
5 suprasternal view (not discussed in this chapter)
(with permission from Springer Science+Business Media: Price [8])



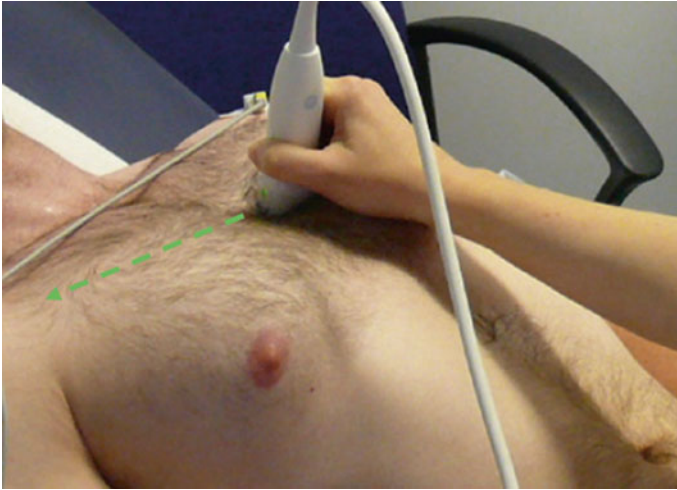


Fig. 14.2 Parasternal LAX probe position shown for a supine patient. The probe is placed in the second intercostal space lateral to the sternum with the indicator (direction noted by *green dashed arrow*) pointed toward the patient's right shoulder (with permission from Springer Science +Business Media: Price [8])

indicating the right side of the ultrasound image) pointing toward the patient's right shoulder, the transducer probe is placed in the second or third intercostal space just lateral to the left sternal border (Fig. 14.2). This view is often one of the easiest to obtain and simultaneously provides a significant amount of information. Structures that are seen and evaluated include the left atrium (LA), left ventricle (LV), left ventricular outflow tract (LVOT), right ventricular outflow tract (RVOT), left-sided valves inclusive of the mitral valve and aortic valve, and the proximal ascending aorta (Fig. 14.3; Video 14.1). When comparing to a similar TEE view, the parasternal long axis is nearly identical to a ME long axis displayed on its side. By increasing the depth of the image, a short-axis view of the descending aorta can be visualized in the far field of the image (Fig. 14.4).

In this echocardiographic window, RV size and systolic function, LV size and systolic function, regional wall motion of the anteroseptal and inferolateral walls, and stenosis or regurgitation of the mitral and aortic valves can be assessed. The parasternal LAX can also be used to identify an anterior or a posterior pericardial effusion as a cause of hemodynamic instability. The utility of this single view cannot be overstated.

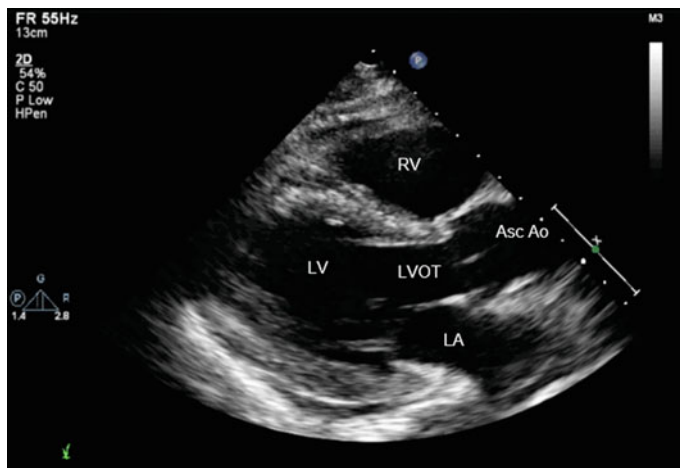


Fig. 14.3 Parasternal LAX view. *LA* left atrium; *LV* left ventricle; *LVOT* left ventricular outflow tract; *RV* right ventricle; *Asc Ao* ascending aorta

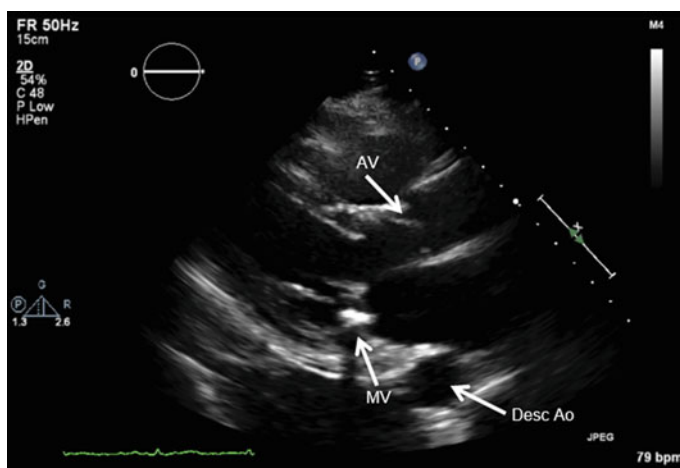


Fig. 14.4 Parasternal LAX view (increased depth). *AV* aortic valve; *MV* mitral valve; *Desc Ao* descending aorta

Parasternal Short-Axis (SAX) View

TEE from its relatively fixed position utilizes the omniplane to develop alternative imaging planes. In the setting of transthoracic imaging, the operator becomes the “omniplane” by holding the probe steady on the chest and simply rotating the probe on the chest in a clockwise or counterclockwise fashion. From the parasternal LAX view, with the patient remaining in the same position, the transducer probe is



Fig. 14.5 Parasternal SAX probe position shown for a supine patient. The indicator is pointed toward the patient's left shoulder (direction noted by *green dashed arrow*). Through angling the probe superiorly to inferiorly as shown by the *white arrow*, the short axis of the aortic valve, mitral valve, and LV can be imaged (with permission from Springer Science + Business Media: Price [8])

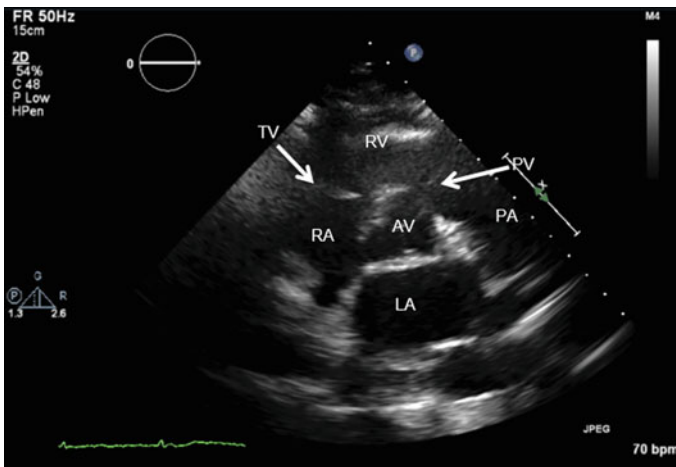


Fig. 14.6 Parasternal SAX view of the AV. LA left atrium; RA right atrium; TV tricuspid valve; RV right ventricle; PV pulmonic valve; PA pulmonary artery; AV aortic valve

rotated clockwise until the indicator is pointed toward the patient's left shoulder to obtain the parasternal SAX (Fig. 14.5). By angling the probe superiorly to inferiorly, a short-axis view of the aortic valve (Fig. 14.6; Video 14.2) and mitral valve (Fig. 14.7; Video 14.3), and LV (Fig. 14.8; Video 14.4) can be assessed. The

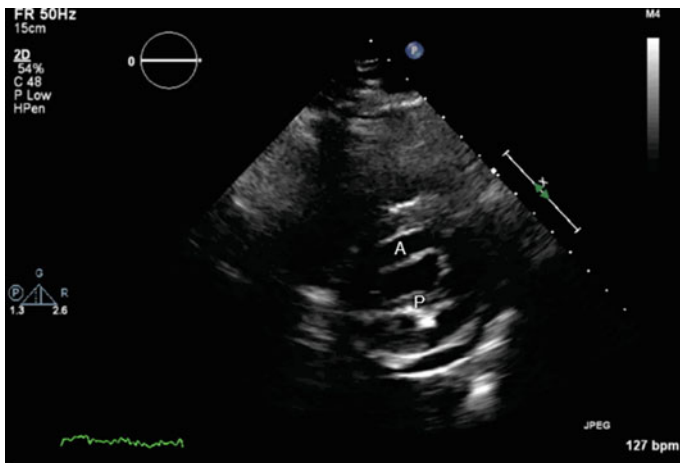


Fig. 14.7 Parasternal SAX basal view of the mitral valve with the leaflets open during diastole. *A* anterior leaflet; *P* posterior leaflet

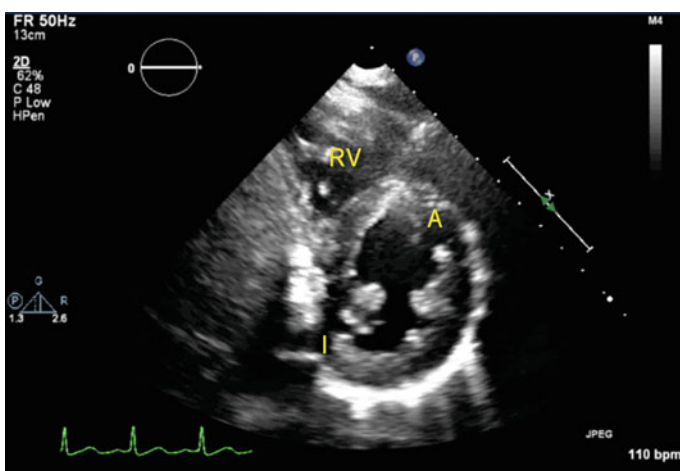


Fig. 14.8 Parasternal SAX mid-papillary view of the LV. *RV* right ventricle; *A* anterior LV wall; *I* inferior LV wall

angling can be analogous to anteflexion and retroflexion of the TEE probe to obtain superior to inferior structures.

In the parasternal SAX view of the aortic valve, overall chamber sizes of the left atrium, right atrium, and right ventricle can be appreciated. This view is analogous to the ME RV inflow-outflow view. Because of the Doppler alignment, the degree of tricuspid and pulmonic regurgitation can be assessed. Finally, in the parasternal SAX of the aortic valve and mitral valve, calcifications and morphology of valves

can be evaluated. Continuing to angle the probe inferiorly, the mid-papillary SAX view of the LV will be imaged. This view allows for evaluation of regional wall motion, degree of LV hypertrophy, and presence of hypovolemia analogous to the TG mid-papillary short-axis view in TEE.

Apical Four-Chamber View

Similar to the ME four-chamber view, a transthoracic four-chamber view can image the same structures, however from the aspect of the LV apex. To obtain the apical four-chamber view, the patient remains in LLD position with the left arm extended above the head and the transducer probe is placed at the apex of the heart identified by the point of maximal impulse. The indicator is pointed toward the patient's left axilla while slight angle adjustments should be made to align the septum in the center of the imaging sector (Fig. 14.9). The four chambers of the heart should be visible, with the left atrium and LV on the right side of the imaging sector and the right atrium and RV on the left side of the imaging sector (Fig. 14.10; Video 14.5).

Though this view can be more difficult to consistently obtain than parasternal views, it yields large amounts of helpful information. All four chambers of the heart can be evaluated for dilation, systolic function of the RV and LV can be assessed, color flow Doppler interrogation of the mitral and tricuspid valves, and pericardial effusions can be appreciated in the apical four-chamber view. Lastly with improved comfort in obtaining this view, mitral valve inflow and lateral wall tissue Doppler imaging may provide insight into diastolic function.

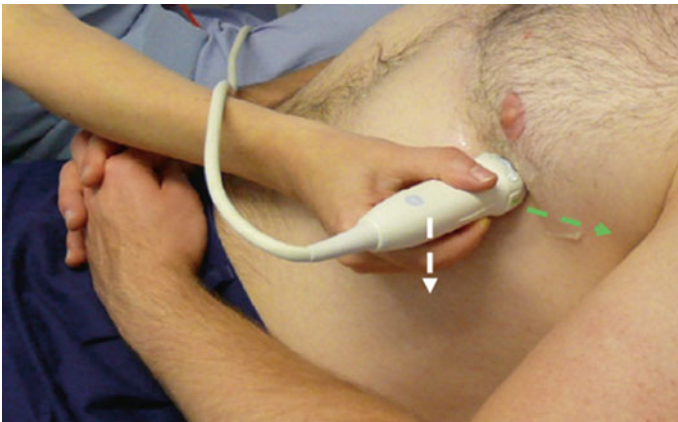


Fig. 14.9 Apical four-chamber probe position shown for a supine patient. The probe is placed at the apex of the heart (point of maximal impulse) and the indicator (*green arrow*) is pointed toward the patient's left side. The *white arrow* indicates the lateral movement of the tail of the probe to center the four chambers on the image (with permission from Springer Science+Business Media: Price [8])

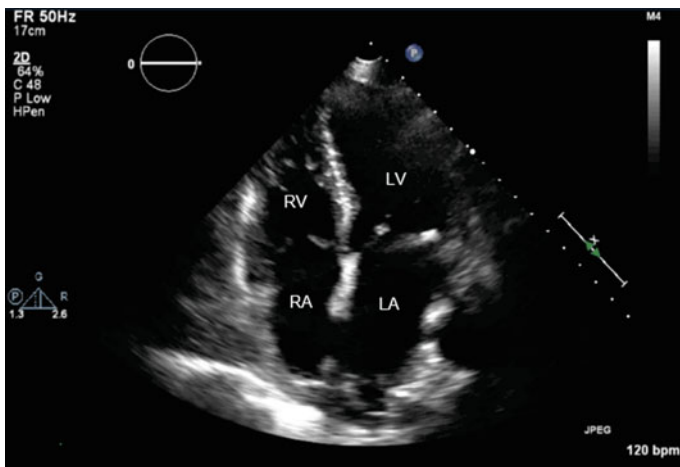


Fig. 14.10 Apical four-chamber view. *RA* right atrium; *RV* right ventricle; *LA* left atrium; *LV* left ventricle

Again envisioning the ultrasound operator as the “omniplane,” counterclockwise rotation of the probe while keeping the location of the probe unchanged will develop the apical four-chamber view to an apical two-chamber view and further to the apical long-axis views. This is akin to increasing the omniplane in TEE from the midesophageal four-chamber view to the midesophageal two-chamber and long-axis views.

Subcostal Views

In critically ill patients, especially those that are receiving positive pressure ventilation and positive end expiratory pressure (PEEP), the parasternal and apical views may be difficult to obtain or of poor quality. The subcostal view can be used in this subset of patients. The increased intrathoracic pressure will “push” the heart in a caudal direction, improving subcostal imaging. The subcostal four-chamber view is obtained by placing the probe just below the xiphoid, with the indicator pointed toward the patient’s left side and the ultrasound beam directed superiorly toward the heart (Figs. 14.11 and 14.12). The inferior vena cava (IVC) entering into the RA can be developed with counterclockwise rotation of the probe (Fig. 14.13; Video 14.6). The diameter and collapsibility of the IVC can be used to aid in the determination of fluid responsiveness and estimates of central venous pressure.

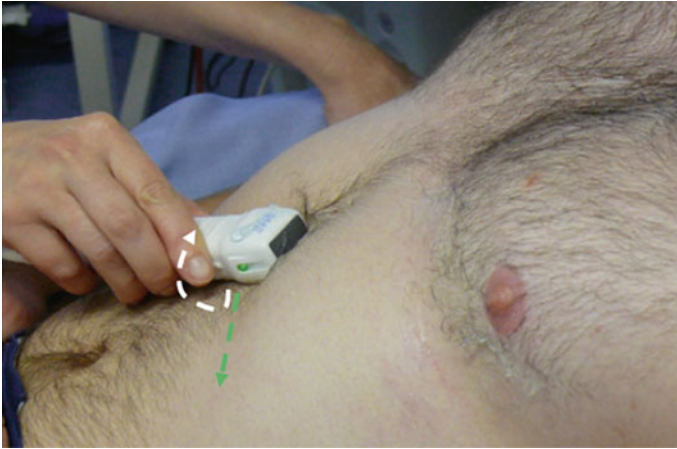


Fig. 14.11 Subcostal probe position shown for a supine patient. The probe is placed just below the xyphoid with the indicator (*green arrow*) pointed toward the patient's left. To view the IVC, the probe is rotated counterclockwise (*white arrow*) (with permission from Springer Science +Business Media: Price [8])

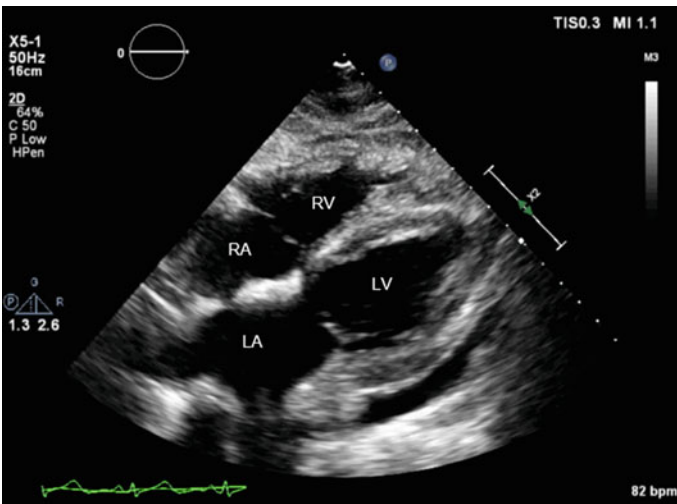


Fig. 14.12 Subcostal four-chamber view. *RA* right atrium; *RV* right ventricle; *LA* left atrium; *LV* left ventricle

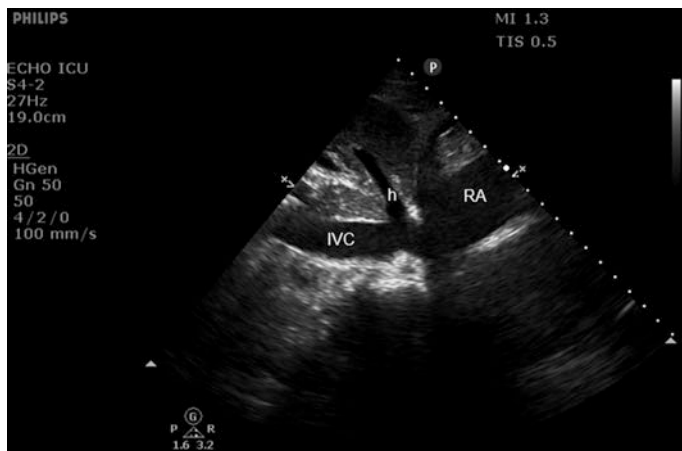


Fig. 14.13 Subcostal IVC view. *IVC* inferior vena cava; *RA* right atrium; *h* hepatic vein

Examples of Hemodynamic Compromise

Bedside TTE is commonly used to assess volume status or fluid responsiveness in the critically ill patient population. Though potentially difficult, estimating fluid responsiveness is important in the management of septic shock as hypovolemia is associated with worse outcomes but over-resuscitation has also been found to increase mortality [5]. In conjunction with other clinical data, a finding suggestive that patients may require additional resuscitation is a collapsed or obliterated LV cavity seen in the parasternal SAX view during systole (Fig. 14.14; Video 14.7). Though the results should be interpreted with caution, respiratory variation of the IVC is also commonly used as a predictor of fluid responsiveness [6]. Patients with a respiratory variation of more than 40 % are more likely to respond to a fluid challenge (Video 14.6).

Life threatening causes of hemodynamic instability that warrant immediate intervention include cardiac tamponade and pulmonary embolism. Cardiac tamponade or concern that a pericardial effusion is causing hemodynamic instability (Fig. 14.15; Video 14.8) requires consultation with a cardiothoracic surgeon immediately. Though a bedside TTE should not be the only tool used to diagnose a pulmonary embolism, there are findings that raise the suspicion that the patient has a pulmonary embolus. Dilation of the RV is often significant, although it is non-specific for a pulmonary embolus (Fig. 14.16). A more specific finding is the distinct echocardiographic pattern of regional RV dysfunction in the mid-free wall with sparing of the apex, also known as the McConnell's sign [7] (Video 14.9). The tethering of the right ventricular apex to the hyperdynamic left ventricle is thought to be responsible for the preserved apical motion. As discussed in Chap. 11, the sensitivity and specificity of McConnell's sign has been called into question. However, this finding raises the level of clinical suspicion for an acute pulmonary embolus.

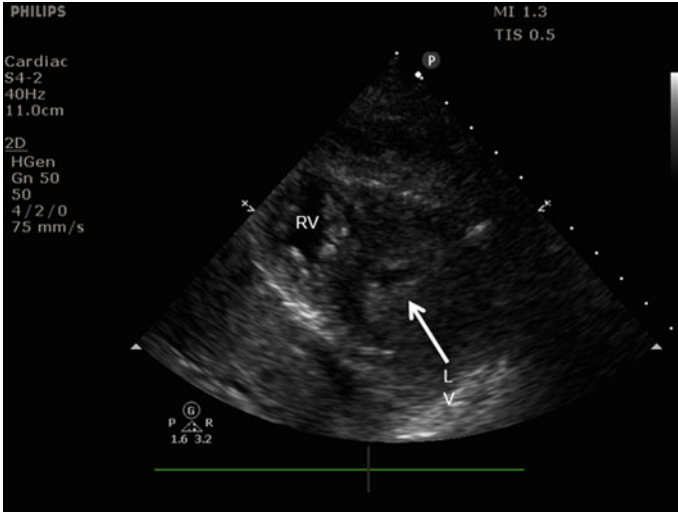


Fig. 14.14 End systolic parasternal SAX view showing an obliterated LV cavity in a patient with hypovolemia. This patient also has significant left ventricular hypertrophy (LVH). *RV* right ventricle; *LV* left ventricle

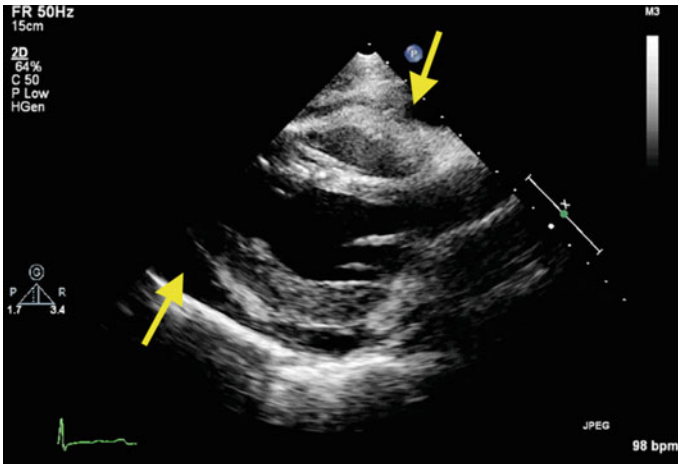


Fig. 14.15 Parasternal SAX view demonstrating a pericardial effusion (yellow arrows) that resulted in hemodynamic instability. Please see Video 14.8 to observe the dynamic component of the effusion

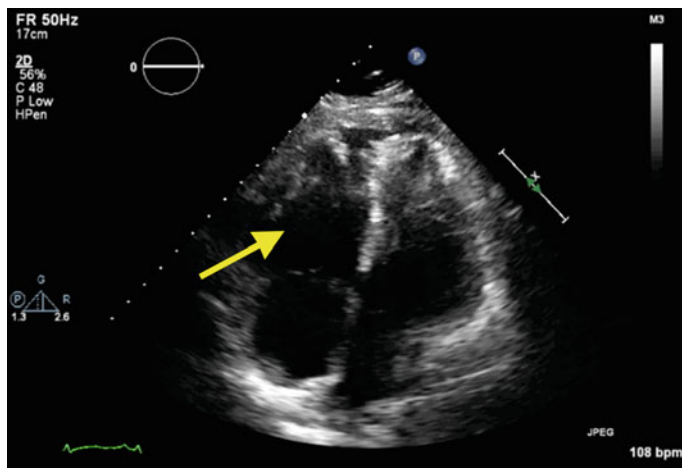


Fig. 14.16 Apical four-chamber view in a patient with a dilated RV (yellow arrow) due to an acute pulmonary embolus

Conclusion

Bedside TTE is a valuable, noninvasive, point-of-care diagnostic tool that has been shown to be helpful in perioperative and hemodynamically unstable patients. Adding TTE to a basis of TEE knowledge requires that the operator learn additional “windows” to the heart, however the normal anatomy, pathologic states, and cardiac physiology remain unchanged. Once past this hurdle of new “windows,” it becomes relatively easy to integrate TTE into practice to identify gross abnormalities in the unstable patient.

References

1. Melamed R, Sprenkle MD, Ulstad VK, Herzog CA, Leatherman JW. Assessment of left ventricular function by intensivists using hand-held echocardiography. *Chest*. 2009;135(6):1416–20.
2. Labovitz AJ, Noble VE, Bierig M, Goldstein SA, Jones R, Kort S, et al. Focused cardiac ultrasound in the emergent setting: a consensus statement of the American Society of Echocardiography and American College of Emergency Physicians. *J Am Soc Echocardiogr Off Publ Am Soc Echocardiogr*. 2010;23(12):1225–30.
3. Oren-Grinberg A, Gulati G, Fuchs L, Pinto DS. Hand-held echocardiography in the management of cardiac arrest. *Anesth Analg*. 2012;115(5):1038–41.
4. Breitkreutz R, Price S, Steiger HV, Seeger FH, Ilper H, Ackermann H, et al. Focused echocardiographic evaluation in life support and peri-resuscitation of emergency patients: a prospective trial. *Resuscitation*. 2010;81(11):1527–33.

5. Boyd JH, Forbes J, Nakada T, Walley KR, Russell JA. Fluid resuscitation in septic shock: a positive fluid balance and elevated central venous pressure are associated with increased mortality. *Crit Care Med*. 2011;39(2):259–65.
6. Muller L, Bobbia X, Toumi M, Louart G, Molinari N, Ragonnet B, et al. Respiratory variations of inferior vena cava diameter to predict fluid responsiveness in spontaneously breathing patients with acute circulatory failure: need for a cautious use. *Crit Care Lond Engl*. 2012;16(5):R188.
7. McConnell MV, Solomon SD, Rayan ME, Come PC, Goldhaber SZ, Lee RT. Regional right ventricular dysfunction detected by echocardiography in acute pulmonary embolism. *Am J Cardiol*. 1996;78(4):469–73.
8. Price S. Hemodynamic monitoring using echocardiography in the critically ill—Chapter 2 Transthoracic echocardiography: normal two-dimensional and doppler imaging. 2011. p. 13–29.

Chapter 15

Ultrasound for Vascular Access

Seth T. Herway, MD, MS

Abstract Ultrasound can be employed to facilitate central and peripheral vascular access. In some cases, such as internal jugular vein cannulation, the use of ultrasound makes the procedure faster and safer while limiting the number of attempts. Complications such as carotid artery puncture or pneumothorax may be reduced. In other procedures, such as subclavian vein cannulation, the role of ultrasound in facilitating the procedure is less clear. Last, peripheral venous access may benefit from observation of patent vasculature and procedure-guidance, however, the reduction of any complications is not documented.

Keywords Internal jugular vein cannulation · Subclavian vein cannulation · Femoral vein cannulation · Ultrasound · Vascular access

Proper vascular access is imperative for appropriate perioperative care and includes the use of peripheral venous access for fluid and drug administration, central venous access for vasoactive infusion and central venous pressure (CVP) monitoring and last, arterial access for continuous blood pressure monitoring and arterial blood sampling. The indications of each type of access are outside of the scope of this text, however, the utility of ultrasound for obtaining the vascular access will be discussed. Ultrasound imaging during vascular procedures can be used to “scout” the anatomy prior to skin puncture, provide image guidance toward the intended structure as well as confirmation of wire placement during a Seldinger technique. The intention of ultrasound imaging is often to reduce complications, reduce the

Electronic supplementary material The online version of this chapter (doi:[10.1007/978-3-319-34124-8_15](https://doi.org/10.1007/978-3-319-34124-8_15)) contains supplementary material, which is available to authorized users.

S.T. Herway, MD, MS (✉)
Department of Anesthesiology, University of California San Diego,
200 W Arbor Drive MC 8770, San Diego, CA 92103, USA
e-mail: sherway@ucsd.edu

time to vascular access, and aid in difficult cannulations, however, this may vary depending upon the vessel selected and the patient's individual anatomy.

General Considerations

Probe Orientation

Unlike the standard orientations found in echocardiography, ultrasound for vascular access can have varying probe and image orientations based on the vessel being cannulated and the operator's position. In general, it is recommended that the probe be oriented to display the same anatomy on the screen that would be visible to the operator from that vantage point. Thus, anatomic structures on the left side of the probe should appear on the left side of the screen and right-sided structures should appear on the right side of the screen. Although it is common for ultrasound probes to have an indicator that denotes one side of the probe that correlates with a specific side of the screen, the user can also briefly confirm anatomic and screen orientation alignment by moving the probe left to right or by applying gentle external pressure on one side of the probe confirming correlation with the image on the screen.

Ultrasound may be used for vascular access both in the long (in-plane) axis (LAX) and in the short (out-of-plane) axis (SAX). Both views may be utilized to guide needle movement, however, the in-plane technique serves to keep the entire needle length in view while the out-of-plane technique catches a cross section of the needle. The advantage that an out-of-plane technique has over an in-plane technique is the ability to visualize surrounding structures during needle movement (e.g., carotid artery during internal jugular cannulation). Oblique views can also be obtained but are not conventionally used and are not addressed further here.

In the SAX view, the probe is placed perpendicular to the desired vessel providing a cross section of the vessel with the needle appearing as a hyperechoic point (Fig. 15.1; Video 15.1). In the LAX view, the probe is placed parallel to the desired vessel, providing an image that shows the course of the vessel across the screen and the needle shaft as it is advanced (Fig. 15.2; Video 15.2). Again, the advantage of the SAX view is that it provides superior visualization of anatomic structures surrounding the vessel of interest. This advantage can be critical because ultrasound is often used to access central veins that run in close proximity to critical arteries. It appears that for novice users, the SAX view also results in faster cannulation times and is perceived to be an easier approach by the operator [1]. The LAX view provides the advantage of better visualization of the needle during its approach to and its course within the vessel. However, maintaining proper alignment of both the ultrasound transducer and the access needle can be challenging. Any malalignment results in the cannulating needle not being imaged and may lead to inadvertent arterial puncture during central venous access.

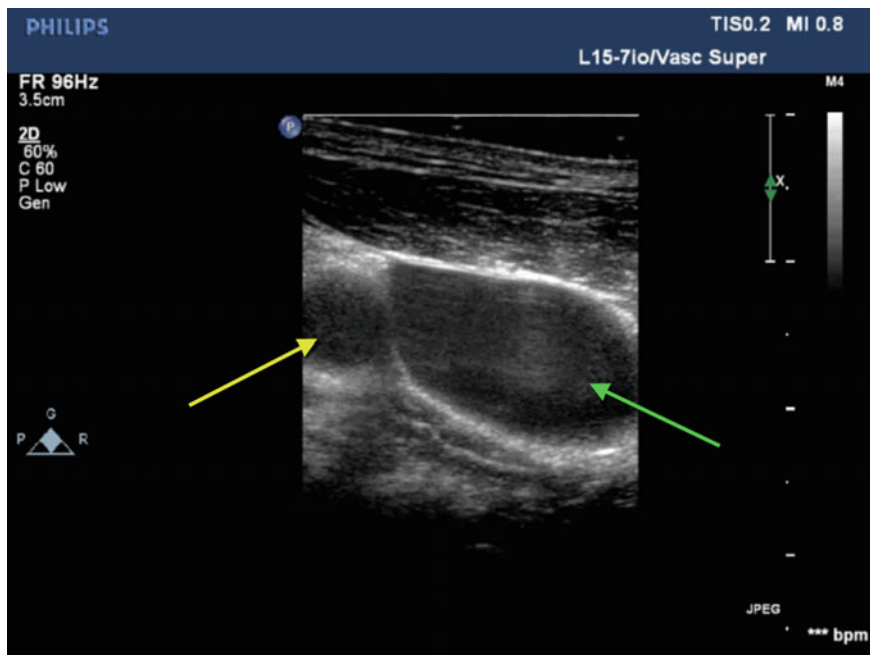


Fig. 15.1 Out of plane imaging or short axis (SAX) of the right internal jugular vein (*green arrow*). *Yellow arrow* indicates the carotid artery just to the medial aspect of the larger, collapsible internal jugular vein

Vessel Selection

There are a number of factors involved in selecting the site for central venous cannulation. Anatomic considerations, patient positioning, patient tolerance, venous drainage, and relative rates of complications should all be considered. In general, larger catheters with more lumens have a higher risk for infections [2]. Subclavian catheters have the lowest risk for infection (1.5–4 %) and thrombosis (1.2–1.9 %). Internal jugular catheters have an infection rate of 4–8 % and a thrombosis rate of 7.6 %. The femoral site has the highest incidence of both infection and thrombosis at 19.8 and 21.5 %, respectively [3].

Vessel Identification

Differentiation of veins from arteries is a critical aspect of appropriate use of ultrasound for obtaining vascular access. Both have anechoic (black) lumens but arteries have thicker walls that are more hyperechoic (white) than the walls of veins. Additionally, arteries are pulsatile and less compressible than veins. Pulsatility and compressibility are the two most useful indicators for differentiation of arteries and

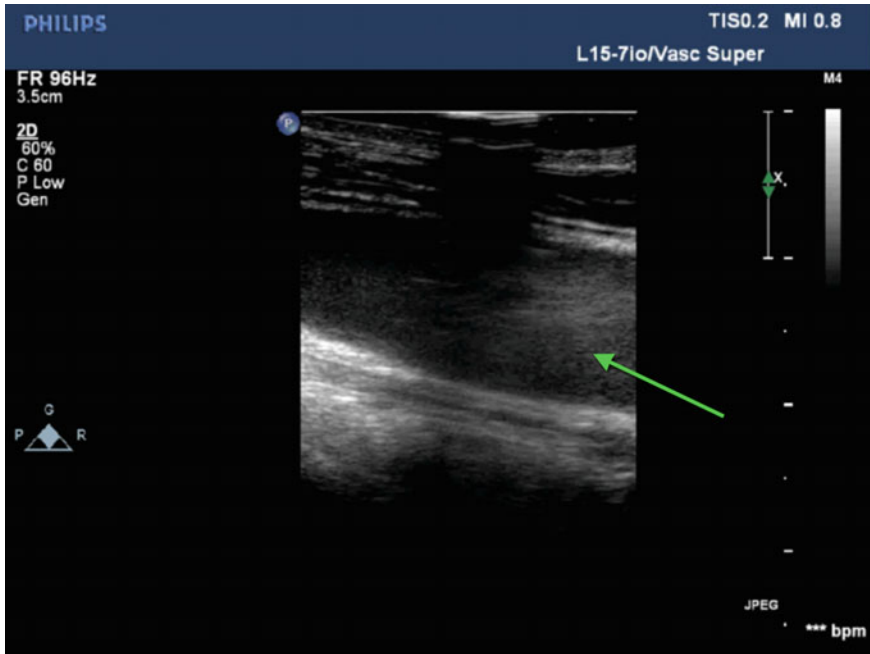


Fig. 15.2 In-plane imaging or long axis (LAX) of the right internal jugular vein (*green arrow*) from the same patient in Fig. 15.1

veins with ultrasound. With the vessel in the short axis, as gentle pressure is applied, veins will compress while nearby arteries will remain patent and pulsatile. However, with excessive pressure both arteries and veins can collapse. Color flow Doppler imaging may also be used to identify pulsatile flow (Figs. 15.3 and 15.4; Videos 15.3 and 15.4). Venous blood flow will be uniform in color, low velocity and may be present during systole and diastole, whereas arterial flow will be higher velocity and detected predominantly during systole. The Doppler scale can be lowered and the color gain increased to detect flow if not initially observed.

Because techniques for vessel identification can be rendered less reliable in low-flow states or cardiac arrest, it is crucial that the operator understands the normal anatomic relationships between arteries and veins surrounding the vessel selected for cannulation. Additionally, other confirmatory measures and verification of correct placement of the guidewire and/or catheter is necessary and will be covered in later sections.

Static Versus Dynamic Imaging

Static imaging uses ultrasound to identify the vessel selected for cannulation and the appropriate site of needle entry after which ultrasound is no longer used to guide the procedure. The dynamic approach uses real-time ultrasound throughout the

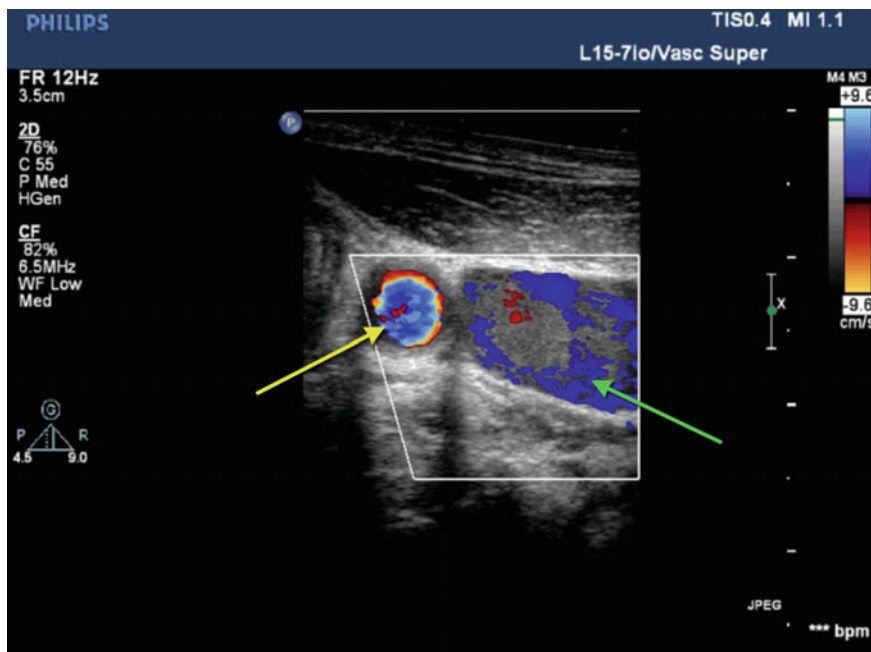


Fig. 15.3 Out of plane imaging (SAX view) of the right internal jugular vein (*green arrow*) with color flow Doppler. *Yellow arrow* indicates the carotid artery. Color flow Doppler imaging demonstrates faster pulsatile laminar flow in the carotid artery with slower flow in the jugular vein

procedure to guide needle placement and vessel entry. Dynamic imaging provides faster cannulation with fewer attempts but complication rates for both techniques are similar [4–6].

Performing the Procedure

Proper positioning of the patient including Trendelenburg positioning when appropriate will aid in vessel detection and in the performance of the procedure by increasing central venous pressure and thereby the size of the vessel on imaging. After identifying the appropriate vessel with ultrasound, the course of the needle to the vessel needs to be determined. Typically, the needle should be directed toward the middle of the vessel which is best determined using the SAX view. If the LAX view is used, the needle should be visualized throughout its course toward and within the vessel. The angle of approach should be such that the needle will avoid nearby arteries both during approach and in the event the needle penetrates through the posterior aspect (“backwall”) of the target vessel. Care should be taken to avoid posterior wall puncture, but having the artery away from the trajectory of the needle will minimize the risk of arterial puncture in the event of accidental posterior wall puncture.

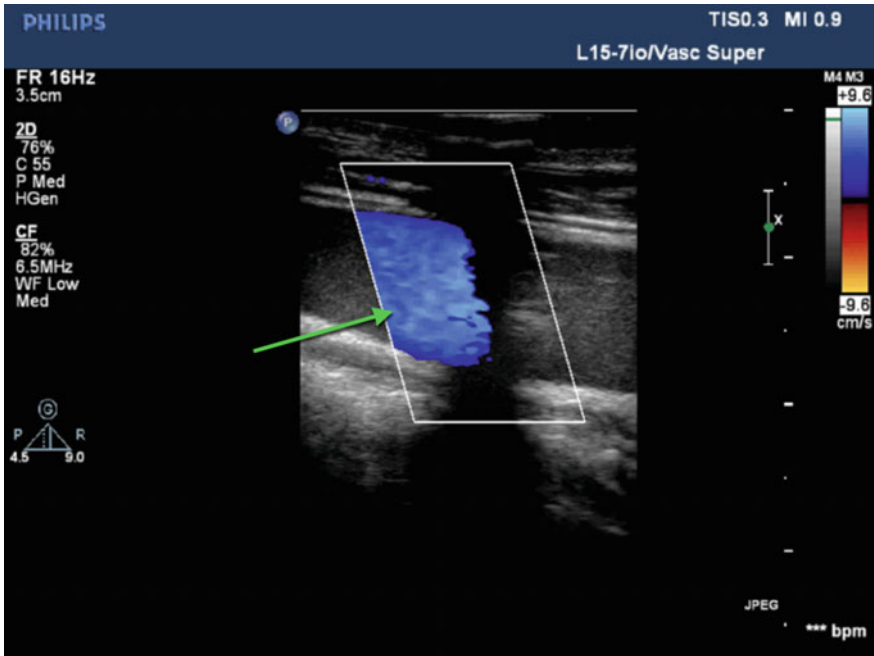
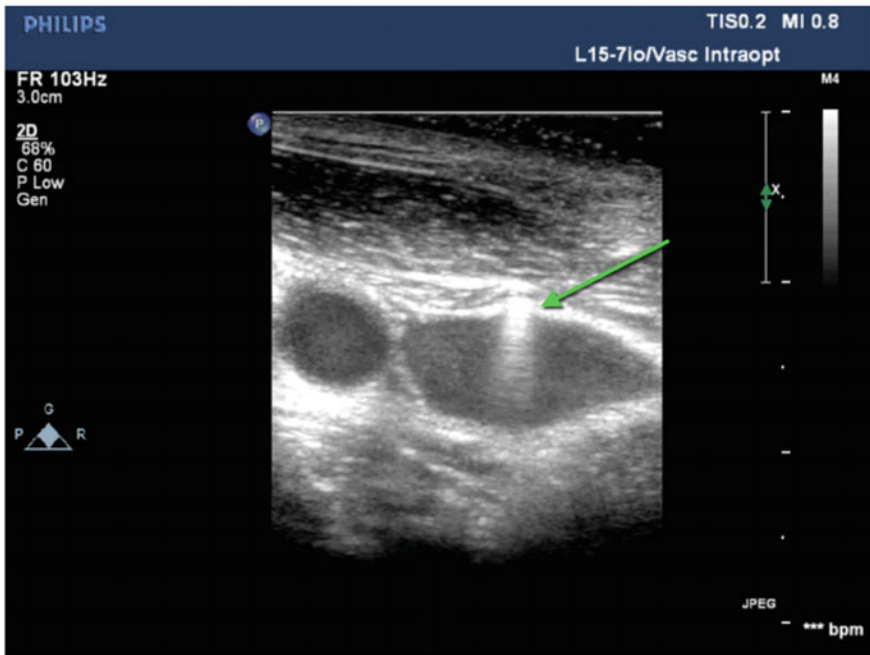


Fig. 15.4 In-plane imaging (LAX view) of the right internal jugular vein (*green arrow*) with color flow Doppler

In the SAX view, the needle tip will be seen to indent the wall of the target vessel. With gentle traction on the syringe connected to the needle, a flash of blood will be seen in the syringe. After placement of the guidewire, ultrasound can be used in both SAX and LAX to confirm that the guidewire is both in the target vessel and not in surrounding vessels (Fig. 15.5a, b; Video 15.5a, b). Other techniques to aid in confirming appropriate vessel cannulation include direct pressure transduction, manometry, blood gas analysis, visualization of the wire with transesophageal echocardiography, and fluoroscopy. With the concurrent use of transesophageal echocardiography, a midesophageal bicaval view can confirm venous placement of the wire, noting the “J” tip of the wire in the right atrium (Fig. 15.6; Video 15.6). The American Society of Echocardiography (ASE) and the Society of Cardiovascular Anesthesiologists (SCA) recommend that real-time ultrasound be used to confirm vessel cannulation. The ASE/SCA recommendation is that if the combination of SAX and LAX is not utilized for confirmation of wire placement, manometry should be used [7].

(a)



(b)

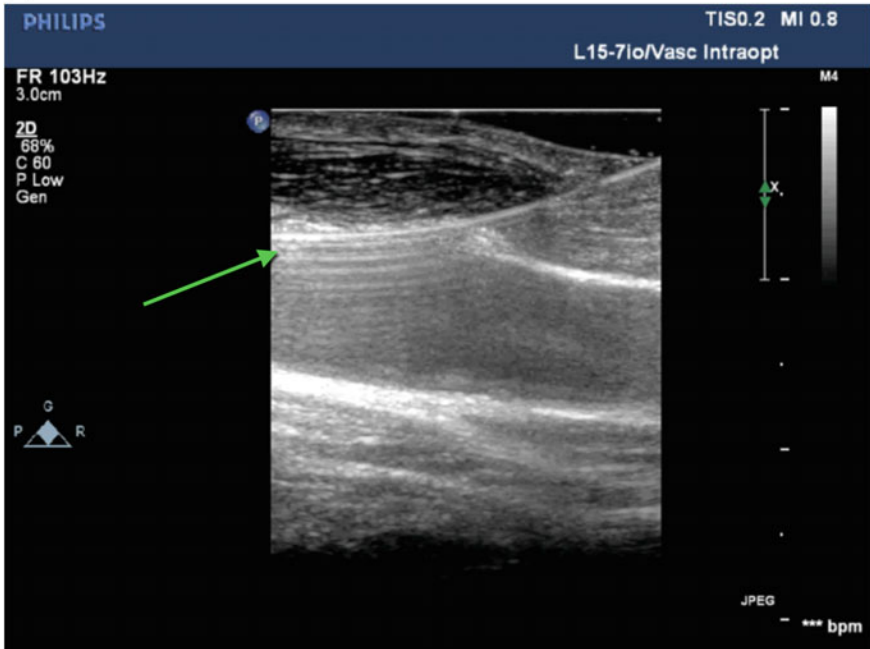


Fig. 15.5 **a** Short axis imaging of right internal jugular vein with a wire within its lumen. **b** Long axis imaging of the right internal jugular vein with a wire noted to be within its lumen (no evidence of “backwall”). *Green arrow* indicates the wire within the jugular vein

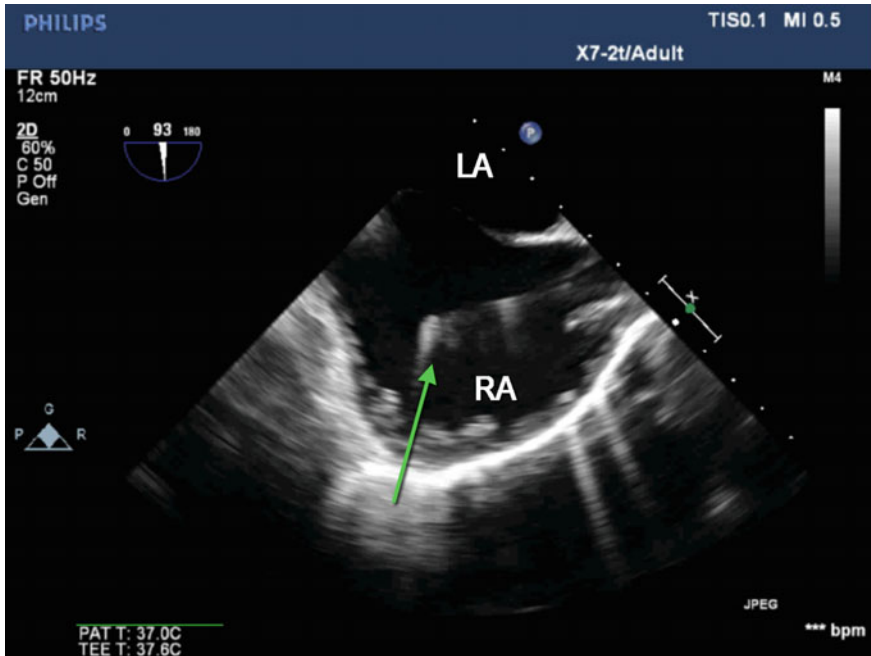


Fig. 15.6 Midesophageal bicaval view demonstrating the “J-tip” of the central access wire within the right atrium confirming venous access. *Green arrow* indicates the “J-tip.” *LA* left atrium; *RA* right atrium

Internal Jugular Vein Cannulation

The superiority of ultrasound guidance over landmark-based techniques for internal jugular (IJ) vein cannulation has been well documented [4, 8–10]. The use of ultrasound improves the overall and first-pass success rate, decreases time to cannulation and rate of arterial punctures, and total number of needle advances [10]. The ASE and SCA recommend that properly trained clinicians use real-time ultrasound for IJ cannulation whenever possible [7].

Any practitioner using ultrasound for IJ vein access should be familiar with the appearance of the local anatomy on ultrasound. The size of the IJ can be increased (potentially improving cannulation success) with Valsalva techniques and Trendelenburg positioning. These maneuvers also decrease the risk of air entrainment in the spontaneously ventilating patient [11, 12]. There is an intimate relationship between the IJ and the carotid artery (CA) at the location where IJ cannulation is typically pursued. This relationship explains the benefit of using ultrasound for IJ cannulation. Overlap between the IJ and the CA can lead to unintentional puncture and/or cannulation of the CA due to a through-and-through puncture of the vein. Ultrasound can be used to angle the approach such that CA

puncture would be avoided in the event of accidental through-and-through puncture [13, 14]. Additionally, ultrasound can be used in both SAX and LAX to visualize the guide wire in the IJ and confirm that the guidewire is not in the CA to avoid accidental CA dilation and cannulation [15]. Real-time ultrasound imaging can also potentially decrease the risk for pneumothorax by allowing for recognition of pleural tissue.

Subclavian/Axillary Vein Cannulation

While ultrasound-guided IJ vein access provides clear complication and success rate benefits over landmark-based techniques, evidence supporting ultrasound-guided subclavian (SC) vein cannulation over landmark techniques is less clear. There are studies, however, that document higher success rates with ultrasound-guided cannulation of the SC vein as compared to landmark techniques [16, 17]. Obese patients and others with obscured external landmarks appear to benefit the most from the use of ultrasound for SC vein cannulation [18, 19].

The ASE and SCA state that the current literature does not support the routine use of ultrasound for uncomplicated patients undergoing SC vein cannulation. However, these associations do indicate that high-risk patients may benefit from the use of ultrasound to identify vessel location and patency prior to cannulation [7].

Although the supraclavicular approach is rarely used with landmark-based techniques because of the high incidence of pneumothorax, it is being used more frequently now as ultrasound identification of supraclavicular vessels is becoming more commonplace. Nevertheless, the infraclavicular approach remains the most common technique for SC vein cannulation with both landmark and ultrasound-guided techniques. The middle third of the clavicle is typically chosen as the site for ultrasound imaging and needle insertion. The vein and artery should be identified just below the distal half of the clavicle (Fig. 15.7; Video 15.7). An SAX approach is usually preferred due to the difficulty of differentiating vein and artery at this location in the LAX. Trendelenburg position does not increase relative SC vein size to the same degree as with the IJ vein and thus, supine positioning is commonly used except in the case of a spontaneously breathing patient where Trendelenburg positioning will reduce the risk for air embolism [20].

Femoral Vein Cannulation

Studies have demonstrated the benefit of ultrasound-guided femoral vein (FV) cannulation in reducing incidence of vascular-related complications to the femoral artery and FV as well as improved first-pass and overall success rates [21–23]. However, the evidence is insufficient to support a recommendation of routine use

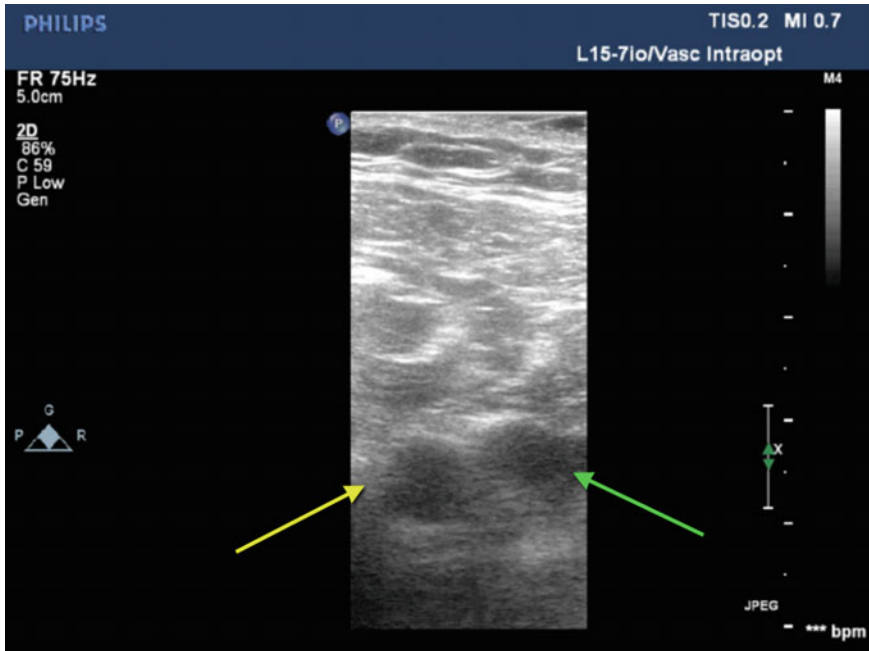


Fig. 15.7 Short axis imaging of the left subclavian artery and vein. The *green arrow* indicates vein and the *yellow arrow* indicates artery

by the ASE and SCA [7]. The ASE and SCA recommend that ultrasound be used *only when feasible* for FV cannulation to identify vessel overlap and patency.

Although infection is one of the most common complications related to femoral catheters, the most common complication related to FV cannulation itself is vascular injury. Of particular concern is common femoral artery puncture which would occur when the needle is directed too laterally or when there is significant vessel overlap. The common femoral artery is typically located at the midpoint of the inguinal ligament connecting the anterior iliac spine to the pubic tubercle. The FV is located just medial to the common femoral artery and it is this close anatomic relationship that makes the use of ultrasound-guided examination prior to cannulation beneficial despite no current recommendation for its routine use (Fig. 15.8; Video 15.8).

Ultrasound for Arterial Access

Ultrasound can be used to guide arterial access at any site at which arterial access is typically obtained including the radial, brachial, femoral, and dorsalis pedis arteries. The cannulation technique should not differ from the techniques used for

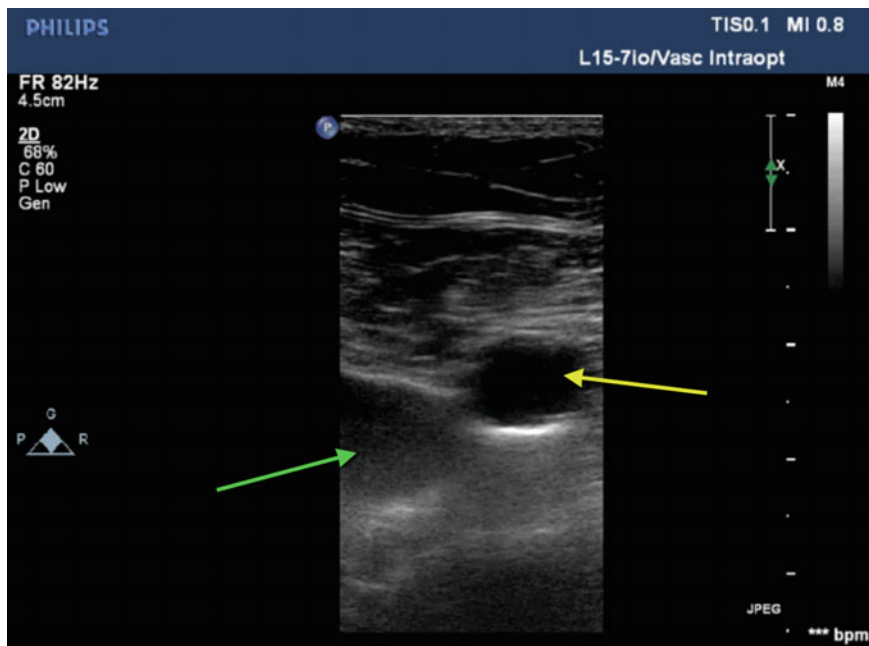
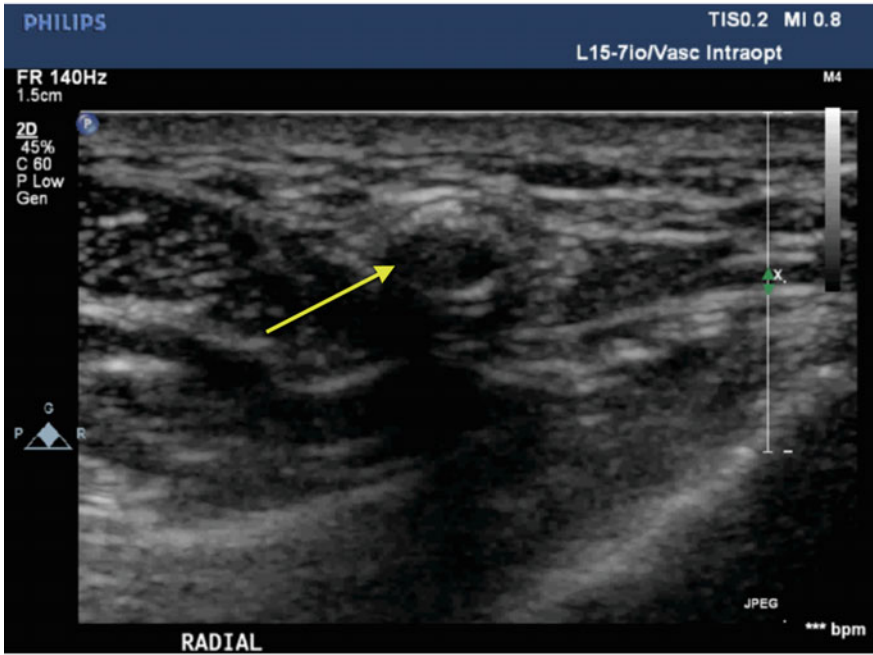


Fig. 15.8 Short axis imaging of the femoral artery and vein. The *green arrow* indicates vein and the *yellow arrow* indicates artery

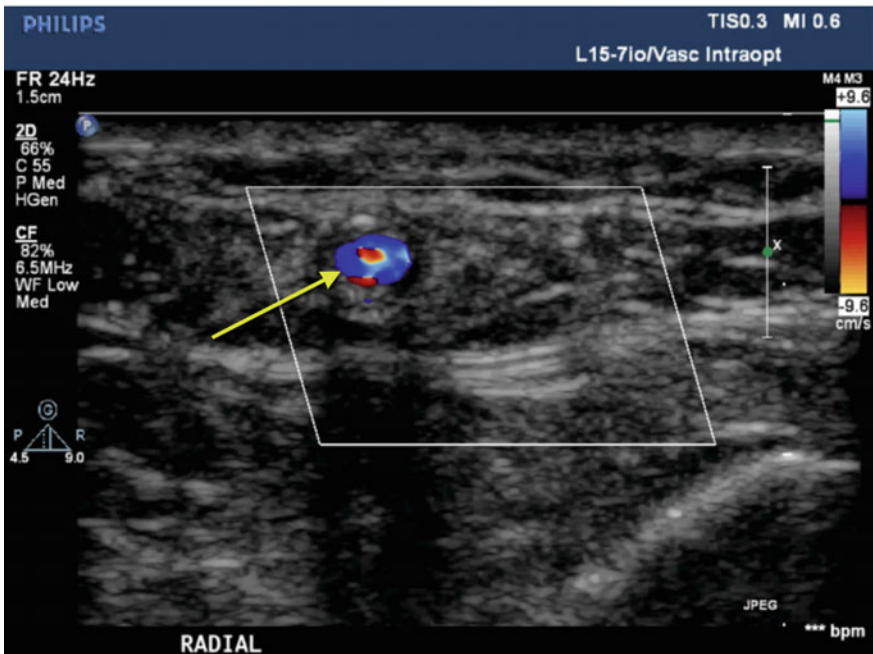
ultrasound-guided central vein access. The patient should be appropriately positioned, the orientation of the ultrasound probe and its correlation with the image on the screen should be confirmed, and measures such as a manual compression with the ultrasound probe and color flow Doppler should be taken to appropriately differentiate the target artery from surrounding vessels. Either the SAX or LAX can be used to cannulate the artery (Fig. 15.9a, b; Video 15.9a, b). The catheter can be inserted either over the needle or utilizing a guidewire.

Use of ultrasound for radial arterial access has been demonstrated to improve both first-attempt and overall success rates and reduce time to cannulation when compared with palpation-based techniques [24–26]. Ultrasound can be particularly useful in patients who are obese, have low perfusion or nonpulsatile blood flow, or who have had previous unsuccessful cannulation attempts [27]. The ASE and SCA recognize the evidence supporting the use of ultrasound to improve first-pass success rates but do not recommend routine use of real-time ultrasound for arterial access [7].

(a)



(b)



◀ **Fig. 15.9** **a** Short axis imaging of the right radial artery. **b** Short axis imaging of the same patient with color flow Doppler imaging. The *yellow arrow* indicates the radial artery

Ultrasound for Peripheral Venous Access

Ultrasound can be used to facilitate peripheral venous cannulation, particularly in deeper veins that are not palpable or visible. There are a number of reports of successful use of ultrasound in both the SAX and LAX for peripheral venous cannulation [28, 29]. Due to the collapsibility of peripheral veins, this can often be a difficult technique to achieve. The use of a tourniquet will increase peripheral pressure improving success (Fig. 15.10; Video 15.10). As well, a through-and-through technique (“backwall”) may be utilized under live ultrasound guidance. Withdrawing of the catheter slowly until blood return occurs allows the passage of a guidewire and subsequent advancement of the catheter. Release of the tourniquet may be necessary to advance the wire. Currently, there are no practice guidelines recommending the routine use of real-time ultrasound for peripheral venous access.

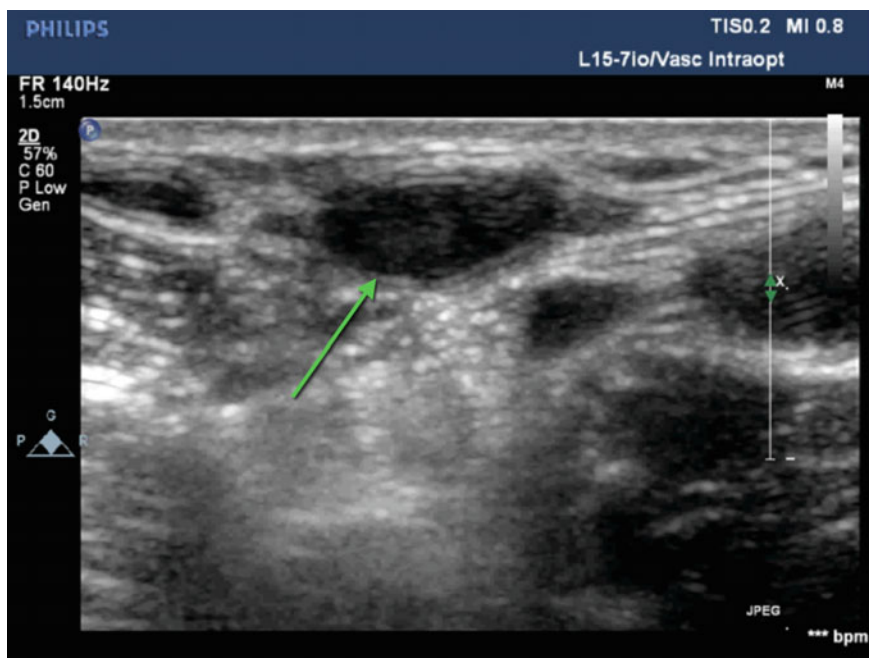


Fig. 15.10 Short axis imaging of a left basilic peripheral vein (*green arrow*)

References

1. Blaivas M, Brannam L, Fernandez E. Short-axis versus long-axis approaches for teaching ultrasound-guided vascular access on a new inanimate model. *Acad Emerg Med.* 2003;10:1307–11.
2. Merrer J. Complications of femoral and subclavian venous catheterization in critically ill patients: a randomized controlled trial. *JAMA.* 2001;286:700.
3. McGee DC, Gould MK. Preventing complications of central venous catheterization. *N Engl J Med.* 2003;348:1123–33.
4. Hosokawa K, Shime N, Kato Y, Hashimoto S. A randomized trial of ultrasound image-based skin surface marking versus real-time ultrasound-guided internal jugular vein catheterization in infants. *Anesthesiology.* 2007;107:720–4.
5. Milling TJ, Rose J, Briggs WM, et al. Randomized, controlled clinical trial of point-of-care limited ultrasonography assistance of central venous cannulation: The Third Sonography Outcomes Assessment Program (SOAP-3) Trial. *Crit Care Med.* 2005;33:1764–9.
6. Schnadower D, Lin S, Perera P, Smerling A, Dayan P. A pilot study of ultrasound analysis before pediatric peripheral vein cannulation attempt. *Acad Emerg Med.* 2007;14:483–5.
7. Troianos CA, Hartman GS, Glas KE, et al. Guidelines for performing ultrasound guided vascular cannulation. *Anesth Analg.* 2012;114:46–72.
8. Denys BG, Uretsky BF, Reddy PS. Ultrasound-assisted cannulation of the internal jugular vein. A prospective comparison to the external landmark-guided technique. *Circulation.* 1993;87:1557–62.
9. Karakitsos D, Labropoulos N, De Groot E, et al. Real-time ultrasound guided catheterization of the internal jugular vein: a prospective comparison with the land mark technique in critical care patients. *Crit Care.* 2006;10:R162.
10. Troianos CA, Jobes DR, Ellison N. Ultrasound-guided cannulation of the internal jugular vein. A prospective, randomized study. *Anesth Analg.* 1991;72:823–6.
11. Bellazzini MA, Rankin PM, Gangnon RE, Bjoernsen LP. Ultrasound validation of maneuvers to increase internal jugular vein cross-sectional area and decrease compressibility. *Am J Emerg Med.* 2009;27:454–9.
12. Terai C, Anada H, Matsushima S, Shimizu S, Okada Y. Effects of mild trendelenburg on central hemodynamics and internal jugular vein velocity, cross-sectional area, and flow. *Am J Emerg Med.* 1995;13:255–8.
13. Blaivas M, Adhikari S. An unseen danger: Frequency of posterior vessel wall penetration by needles during attempts to place internal jugular vein central catheters using ultrasound guidance. *Crit Care Med.* 2009;37:2345–9.
14. Stone MB, Hern HG. Inadvertent carotid artery cannulation during ultrasound guided central venous catheterization. *Ann Emerg Med.* 2007;49:720.
15. Moak JH, Lyons MS, Wright SW, Lindsell CJ. Needle and guidewire visualization in ultrasound-guided internal jugular vein cannulation. *Am J Emerg Med.* 2011;29:432–6.
16. Balls A, LoVecchio F, Kroeger A, Stapczynski JS, Mulrow M, Drachman D. Ultrasound guidance for central venous catheter placement: results from the Central Line Emergency Access Registry Database. *Am J Emerg Med.* 2010;28:561–7.
17. Gualtieri E, Deppe SA, Sipperly ME, Thompson DR. Subclavian venous catheterization. *Crit Care Med.* 1995;23:692–7.
18. Beaulieu Y. Bedside ultrasonography in the ICU. *Chest.* 2005;128:1766.
19. Hind D. Ultrasonic locating devices for central venous cannulation: meta-analysis. *BMJ* 2003;327:361–70.
20. Tan B-K, Hong S-W, Huang MHS, Lee S-T. Anatomic basis of safe percutaneous subclavian venous catheterization. *J Trauma Inj Infect Crit Care.* 2000;48:82.
21. Iwashima S, Ishikawa T, Ohzeki T. Ultrasound-guided versus landmark-guided femoral vein access in pediatric cardiac catheterization. *Pediatr Cardiol.* 2007;29:339–42.

22. Kwon T, Kim Y, Cho D. Ultrasound-guided cannulation of the femoral vein for acute haemodialysis access. *Nephrol Dial Transplant*. 1997;12:1009–12.
23. Seto AH, Abu-Fadel MS, Sparling JM, et al. Real-time ultrasound guidance facilitates femoral arterial access and reduces vascular complications. *JACC: Cardiovasc Interv*. 2010;3:751–8.
24. Levin PD, Sheinin O, Gozal Y. Use of ultrasound guidance in the insertion of radial artery catheters. *Crit Care Med*. 2003;31:481–4.
25. Shiloh AL. Ultrasound-guided catheterization of the radial artery. *Chest*. 2011;139:524.
26. Shiver S, Blaivas M, Lyon M. A prospective comparison of ultrasound-guided and blindly placed radial arterial catheters. *Acad Emerg Med*. 2006;13:1275–9.
27. Sandhu NS, Patel B. Use of ultrasonography as a rescue technique for failed radial artery cannulation. *J Clin Anesth*. 2006;18:138–41.
28. Keyes LE, Frazee BW, Snoey ER, Simon BC, Christy D. Ultrasound-guided brachial and basilic vein cannulation in emergency department patients with difficult intravenous access. *Ann Emerg Med*. 1999;34:711–4.
29. Sandhu NPS. Mid-arm approach to basilic and cephalic vein cannulation using ultrasound guidance. *Br J Anaesth*. 2004;93:292–4.

Index

Note: Page numbers followed by *f* and *t* indicate figures and table respectively

A

- Adult congenital heart disease
 - atrial septal defect
 - coronary sinus, 251
 - echocardiographic examination for, 252, 253–254
 - ostium primum, 249, 251, 252*f*
 - ostium secundum, 248–249, 251*f*
 - PFO, 248
 - sinus venosus, 251, 253*f*
 - PDA/aorticopulmonary window, 258–259
 - persistent left SVC, 257
 - ToF, 259–260
 - ventricular septal defect
 - echocardiographic examination of, 256–257
 - inlet, 255
 - muscular defects, 255
 - outlet, 255–256
 - perimembranous defects, 254
- American Society of Anesthesiologists (ASA), 6
- American Society of Echocardiography (ASE), 6, 206
- Aortic aneurysms
 - echocardiographic approach, 197
 - normal adult thoracic aortic diameters, 196, 198*t*
- Aortic atheroma, 199–201
- Aortic dissection
 - classification systems, 188
 - CT/MRI, 188
 - DeBakey system, 188
 - dissection flap identification, 189–191
 - identifying complicating pathologies, 193–196
 - Stanford system, 188
 - true and false lumens, differentiation of, 191–193, 193*t*
- Aortic regurgitation (AR)
 - aortic root dilatation, 136
 - cuspid integrity, 136
 - echocardiographic evaluation, 137–143
 - color flow Doppler, 138
 - spectral Doppler, 140–141
 - two-dimensional assessment, 137–138
 - excessive cuspid motion, 136
 - groups, 136
 - quantification of (*see under* Color flow Doppler)
- Aortic stenosis (AS)
 - echocardiographic evaluation
 - color flow Doppler, 131
 - spectral Doppler, 132–136
 - TEE, three-step approach, 128
 - two-dimensional assessment, 128–131
 - rheumatic causes, 127
 - sclerotic thickening, 127
 - ventricular relaxation, 127
- Aortic valve (AV)
 - aortic regurgitation. *see* Aortic regurgitation
 - aortic root dilatation, 136
 - cuspid integrity, 136
 - echocardiographic evaluation, 137–143
 - excessive cuspid motion, 136
 - groups, 136
 - aortic stenosis
 - echocardiographic evaluation, 128–136
 - rheumatic causes, 127
 - sclerotic thickening, 127
 - ventricular relaxation, 127
 - intervalvular septum, 127
 - LVOT, 127
 - structure of, 126
 - Valsalva sinuses of, 126
- ASE. *See* American Society of Echocardiography (ASE)
- Atheromatous disease, 199

echocardiographic grading, 200, 201*t*
 Atrial contraction, 171
 Atrial septal defect (ASD)
 coronary sinus, 251
 echocardiographic examination for, 252, 253–254
 ostium primum, 249, 251, 252*f*
 ostium secundum, 248–249, 251*f*
 PFO, 248
 sinus venosus, 251, 253*f*

B

Basic examination, TEE
 complications, 8–9, 8*t*
 contraindications, 7–8, 7*t*
 indications, 6–7
 Basic view, TTE
 apical four-chamber view, 272–273
 parasternal LAX view, 267–269
 parasternal SAX view, 269–272
 subcostal views, 273, 274*f*
 Bicuspid mitral valve, 96
 Blood flow velocity, 50, 51*f*
 Blunt aortic injury, 202

C

Cardiac output (CO), 222
 Color flow Doppler (CFD), 88, 131, 207
 aortic regurgitation, quantification of
 jet width to LVOT diameter, 139–140
 vena contracta, 138–139, 140*f*
 aortic stenosis, 131
 hemodynamics, 116
 mitral regurgitation (MR) jet, 110
 PISA, 115–116, 115*f*
 pulmonary venous flow profile, 113, 114*f*, 115
 vena contracta, 113, 114*f*
 Coronary artery
 anatomy
 LAD, 78
 LCA, 78
 LCx, 78
 RCA, 79
 17-segment model, 80, 80*f*
 coronary perfusion, 80
 mid-esophageal (ME)
 long axis view, 83, 84*f*
 two-chamber view, 83, 84*f*
 myocardial ischemia, complications from
 diastolic dysfunction, 89
 myocardial infarction, 90–91
 papillary muscle, 89–90
 stunned myocardium, 89

 ventricular free wall rupture, 90
 regional wall motion abnormality
 akinesis/dyskinesia, 87
 grading of, 85*t*
 M-mode, 88, 88*f*
 transgastric midpapillary short axis view, 81, 82*f*
 Coronary sinus (CS), 257

D

DeBakey system, 188
 Diastasis, 171
 Diastology
 clinical implications of
 intraoperative echocardiography, 180
 left atrium (LA) and left ventricle (LV), 179
 S-wave, 180
 phases of, 170–171
 properties, 170
 pulse-wave Doppler echocardiography
 LA inflow/pulmonary venous flow, 172, 173*f*
 LV/transmitral inflow profile, 171–172
 tissue Doppler imaging, 174–175
 stages of, 176*t*
 impaired relaxation, 176–177
 pseudonormalization, 177–178
 restrictive stage, 178
 spectrum of, 176*f*
 D-shaped left ventricle, 157, 158*f*

E

Early rapid filling, 171
 Eccentricity index (EI), 158
 EF. *See* Ejection fraction (EF)
 Effective regurgitant orifice area (EROA), 115–116
 EI. *See* Eccentricity index (EI)
 Ejection fraction (EF)
 ASE definition, 62
 3D EF calculation, 72, 73*f*
 visual estimation of, 63

F

Femoral vein cannulation, 287–288
 Focused cardiac ultrasound (FOCUS), 266
 Fractional area change (FAC), 66
 RV FAC, 155
 Fractional shortening, 63–66
 Functional mitral regurgitation (FMR), 108

G

Global longitudinal strain (GLS), 73, 74*f*

Grading severity
 color flow Doppler, 109–110, 111*f*, 112*f*
 two-dimensional echocardiography,
 108–109

H

Hemodynamic assessment, 52
 flow, 53–54
 pressure gradient estimation, 55, 57
 valvular area, 54–55

Hemodynamic compromise, 3–4, 6
 examples of, 275, 276*f*, 277*f*

Hemodynamic instability, 16, 206, 207

Hemodynamics, 116

Hypovolemia

cardiac output, 222
 LVEDA, 219
 LVESA, 220
 LVOT diameter, 220
 stroke volume, 220, 222–223
 VTI, 222

I

Inlet VSDs, 255

Interatrial septum, 159–160

Internal jugular (IJ) vein cannulation, 286–287

Intervalvular septum, 127

Interventricular septum (IVS), 78
 shape and motion of, 157–158

Intra-aortic balloon pump (IABP), 187

Isovolumetric relaxation, 171

J

Jugular vein, 282, 283*f*, 284, 285*f*. *See also*
 Internal jugular (IJ) vein cannulation

K

Knowledge

lack of, 231–232
 of normal anatomy, 4, 243
 of principles of echocardiography, 4, 183
 TEE knowledge, 277

L

Left anterior descending (LAD) artery, 78

Left atrial appendage (LAA), 19

Left circumflex (LCx) artery, 78

Left coronary artery (LCA), 78

Left ventricular end-diastolic area (LVEDA),
 66, 179, 216, 219, 224, 225*t*

Left ventricular end diastolic pressure
 (LVEDP), 179

Left ventricular end-systolic area (LVESA), 66,
 179, 216, 219, 224, 225*t*

Left ventricular outflow tract (LVOT), 127
 jet width to LVOT diameter, 139–140
 pulse wave Doppler of, 132–133, 133*f*

Left ventricular systolic function
 ejection fraction

ASE definition, 62
 3D EF calculation, 72, 73*f*
 visual estimation of, 63

fractional area change, 66

fractional shortening, 63–66

GLS, 73, 74*f*

LV geometry, measurements of

mass calculation, 75
 wall thickness, 74

LV volumes, 67–68

modified Simpson's method

dP/dt, 69–71
 mid-esophageal four-chamber view, 68,
 69
 mid-esophageal two-chamber view, 68,
 69

tissue Doppler imaging, 71, 72*f*

Long axis (LAX) view, 280, 284

mid-esophageal, 19–20, 103, 105, 113, 207*t*

ascending aortic, 23–25, 38*t*

AV, 29–30

descending aortic, 26–27, 39*t*, 43*t*

parasternal, 267–269

TG, 31–32

deep-TG, 32–34, 207*t*

upper esophageal (UE), aortic arch, 35, 43*t*

LVEDP. *See* Left ventricular end diastolic
 pressure (LVEDP)

M

ME views. *See* Mid-esophageal (ME) views

Mid-esophageal (ME) views

ascending aortic SAX and LAX views,
 23–25

AV SAX, 20–21, 20*f*

bicaval view, 22–23, 23*f*

four-chamber view, 17–18

LAX view, 19–20, 20*f*

RV inflow–outflow view, 21–22, 22*f*

two-chamber view, 19, 19*f*

Mitral stenosis (MS)

PHT, 120, 122

PISA, 122–123, 122*f*

planimetry, 123

pressure gradients, 119, 120*f*, 121*f*

quantitative assessment of, 119, 119*t*

two-dimensional echocardiography,
 117–119

Mitral valve (ML)

- Mitral valve (ML) (*cont.*)
- anatomy and function of
 - anterior leaflet, 96
 - bicuspid mitral valve, 96
 - components of, 95, 96f
 - mitral leaflets, 96, 98
 - posterior leaflet, 96
 - color flow Doppler
 - hemodynamics, 116
 - MR jet, 110
 - PISA, 115–116, 115f
 - pulmonary venous flow profile, 113, 114f, 115
 - vena contracta, 113, 114f
 - mid-esophageal views
 - four-chamber view, 98
 - LAX view, 103
 - mitral commissural view, 103
 - two-chamber view, 103
 - MS (*see* Mitral stenosis (MS))
 - regurgitation
 - excessive leaflet motion, 105
 - FMR, 108
 - mechanism of, 105
 - normal leaflet motion, 105
 - restricted leaflet motion, 108
 - two-dimensional echocardiography, 108–109
 - types of, 105
 - TEE imaging of, 98, 100–102f
 - transgastric
 - basal SAX view, 104
 - two-chamber view, 104
- Myocardial ischemia, complications from
- diastolic dysfunction, 89
 - myocardial infarction, 90–91
 - papillary muscle, 89–90
 - stunned myocardium, 89
 - ventricular free wall rupture, 90
- Myocardial performance index (MPI) 155, 157
- N**
- National Board of Echocardiography (NBE), 5
- Non-cardiac surgery, 3–5
- Normal adult thoracic aortic diameters, 196, 198r
- Normal anatomic variants and misdiagnoses, TEE
- Arantius, nodules of, 237, 239f
 - Chiari network, 233, 234f
 - Coumadin ridge, 237, 239f
 - crista terminalis, 235, 235f
 - epicardial fat, 232, 233f
 - Eustachian valve, 233, 234f
 - Lambl's excrescences, 236, 237f
 - moderator band, 235
 - papillary fibroelastoma, 236, 238f
- Normal leaflet motion, 105
- O**
- Ostium primum, 249, 251, 252f
- Ostium secundum, 248–249, 251f
- P**
- PAP. *See* Pulmonary artery pressure (PAP)
- PASP. *See* Pulmonary artery systolic pressure (PASP)
- Patent ductus arteriosus (PDA), 258–259
- Patent foramen ovale (PFO), 159–160, 248
- PDA. *See* Patent ductus arteriosus (PDA)
- PE. *See* Pulmonary embolism (PE)
- PEEP. *See* Positive end expiratory pressure (PEEP)
- Perioperative transesophageal echocardiographic (PTE) examination
- ASE and SCA views
 - basic, 37–39r
 - descending aortic SAX and LAX views, 26–27, 27f, 28f
 - ME ascending aortic SAX and LAX views, 23–25
 - ME AV SAX, 20–21, 20f
 - ME bicaval view, 22–23, 23f
 - ME four-chamber view, 17–18
 - ME LAX view, 19–20, 20f
 - ME RV inflow–outflow view, 21–22, 22f
 - ME two-chamber view, 19, 19f
 - TG midpapillary SAX view, 25–26, 26f
 - comprehensive TEE, 39r–43r
 - deep TG LAX view, 32, 33f, 34
 - ME AV LAX view, 29–30, 30f
 - ME mitral commissural view, 29, 29f
 - TG basal SAX view, 30–31
 - TG LAX view, 31–32, 33f
 - TG RV inflow view, 34, 34f
 - TG two-chamber view, 31, 32
 - UE aortic arch LAX and SAX views, 35, 35f
 - TEE perioperative guidelines, 16
- Plaque, 200
- Positive end expiratory pressure (PEEP), 273
- Pressure half time (PHT), 120, 122
- Proximal isovelocity surface area (PISA), 115–116, 115f
- EROA, 115–116
- mitral valve area, calculation of, 122f

- Pulmonary artery pressure (PAP), 148
 - Pulmonary artery systolic pressure (PASP), 163
 - Pulmonary embolism (PE), 164, 212, 214–215
 - risk factors associated, 214*t*
 - Pulmonary hypertension, adaptations to, 148
 - right ventricular enlargement, 149
 - right ventricular hypertrophy, 149–150
 - Pulmonary vascular resistance (PVR), 148
 - Pulseless electrical activity (PEA), 266
- Q**
- Qualitative evaluation of RV, 147–148
 - Quantitative assessment of mitral stenosis, 119, 119*t*
 - Quantitative assessment of RV
 - FAC, 155
 - MPI, 155, 157
 - TAPSE, 152, 154, 154*f*
 - TDI, 155, 157*f*
- R**
- Regional wall motion abnormality (RWMA)
 - akinesis/dyskinesia, 87
 - grading of, 85*t*
 - M-mode, 88, 88*f*
 - Rescue echocardiography
 - acute valvular and aortic pathology, 207
 - cardiac tamponade
 - echocardiographic diagnosis of, 209
 - pericardial effusions, 208
 - RV inflow–outflow, 210
 - two dimensional manifestations of, 210, 211*t*
 - cardiovascular system, 206
 - hypovolemia
 - cardiac output, 222
 - LVEDA, 219
 - LVESA, 220
 - LVOT diameter, 220
 - stroke volume, 220, 222–223
 - VTI, 222
 - left ventricular dysfunction
 - dagger shape, 218, 219*f*
 - FAC, 216
 - pathophysiologic settings, 217, 217*t*
 - low afterload, 224–225
 - pulmonary embolism
 - risk factors, 212, 214*t*
 - RV and LV dysfunction, 215
 - right ventricular dysfunction, 211
 - TEE exam, 206, 207*t*
 - Right atrium (RA), 159, 210
 - Right coronary artery (RCA), 79
 - Right heart, 83
 - RV (*see* Right ventricle/cular (RV))
 - transgastric midpapillary short axis view, 211
 - Right ventricle/cular (RV)
 - acute PE, echocardiographic findings in, 164–166
 - IVS, shape and motion of, 157–158
 - pulmonary hypertension
 - classification, 148, 149*t*
 - enlargement, 149
 - RVH, 149–150
 - quantitative assessment of (*see* Quantitative assessment of RV)
 - RA adaptation
 - interatrial septum position, 159–160
 - pulmonary artery, 163–164
 - tricuspid regurgitation, 160–163
 - structure and function, 146–147
 - TEE views
 - ME ascending aortic short axis view, 148
 - ME bicaval view, 147–148
 - ME four-chamber, 147
 - ME RV inflow–outflow view, 147
 - TG midpapillary short axis view, 148
 - TG RV inflow view, 148
 - Right ventricular outflow tract (RVOT), 21
- S**
- Septomarginal trabecula, 235
 - Short axis (SAX) view, 280, 287
 - mid-esophageal (ME)
 - aortic valve, 20–21, 241*f*, 253
 - ascending aortic, 23–24
 - descending aortic, 26–27, 43*t*
 - parasternal, 270, 270*f*, 271, 271*f*, 275
 - end-systolic, 276*f*
 - right internal jugular vein, 281*f*, 283*f*
 - transgastric (TG)
 - basal, 30–31, 42*t*, 104
 - midpapillary, 25–26, 65*f*, 216
 - upper esophageal (UE) aorta, 35–36
 - Society of Cardiovascular Anesthesiologists (SCA), 6, 206
 - Spectral Doppler
 - aortic regurgitation
 - flow, descending aorta reversal of, 141–142, 143*f*
 - PHT, 140–141
 - aortic stenosis
 - LVOT, pulse wave Doppler of, 132–133, 133*f*
 - mean pressure gradients, 135–136

- VTI measurements, 135
- Stanford system, 188
- Stroke volume (SV), 220, 222–223
- Superior vena cava (SVC), persistent left, 257
- T**
- Takotsubo cardiomyopathy, 216
- TEE. *See* Transesophageal echocardiography (TEE)
- Tetralogy of fallot (ToF), 259–260
- Thoracic aorta
 - aortic aneurysms, 196–199
 - aortic atheroma, 199–201
 - aortic dissection
 - classification systems, 188
 - CT/MRI, 188
 - DeBakey system, 188
 - dissection flap identification, 189–191
 - identifying complicating pathologies, 193–196
 - Stanford system, 188
 - true and false lumens, differentiation of, 191–193, 193*t*
 - TEE, aortic views
 - anatomical sections, 184
 - short and long axis views, 186
 - trauma, 202
- Tissue Doppler imaging (TDI), 155, 157*f*
- Transesophageal echocardiography (TEE)
 - aortic views
 - anatomical sections, 184
 - cranial aspect, 185
 - short and long axis views, 186
 - artifacts
 - acoustic shadowing, 241
 - dropout, 240–241, 240*f*
 - mirroring, 243, 244*f*
 - reverberation, 242, 243*f*
 - side lobe, 241–242, 242*f*
 - avoiding pitfalls, 243–244
 - basic examination
 - complications, 8–9, 8*t*
 - contraindications, 7–8, 7*t*
 - indications, 6–7
 - basic perioperative, certification in, 5–6
 - hemodynamic instability, 206, 207
 - normal anatomic variants and misdiagnoses (*see* Normal anatomic variants and misdiagnoses, TEE)
 - non-cardiac surgery, 3–5
 - reporting and image storage, 13
 - using TEE probe
 - insertion, 9
 - manipulation, 9–11
 - orientation, 12, 12*f*
- Transthoracic echocardiography (TTE), 4
 - basic view
 - apical four-chamber view, 272–273
 - parasternal LAX view, 267–269
 - parasternal SAX view, 269–272
 - subcostal views, 273, 274*f*
 - hemodynamic compromise, examples of, 275, 276*f*, 277*f*
 - noninvasive, 266
 - pseudo-PEA, 266
- Tricuspid annular plane systolic excursion (TAPSE), 152, 154, 154*f*
- Tricuspid regurgitation (TR), 160–163
- Tricuspid valve (TV), 160
- U**
- UE aortic arch. *See* Upper esophageal (UE) aortic arch
- Ultrasound
 - arterial access, 288–289
 - peripheral venous access, 291
- Ultrasound physics
 - basic, 45–46
 - density interfaces, 48
- Doppler
 - blood flow velocity, 50, 51*f*
 - CFD and PWD, 52
 - characteristics and clinical use of, 51, 51*t*
 - effect, 50
 - principle, 51
 - Wagon Wheel effect, 52, 52*f*
- hemodynamic assessment
 - flow, 53, 54
 - pressure gradient estimation, 55, 57
 - valvular area, 54, 55
- history of, 46, 46*f*
- probes
 - axial resolution, 48, 49*f*, 50
 - effects of, 49, 50*f*
 - lateral resolution, 48, 48*f*, 50
 - sound frequencies, 46, 47*f*
 - sound waves, characteristics of, 46, 46*f*
- Upper esophageal (UE) aortic arch, 35
 - LAX views, 43*t*, 35*f*
 - SAX views, 36*f*, 43*t*
- V**
- Vascular access, ultrasound for
 - femoral vein cannulation, 287–288
 - IJ vein cannulation, 286–287
 - performance, 283, 284
 - probe orientation, 280

- proper vascular access, 279
 - static vs. dynamic imaging, 282–283
 - subclavian/axillary vein cannulation, 287
 - vessel identification, 281–282
 - vessel selection, 281
 - Velocity–time integral (VTI), 119, 132
 - Ventricular septal defect (VSD)
 - echocardiographic examination of, 256–257
 - inlet, 255
 - muscular defects, 255
 - outlet, 255–256
 - perimembranous defects, 254
 - VTI. *See* Velocity–time integral (VTI)
- W**
- Wall motion abnormalities (WMA), 18